Vision-dependent avoidance behaviours as a non-invasive assessment of visual function in mice.

Mónica Maria Fernandes Freitas Martins

A dissertation submitted in partial fulfilment of the requirements for the degree of

Doctor of Philosophy

of

University College London

University College London

Declaration of originality

I, Mónica Maria Fernandes Freitas Martins, hereby declare that the work presented in this thesis is my own. Where information has been derived from other sources, I confirm that this has been indicated.

Abstract

The development of therapies for retinal degeneration relies heavily on mouse models. Here, I seek to translate a recently described visual stimulus-induced spontaneous behaviour into use as a low-severity test of vision, to determine retinal (dys)function and treatment effect and to understand the biology underpinning these stereotyped behaviours. Using wild-type (C57BL/6J) mice I first established a standardised framework where the impact of intra- and inter-animal variability and organisation of test sessions was assessed. On each session a mouse was placed in an arena that contained a refuge and stimuli presented, either a moving black disc of constant size (Sweep) or a rapidly expanding black disc (Loom).

As expected, mice usually ran to refuge (escape) upon Loom stimulus, or briefly ceased moving (freezing) upon Sweep stimulus. This set of experiments allowed me to establish an optimized protocol and further perform a cross-sectional study of response against strain, age, and sex where behaviour responses were remarkably consistent. The longitudinal study revealed a consistent response profile across ages, with a decrease in escape responses to the loom stimuli in older (1 year) mice, whilst the strain study showed that whilst some strains exhibit reduced exploratory behaviours the type of response was maintained across strains.

Next, I sought to explore some of the biology underlying these innate behaviours, by comparing responses both in non-degenerative animals that lack functioning rod or cone photoreceptors and/or melanopsin-sensitive cells and in models of progressive photoreceptor degeneration. My findings revealed an important role of intact rod function in mediating effective avoidance behaviours. This discovery resonates with the observed heightened responses at scotopic light levels in wild-type (C57BL/6J) mice, as well as with evolutionary principles.

Further, I sought to examine how vision-dependent avoidance behaviours might be implemented alongside other modes of visual

assessment as means of assessing therapeutic rescue. The variability observed in therapeutic rescue, even within individual animals, posed challenges in interpreting the Loom and Sweep data.

The consistency of the data reported under this thesis suggest that vision-dependent avoidance behaviours could be a reliable and robust method to assess visual function in mice.

Impact Statement

The development of therapies for retinal degeneration relies heavily on mouse models, yet conventional vision-guided behavioural tasks are often laborious and involve stressful techniques. Thus, there's a pressing need for non-invasive, repeatable, and reliable methods to measure visual sensitivity. This thesis addresses this challenge by leveraging visually induced innate escape and freeze avoidance behaviours to assess low- and high-level visual function in murine models of retinal dysfunction and recovery. This simple framework, utilizing visual stimuli like Loom and Sweep, complements existing readouts and aids in evaluating therapeutic success in eye diseases.

While similar behavioural tests have been employed in other studies, this study delves deeper into its application for pre-clinical ophthalmology research. It thoroughly examines protocol design, optimization, variability, and the influence of sex, age, wild-type strains and vision-impaired mouse models on these visually triggered innate behaviours. As a result, a substantial dataset of behavioural responses to visual stimuli across various conditions was generated. This comprehensive dataset, upheld by consistency in the protocol and experimental design, significantly contributes to the broader research.

Optimization of the Loom and Sweep design protocol was crucial for generating consistent data, with valuable insights shared globally. This thesis proposes some key findings: visual stimuli reliably trigger innate behaviours, and individual mice exhibit consistent responses regardless of exposure frequency.

Future research can delve into the mechanistic details underlying these visually triggered behaviours, paving the way for novel therapies for retinal degeneration and visual pathway disorders. This project was developed as a collaboration between gene and cell therapy ophthalmological and behavioural neuroscience groups fostering knowledge exchange and driving progress in both fields. By providing a simple framework for testing eye therapies, this project may attract new researchers and advance pre-clinical ophthalmology and behavioural neuroscience research.

Ultimately, this study explores the potential of utilizing innate behavioural responses as a metric for assessing visual function in mice, particularly in the context of gene therapy intervention in a well-established mouse model of retinal degeneration. The dissemination of this research will contribute to a deeper understanding of visually induced behaviours, thereby informing future studies aimed at enhancing therapies for patients and ultimately improving their quality of life.

Acknowledgements

I would like to thank Rachael Pearson and Sam Solomon for their valuable contributions to the design, execution, and analysis of the experiments incorporated into this thesis. Additionally, I wish to extend my gratitude to the members within the Pearson, Solomon, and Robin Ali labs for their support in the carrying out of the project.

Over the past few years, we've relentlessly pursued progress, pushing boundaries and striving for excellence even in the face of overwhelming challenges. Truth be told, it has been a bittersweet journey, one that I could never have foreseen would lead me to this very point. Against all odds, I've grasped each opportunity, worked tirelessly, and chased after every glimmer of potential that has brought me to this very moment.

Mom, amidst everything else, I hold dear the greatest gift you've bestowed upon me - the courage to relentlessly fight for what I believe in, no matter how daunting the obstacles may seem. For this invaluable lesson, I am profoundly grateful.

Tiago, from the beginning of our academic journey and throughout our lives, your steadfast presence has been an incredible blessing. Your unwavering belief in me and your constant encouragement have served as the bedrock upon which I've constructed my path forward.

Olívia, may this journey serve as a testament to the boundless possibilities within your reach, regardless of your background or circumstances. While the path ahead may be sometimes arduous, know that with steadfast commitment, unwavering dedication, and the right people, you possess the power to achieve your wildest aspirations. My deepest wish for you is that you always find the courage to pursue your dreams, and should doubt ever cloud your vision, may those around you serve as steadfast beacons, reminding you of your limitless potential.

You are the greatest gifts life has bestowed upon me, and for that, I am endlessly grateful. It is with profound love that I dedicate this thesis to you both.

“Everything is theoretically impossible until it is done.” – Robert A. Heinlein

Table of Contents

Table of Figures and Tables

Abbreviations

ONL - outer nuclear layer
INL - inner nuclear layer
GCL - ganglion cell layer
RGCs - retinal ganglion cell
dLGN - dorsal lateral geniculate nucleus
V1 - primary visual cortex or striate cortex
IPL - Inner plexiform layer
SC - superior colliculus
UV - ultraviolet
ERGs - Electroretinograms
LP - lateral posterior nucleus of the thalamus
PAG - periaqueductal gray
Ca^{2+} - salcium
Na^{2+} - sodium
cGMP - cyclic guanosine monophosphate
K^{+} - Potasium
GDP - Guanosine diphosphate
GTP - guanosine triphosphate
iRBP - interphotoreceptor retinoid-binding protein
GUCA - guanylyl cyclase regulated by a GC-activating protein
GCAP - guanylyl cyclase regulated by a GC-activating protein
GC - guanylyl cyclase
GRK - rhodopsin kinase
LGN - lateral geniculate nucleus
GNAT1 - rod α-transducin knockout mouse
CNGA3 - cyclic nucleotide gated channel α3 subunit
CNGB3 - cyclic nucleotide gated channel β3 subunit
CNG - cyclic nucleotide gated channel
OGC - *Opn4*$^{-/-}$; *Gnat1*$^{-/-}$; *Cnga3*$^{-/-}$ triple knockout mice model
ipRGC - intrinsically photosensitive retinal ganglion cell
OPN4 - melanopsin
PDE6β$^{rd1/rd1}$ - β subunit of phosphodiesterase 6 rapid degeneration mice model
PDE6 - phosphodiesterase 6
P10 – postnatal day 10
P25 – postnatal day 25
DAPI - 4′,6-diamidino-2-phenylindole
AAV - adeno-associated virus
AAV2/7 - adeno-associated virus serotype 2/7
AAV2/8 - adeno-associated virus serotype 2/8
LCA - leber congenital amaurosis
RPE65 – retinal Pigment epithelium 65
AAV2/2 - adeno-associated virus serotype 2/2
Kb - kilobases

Rd1 – rapid retinal photoreceptor degeneration mouse model 1
PFA - paraformaldehyde
PBS - phosphate-buffered saline
OCT - optimal cutting temperature compound
s - second
cm - centimeter
ms - milisecond
° - degree
min - minutes
m^2 – square meter
candela - unit of luminous intensity
kohm - kiloohm
c/d – cycle per degre
% - percentage
μg - micrograme
ml - mililiter
μl - microliter
h - hour
°C – degree Celcius
um - micrometer
cDNA – complementar deoxyribonucleic acid
AAV8 - adeno-associated virus serotype 8
DNA - deoxyribonucleic acid
DMEM - dulbecco's modified eagle medium
mM - milimolar
pH – potencial of hydrogen: a figure expressing the acidity or alkalinity of a solution on a logarithmic scale.
M - molar
PCR – polimerase chain reaction
ANOVA – analysies of variance statistical method
r-value - correlation coeficient
p-value - probability that a particular statistical measure is significant
n – number of independent experiments
UCL – University College London
KCL – Kings College London
S - session
T - trial
COVID-19 - coronavirus disease
D - day
M - month

Chapter 1: Introduction

The eye stands out as our paramount sensory organ, offering profound insights into the intricacies of visuospatial consciousness, a dominant aspect of our conscious experience. Notably, approximately 80% of external input processed by the brain is processed through the visual system (Jerath et al., 2015). The eye is also the most energy intensive tissue in the human body, requires precise development, and lacks redundancy in many of its functions. Vision loss is therefore debilitating and imposes significant costs on public funds, and private expenditure, as well as personal health. As the vast majority of vision loss is associated with aging, it is crucial to understand and develop novel therapeutic approaches for the treatment of neural degeneration (Aghaizu et al., 2017; Auricchio et al., 2017). At the same time, the anatomical characteristics of the eye make it an ideal organ to target and to test numerous therapeutic approaches. The eye's development and degeneration mechanisms have been studied extensively and it benefits from a partial immune privilege provided by the blood-retina barrier, allowing the use of different therapeutics strategies tools, as viral vectors, cells, and implants with no major reactions. Furthermore, it is anatomically discrete and easily approachable surgically.

The pre-clinical development of therapies for the treatment of retinal degeneration relies heavily on mouse models. Conventional vision-guided behavioural tasks are laborious and often involve stressful techniques such as fear conditioning, food- and water-regulation, and water-maze therefore, the development of new non-invasive, repeatable, and reliable methods for behavioural measurements of visual sensitivity is crucial. Here, I seek to utilise visually-induced innate escape and freeze avoidance behaviours (Yilmaz and Meister, 2013; De Franceschi et al., 2016) to develop a non-invasive method to assess low- and high-level visual function in murine models of retinal dysfunction and recovery.

I will first provide a general overview of the primate visual system with particular focus on humans. Then, I compare the primate and the rodent visual

systems, highlighting specific key features of both species. Further, as this study aims to characterise a behavioural test to be used as a readout of visual improvement after the treatment of retinal degeneration, I give an overview of retinal degeneration, and the avenues being pursued to tackle this and improve the quality of life of affected people.

1.1. Structure of the early visual system in humans and primates

The fundamental steps in the process of seeing are the transmission and refraction of light by the eye, the transduction of light into electrical signals by the photoreceptors present in the retina, and the refinement of these signals by synaptic interactions within the neuronal circuits of the retina.

The information extracted by the retina is transmitted by ganglion cell axons through the optic nerve to retinorecipient regions of the brain, where further processing leads to the ability to perform all the different functions from visual perception: high acuity, colour, motion; to the circadian rhythms, pupil size adjustment, and the movement of head and eye to or away from a visual stimulus (Celesia and DeMarco, 1994; Martersteck et al., 2017).

As illustrated in **Figure 1** - figure reproduced with permission from Aikaterini A. Kalargyrou et. al, Front. Mol. Neuroscience, 15:1042469, 2023 – the anatomical structure of the eye resembles a fluid-filled sphere surrounded by three layers of tissue. Among these layers, only the innermost, known as the retina, harbours neuronal cells that possess light sensitivity, enabling the transmission of visual signals. Adjacent to the retina lies the uveal tract, a layer of tissue composed by the choroid, the ciliary body, and the iris. The choroid is the larger component of this layer, highly vascularized to support and nourish the photoreceptors present in the retina, and rich in melanin a light absorbing pigment. Extending from the choroid towards the front of the eye is the ciliary body, a ring of tissue encircling the lens. This structure is composed of a muscular and a vascular component that are important for adjusting the refractive power of the lens. This is achieved by altering the thickness of the lens in response to the contraction of the ciliary muscle, which relieves tension

in the lens, allowing it to increase in thickness. The aqueous humorfluid that fills the eye is important as a source of nutrients. The last and most anterior compartment of the uvea tract is the iris, specialised in controlling the diameter and size of the pupil limiting the amount of light that enters the eye. This structure is also where the eye colour is determined. The outermost layer of eye tissue is the sclera, a tough, white, fibrous tissue. This layer assumes a specialized, transparent composition at the front of the eye, known as the cornea, facilitating the entry of light into the eye (Hejtmancik and Nickerson, 2015; Busse, 2018; Kalargyrou et al., 2023).

As light enters the eye through the cornea, it is focused by the lens onto the photoreceptors cells present in the retina. The retina is a light sensitive multilayer structure composed of six major classes of neurons, and non-neuronal Müller glial cells. Three nuclear layers (**Figure 1**) can be distinguished, which are, from posterior to anterior (i.e. from outer to inner): the outer nuclear layer (ONL), the inner nuclear layer (INL) and the ganglion cell layer (GCL), separated by the outer and inner plexiform layers, in which synaptic contacts occur. The ONL is composed of photoreceptor cell bodies, which project their outer segments towards and interdigitate with the retinal pigmental epithelium. This retinal pigmental epithelium is crucial for maintenance of the photoreceptors and the recycling of photopigments (Hejtmancik and Nickerson, 2015; Busse, 2018). Absorption of light by the photopigments present in the outer segments of the photoreceptors initiates a cascade of biochemical processes that transform light into the electrical energy of neuronal signals called the phototransduction.

Photoreceptor cells, integral to the process of vision, are specialised and photosensitive cells characterised by distinct structural components. These components include an outer segment, which houses membranous disks containing light-sensitive photopigment molecules, an inner segment, a cell body, and a synaptic terminal. There are two identified types of photoreceptors: rods and cones. While they share fundamental structural elements, they vary in shape, the type of expressed photopigment, distribution across the retina, and the pattern of synaptic connections. These differences contribute to the specialised and unique features of each photoreceptor type.

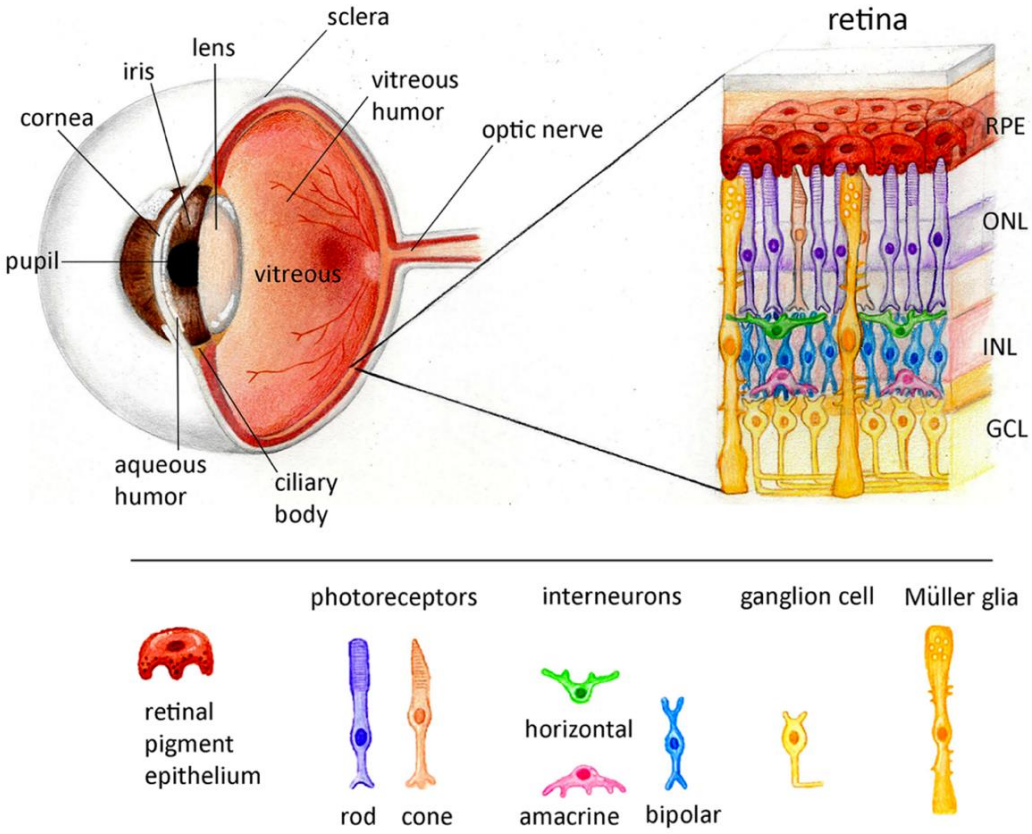

Figure 1: Schematic representation of the eye and retina of humans and primates.

The eye is anatomically divided in three layers. The external layer of the eye consists of the cornea, and sclera. The intermediate layer includes-at the anterior-the iris and ciliary body and in the posterior the choroid (not shown here). The internal layer is comprised by the retina. The space is filled with fluid called the aqueous humor, at the anterior chamber, or vitreous humor between the lens and the retina. The retina is divided in two compartments: one non-neuronal, the retina pigment epithelium (RPE) and one neuronal, the neuroretina. The vertebrate neuroretina is laminated in three layers of nerve cell bodies and two layers of synapses. The outer nuclear layer (ONL) consists of the somata of the rods and cones, the inner nuclear layer (INL) consists of the cell bodies of the bipolar, horizontal and amacrine interneurons and the ganglion cell layer (GCL) contains cell bodies of ganglion cells and some displaced amacrine cells. The axons of the ganglion cells are forming the optic nerve interconnecting the retina with the brain. Figure reproduced with permission from Aikaterini A. Kalargyrou et. al, Front. Mol. Neuroscience. 15:1042469, 2023.

Rod photoreceptors are notably more abundant in the retina, except in the fovea - a region exclusively dedicated to cones in the primate retina. These rods express the photopigment rhodopsin and play a crucial role in facilitating vision under low or dim light conditions, making them particularly vital for night

vision (scotopic vision). Notably, rods are sensitive solely to the intensity of light and lack the ability to perceive its wavelength, resulting in the representation of images exclusively in monochromatic vision. Conversely, cone photoreceptors operate on a similar principle, but the presence of multiple cone types allows for the comparison of wavelengths. This capability enables the cone system to distinguish between different wavelengths and perceive colour. While cones are fewer in number in the retina, their spacing in the central macula is very dense. The macula, rich in cone photoreceptors, includes at its centre the fovea a region exclusively composed by cone photoreceptors in primates. Human cones express one of three different photopigments - blue, green, or red opsin - reflecting their maximal absorption of short, medium, and long wavelengths, respectively. This unique feature equips cones to mediate colour vision and high-acuity spatial vision under daylight conditions (photopic vision). Although scotopic and photopic visual signals initially follow separate neuronal pathways, they eventually converge in the visual processing pathway.

In the outer plexiform layer, photoreceptor synaptic terminals contact with bipolar cells, which are responsible for transmitting the visual signal received onwards to the inner retina. The dendrites of rod bipolar cells are highly branched, and receive input from as many as 120 rods, conferring high sensitivity but low spatial acuity. In contrast, cones are responsible for higher-acuity vision, compared with rods, and cone bipolar cells transmit signals from just a few cones and drive ganglion cells. In addition to synapsing with bipolar cells at the plexiform layer, photoreceptors also synapse with horizontal cells known to provide negative feedback to photoreceptors via lateral inhibition, modulating multiple photoreceptor input to bipolar cells and controlling bipolar activation. These properties contribute to background light adaptation, making it possible to analyse on low-contrast details in a visual scene. Similarly, the input from bipolar cells to ganglion cells undergoes modulation by amacrine cells, a diverse group primarily consisting of inhibitory interneurons. One of the defining features of amacrine cells is their remarkable diversity in terms of morphology and function. Different subtypes of amacrine cells contribute to specific aspects of visual processing. Some are dedicated to lateral inhibition,

enhancing contrast and sharpening edges in visual stimuli. Others participate in temporal processing, influencing the timing of signals transmitted through the retina. The variety of amacrine cell functions underscores their significance in orchestrating the complex symphony of retinal signal processing. Further amacrine cells exert a substantial influence on ganglion cells, the output neurons of the retina. Through intricate synaptic interactions, amacrine cells modulate the responses of ganglion cells to visual stimuli. This modulation extends beyond simple inhibition, contributing to the extraction of features such as motion, direction, and colour from the visual scene.

The ganglion cell layer constitutes the output neurons of the retina, responsible for encoding visual information through the rate and timing of action potentials. These action potentials travel along the axons of ganglion cells over long distances, reaching higher visual centers in the brain. As a critical component of the vertebrate visual system, retinal ganglion cells play a pivotal role in transmitting visual information from photoreceptors to various visual processing centers in the brain. Their physiological and morphological diversity enables the processing of various aspects of visual information.

Morphologically, retinal ganglion cells can be classified into different types, such as ON (sustained) and OFF (transient) types, responding to changes in light intensity. Functionally, they can be categorized based on their receptive field properties, including center-surround organization and the presence of colour opponent receptive fields. Some retinal ganglion cells are specialized for processing specific visual features like motion, direction, or spatial frequency. In the visual pathway, retinal ganglion cells play a crucial role in transmitting visual information to the brain, where it undergoes further processing and interpretation.

Each ganglion cell receives input from a specific region of the visual field known as its receptive field, determining the type of visual information it encodes. These cells integrate and transform signals from photoreceptors and retinal interneurons, adjusting their output based on visual stimulus properties. Different types of retinal ganglion cells project to different visual centers in the

brain, each contributing uniquely to various aspects of visual perception, thus encoding specific types of visual information.

In primates, the axons of retinal ganglion cells form the optic nerve, carrying retinal output to central brain structures involved in visual processing. At the optic chiasm, 60% of the axon fibers cross, while the remaining 40% continue along the optic tract towards the diencephalon and midbrain. This partial crossing allows information from both retinas to be processed by the same cortical site in each hemisphere(Celesia and DeMarco, 1994; Hejtmancik and Nickerson, 2015).

As illustrated in **Figure 2** - figure reproduced with permission from Solomon and Lennie, Nature Reviews Neuroscience 8(4): 276-86, 2007 - a notable observation in primates is that the predominant destination for the axons of the vast majority of retinal ganglion cells in the optic tract is the diencephalon. Specifically, these axons terminate in the dorsal lateral geniculate nucleus (dLGN) of the thalamus. In contrast, in rodents, a significant target for these axons is the superior colliculus (SC). The dLGN contains neurons that send their axons to the primary visual cortex, or striate cortex (V1), in the cerebral cortex. The retino-geniculo-cortical pathway is comprised to large extent (80%) of midget RGCs (Callaway, 2005); these cells have small cell bodies and dendritic trees that densely tile the IPL of the primate fovea, promoting high-acuity and colour vision (Sinha et al., 2017). In addition, parasol and small bistratified RGCs, together with about a dozen other RGC types (Field and Chichilnisky, 2007; Busse, 2018) also project to the dLGN, the first-order thalamic relay for vision. Further, in the retino-geniculo-cortical pathway, input from the contralateral half of the visual field is directed to the visual cortex in each hemisphere thus, different areas of the visual cortex process various aspects of visual information, such as form, colour or movement (Busse, 2018). Studies have shown that V1 is crucial for vision and plays a major role in conveying most of the information that is essential for the process of seeing (Hejtmancik and Nickerson, 2015).

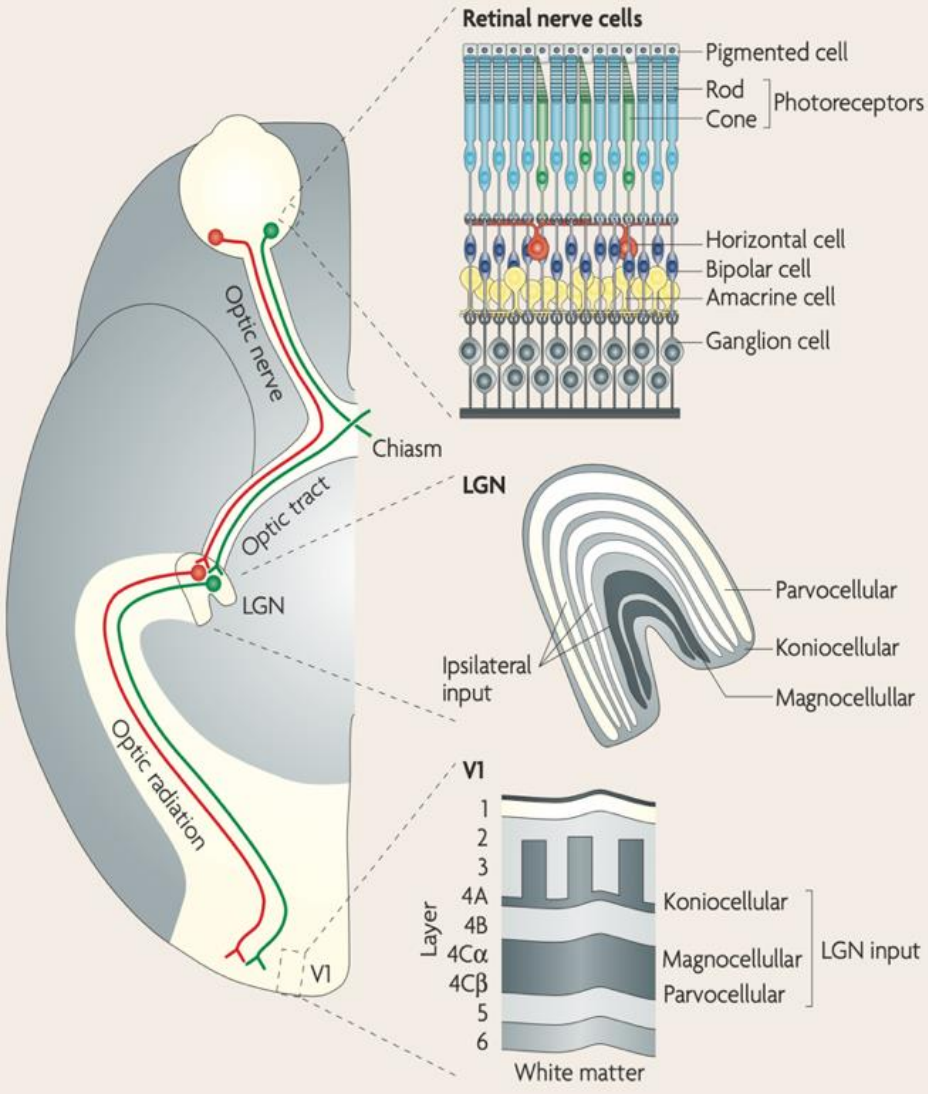

Figure 2: The visual pathway in primates.

The left panel shows a schematic drawing of the pathway from the retina to the primary visual cortex (V1) through the dorsal lateral geniculate nucleus (LGN) of the thalamus. The right panels highlight the important anatomical structures. Ganglion cells from the temporal retina project to the ipsilateral LGN (red lines) and those from the nasal retina project to the contralateral LGN (green lines). The axons of LGN neurons project almost exclusively to V1, where they terminate primarily in layer 4 and form ocular dominance columns. The termination site within layer 4 depends on the layer in which the LGN neuron is found: parvocellular (P) cells project mainly to layer 4Cβ, magnocellular (M) to layer 4Cα, and koniocellular (K) cells to layer 4A and lower layer 3. The shading depicts the distinct pattern that emerges when slices through V1 are stained for cytochrome oxidase activity. Reactivity is particularly high in layer 4 and in patches that dot the superficial layers 2 and 3. Figure reproduced with permission from Solomon and Lennie, Nature Reviews Neuroscience 8(4): 276-86, 2007.

The pretectum, a region between the thalamus and midbrain, is also a major target of the RGCs axons in the optic tract. This structure is important for coordinating the diameter of the pupil in response to the amount of light received by the retina, also known as the pupillary light reflex. The pupillary reflex has been successfully used as a diagnostic tool to test the visual sensory apparatus and the central pathways that mediate this reflex (Hall and Chilcott, 2018).

RGCs have several other retino-recipient targets including amongst others the suprachiasmatic nucleus of the hypothalamus, which is important for establishing the circadian rhythm, and the superior colliculus (SC), which is important in coordinating head and eye movements to visual targets (Busse, 2018).

Retinal ganglion cells perform a range of computational operations to extract and encode visual information. They integrate and transform signals received from photoreceptors and retinal interneurons, modulating their output based on the visual stimulus properties. RGCs exhibit receptive field properties that enhance the detection of edges, boundaries, and specific features in the visual scene. Additionally, they exhibit various spatiotemporal response properties, allowing for the detection of motion, direction, and other visual stimuli. It is the diversity of RGCs types and their target that supports the processing of the complex and multiple types of visual information required to perform all the different functions of visual perception: high acuity, colour, motion, as well as modulating circadian rhythms, pupil size, and the movement of head and eye towards or away from visual stimulus.

1.2. Phototransduction

As part of the central nervous system the retina exhibits complex neuronal circuitry. However, photoreceptors do not exhibit action potential as most sensory cells do, instead light activation generates a graded change in membrane potential and consequently a change in the rate of glutamate

transmitter release onto post-synaptic bipolar and horizontal cells. Transmitter release from the synaptic terminals of the photoreceptors is voltage-sensitive to calcium (Ca^{2+}) channels present in the terminal's membrane. The activation of the photoreceptors, either rods or cones, by light causes membrane hyperpolarization. Hence, in the dark photoreceptor's cells are in a depolarized state with high numbers of open Ca^{2+} channels and consequently with a high rate of transmitter release into post-synaptic neurons. As illumination intensity increases the photoreceptors cells hyperpolarize, the membrane potential becomes more negative (more polarised), leading to a reduction in opened Ca^{2+} channels and subsequently a decrease in transmitter release.

Under dark conditions sodium (Na^{+}) and Ca^{2+} flow into the outer segment through the membrane channels gated by nucleotide cyclic guanosine monophosphate (cGMP). This inward current of cations is opposed by an outward current mediated by potassium (K^{+}) selective channels in the inner segment. Absorption of light leads to a decrease in cGMP concentration in the outer segment leading to a closure of cGMP-gated channels and consequently a reduction in the inward flow of Na^{+} and Ca^{2+} leading to the cell becoming depolarised. As cGMP concentration decreases, cGMP-gated channels will close, preventing depolarization induced by the influx of Na^{+} and Ca^{2+} (Pahlberg and Sampath, 2011).

When a photon of light is absorbed by the photopigments present in the photoreceptor's outer segment disks, a series of biochemical changes occurs leading to the decrease of cGMP levels. Photopigments contain the light absorbing chromophore, retinal, coupled with one of several potential opsins that depends on the particular type of photoreceptor. As described above these different opsins determine the spectrum of light absorption, allowing the functional and unique specialization of rods and cones photoreceptors. Rhodopsin, the opsin present in rods, is perhaps the most well characterised photopigment and has been of extreme importance to shine light on the molecular events that occur during phototransduction. Rhodopsin is composed by two parts: an opsin molecule linked to a chromophore, 11-cis-retinal (Athanasiou et al., 2018). When light activates rhodopsin,

phototransduction occurs, its configuration changes from 11-cis isoform to all trans retinal leading to several changes in the opsin component of the molecule. The changes in opsin lead to the exchange of GDP for GTP on the G-protein consequently activating an intra cellular messenger, transducin, which activates cGMP hydrolysis through a cGMP phosphodiesterase complex (Pahlberg and Sampath, 2011). As cGMP concentration decreases on the disk membrane of the outer segments, cGMP-gated channels will close, preventing depolarization induced by the influx of Na^+ and Ca^{2+}. Activated rhodopsin is rapidly phosphorylated by its kinase, which allows the protein arrestin to bind to rhodopsin. This binding blocks the activation of transducin and consequently prevents the initiation of the phototransduction cascade.

The restoration of retinal to a form capable of photon capture is a crucial step in the visual pathway as it maintains the light sensitivity of the photoreceptors. This complex process is known as the retinoid cycle. All-trans-retinal dissociates from opsin and diffuses into the outer segments cytosol where is converted to all-trans-retinol and transported to the pigmented epithelium. It is within the pigmented epithelium layer that appropriated enzymes convert all-trans-retinal to 11-cis retinal, that is then transported back to the outer segment via the same chaperon protein interphotoreceptor retinoid-binding protein (IRBP). While comprehensive description of phototransduction it is not this study focus, **Figure 3** offers a concise overview of the molecular events occurring following the stimulation of rhodopsin by a single photon.

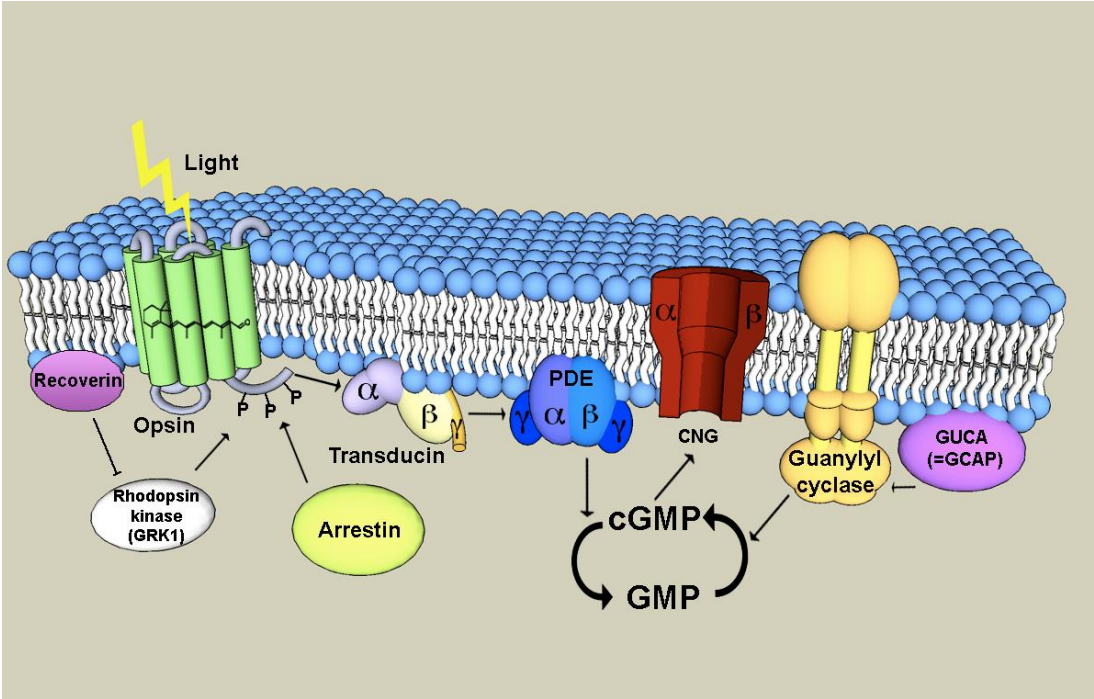

Figure 3: Schematic illustration depicting the phototransduction cascade in a vertebrate rod and cone photoreceptor cell.

Upon photon absorption, opsin molecules are activated and 11-cis-retinal within the opsin undergoes conversion to all-trans-retinal. This activation triggers transducin, a G protein comprising three subunits (α, β, and γ). Subsequently, transducin activates phosphodiesterase 6 (PDE), forming a dimer with α and β (or two α subunits), inhibited by two γ subunits. Active PDE catalyzes the hydrolysis of cyclic GMP into GMP, leading the cyclic nucleotide ion channel (CNG, a tetramer with α and β subunits) to close. Guanylyl cyclase (GC), regulated by a GC-activating protein (GUCA or GCAP), generates new cGMP. Finally, rhodopsin kinase (GRK) deactivates the opsin via phosphorylation, regulated by recoverin. Arrestin binds to the phosphorylated opsin and inhibits its signalling to transducin. Figure reproduced with permission from Larhammar, D., Nordström, K. and Larsson, T. A., Philosophical Transactions of the Royal Society B: Biological Sciences.10:1098, 2009.

The magnitude of phototransduction is dependent of the prevailing of illumination, a phenomenon known as light adaptation. As levels of illumination increase the sensitivity of the receptor is reduced. This decrease in sensitivity prevents the saturation of photoreceptor cells and greatly extends the range of light intensity over which they are operational. The concentration of Ca^{2+} in the outer segments is crucial for this light modulation of photoreceptor sensitivity. As described above, the closure of cGMP-gated channels upon light activation leads to a decrease in net concentration of Ca^{2+}. This decrease promotes important changes that tend to reduce the sensitivity of the receptor

such as increase in the activity of several kinases, guanylate cyclase enzyme (cGMP synthesis kinase) and rhodopsin kinase, that lead respectively to an increase of cGMP levels and of rhodopsin molecules that able to bind with arrestin. Further there is an increase affinity of the cGMP-gated channels for cGMP, reducing the impact of light induced reduction of cGMP levels. As described, low concentrations of internal Ca^{2+} at the photoreceptors outer segments membranes is one of the mechanisms crucial for light adaptation (Mannu, 2014; Armstrong and Cubbidge, 2019).

1.3. Comparison of rod and cone system

Within the retina, the rod and cone photoreceptor systems represent two distinct pathways for processing visual information. Understanding the characteristics and differences between these systems is crucial for unravelling the complexities of vision. The beautiful alignment of rods and cones can be visualised in vertical sections of retina prepared for light microscopy. Rods and cones can be distinguished rather easily due to individual characteristic shape, but also differ in the type of photopigment expressed, distribution across the retina and pattern of synaptic connections, giving them specialised and unique features for the different aspects that vision requires. Indeed, as described above, in primates the dynamics and organization of the rod system means it is specialized for light sensitivity at the expense of resolution, whereas the cone system has a very high spatial resolution at expense of sensitivity (Hejtmancik and Nickerson, 2015).

Under dark conditions, only rods are activated, and rod-mediated vision is known as scotopic vision. As illumination level increases the contribution of cone system becomes larger, and at light levels close to what is observed at twilight, both rods and cone contribute for mesopic vision. Rod contribution is impaired as their response to light saturates, leading to no change in their membrane potential as a function of illumination (as all the membrane channels are closed). Beyond this point, in normal indoor lighting or sunlight, the cone system is crucial for determining what is seen and vision supported by cone function is defined as photopic vision.

The capability of the two types of photoreceptors to respond to different ranges of light intensity relies on differences in their transduction mechanisms. Rods can produce reliable responses to a single photon of light whereas more than a hundred photons are needed to produce a comparable response in a cone. Further, rods saturate as light intensity increases but individual cones do not saturate at high levels of light illumination. It is important to highlight that both types of receptors have an adaption mechanism that allows them to operate over a range of luminance values, although the cone mechanism for light adaptation is thought to be more effective. This difference in adaptation mechanism is clearly observed in the slower recovery of response of rods to a bright light flash (about 200 milliseconds), whereas the cone response recovery is four times faster (Clark et al., 2013; Howlett et al., 2017).

The organization of circuits transmitting information from rods and cones to retinal ganglion cells plays a pivotal role in shaping the distinctive features of scotopic and photopic vision. In most regions of the retina, signals from rods and cones converge onto the same ganglion cells, meaning that individual ganglion cells respond to both rod and cone inputs depending on the light level.

Despite this convergence, the initial stages of the pathways connecting rods and cones to ganglion cells operate independently. Depending on the level of illumination, ganglion cells respond to both type of receptors, although the pathway from rods involves a specific class of rod bipolar cells known as rod bipolar. Unlike cone bipolar cells, these rod bipolar cells do not directly connect with retinal ganglion cells. Instead, rod bipolar cells establish synapses with the dendritic processes of amacrine cells that form gap junctions and chemical synapses with the terminals of cone bipolar cells. These bipolar cells in turn make synaptic contacts on the dendrites of ganglion cells in the inner plexiform layer. Each rod bipolar cell is contacted by several rods, and many rods bipolar cells in turn contact a given amacrine cell. This convergence allows the rod system to be much more capable of detecting light, as small signals from many rods are pooled together to generate a larger response in bipolar cells. Consequently, convergence comes at the expense of spatial resolution, since the source of a response in a rod bipolar cell can arise from a relatively large

area of the retina surface diminishing the ability to precisely pinpoint the location of a visual stimulus.

A significant distinction lies in the degree of convergence between the rod and cone systems, a factor contributing significantly to their unique properties. The cone system exhibits far less convergence. In central vision-dominating retinal ganglion cells, known as midget ganglion cells, each receives input from only one cone bipolar cell, which is, in turn, connected to a single cone. This lack of convergence enhances the precision of the cone system, allowing for a one-to-one relationship that is crucial for spatial resolution and maximize acuity (Masland, 2012; Lucas et al., 2012; Howlett et al., 2017).

It is important to highlight that the distribution of rods and cones across the retina is crucial for vision. The density of rods is much greater than of cones throughout most of the retina, even though perception in typical daytime light levels is dominated by cone-mediated vision. It has been estimated that the healthy human retina has approximately 90 million rod photoreceptors and 4.5 million of cones. The density of rods is greater than of cones apart from the fovea, a highly specialized region in the centre of the macula. In this circular region that measures approximately 1.2 millimetres in diameter, the cone density increases almost 200-fold, and there is a sharp decline in the intensity of rods present in this area - in fact the most centre portion of the fovea is rod free. This high density of cones in the fovea and their one-to-one relationship with bipolar and retinal ganglion cells, provides the cone system with the capacity to mediate the highest levels of visual acuity. With distance away from the fovea (eccentricity), the cone density declines, accompanied by an increase in convergence onto retinal ganglion cells, and acuity is reduced.

1.4. Central visual pathways

The process of visual perception is a complex orchestration involving intricate neural circuits that transmit and process visual information from the eyes to the brain. These pathways, known as visual streams, not only shape

our understanding of the visual world but also play a crucial role in regulating behaviours linked to the day-night cycle and adjusting pupil size.

Once visual information reaches the brain, it follows specific pathways to different visual centers for further processing. Key structures involved in these pathways include the lateral geniculate nucleus (LGN) in the thalamus and the superior colliculus. The Lateral Geniculate Nucleus serves as a relay station for visual information on its way to the primary visual cortex (V1). It consists of distinct layers dedicated to processing different aspects of visual stimuli, such as spatial resolution and contrast sensitivity. In humans, the LGN plays a critical role in processing colour vision, whereas in rodents, its function may be more focused on contrast sensitivity and motion detection.

The superior colliculus is involved in orienting responses, sensorimotor transformations, and visual-motor coordination. In rodents, the SC receives direct input from retinal ganglion cells and plays a significant role in visuomotor behaviours and defensive responses. Its involvement in processing looming visual stimuli highlights its importance in detecting and responding to potential threats in the environment.

After initial processing in subcortical structures such as the LGN and SC, visual information is transmitted to the primary visual cortex (V1) and higher-order visual areas in the occipital, parietal, and temporal lobes. These cortical regions further analyse and integrate visual signals, allowing for complex visual perception, object recognition, and spatial awareness.

The occipital lobe is one of the visual processing areas of the cerebral cortex. It is associated with visuospatial processing, distance and depth perception, colour determination, object and face recognition, and memory formation. The primary visual cortex surrounds the calcarine sulcus on the occipital lobe and receives the visual information from the retina via the thalamus. Surrounding the primary cortex is the secondary visual cortex, which receives information from it. Although still a topic of controversy, the primary visual cortex transmits information through two pathways: the dorsal and ventral stream. The dorsal stream is associated with object location and

motion and carries visual information to the parietal lobe. While the ventral stream has associations with object recognition and transmits visual information to the temporal lobe (Field and Chichilnisky, 2007; Hejtmancik and Nickerson, 2015; Busse, 2018; Armstrong and Cubbidge, 2019).

The primary visual pathway consisting of retina, optic nerves, optic chiasm, optic tracts, lateral geniculate nucleus, optic radiations, and visual cortices is by far the most studied and thought to be the most important component of the conscious (perceptual) visual system (Field and Chichilnisky, 2007; Hejtmancik and Nickerson, 2015; Busse, 2018). Within this pathway different classes of neurons encode a variety of visual information, luminance, spectral differences, contour orientation, and motion that enables the perception of the visual scene. The parallel processing of different categories of visual information continues in cortical pathways that extend beyond primary visual cortex, supplying visual areas in the occipital, parietal and temporal lobes.

The diverse functions supported by the visual pathway could be attributed to the diverse targeting of ganglion cells. Ganglion cells axons that exit the retina trough the optic disk, double together forming the optic nerve which carry the retinal output to central brain structures involved in visual processing. At the optic chiasm, some axon fibres cross, allowing both eyes' information to be processed by the same cortical site in each hemisphere (Celesia and DeMarco, 1994; Hejtmancik and Nickerson, 2015). The retinogeniculostriate pathway relays information to the thalamus's dorsal geniculate nucleus, then to the primary visual cortex, crucial for perceiving visual information.

Another target for ganglion cells is the pretectum, a region between the thalamus and midbrain, essential for coordinating pupillary light reflex, adjusting pupil size based on light exposure. Additionally, ganglion cells target structures like the suprachiasmatic nucleus, involved in circadian rhythm regulation, and the superior colliculus, essential for coordinating head and eye movements towards visual targets.

The diverse functions supported by the visual pathway result from ganglion cells' diverse targeting. Specific ganglion cell types of projects to different brain regions, mediating various aspects of visual perception, such as acuity, colour, motion, and luminance changes. The retina's diverse ganglion cell types, including those expressing melanopsin, contribute to this diversity. These cells have distinct light-sensitive properties, allowing them to modulate their response to light levels independently of rod and cone signals (Barnard et al., 2004; Lucas et al., 2012; Kim et al., 2021).

1.5. Comparison of rodent and human visual system

A natural environment is an ever-changing sensory landscape. Sensory systems adapt to these changes, increasing an animal's ability to extract important information and survive under a wide range of conditions. Rodents, and in particular mice, are the dominant model for understanding of the normal and abnormal structure, function, and development of the visual system, due to their small size, relatively low maintenance costs and the genetic tractability to model diseases and genetic conditions observed in humans. The visual systems of rodents and humans, while sharing fundamental principles, exhibit notable differences in their anatomical structures and functional features. This section explores the potential distinctions in types and functions of retinal elements and investigates similarities and differences in some central targets, emphasizing regions like the Suprachiasmatic nucleus and the pretectum, while contrasting the Lateral Geniculate Nucleus (LGN) and Superior Colliculus (SC).

Rodents and humans share the basic architecture of the retina, featuring photoreceptors (rods and cones), bipolar cells, horizontal cells, amacrine cells, and ganglion cells. However, the ratio and distribution of these elements may vary, influencing visual capabilities. Rodents, being crepuscular or nocturnal, often possess a higher density of rod photoreceptors, specialized for low-light conditions, whereas humans, adapted to diurnal vision, have a greater concentration of cone photoreceptors for daylight vision and colour

discrimination. The rodent retina is rod-dominant and lacks the foveal specialization of primates, resulting in poor visual acuity (Prusky et al., 2000; Van Hooser, 2007). In addition, and in contrast to primates, mouse cone photoreceptors only express two types of opsins, blue and green, and both opsins can be co-expressed in the same photoreceptor, although most cones show an increased sensitivity for one or other wavelength.

In terms of visual system circuitry, both rodents and humans exhibit a suprachiasmatic nucleus in the hypothalamus, crucial for circadian rhythm regulation. This nucleus receives input from retinal ganglion cells expressing melanopsin, responding to light levels and aiding in the synchronization of the internal biological clock. Further, both species rely on a region positioned between the thalamus and midbrain, the pretectum, for adapting to changes in ambient light conditions. The pretectum plays a role in the pupillary light reflex as it coordinates adjustments in pupil size based on light exposure.

However, differences arise in targets like the lateral geniculate nucleus (LGN) and superior colliculus (SC). Humans have a complex, six-layered LGN dedicated to visual information processing, whereas rodents have a simpler, two-layered LGN, reflecting variations in visual processing complexity. Similarly, the SC, vital for coordinating eye and head movements, plays a more substantial role in visuomotor functions in rodents compared to humans, where cortical processing may dominate.

In the rodent brain, the superior colliculus is a retinal recipient structure involved in visual information processing, sensorimotor transformation, and cognitive functions. In addition to mediating orienting responses, the rodent superior colliculus strongly contributes to triggering defensive behaviours. Notably, early seminal studies of the superior colliculus indicated that distinct defensive behavioural patterns can be triggered by stimulation at different sites in the superior colliculus (Ellis et al., 2016; Huang et al., 2017; Shang et al., 2018). These studies were followed by the identification of looming-sensitive cells in specific layers of the superior colliculus. These behavioural and physiological data suggest that, among the

intermingled diverse cell types in the superior colliculus a subset of neurons may detect looming visual stimuli and participate in the generation of dimorphic defensive behaviours (Shang et al., 2018).

The target of the vast majority of mouse RGCs (at least 85%) is the superior colliculus (Ellis et al. 2016), thought to be involved in visual-motor guidance behaviours. It is estimated that in rodents the proportion of dLGN-projecting RGCs vary between 25%-50%. Interestingly, of these dLGN-projecting RGCs more than 80% send a collateral axon to the SC (Seabrook et al., 2017; Busse, 2018). The numerical dominance of the projection to the superior layers of the SC in mice suggests the important role that the SC has in mouse vision. In addition, as for primates, mouse RGCs are also very diverse and target many areas in the brain.

Further, functional considerations further highlight disparities in visual adaptations. Rodent vision prioritizes motion detection and low-light sensitivity, suiting their nocturnal lifestyle, while human vision emphasizes colour discrimination, high acuity, and intricate visual processing.

Despite the notable differences between rodent and human visual systems, the striking similarities, particularly in the early stages of visual processing, enable us to investigate the pathways and circuitry underlying the mouse visual system. By leveraging these similarities, researchers can glean valuable insights into the mechanisms of human vision. Furthermore, the advantages provided by mouse models, such as their genetic tractability, cost-effectiveness, ease of experimental manipulation, and potential for translational research, establish them as indispensable tools for advancing our comprehension of vision. These attributes make rodents an indispensable tool for advancing our understanding of vision and developing novel treatments for vision-related conditions.

1.6. Retinal degeneration

Vision is perhaps the sense that humans rely on most to gain information about the environment that surrounds us, allowing us to navigate the world, make decisions, and perform complex tasks. For this reason, vision loss is therefore debilitating and imposes significant costs on public funds, private expenditure, and health. Most of vision loss has been associated with age, injury, or disease, where the death of the photoreceptor cells or their support cells in the mammalian retina leads to impairment of visual function. Most commonly, patients display rod degeneration, where rod photoreceptors are the primary cell affected, cone degeneration, where cone's function is disturbed, or a mixed rod/cone degeneration where both photoreceptor types are affected. The progressive loss of light sensitive photoreceptors cells, retinal degeneration, in all these disorders lead to irreversible sight-loss (Auricchio et al., 2017; Aghaizu et al., 2017; Kalargyrou et al., 2023).

Alongside cell loss, the retina undergoes neuronal rewiring and reprograming, including changes in gene expression and metabolic rate of some cells as well as migration of neurons across the retina. It is important to highlight that despite the loss of neurons in the outer nuclear layer, the inner nuclear layer and ganglion cell layers remain intact for several years, opening avenues for possible optogenetic therapeutic approaches to restore vision.

The diversity of the molecular and environmental factors that lead to retinal degeneration alongside with the incapability of regeneration makes the treatment of retinal diseases very challenging. Understanding the mechanisms underlying these pathologies would be crucial for the develop of novel therapeutic approaches for the treatment of neural degeneration not only in the retina but more broadly in the central nervous system (Aghaizu et al., 2017; Auricchio et al., 2017).

The most frequent form of inherited retinal disorders is known as inherited retinal dystrophies and affects 1 in 3000 people in Europe and in the United States. This genetically and phenotypically heterogenous group, comprises of

diseases that leads to vision loss associated with mutations in more than 100 genes. Although the molecular mechanism underlying many of these disorders remain unclear, this group of retinal dystrophies have been crucial to impulse the development of new therapeutic approaches as pharmacological inhibitors, gene therapy and cell replacement therapies.

1.7. Mouse models to study retina dystrophies

Mouse models have been pivotal in advancing our understanding of retinal dystrophies and in the study for potential therapies. These models, ranging from naturally occurring mutants to genetically engineered counterparts, provide valuable insights into disease mechanisms. Highlighted below are several pertinent models utilized in this research domain.

The rod α-transducin knockout mouse, Gnat1$^{-/-}$, represents stationary night blindness, characterised by a non-progressive impairment in rod phototransduction (Calvert and Brammer, 2000; Calvert et al., 2006). While exhibiting gradual retinal changes beginning around 4 weeks old, significant alterations become evident around 13 weeks of age where the rod outer segments length is slightly shortened and outer nuclear layer thickness is reduced by ~10% (Calvert and Brammer, 2000; Calvert et al., 2006; Barber et al., 2013).

The CNGA3$^{-/-}$ mouse (herein referred to as “CNGA”) serves as a model for achromatopsia, a rare disorder characterized by cone dysfunction and severe colour vision deficiency (Wissinger et al., 2001; Pang et al., 2012; Wang et al., 2021). This disorder is associated with mutations in genes responsible for components of the cone phototransduction cascade where CNGA3 and CNGB3 mutations account for approximately 80% of all achromatopsia cases, with varying prevalence among different populations. Missense mutations in the CNGA3 gene are associated with significant impairments in the photoreceptor cyclic nucleotide gated (CNG) channels,

situated on the photoreceptor outer segments that is crucial for phototransduction, contributing to the core deficiencies observed in achromatopsia(Michalakis et al., 2010; Wang et al., 2021).

The OGC mice is a triple knout model lacking genes crucial for rod, cone, and intrinsically photosensitive retinal ganglion cell (ipRGC) function. The targeted deletion of the genes encoding for Gnat1, cone cyclic nucleotide gated channel α3 subunit (Cnga3), and melanopsin (Opn4) is expected to completely abolish photoreception in the OGC triple-knockout mouse model (herein referred to as “OGC”), since rods, cones, and melanopsin-containing intrinsically photosensitive RGCs (ipRGCs) are understood to account for all photosensitivity in the mammalian retina (Hattar et al., 2003). However, researchers have demonstrated that despite lacking these essential components, OGC mice still display consistent some visual responses (Allen et al., 2010).

The PDE6β$^{rd1/rd1}$ mouse replicates autosomal recessive forms of retinitis pigmentosa (Keeler, 1924; Carter-Dawson et al., 1978; Chang et al., 2002), manifesting rapid photoreceptor degeneration attributed to a mutation affecting the expression of the β subunit of phosphodiesterase 6 (PDE6). In the PDE6β$^{rd1/rd1}$ mouse, rod degeneration begins as early as P10 with progressive loss of the ONL and all rods are lost by P25 (Bowes and Farber, 1987).

1.8. Approaches for treating retinal degeneration.

Huge efforts have been made to understand retinal degeneration and how to slow down disease progression. One approach that aims to preserve the remaining healthy cells, mostly photoreceptors, is gene therapy to correct the genetic mutations that leads to degeneration (Auricchio et al., 2017; Athanasiou et al., 2018). Although this strategy has shown some efficacy it has its limitations specially when retina degeneration is diagnosed at later stages of disease and a significant number of cells have been lost already. In

these scenarios optogenetic or cell replacement strategies may be an alternative and more proficient approach to account for the cell loss.

Retinal diseases that are caused by a known genetic mutation can be diagnosed and possibly treated with a gene therapy approach. This therapeutic manipulation at the genetic level is dependent on the type of mutation: loss-of function or abnormal gain-of-function and consequently the resulting encoded protein. Respectively, gene therapy aims to introduce a normal version of the missing or defective gene, silence the mutant gene, or provide a correct gene so that cells with corrected versions of the proteins affected will restore cell physiology and ultimately vision function.

The most used strategy to deliver the gene of interest to the eye relies in the use of viral particles, such as adeno-associated virus (AAV) or lentivirus. The use of viral vectors, specifically AAV, has shown to have serval advantages, as it's known non-pathogenic and its ability to efficiently infect and transduce photoreceptors and retinal pigmented epithelium cells mediating stable expression of the gene of interest for several years (Sundaram et al., 2012; Auricchio et al.,2017).

In 1996, Ali et al. (Ali et al., 1996) conducted a study involving the delivery of an AAV virus with the serotype 2/2 to the mouse retina through sub-retinal injection. This specific serotype demonstrated the ability to transduce both photoreceptors and retinal pigmented cells, reaching its peak transgene expression four weeks post sub-retinal delivery. While various studies have explored the transducing capabilities of different serotypes in the retina, AAV2/7 and 2/8 have exhibited superior efficiency and stable transduction of cells in the mammalian retina when compared to other serotype combinations (Auricchio et al., 2017). The identification of AAV2/7 and 2/8 as efficient and rapid transducers of murine photoreceptors had a significant impact on the development of therapies for severe inherited photoreceptor diseases.

In 2008, a pivotal breakthrough occurred during clinical trials involving patients with Leber Congenital Amaurosis (LCA), a severe retinal dystrophy resulting from mutations in the gene encoding retinal pigment epithelium

specific RPE65. This clinical trial marked the first instance of evidence showcasing the improvement of visual-guided mobility and minimal adverse effects following the sub-retinal delivery of AAV2/2 encoding RPE65 (Bainbridge et al., 2008). Despite sustained visual improvement over an extended period, individuals treated for LCA still exhibited a progressive, degenerative loss of photoreceptor cells (Cideciyan et al., 2013; Bainbridge et al., 2015).

Several clinical trials have targeted genes involved in autosomal recessive disorders, by supplementing the gene to produce a functional protein (Botto et al., 2022). Hundreds of genes have been implicated in inherited retinal dystrophies, meaning gene- or mutation-specific gene therapy approaches are currently impractical. Moreover, the small packing capacity (4.7kb) of AAV vectors makes it challenging for diseases caused by mutations within large genes. An interesting point to note is that indeed, once the light sensitive cells of the retina are lost, leading to remodelling and rewiring, the inner retinal neural circuitry from bipolar cells to retinal ganglion cells often remains intact. This preservation could open avenues for alternative gene therapy approaches, where the surviving non-light sensitive retinal cells could be targeted to produce light-sensitivity proteins. Such optogenetic strategies would enable other neuronal cells of the retina synaptic network to become photoreceptor-like. However, the sensitivity of currently available optogenetic tools is low, so further research to improve optogenetic tools is worth pursuing as it could bring major improvement to patients with advanced retinal degeneration (McClements et al., 2020; Botto et al., 2022).

In most of visually impaired patients, loss of vision is the consequence of the loss of photoreceptor cells, therefore one could hypothesise that the direct replacement of photoreceptors would be an interesting strategy to restore visual function in advanced degeneration. Indeed the idea of re-introducing cells back to the eye has been one strategy that has been pursued to help restore visual function in patients with retinal degeneration. Moreover, the discovery of pluripotent stem cells offered much hope that these cells could

be generated in high purity and specifically drive to replace the cell types lost to disease (West et al., 2020) .

The approaches briefly described here are the major avenues for treating inherited retinal dystrophies that are being pursued today. They all benefit from the deeper understanding of retinal dystrophy disease mechanism alongside with the emergence of efficient and safe delivery to the eye of viral vectors (in particular, the adeno-associated virus) or cell transplants showing some promises in restoring the vision circuitry that is affected in disease.

1.9. Tests of visual function in mouse

The mouse eye is at the forefront of the development of novel therapeutic approaches for the treatment of neural degeneration. The pre-clinical development of new treatments for retinal disease, such as gene and cell therapies, requires the ability to screen mouse models repeatedly and reliably for visual function before, during and after treatment. Often these methods are limited to electrophysiological recordings, such as electroretinograms (ERGs), which provide a useful measure of gross retinal function but tell us little about the quality of the visual information received by the rest of the brain. Similarly, commonly used behavioural assays of visual function, such as the pupillary light reflex, optokinetic and optomotor reflexes are thought to involve very specialised subcortical pathways that may not contribute to the visual processing required for higher order behaviours and perception (Abdeljalil et al., 2005; Hall and Chilcott, 2018). All the current methods that are thought to allow measurement of higher visual function rely on learning. As such, these typically involve stressful techniques of moderate severity rating (UK Home Office classification) including fear conditioning, food- and water-deprivation, water-mazes or similar. These techniques usually require lengthy training, which limits their use in progressively visually-impaired animals, and can be further impaired by inter-animal differences in learning abilities (Prusky et al., 2000). There is thus a significant need for new, non-invasive, repeatable, and reliable methods for behavioural measurements of visual sensitivity.

1.10. Avoidance behaviours

In prey species such as mice, avoidance of predators is key to survival and drives instinctual behaviours like freeze or flight (escape). Escape behaviour is a well-established and characterised behaviour that can be easily triggered by a rapidly expanding overhead stimulus mimicking the approach of a predator, such that rodents typically flee to an available refuge. Conversely, a small moving disk sweeping overhead stimulus is sufficient to induce freeze behaviour in mice (De Franceschi et al., 2016). These “Loom” and “Sweep” stimuli provide visual triggers for opposing escape and freeze behaviours, providing evidence that mice make behavioural choices based on vision alone.

These behaviours have gained interest and studies have aimed to elucidate the circuits underlying these opposing behaviours. There appears to be a substantial involvement of the primary visual cortex and higher thalamic nuclei, as well as spatial memory, indicating that these behaviours are not simple sub-conscious reflexes but instead may involve processing by higher image forming pathways and other forms of high level integration (Wei et al., 2015; Shang et al., 2018). Perhaps due to its anatomical connectivity and consequent behavioural diversity, the mouse superior colliculus has received much attention. In mice, most output neurons of the retina project to the SC and some SC neurons can respond to sweeping (Gale and Murphy, 2016) and looming stimuli (Zhao et al., 2014). Activating SC neurons can drive both freezing (Zingg et al., 2017) and flight behaviour (Evans et al., 2018). There is also evidence that two targets of the SC, the lateral posterior nucleus of the thalamus (LP) and the periaqueductal gray (PAG), may be important in these behaviours. Activation of SC terminals in the LP (Wei et al., 2015) and the PAG (Evans et al., 2018) can drive freezing and flight responses, respectively. In addition, inhibiting the terminals of SC neurons in the PAG reduces flight responses to a looming stimulus (Evans et al., 2018).

Recent studies have begun to address the involvement of the retina in innate avoidance behaviours, particularly in responses to looming threats. Two

populations of retinal ganglion cells (RGCs) have been identified as potential mediators of these behaviours: the OFF-transient alpha cells (Münch et al., 2009) and the bistratified RGCs (Huang et al., 2017). In addition to these findings, recent research has investigated how signals from RGCs are transmitted to the superior colliculus, a key brain region involved in processing visual information and coordinating behavioural responses. With studies also exploring the preferences exhibited by diverse superior colliculus neurons in response to various types of moving stimuli (Gale and Murphy, 2014; 2018; Reinhard et al., 2019). Furthermore, the altered responses to visual stimuli observed in genetically modified mice lacking specific types of RGCs (Lees et al., 2020) suggest that the processing of threatening visual stimuli may occur at the retinal level, rather than solely within higher brain structures.

Innate avoidance behaviours are thought to be crucial for mice survival, are rapidly induced and short lived. Therefore, it should be possible to repeat a visual stimulus multiple times in a single experimental session, increasing the behaviour data acquired per session per animal. It thus becomes crucial to understand if these behaviours could extinguish upon multiple presentation of visual stimuli, or if increasing session intensity would lead to habituation and decrease the reliability of this method to access visual function. Encouragingly, Storchi et al (2019) showed that innate behaviours responses triggered by visual stimuli, including a “full field flash” and a modified “loom” stimulus, could indeed be used to measure visual acuity in healthy animals and discriminate degrees of visual dysfunction in Rd1 mice, a model of severe retinal degeneration (Storchi et al., 2019).

This suggests that it may be possible to use innate avoidance behaviours in response to sweeping and looming visual stimuli to assess visual function in healthy and diseased mice. The overarching aim of this project is thus to exploit these behaviours to develop a high-sensitivity, repeatable behavioural measurement of functional vision in murine models of retinal dysfunction and recovery. Furthermore, it seeks to improve our understanding of the biological contributions of photosensitive cells towards these behaviours.

Research Aims and Objectives

This project aims to provide a comprehensive understanding of innate behaviours of mice in response to two visual stimuli, herein termed ‘Loom’ and ‘Sweep’. Further, it seeks to determine if it is possible to translate a visual stimulus-induced spontaneous behaviour into use as a low-severity test of vision to determine retinal (dys)function and treatment effect and to understand the biology underpinning these stereotyped behaviours. To address this, the project will:

Aim 1: Provide a standardized framework for measuring visual stimulus-induced escape and freeze responses in wild-type mice.

i) Optimal measurement regime. Male and female wildtype (*C57BL/6J*) mice will be presented with one of three different stimulus regimes (5 trials in one day, 5 trials per day for five days and 1 trial per day for five days). All mice will be re-tested 1 month later to determine if initial number or arrangement of trials predicts future habituation. Findings will inform the number of trials/animal used hereafter and about any potential differences related to sex.

ii) Cross-sectional study of age and strain. The response characteristics will be determined using naïve cohorts of *C57BL/6J* mice at either 21 days, 1, 2, 6, 12 and 15 months of age. A further cohort of *C57BL/6J* mice will be tested at all of the above time points to assess longitudinal changes within individuals. To understand if different mice strains respond in the same manner, Loom and Sweep responses will be examined in two further commonly used strains of wildtype mice with normal vision, *129/SV* and *DBA1/J*.

Aim 2: Determine contribution of different photosensitive cells to Escape and Freeze responses.

i) The contributions of rods, cones and photosensitive ganglion cells to the behaviours observed in response to looming and sweeping visual stimuli will be examined in mouse models lacking function in these cells. *Gnat1*$^{-/-}$ (a mouse model of stationary night blindness due to non-functional rods photoreceptors), *Cnga3*$^{-/-}$ (a mouse model for early-onset cone-specific degeneration) and OGC (triple-knockout mouse for *Gnat1*$^{-/-}$, *Cnga3*$^{-/-}$ and the melanopsin gene, *Opn4*$^{-/-}$) mice will be assessed under scotopic ('night vision') and photopic ('day vision') light conditions, along with *C57BL/6J* mice as wildtype controls. Animals will be tested following appropriate dark/light adaptation using the optimal protocol as determined in (1i).

Aim 3: Evaluation of visual stimulus-induced innate response as method of assessing changes in visual function resulting from retinal degeneration and after therapeutic rescue.

i) Responses to loom and sweep stimuli will be assessed in the PDE6β$^{rd1/rd1}$ mouse model of rapid photoreceptor degeneration. This model can be rescued by gene therapy (AAV2/8.RHO.PDE6β vectors) (Nishiguchi et al., 2015); therefore, cohorts of mice will receive 1.5 μl of double subretinal injections at post-natal day 10 and tested at 6 weeks post-treatment, compared to untreated controls. The Loom and Sweep responses will be compared with more traditionally used tests of retinal function, including electroretinogram recordings and optokinetic head tracking.

CHAPTER 2: Materials and Methods

All procedures were conducted in accordance with the UK Animals Scientific Procedures Act (1986). Experiments were performed at University College London or King's College London under personal and project licenses released by the Home Office following appropriate ethics review.

2.1. Murine animal models

All mice models used for this project were maintained on a standard 12/12-hour light dark cycle, housed in same sex groups or sustained breeding pairs wherever possible and provided with fresh bedding, nesting material, food, and water *ad libitum*. All measurements were made during the light phase of the cycle. In order to retain natural behaviours, all mice used in this study were kept under a minimal handling protocol and any handling was performed using transfer tubes.

To establish a standard framework for visual stimulus-induced escape and freeze responses, the impact of different testing regimes on the responses of wildtype mice aged 2 (±1) months was assessed. Wildtype mice (*C57BL/6J*) were purchased from Harlan, UK and brought into the animal facility at the age of 6-8 weeks and either used for procedures or breeding. Mice were randomly allocated to one of three designs: "Tonic" (x1 session per day for 5 days), "Burst" (x5 sessions in 1 day) or "Intense" (x5 sessions per day for 5 consecutive days) (**Figure 4 D**). All protocols were tested on female mice (with 6 animals assigned to each protocol), and "Tonic" and "Burst" protocol were additionally tested on male mice (6 animals in each protocol). All mice were re-tested within the same protocol one month later to determine impact of design on habituation.

As will be shown in Chapter 3, this first set of experiments yielded an 'Optimised' protocol design, which combined the "Tonic" and "Burst" protocols and by conducting x3 sessions per day for two consecutive days. Further, these experiments showed that male and female animals behaved similarly in response to these visually-induced innate behaviours. Hereafter, all

experiments were performed on male and female mice, regardless of sex, in accordance with availability of the required model and age.

To determine the effects of both age and cumulative repeated measurements, naïve cohorts of *C57BL/6J* mice at either 21 days, 1, 2, 6, 12 or 15 months of age were tested. An additional cohort was tested at each of the time points mentioned, to assess longitudinal changes within individuals and further account for habituation/extinction of these innate behaviours.

To assess potential differences in behaviour arising from different backgrounds, two additional commonly used strains of wildtype mice with normal vision, *129/SV* and *DBA1/J* (both purchased from Harlan and then bred in house), were subject to the optimised protocol at 2 ± 1 months of age, and re-tested one month later, to assess possible changes in habituation and/or behavioural extinction. A control group of *C57BL/6J* was used alongside. All mice were treated equally and received minimal handling to prevent taming and potential reductions in escape response.

To examine the relative contributions of photosensitive cells to Escape/Freeze responses, I tested cohorts of mice with specific genetic mutations: *Gnat1*$^{-/-}$ (on a mixed *129/SV* and *C57BL/6J* background), *Cnga3*$^{-/-}$ (also on a mixed *129/SV* and *C57BL/6J* background) and *Opn4*$^{-/-}$*; Gnat1*$^{-/-}$; *Cnga3*$^{-/-}$ *(*herein known as *OGC*) mice. The *OGC* mice likely have mixed *129/SV* and *C57BL/6J* although there's no information about this aspect on the original paper (Hattar et al., 2003). Alongside, I tested a control cohort of *C57BL/6J* mice. All mice were bred in house and were tested at 2 ± 1 months of age and under scotopic and photopic conditions, following appropriate dark/light adaptation.

To evaluate whether visual stimulus-induced innate response is an appropriate method of assessing visual function upon therapeutic rescue, a well characterized model of rapid photoreceptor degeneration was used. *PDE6β*$^{rd1/rd1}$ (on a *C3H/HeJ* background and bred in house) is an animal model for autosomal recessive forms of retinitis pigmentosa (Carter-Dawson et al., 1978). It is characterized by a rapid loss of photoreceptors (starting around

P10 and complete loss of all rods by P25) due to a mutation affecting the expression of the β subunit of phosphodiesterase 6 (PDE6), which can be rescued by AAV-mediated gene supplementation (Nishiguchi et al., 2015). A cohort of untreated RD1 mice served as controls in the study.

2.2. Assessment of visual function in mice

2.2.1. Innate behaviour environment and experimental design

The arena in which the behavioural tests were performed was a custom-built 45 cm wide × 40 cm deep × 33 cm high infrared acrylic box whose walls were coated with white card. At the base of one wall was a hole (5 cm x 8 cm) that gave access to a refuge, a small black plastic box (20 cm wide × 12 cm) (**Figure 4 A**). Visual stimuli were generated by a Dell Precision 3630 computer(Intel Core i5-8500, 6 Core, 9MB Cache, 3.0GHz, 4.1Ghz Turbo w/UHD Graphics 630), by the freely available software BonVision/Bonsai (Lopes et al., 2015; 2020) and projected via a GT760ST Projector (Optoma, UK) onto a rear projection sheet (75 cm × 65 cm) placed 30 cm above the floor of the arena. The sheet provided a constant illumination (mean luminance 30 to 40 candela/m^2) to the arena. Mouse movements were video recorded with a Blackfly S Mono camera (Clear View Imaging, UK) sampled by Bonsai at 60 Hz. The camera was fitted with a Kowa 3.5/F1.4 monofocal lens (Alrad Imaging, UK) and an infrared filter, and positioned above and to one side of the arena. To align video and visual stimulus, an infrared LED placed just outside the arena was briefly illuminated by a Leonardo Arduino MCU (RS Components, UK) under the control of the same computer that generated the visual stimuli.

The “Loom” stimulus was a 1 cm (thus a visual angle of diameter 2° when directly over the animal) black disk rapidly widening to 25.5 cm (50°) in 250 ms and remaining on the screen at this size for an additional 500 ms (**Figure 4 B Bottom**). The “Sweep” stimulus was a 2.5 cm (5°) black disk that appeared at one side of the monitor and then translated smoothly to the opposite side over 4 s (21 °/s) (**Figure 4 B Top**).

As illustrated in **Figure 4 C**, animals were allowed to habituate to the arena for 10 min; in subsequent sessions the habituation period was reduced to 5 min. After habituation, a maximum of 20 minutes was allowed to deliver a sequence of two Sweep and two Loom trials that were always presented in the same sequence: 1st Sweep → 1st Loom → 2nd Sweep → 2nd Loom, with at least one minute between the presentation of successive stimuli (**Figure 4 C**). Thus Habituation + 1st Sweep → 1st Loom → 2nd Sweep → 2nd Loom comprises a single "session". If it was not possible to present all four stimuli within the allocated time, mice were removed from the testing arena after the 20 minutes period; this is reflected in reduced and variable trial numbers for a given animal where applicable.

Presentation of the visual stimulus was triggered by the experimenter when the animal was approximately in the centre of the arena (observed via video). For "Sweep" stimuli, we predicted that the speed of the mouse would decrease on response to the stimuli, so it was important that the mice were moving when the stimulus was delivered. Therefore, for consistency, the presentation of the visual stimuli was preferentially triggered when the mice were moving at a moderate speed across the arena, and avoiding when animal were rearing, grooming or distracted, or running rapidly.

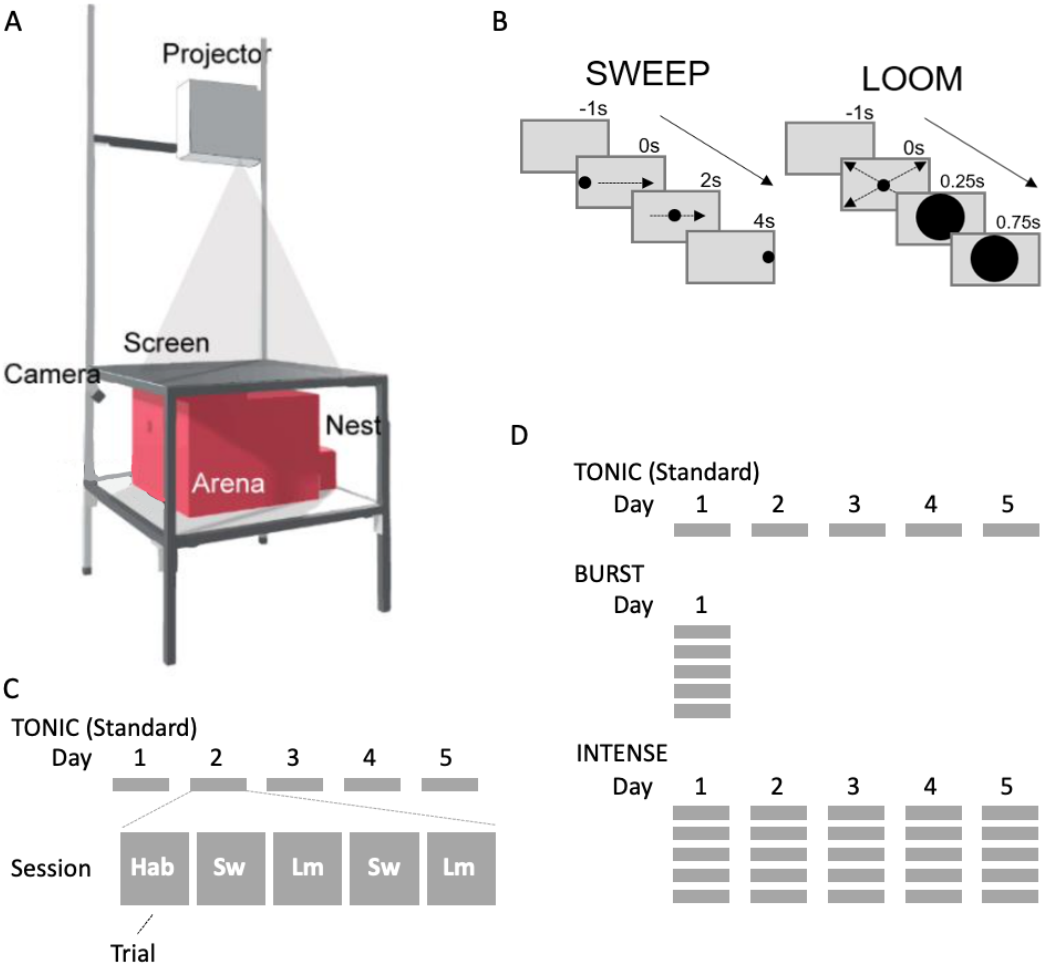

Figure 4: Experimental design for assessing visual stimulus-induced escape/freeze responses.

(A) Schematic representation of the behavior set up. (B) Stimuli Schematic Illustrations. Top: Sweep Stimuli. Bottom: Loom Stimuli. (C) Schematic workflow of a session. (D) Schematic representation of the three Protocol Designs tested.

Unless otherwise stated, all experiments were performed under photopic conditions (mean luminance 30 – 40 candela/m^2). Where scotopic conditions were required (Chapter 4), a neutral density filter was placed just below the projector. The filter was held by a made-to-measure black opaque plastic cylinder that could hold multiple disks of neutral density filter (Pro Centre Limited, UK) to reduce light intensity sufficient to maintain a constant scotopic illumination (mean luminance 0.1 candela/m^2) to the arena.

2.3. Innate behaviour analysis

Video recordings were acquired by the same Bonsai routine that presented the visual stimulus, and we used inbuilt Bonsai nodes (*BackgroundSubtraction, FindContours, BinaryRegionAnalysis*) to extract the position (centroid) of the animal in each frame. The angle and oblique orientation of the camera introduces projective distortions in the image, so we estimated this distortion by calculating the requisite polynomial transformation matrix from daily calibration images using the function *cp2tform* in MATLAB (version R2019a, Mathworks, NA). The inverse of this matrix was used to transform positional estimates from image space to arena space, using the function *tforminv*. We used the xy coordinates to find the animal's speed for each frame and paired this with the timing of each stimulus to calculate more accurate variables. When analysing the animal's response to stimuli, we concentrated on the xy coordinates and speed for each frame within 5 seconds after stimulus onset. We followed De Franceshi et al. (2016) and defined escape responses as a phase of movement following stimulus onset during which mouse speed was higher than 40 cm/s and the mouse returned to the nest within 5 s of the stimulus. Freezing behaviour was defined as periods of time during which the speed of movement decreased to less than 2.5 cm/s for at least 0.2 s after stimuli onset.

2.4. Electroretinography recordings

Electroretinography (ERG) is a commonly employed method for assessing the electrical activity of the eye in response to light stimuli. Typically, ERG recordings reveal two distinguishable waves known as the a-wave and b-wave. Although additional components can be discerned under various conditions, they were not the focus of the experiments discussed here (Einthoven and Jolly 1908). When light enters the eye, an initial negative deflection, termed the a-wave, is observed in the ERG. This is caused by the reduction of the dark current generated by photoreceptor cells due to the closure of cGMP-

gated ionic channels and subsequent hyperpolarization of the photoreceptors upon exposure to light. Following the a-wave, a positive deflection known as the b-wave appears. The b-wave primarily originates in post-synaptic retinal cells, notably Müller and on-bipolar cells. The hyperpolarization of photoreceptor cells reduces glutamate release, leading to the depolarization of post-synaptic cells. This increase in extracellular potassium ions generates an electrical current that depolarizes post-synaptic cells, resulting in a corneal-positive deflection (Gotch 1903; Einthoven and Jolly 1908).

For the experiments described on this thesis, ERG recordings were conducted on both eyes of treated and untreated mice following overnight dark adaptation. We employed standardized procedures using commercially available equipment (Celeris, Diagnosys LLC, Cambridge, UK) under dim red-light conditions. Mice were anesthetized via intraperitoneal injection (details provided in section 2.3) and their pupils were dilated with 2.5% phenylephrine and 1% tropicamide eye drops (Minims, Bausch and Lomb, Kingston-upon-Thames, UK). To maintain hydration and electrode contact, a water-based ocular lubricant (Viscotears, Novartis Pharmaceuticals UK Ltd, Camberley, UK) was applied to the eyes. ERG recordings from both eyes were obtained simultaneously. Midline reference and ground electrodes were carefully positioned subdermally at the center of the forehead and the base of the tail, respectively, for each animal. A thin layer of Viscotears was applied to the eyes followed by a corneal contact electrode. Before recording, we ensured symmetrical impedance (between 5 and 8 kOhm) and low background noise for both electrodes. Dark-adapted recordings were obtained at progressively increasing light intensities ranging from 0.001 to 30 candela.s/m^2, while light-adapted recordings were conducted at intensities from 0.1 to 50 candela.s/m^2. A light adaptation step of 5 minutes with a continuous light intensity of 30 candela/m^2 preceded the light-adapted recordings. Three sweeps were averaged for each intensity step, and the amplitudes of the a-wave and b-wave were analysed using Espion software (Diagnosys LLC, Cambridge, UK).

2.5. Optomotor assessment

The optomotor assessment is a behavioural test that relies on animals' natural optokinetic (eye movement) and optomotor (head movement) reflexes, which aid in stabilizing the image of a moving environment. These reflexes involve compensatory head movements triggered by global shifts in the visual scene during the animal's locomotion or position adjustments. Optomotor reflexes are easily observable, require no prior learning, and have proven valuable for quickly evaluating retinal function. Moreover, this response can be utilized to gauge contrast sensitivity and/or acuity (Thaung et al., 2002; Abdeljalil et al., 2005; Kretschmer et al., 2017).

In this study, contrast sensitivity of both treated and untreated mice was assessed using an OptoDrum system (developed and distributed by Striateck GmbH, Tübingen, Germany). Mice were subjected to rotating sinusoidal gratings, and their optomotor responses were measured. Typically, mice reflexively move their heads in the direction of grating rotation; the right and left eyes exhibit sensitivity to counterclockwise and clockwise rotations, respectively. For this research, contrast sensitivity was evaluated using specific stimulus components with spatial frequencies of 0.1, 0.2, and 0.4 cycles per degree (c/d). The contrast of the vertical rotating bars displayed on screens varied, ranging from black and white bars (100% contrast) to grayscale with decreasing contrast between the two gray bars. During testing, mice were positioned on a platform at the center of an arena surrounded by four screens displaying the stimulus. The experimenter configured the program and selected the direction of the bars, while the software automatically determined the direction in which the animal moved its head based on pre-programmed algorithms. Mice were randomly selected and tested twice daily (in clockwise and counterclockwise directions) over a period of three days. Between each mouse, the arena and platform were sanitized with 70% ethanol. All experiments were conducted under consistent light levels and overseen by the same investigator each time to minimize inter-operator variability.

Final contrast sensitivity values were calculated using the formula: 1 ÷ (Value Obtained given by Optomotor software ÷ 100).

2.6. Anaesthesia

For the gene therapy treatment of mice by subretinal injection and ERG recordings, mice were anaesthetized with a mixture of medetomidine hydrochloride (1 mg/mL, DormitorTM Pfizer Animal Health, Kent, UK), ketamine (100 mg/mL, Fort Dodge Animal Health, Southampton, UK) and dH20 in a ratio of 5:3:42. Anaesthesia was injected intraperitoneally (10 µl per g body weight) and the mouse placed in a pre-warmed anaesthesia chamber. Surgery was performed under aseptic conditions on a clean, covered heat mat to maintain body temperature. Local anaesthesia using topical 0.5% amethocaine drops (Minims, Bausch and Lomb Ltd, Kingston-upon- Thames, UK) was administered prior to subretinal injections, and topped up when necessary. Anaesthesia was reversed by intraperitoneal injection of an amount of AntiSedanTM (Pfizer Animal Health, Kent, UK) equal to the volume of anaesthesia used. Body temperature was maintained using a heat mat and mice were only returned to the cage when mobile and responsive. Pups undergoing anaesthesia were moved back into the maternal cage once moving around and closely monitored until fully recovered.

2.7. Subretinal injection

Under general anaesthesia, a drop of 1% tropicamide (Minims, Bausch and Lomb Ltd, Kingston-upon- Thames, UK) was applied to the eyes of the animals to dilate the pupils. Liberal application of Viscotears (Novartis Pharmaceuticals UK Ltd., Camberely, UK) prevented the eyes from dehydrating and kept the cornea clear for visualisation during surgery. Subretinal injections were performed under direct retinoscopy through an operating microscope (Zeiss). The tip of a 0.8 cm, 34-gauge hypodermic needle (Hamilton) was inserted tangentially through the sclera of the mouse eye, causing a self-sealing wound tunnel. The needle tip was brought into focus at the subretinal space, and the viral particles were injected. The needle

was then withdrawn under great care to support self-sealing of the injection wound. In some cases, animals received double injections of 1.5 µl rAAV each to produce bullous retinal detachments in the superior and inferior hemisphere around the injection sites.

2.8. Histology

Mice were euthanised by cervical dislocation. The eyes were dissected, removed from the eye socket and the cornea, iris, and lens were removed. All samples were fixed for 1h in 4% paraformaldehyde (PFA), cryopreserved overnight at 4ºC in 20% sucrose in phosphate buffered saline (PBS) and embedded in optimal cutting temperature medium (OCT, Tissue Tek Raymond Lamb, Eastbourne, UK). Embedded samples were immediately frozen in dry ice and stored at -20ºC. Retinal cryosections were cut in sagittal orientation at a thickness of 15 µm using a cryostat (Bright OTF 5000, Huntingdon, UK). Sections were collected on poly-lysine coated slides (Thermo Fisher Scientific, Loughborough, UK), air-dried, and stored at -20°C until used for immunohistochemistry experiments. To assess treatment efficacy, a straightforward staining protocol was employed to examine the DAPI (1:1000, Sigma-Aldrich), allowing visualization of photoreceptor nuclei. This facilitated observation to determine whether the treatment had effectively prevented retinal degeneration.

2.9. Virus production

The transgene construct, pD10/hRho-hPDE6β was kindly provided by Professor Alberto Auricchio (TIGEM Institute, Naples, Italy) and contains the human cDNA sequence of the PDE6β gene downstream of the short human rhodopsin promoter, as described previously (Nishiguchi et al. 2015). The plasmids were packaged into AAV8 to generate the recombinant AAV viral vectors AAV8.hRho.hPDE6β (Nishiguchi et al. 2015) as briefly summarized below. Recombinant AAV8 virus was produced through a triple transient

transfection method. The plasmid construct (pD10), AAV serotype-specific packaging plasmid and helper plasmid, in a ratio of 1:1:3 at 20 mg total DNA per ml of DMEM, were mixed with Polyethylenimine (Polysciences Inc.) to a final concentration of 50 mg/ml and incubated for 10 minutes at room temperature to form transfection complexes, which were added to 293 T cells at 50 mg DNA per 15-cm plate and left for 72h. The cells were collected, concentrated, and lysed by a three-time freeze–thaw process in PBS to release the vector. AAV8 was bound to an AVB Sepharose column (GE Healthcare) and eluted with 50 mM Glycine pH2.7 into 1 M Tris pH 8.8. Viral particle titres were determined by comparative PCR prepared from purified viral stocks and defined plasmid controls. The purified vector titres used for all experiments were $2x10^{12}$ viral particles per ml^{-1} as used previously (Nishiguchi et al. 2015).

2.10. Statistical analysis

Data analysis presents means ± standard deviation of the mean, unless stated otherwise. MATLAB R2019a was utilized for statistical analyses of behavior data derived from the Loom and Sweep behavior test. Statistical significance was determined using one-way ANOVA, followed by Tukey post hoc test for multiple comparisons, to identify significant differences among groups. For non-Gaussian distributions, non-parametric tests including the Wilcoxon rank-sum test or Kruskal–Wallis test were employed.

Pearson correlation analysis was conducted to calculate the coefficient (r) to compare the cumulative probability of response types between the initial and subsequent (re-testing 28 days later) testing events, with associated p-values determined using MATLAB R2019a.

Unpaired t-tests were utilized in Prism for optomotor and ERG analysis, performed using GraphPad Prism 5 (GraphPad Software, La Jolla, CA), comparing treated Rd1 mice to the untreated cohort.

The respective number of animals is described in individual figure legends and in each chapter of this thesis.

Statistical significance was considered for p-values < 0.05. P-values were categorized as follows: $p < 0.05$ = statistically significant (*), $p < 0.005$ = very significant (**), $p < 0.001$ = highly significant (***).

Glossary

For the purpose of clarifying project-specific terms used throughout this thesis, a list of definitions is provided:

Trial - the presentation of one visual stimulus.

Session - a session started with the placement of the mouse in the middle of the arena, followed by the habituation period and up to 20 minutes of time in which we attempted to deliver the pre-established sequence of visual stimuli. The session finished after this allocated time and the mouse was removed from the testing arena. Therefore, each session has a maximum duration of either 30 minutes (for the first session where the habitation time was of 10 minutes plus the fixed 20 minutes for stimuli delivery) or 25 minutes (for the remaining sessions where the habituation period is of 5 minutes plus the fixed 20 minutes for stimuli delivery). Depending on mouse behaviour throughout the session, the maximum number of stimulus presentations in a single session is four but may be less; this is reflected in the reduced and variable trial numbers for a given animal, where applicable.

Tonic protocol - each mouse allocated to this protocol designed is exposed to one session per day for five consecutive days. Therefore, a total number of 5 sessions will be recorded for each mouse under this experimental design.

Burst protocol - each mouse allocated to this protocol designed is exposed to five sessions in one day. Thus, a total number of 5 sessions will be recorded for each mouse under this experimental design.

Intense protocol - each mouse allocated to this protocol designed is exposed to five sessions per day for five consecutive days. Accordingly, a total number of 25 sessions would be recorded for each mouse under this experimental design.

Optimised protocol – the optimal distribution and organisation of sessions, following assessment of the tested “Tonic”, “Burst” and “Intense” protocols. In the optimised protocol, each mouse was exposed to three sessions per day for two consecutive days. Thus, a total of 6 sessions would be recorded for each mouse under this experimental design. Except for aim 1, where I specifically compare the protocols design and distribution and organisation of sessions, all subsequent experiments were performed under the optimised protocol.

“Escape” response - defined as when a mouse both i) exhibited speeds of movement higher than 40 cm/s, and ii) returned to the nest, within 5 seconds of stimuli onset.

“Freeze” response - defined as periods of time during which the speed of movement decreased to less than 2.5 cm/s for at least 0.2 s after stimuli onset.

“Freeze+Escape” response – defined as when a mouse exhibits a period of freezing behaviour followed by an escape response, according to the parameters stated above. This combination response behaviour has been observed previously (De Franceschi et al. 2016).

“Detection” response – mice may show more than one behaviour in response to the same type of single visual stimulus: mice can freeze only, escape only, or freeze and then escape. The presence of any of these responses is defined in this report as “detection” and reflects the overall likelihood of any given mouse showing some form of behavioural response to a visual stimulus (by freezing and/or escaping behaviours).

“Loom” - The “Loom” stimulus was a 1 cm (thus a visual angle of diameter 2° when directly over the animal) black disk rapidly widening to 25.5 cm (50°) in 250 ms and remaining on the screen at this size for an additional 500 ms.

“**Sweep”** - The “Sweep” stimulus was a 2.5 cm (5°) black disk that appeared at one side of the monitor and then translated smoothly to the opposite side over 4 s (21 °/s).

CHAPTER 3: Standardized framework for visual stimulus-induced escape and freeze responses in wild-type mice.

3.1 Optimization of a Loom/Sweep behavioural assessment arena.

Visually induced avoidance responses (escape or freeze) may be used as a measure to assess visual function in mice. To begin to develop this as a reproducible test, I started by improving the experimental arena described by De Franceschi et al. (2016). As described in the Methods chapter and illustrated in **Figure 5 A**, a metal frame structure was built, providing a stable base, and the arena was placed over a thick white plastic base on the bottom of the frame. The stimuli projection was also improved by replacing the monitor that previously surmounted the arena with a projector and a projection sheet that was placed above the arena, allowing greater freedom in visual stimuli / experimental and therefore more opportunity to deliver the visual stimuli. An infrared camera was attached to the metal frame above the side of the arena opposite the nest. The camera was placed below the projection sheet and was adjusted to an angle and height that would allow imaging through the infrared wall, visualising all the arena including the door to the nest. The arena was built with infrared black acrylic with white plastic covering most of the walls to avoid reflections. Another important alteration to this set up was providing a shelter/nest (a black acrylic box) that was placed outside the arena and accessed through a hole in one of the arena walls, freeing up more space for the mice to move and, consequently, more opportunity to trigger the visual stimulus at a central location in the arena.

3.2 Visual stimuli induce instinctive avoidance behaviours in mice.

The first aim of this project was to establish a standardized framework for assessing visual stimulus-induced avoidance responses in adult (2 ± 1 month old) wild-type (C57BL/6J) mice in any given "Session" (**Figure 5 C**), a mouse was placed in the arena and allowed to explore for a brief period (10 minutes on first exposure, 5 minutes subsequently). During this time the projector was held at the mean luminance. Subsequently, each mouse was presented with a pre-established sequence of 4 trials: 1st Sweep → 1st Loom → 2nd Sweep → 2nd Loom, with at least 1 minute in between each stimulus presentation (**Figure 5 C**). A maximum of 20 minutes was allowed for each Session, in which I aimed to deliver all 4 trials. As this was not always possible within the 20 minutes period, for example if the mouse was reluctant to navigate the centre of the arena and remained inside the nest or at the corner it made stimuli delivery challenging, this is reflected in the reduced and variable trial numbers for a given animal (and therefore experimental cohort), where applicable.

I first measured behavioural responses when animals were tested in once-daily experimental sessions, similar to most previous work. As reported by De Franceschi et al. (2016), mice exhibit clear and distinct behavioural responses to well characterized visual stimuli, 'Loom' and 'Sweep' stimuli **Figure 5 B**. Randomly allocated wild-type mice (n=12, 6 females and 6 males) were exposed to a single session per day for five consecutive days (herein termed the "Tonic" protocol). Ideally, this protocol would yield responses in 20 trials (2 Loom and 2 Sweep in each of 5 sessions) for each mouse, and therefore a total of 240 trials over all animals (**Figure 5 C**).

Most presentations of a Loom stimulus evoked a behavioural response. I defined behaviours as described in De Franceschi et al. (2016). 'Escapes' are a rapid movement (exceeding 40 cm/s) towards the refuge, and I found escapes on 55% (62/112) trials. 'Freezes' are epochs where mouse movement is less than 2 cm/s, for at least 0.5 s, and I found freeze behaviours

on 38% (43/112) trials. In some trials ('Freeze + Escape'; 10/112), escapes were preceded by freeze behaviour. The presence of either or both of freeze and escape behaviours defines the 'Detection' probability for a Loom stimulus and was 86% (95/112 trials) (**Figure 5 D**).

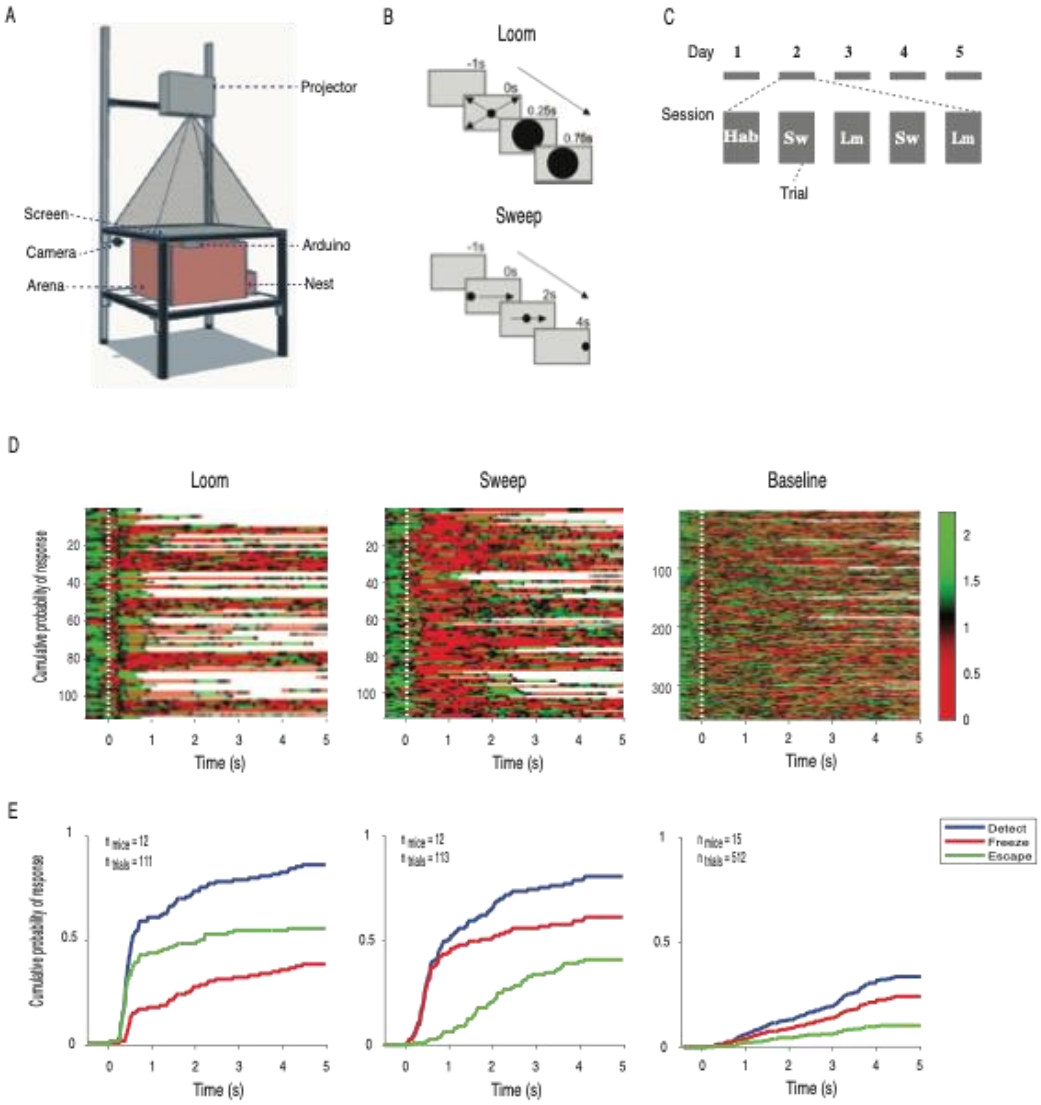

Figure 5: *Visual Stimuli induce instinctive avoidance behaviours in mice.*

(A) Schematic representation of the behaviour set up developed for assessing visual stimuli-induced behaviour responses in mice. (B) Schematic illustrations of stimuli. Top - Loom Stimuli: 1 cm black disk (thus a visual angle of diameter 2° when directly over the animal) rapidly widening to 25.5 cm (50°) in 250 ms and remaining on the screen at this size for an additional 500 ms; Bottom - Sweep Stimuli: 2.5 cm (5°) black disk that appeared at a smaller side of the monitor and then translated smoothly to the opposite side over 4 s (21 °/s). (C) Schematic representation of a protocol design tested – "Tonic" where mice were tested 5

sessions, one session per day for 5 days. Regardless of the design protocol the session workflow schematically highlighted was maintained throughout experiments. (D) Images of the natural logarithm of movement speed in each trial (one trial per row) of the tonic protocol during Loom (1st panel), Sweep (2nd panel) and Baseline (3rd panel). Where red indicates low speed; green indicates high speed; black indicates speeds close to the mean across animals; white indicates times when the animal was in the refuge and therefore not detected. (E) Graphs representing the cumulative probability of detection, having observed either an escape and/or freeze response (*blue*), an escape response (*green*) and a freeze response (*red*) over time on the Tonic protocol.

Sweep stimuli also evoked behaviours on most trials (**Figure 5 B**). The detection probability for Sweep trials was 81% (91 / 113 trials). Unlike for Loom, most trials elicited freeze behaviour (61%, 69/113 trials), and fewer resulted in escape behaviour (41%, 46/113 trials) (**Figure 5 D and E**). About half of escapes were preceded by freeze behaviour (freeze+escape: 21%, or 24/113 trials).

To account for mouse behaviour that might include pauses while foraging, or return to the refuge, even in the absence of a real threat, we have analysed 5 min of the habituation period (before any visual stimulus), analysing only those epochs where the animal approached the centre of the arena and applying the same criteria for escape and freeze as used above. As seen in the baseline data in **Figure 5 D and E, the** chance probability of escape and freeze was much lower compared to the stimulus-induced responses.

The reader's attention is drawn to the fact that our analyses classifies the responses *after* stimuli onset; if mouse movement speed is less than 2.5 cm/s for at least 0.2 s, this is classified as freeze behaviour and contributes to the freeze probability, while if in response to the same visual stimuli the mice speed exceeds 40 cm/s as it returns to the refuge this would be classified as escape behaviour and will contribute for the probability of escape. Therefore, the probabilities shown throughout this report are cumulative and not exclusive, meaning that we considered that any given mouse can show more than one behaviour in response to the same stimulus: freeze only, escape only, or freeze and escape in response to a single visual stimulus. This is also reflected in the probability of observing either: freeze and/or escape behaviours.

3.3 Influence of number and frequency of Sessions on behavioural responses.

Prior to this study, established protocols in the literature have typically employed a testing regimen that involved mice participating in a single daily session on each of three to six days (De Franceschi et al. 2016; Vale, Evans, and Branco 2017; Storchi et al. 2019), a format similar to the “tonic” protocol above **Figure 5**. Though not explicit, the rationale for once-daily sessions appears to be the concern that more intense testing regimes may be more likely to induce habituation, or otherwise alter these instinctive behaviours. In a preclinical setting, this testing regimen may present challenges, due to the extended duration of the experiments and the considerable number of mice required to account for various treatments or conditions. Consequently, I evaluate the feasibility of obtaining measurements of visually evoked avoidance behaviour by re-exposing the same mice to visual stimuli within a single day. With these considerations in mind, I explored two additional experimental protocols. As illustrated in **Figure 6** these protocols are as follows:

"Burst" Protocol: five sessions conducted within a single day.

"Intense" Protocol: five sessions are administered each day for five consecutive days.

This approach allows us to distinguish which experimental design aligns more effectively with the specific objectives of this study. In this study, the primary focus revolves around employing visually triggered avoidance behaviours in preclinical research as the key metrics to evaluate the outcomes of gene and cell therapies for ocular applications.

The “Burst” protocol consisted of the same total of five sessions but conducted within a single day. This experimental design involved a cohort of twelve mice, comprising six males and six females. Ideally, this protocol would yield responses in 20 trials (2 Loom and 2 Sweep in each of 5 sessions) for each mouse, and therefore a total of 240 trials over all animals. I found a subtle distinction in the probability of detecting the loom stimulus between the cohort

of mice tested under the “Burst” protocol and the cohort of mice tested under the “Tonic” protocol (**Figure 6 B and C)**. Under the “Burst” protocol, the likelihood of detecting a Loom stimulus was higher (detection probability 90%; 110/122 trials). With a pronounced prevalence of escape responses (76%; 93/122 trials). In contrast, freezing behaviour was lower, 16% (18/112 trials) in the “Burst” protocol (**Figure 6 C**).

The “Intense” protocol, marked by five daily sessions conducted over a continuous span of five days, allowed us to investigate how the distribution of sessions over consecutive days may influence avoidance behaviours. Ideally, this protocol would yield responses in 20 trials (2 Loom and 2 Sweep in each of 5 sessions per day) for each mouse, and therefore a total of 600 trials over all animals. These experiments were conducted on a cohort of 6 female mice. This is because it became clear during the course of experiments that the substantial time commitment required for this protocol made this design impractical for future assessments.

The overall probability of detecting the loom stimuli, by responding to it by escaping and or freezing, was 87% (191 out of 220 trials) (**Figure 6 B and D**). Escape responses were more prevalent, occurring in 62% of trials (136 / 220 trials), while freezing behaviour was exhibited in 29% (64 / 220 trials) (**Figure 6 D**).

Responses to Sweep stimuli were consistent across “Tonic”, “Burst” and “Intense” protocols as demonstrated in **Figure 6 A, B, D** (**middle panels**). Specifically, the likelihood of any mouse detecting the sweep stimuli was 78% (101 / 130 trials; 12 mice) for the “Burst” protocol and 79% (192 / 243 trials; 6 mice) for the “Intense” protocol (**Figure 6 E (middle panel)**). Mice allocated to the “Burst” protocol exhibited an interesting behaviour pattern in response to Sweep stimuli, where the probabilities of both freezing and escaping behaviour were nearly identical. Freezing responses were observed, on average, in 52% (68 / 130) trials (**Figure 6 D (middle panel)**). It is worth noting that within a subset of 34 trials (26 % of sweep trials), those mice displayed a freeze+escape behaviour in response to the sweep stimuli.

The “Intense” protocol required five daily sessions over each of five consecutive days. Despite the enhanced session frequency, the probability of observing avoidance behaviours (freezing, escaping, or both) remained similar to the “Tonic” and “Burst” protocols, as seen in **Figure 6 A, B, C, and D**. Specifically, mice detected 79% (192 / 243 trials) sweep stimuli with freeze behaviour observed in 50% (122 / 243 trials), escape in 46% (112 / 243 trials), similar to those for “Tonic” and “Burst” protocols (**Figure 6 E (middle panel)**). Freeze+escape responses were seen in 16% (39 / 243 trials).

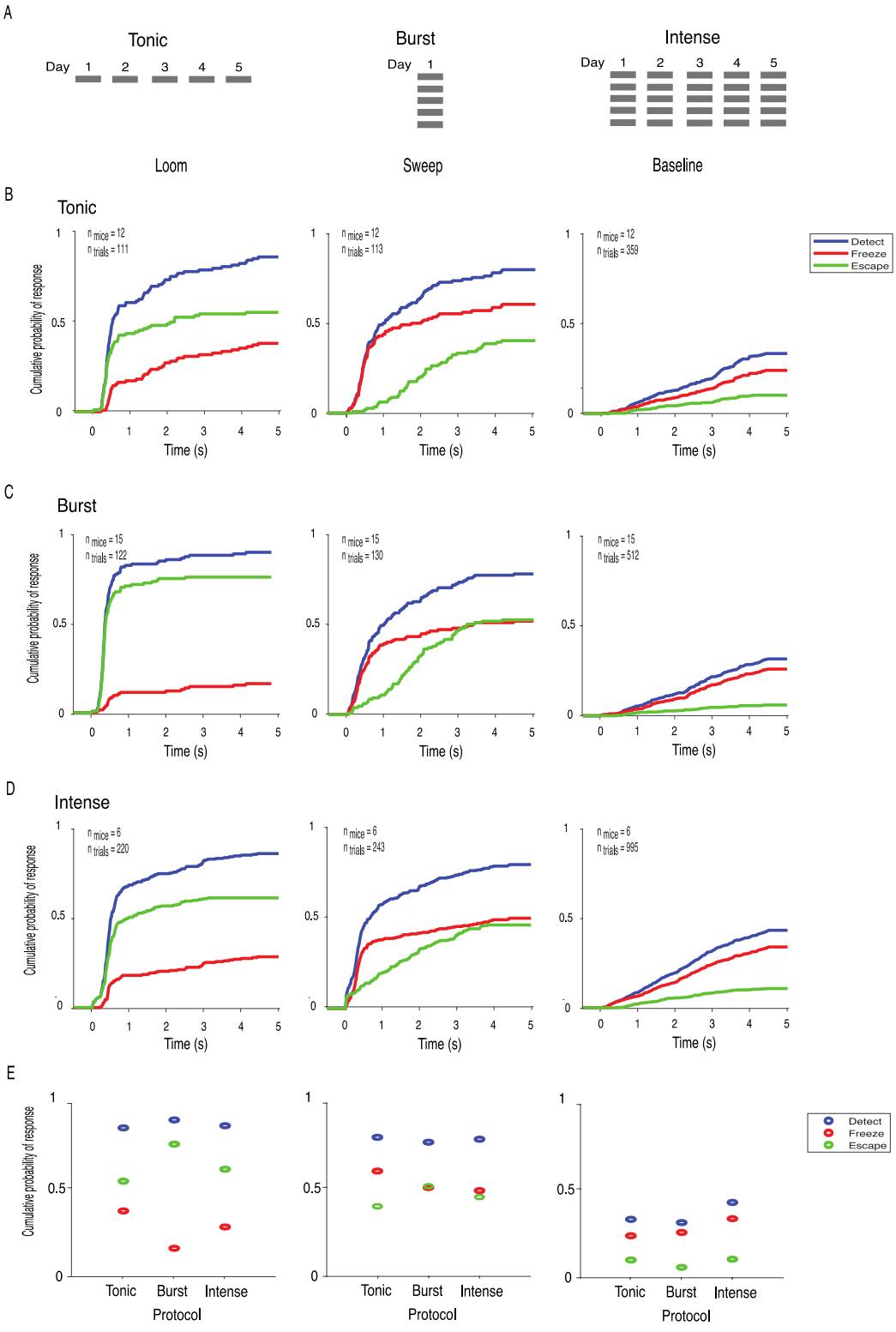
A
Tonic
Day 1 2 3 4 5
Burst
Day 1
Intense
Day 1 2 3 4 5
Loom
Sweep
Baseline
B
Tonic
n mice = 12
n trials = 111
n mice = 12
n trials = 113
n mice = 12
n trials = 359
Detect
Freeze
Escape
Cumulative probability of response
Time (s)
C
Burst
n mice = 15
n trials = 122
n mice = 15
n trials = 130
n mice = 15
n trials = 512
D
Intense
n mice = 6
n trials = 220
n mice = 6
n trials = 243
n mice = 6
n trials = 995
E
Tonic Burst Intense
Protocol

Figure 6: Influence *of experimental design on behavioural responses.*

(A) Schematic representation of the protocol designs tested – “Tonic” where mice were tested 5 sessions, one session per day for 5 days; “Burst” where mice were tested 5 sessions conducted within a single day; "Intense" where mice were tested 5 sessions each day for five consecutive days. (B-D): Graphs representing the cumulative probability of having observed either an escape and/or freeze response (*blue*), an escape response (*green*) and a freeze response (*red*) over time on the Tonic, Burst and Intense protocols. Cumulative probability of responses to the (Left) Loom stimuli, (Middle) Sweep stimuli, and during (Right) baseline assessment where no visual stimuli was triggered. (E) Comparisons of the average cumulative probability of detecting either of the visual stimuli by having observed either an escape and/or freeze response (*blue*), an escape response (*green*) and a freeze response (*red*) in response to the stimuli. Cumulative probability of responses to (*Left*) Loom stimuli, (*Middle*) Sweep stimuli, and (*Right*) during baseline assessment where no visual stimuli was triggered.

While overall pattern of avoidance responses was consistent across protocols, session intensity was associated with subtle differences (**Figure 6 E**). Of note, increased session intensity significantly impacted the mice's willingness to explore the arena, making it challenging to deliver stimuli effectively when they were optimally located.

Baseline data, reflecting mouse behaviour before stimuli presentation, consistently showed low cumulative probabilities of escape, freeze, or escape+freeze responses across all protocol designs. This baseline data validates that the behaviours observed were primarily responses to the visual stimuli presented. It is worth noting that behavioural differences emerged between different cohorts of mice, even at baseline, particularly in the “Intense” protocol (**Figure 6 E, Right panel**). These differences could reflect animal variability and should be considered in the overall analysis.

Nevertheless, the average detection probabilities for both visual stimuli across the three tested design protocols were very consistent: “Tonic” (probability of detection $_{Tonic}$ = 84 %, n $_{Tonic}$ = 187 / 224 trials), “Burst” (probability of detection $_{Burst}$ = 84 %, n $_{Burst}$ = 211 / 252 trials), and “Intense” (probability of detection $_{Intense}$ = 83 %, n $_{Intense}$ = 382 out of 463 trials). As previously noted, animals subjected to the “Burst” protocol exhibited a higher likelihood of displaying escape responses to both types of visual stimuli (loom:

probability of escape $_{Burst}$ = 76 %, n $_{Burst}$ = 93 out of 122 trials; sweep: probability of escape $_{Burst}$ = 52 %, n $_{Burst}$ = 68 out of 130 trials) compared to the “Tonic” and “Intense” protocols (see **Figure 6 E**). Consequently, a reduced probability of observing freeze responses to loom and sweep visual stimuli under the “Burst” protocol was noted. These small differences aside, **Figure 6 E** highlights the striking similarity in the behavioural profiles of mice tested across the “Tonic”, “Burst”, and “Intense” protocols in terms of their overall response to any visual stimulus, and their preferred behavioural responses to these stimuli.

3.3.1 Parameters of behaviour response.

Similarity in categorical response (‘freeze’, ‘escape’) may mask finer-grained differences in features of that response, such as running speed or latency. I next sought to provide a more detailed characterization of the obtained responses by examining various parameters. Latency of escape and freezing responses, representing the time from stimulus onset to the initiation of escape or freezing events, was measured.

Additionally, peak escape speed, defined as the maximum speed achieved between the initiation of escape and reaching the nest and freeze duration, defined as the time between the initiation and the end of a freeze response was considered. In **Figure 7** (and **Table 3**), the violin plots of the distribution and probability density of each parameter across different experimental conditions is presented. Analysing the escape latency to loom stimuli across the various protocols tested (median of escape latency Tonic = 0.37 s, Burst = 0.46 s, Intense = 0.5. s), mice assigned to the Burst protocol exhibited a faster response compared to those in the Tonic and Intense protocols (ANOVA: Tonic vs Burst p = 0.0089, Burst vs Intense p = 0.0837) (**Figure 7 A)**. However, there were no significant differences in freeze latency, max escape speed, or freeze duration (**Figure 7 B, C and D)** among the groups analysed.

There were also slight differences in parameters of response to sweep stimuli. Escape latency varied across the protocols **Figure 7 A** (median of escape latency: Tonic = 1.977 s, Burst = 1.704 s, Intense = 1.353 s), a significant difference was observed between the Tonic and Intense protocols (ANOVA, Tonic vs Intense p = 0.0036). This trend was consistent when looking at freeze latency (median of escape latency: Tonic = 0.552 s, Burst = 0.47 s, Intense = 0.353 s), with a significant difference noted between the Tonic and Intense protocols (Kruskal-Wallis: Tonic vs Intense p = 0.0092) (**Figure 7 B**). Max escape speed also displayed differences between the groups tested (median of max escape speed: Tonic = 67.29, Burst = 61.51, Intense = 73.67); mice assigned to the Intense protocol exhibited a statistically significantly higher escape speed compared to those in the Burst protocol (ANOVA: Burst vs Intense p = 0.016) (**Figure 7 C**). Significant differences in freeze duration (median of freeze duration: Tonic = 1.13 s, Burst = 0.76 s, Intense = 0.89 s) were observed in **Figure 7 D**, indicating that mice in the "Tonic" protocol froze for longer periods compared to those in the Burst protocol, aligning with previous observations of a higher proportion of freeze+escape responses in the "Burst" protocol to sweep stimuli. The exploration of these parameters offers valuable insights into the nuanced aspects of the responses, contributing to a more comprehensive understanding of the observed behaviours under different experimental conditions.

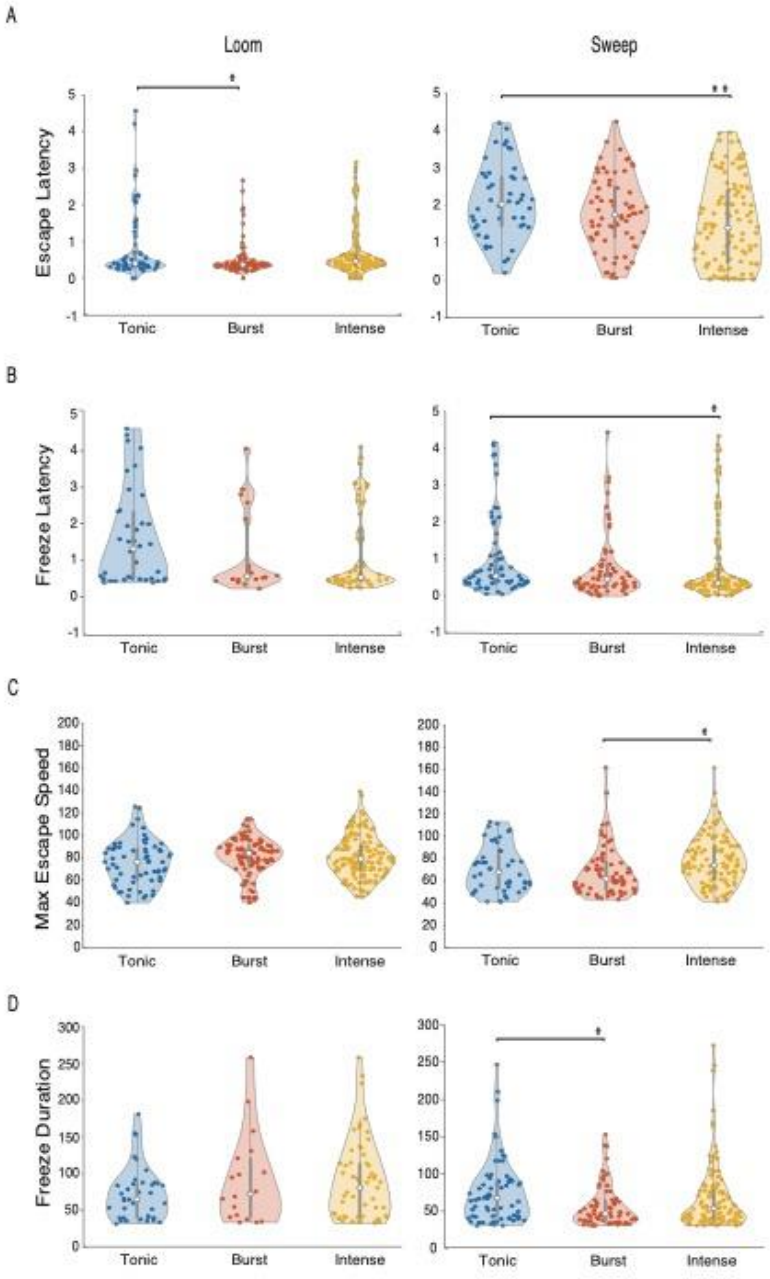
A
Loom
Sweep
Escape Latency
*
**
Tonic
Burst
Intense
B
Freeze Latency
*
C
Max Escape Speed
*
D
Freeze Duration
*

Figure 7:Influence of experimental design on the response characteristics of visually induced avoidance behaviours in mice.

Visual representation of the distribution and probability density of behavioural response characteristics: escape latency, freeze latency, maximum escape speed and freeze duration. Latency of escape and freezing responses were defined as the time between stimulus onset and the initiation of escape or freezing events respectively. Peak escape speed was defined as the maximum speed achieved between the initiation of an escape response and, freeze duration was defined as the time between the initiation and ceased of a freeze response. Left Panel: Violin plots of the distribution and probability density of behavioural response characteristics: escape latency (A), freeze latency (B), maximum escape speed (C) and freeze duration (D) for the Tonic, Burst and Intense protocol designs to Loom stimuli. Right Panel: Violin plots of the distribution and probability density of behavioural response characteristics: escape latency (A), freeze latency (B), maximum escape speed (C) and freeze duration (D) for the Tonic, Burst and Intense protocol designs to Sweep stimuli. $p<0.05$= statistically significant *, $p<0.005$ = very significant **

This analysis of session organization illustrates the variations in behavioural responses among the different designs. While the “Tonic” and “Intense” protocols displayed many similarities in their overall response probabilities and behavioural response profiles to the Loom stimuli, the “Burst” protocol exhibited distinct patterns. Notably, the “Burst” protocol presented an elevated detection probability, and more escape responses were observed in response to the loom stimuli. These response patterns, characterized by heightened detection rates and pronounced escape behaviours, highlights the impact of repeated presentations within a short time frame within the context of our study. Interestingly, I observed that the increment in sessions within a day did not affect mice exploratory behaviour and consequently occupancy maps of mice that underwent the Burst protocol, contrary to what was observed for the Intense protocol where a proportional reduction in mice exploratory behaviour throughout the sessions within one day. Taking into consideration the design of the burst protocol we could only attribute this effect to intra-animal variability.

3.4 An Optimised protocol for assessing visually evoked innate behaviours.

In order to establish a simple test to visually evoked innate behaviours in mice, I have explored various experimental design protocols, scrutinizing the impact of session organization and repeated measurements. As this data was examined, it became evident that these intricate and multifaceted behaviours can be influenced by different factors, from the design of the experimental protocol and by the individual mouse itself. With this understanding, I set out to define a protocol that would balance both usability and the consistency of behavioural outcomes. The optimised protocol, designed with the intention to be the primary protocol for the subsequent phases of our study, consists of three sessions per day for two consecutive days.

To establish a baseline for the subsequent studies following this protocol design, and to be able to set comparison between the different design protocols I measured the behavioural responses of adult (2 ± 1 month old) wild-type (C57BL/6J) mice (n=7, comprising 2 females and 5 males) to Loom and Sweep visual stimuli. Each mouse subjected to this protocol underwent a total of six sessions, with the same session structure (Sweep-Loom-Sweep-Loom) as previous and as illustrated in **Figure 4 C**. In an ideal scenario, where mice continuously explore the arena for the entire session duration, the maximum number of responses captured would number 168. Half of these trials would feature loom stimuli, while the other half would involve sweep stimuli.

The cumulative probability of responses to both stimuli is illustrated in **Figure 8** and summarized in **Table 2**. Cumulative probability detection was 87 % for both loom (71 /82 trials) and sweep (72 / 83 trials) (**Figure 8 A**). Looking at the type of triggered innate behaviours, Loom stimuli triggered escape in 38 % (31 / 71 trials); this was a surprisingly lower probability of escape to what was observed previously for the other design protocols. In fact, as illustrated in **Figure 8 A**, mice allocated to this protocol design showed a

higher probability of freezing, 54 %, in response to loom trials (44 / 71 trials). Sweeps evoked freezing behaviour in 82 % (44 / 71 trials), and escape responses in 22 % (16 / 71 trials) (**Figure 8 A**). The unexpectedly low probability of escape observed across animals assigned to the Optimal protocol illustrates a degree of variability between cohorts with respect to these visually triggered innate behaviours. While various factors, such as changes in BSU staff, alterations in husbandry routines, and external disruptions during the pandemic could contribute to these differences, the observed variations seem more animal-specific, indicating a high inter-animal variability, as discussed in subsequent sections.

Despite our best efforts to maintain a tight time frame and consistency between sites, the Covid-19 pandemic and a change of laboratories between Universities may be responsible for some of the observed variability in behavioural responses. To provide transparency, details such as experiment dates, locations, and users are clearly indicated in the summary **Table 1**, allowing readers to consider variations due to changes in experimental environments. At King's College London (KCL), I observed a different behavioural response profile under the Optimised protocol, compared to those tested at UCL. Following a period of acclimatization to the new animal facility, we established new breeding pairs, prioritizing litters from these pairs for experiments. Adult wild-type (C57BL/6J) mice (2 females and 3 males), aged 2 ± 1 month, were assigned to the “Optimised” experimental protocol. As depicted in **Figure 10 B**, detection of Loom (84 %, 32 / 38 trials) or Sweep stimuli (83 %, 34 / 41 trials) was similar to cohorts tested at UCL (**Figure 5 and 6**). Loom stimuli prompted escape responses in 68 % of trials (26 / 38 trials), with freezing in 6 / 38 loom trials (16 %). Sweep stimuli evoked escape (63 %, 26 / 41 trials), and freeze behaviour (49 %, 20 / 41 trials) (**Figure 8 B**). These were notably different to what was observed for the cohort of mice tested under the ‘Optimised’ protocol at UCL, but the behaviour profile seen at KCL seems to be more aligned to what was described during protocol comparisons at UCL **Figure 8 D** (**left panel**). For example, animals tested under the "Burst" protocol design at UCL (**Figure 8 B**) also exhibited a high escape probability to sweep stimuli (52 %, 68 / 130 trials).

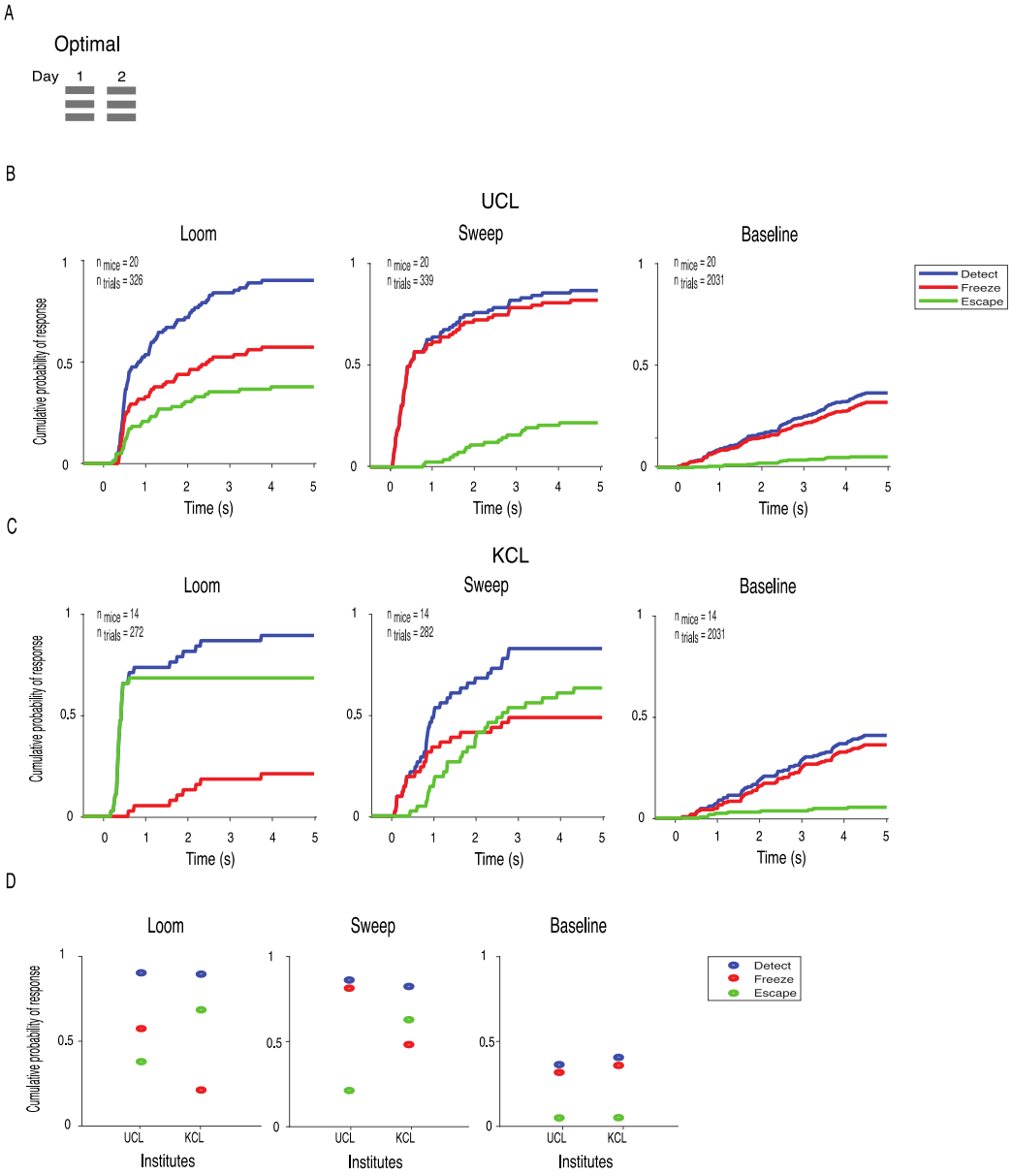
A
Optimal
Day 1 2
B
UCL
Loom
Sweep
Baseline
n mice = 20
n trials = 326
n mice = 20
n trials = 339
n mice = 20
n trials = 2031
Detect
Freeze
Escape
Cumulative probability of response
Time (s)
C
KCL
Loom
Sweep
Baseline
n mice = 14
n trials = 272
n mice = 14
n trials = 282
n mice = 14
n trials = 2031
D
Loom
Sweep
Baseline
UCL
KCL
Institutes

Figure 8: The influence of different sites on the visual triggered innate behaviour responses in an optimised protocol.

(A) Schematic representation of the Optimised protocol design where mice were tested 6 sessions, 3 sessions per day for two consecutive days. (B-C) Graphs representing the cumulative probability of having observed either an escape and/or freeze response (*blue*), an escape response (*green*) and a freeze response (*red*) over time on the optimised protocol recorded at UCL and KCL Institutes. Cumulative probability of responses to (*Left*) Loom stimuli, (*Middle*) Sweep stimuli, and (*Right*) during baseline assessment where no visual stimuli was triggered. (D) Comparisons of the average cumulative probability of detecting either of the visual stimuli by having observed either an escape and/or freeze response (*blue*), an escape response (*green*) and a freeze response (*red*) in response to the stimuli. Cumulative probability of responses to (*Left*) Loom stimuli, (*Middle*) Sweep stimuli, and (*Right*) during baseline assessment where no visual stimuli was triggered.

It is important to consider that the UCL Optimised experiments were done at a period of returning to work after the pandemic (August 2020) and perhaps the differences observed could be attributed to external factors and potential environmental influences on specific cohorts. Nevertheless, it is intriguing that the KCL cohorts (recorded on May 2021) exhibited behaviour profiles resembling earlier response profiles observed at UCL.

3.4.1 Parameters of behaviour response.

Further characterization of the behavioural responses was done looking at parameters including response latencies, maximum escape speed, and freeze duration for the optimized protocol in each institution as depicted in **Figure 9** and summarized in **Table 3**. No significant differences were found in escape latency (median: UCL = 0.87 s, KCL = 0.37 s) or maximum escape speed (median: UCL = 61.37, KCL = 84.07). However, freeze latency (median: UCL = 0.69 s, KCL = 2.02 s), mice tested at KCL took longer to initiate their freeze responses upon stimuli detection compared to mice tested at KCL (Rank Sum p = 0.0328) (**Figure 9 B**). Furthermore, as depicted in **Figure 9 D**, freeze

responses were longer at UCL (median: UCL = 1.49 s, KCL = 0.63 s, Rank Sum p = 0.0138).

As my understanding deepened regarding the variable nature of these visually triggered innate behaviours, it became clear that, despite our efforts to minimize changes in experimental conditions, handling procedures, user consistency, and protocol design, different mice exhibit different behavioural responses to loom and sweep stimuli. While it is true that the most prevalent behaviour observed for loom is an escape response, and sweep stimuli tend to trigger more freeze responses, it is essential to recognize that this may not hold true for every animal. This awareness is crucial for designing studies and interpreting data. Despite the variability observed, the primary goal of this study - to understand if visually triggered innate behaviours could serve as a reliable outcome measure of vision capability - remains unaffected. I was not overly concerned with this variability, and I remain reassured that regardless of site changes during the study's execution, mice consistently respond and detect both loom and sweep stimuli. Establishing the 'Optimised Protocol' not only underscores our dedication to practicality, but also guarantees the scientific soundness of our research, establishing a foundation for the chapters that follow.

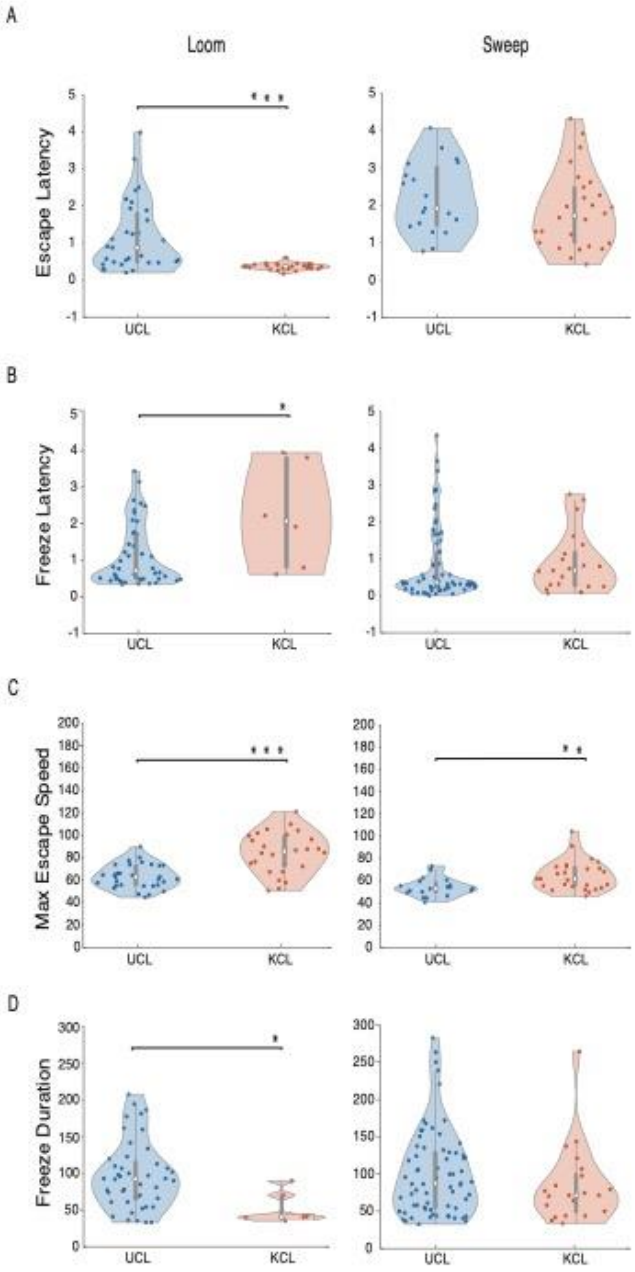
A
Loom
Sweep
Escape Latency
***
UCL
KCL
B
Freeze Latency
*
C
Max Escape Speed
***
**
D
Freeze Duration
*

Figure 9: The influence of different sites on the characteristics of visual triggered innate behaviour responses in the optimised protocol.

Visual representation of the distribution and probability density of behavioural response characteristics: escape latency, freeze latency, maximum escape speed and freeze duration. Latency of escape and freezing responses were defined as the time between stimulus onset and the initiation of escape or freezing events respectively. Peak escape speed was defined as the maximum speed achieved between the initiation of an escape response and, freeze duration was defined as the time between the initiation and ceased of a freeze response. Left Panels: Violin plots of the distribution and probability density of behavioural response characteristics: escape latency (A), freeze latency (B), maximum escape speed (D) and freeze duration (E) for a cohort of mice tested using the Optimised Protocol whilst housed at UCL. Right Panels: Violin plots of the distribution and probability density of behavioural response characteristics: escape latency (A), freeze latency (B), maximum escape speed (C) and freeze duration (D) for a different cohort of mice tested using the Optimised Protocol whilst housed at KCL. $p<0.05$= statistically significant *, $p<0.005$ = very significant **, $p<0.001$= highly significant ***

3.5 The reproducibility of visually induced avoidance behaviour in mice.

Previous research has overlooked a crucial aspect: the reproducibility of visually induced behaviours in mice. In this study every mouse, irrespective of the assigned experimental protocol, was subject to a minimum of five test sessions. Consequently, this enabled me to conduct a comprehensive analysis across various datasets, encompassing different design protocols such as “Tonic”, “Burst”, “Intense”, and “Optimised” designs all conducted within the same research institution. Specifically, focused on the initial five sessions for each design protocol, regardless of whether more were performed. The primary objective was to investigate how mice responded to both visual stimuli during the initial five sessions and assess if these responses exhibited significant changes over subsequent sessions. In **Figure 10 A**, the detection percentage, reflected in mice freezing and/or escaping, is depicted across the first five sessions for 40 mice. Session 1 showed the lowest percentage of detection responses (67 %; $n_{Session1}$ = 107 / 160 trials), compared to the subsequent sessions, which were consistently around 80%

(S2 = 83 %, 125 /151 trials; S3 = 86 %, 120 / 140 trials; S4 = 87 %, 117 / 134 trials and S5 = 89 %, 133 / 118 trials). Indeed, for the first sessions, it was observed similar probability of escape and freeze responses of 36 % ($n_{S1\ Escape}$ = 58/160 trials, $n_{S1\ Freeze}$ = 58/160 trials. There are two differences between the first and the subsequent sessions: 1) cumulative habituation time to arena, 2) different prior exposure to stimuli. The first session included a habituation period of 10 minutes while in all subsequent sessions, this was reduced to 5 minutes. As for the detection probability, it was observed no bias towards a specific behaviour in the remaining sessions, as the probabilities of observing freeze or escape responses were very similar and remained consistent across the four remaining sessions analysed.

This experimental design also allowed me to establish how response varied within a session. As described previously, a predetermined sequence of four visual stimuli or trials: 1st Sweep ➔ 1st Loom ➔ 2nd Sweep ➔ 2nd Loom was employed throughout all experiments. This dataset demonstrates strikingly similar response probabilities across various trials (**Figure 10 B**). Specifically, responses in Trial 1 (probability detection $_{Trial1}$ = 74 %, n detection $_{Trial1}$ = 144 / 195 trials) were comparable to those in Trial 3 (80 %, 137 / 171 trials), and those in Trial 2 (86 %, 157 / 183 trials) were comparable to Trial 4 (87 %, 142 / 163 trials). These findings suggest that prior stimuli presented within the same session do not significantly influence subsequent responses (**Figure 10 B**).

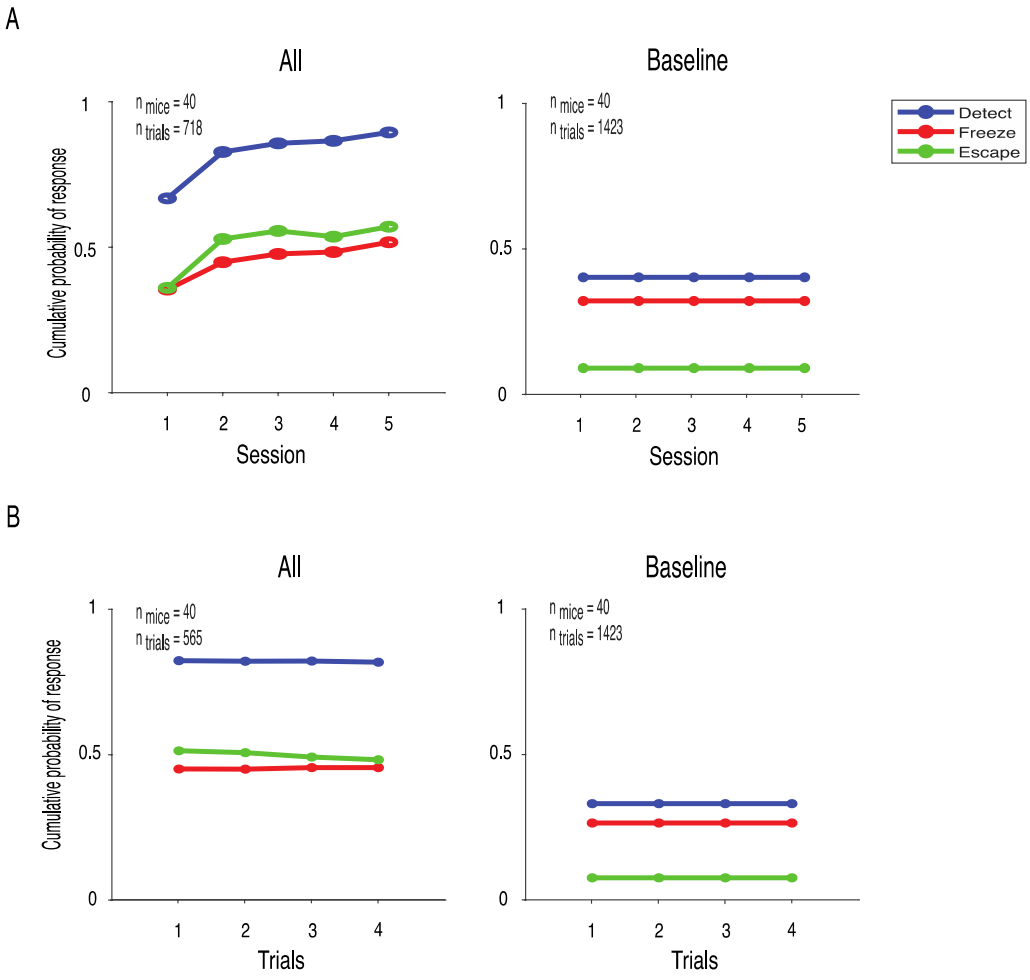

Figure 10: The reproducibility of visually induced avoidance behaviour in mice.

(A and B) Average cumulative probability of having observed either an escape and/or freeze response (*blue*), an escape response (*green*) and a freeze response (*red*) over time across all data set. A: Session analysis across all datasets. B: Trials analysis across all datasets.

Little change in probability of specific behaviours across the duration of a Session was observed. For Loom stimuli (Trials 2 and 4), it was observed similar frequency of escape response (T2 58 %, 82 / 195 trials; T4 63 %, 103 / 163 trials). Similarly, for Sweep stimuli (Trials 1 and 3), probability of escape was 42 % (82 / 95 trials) on Trial 1 and 42 % (72 / 171) on Trial 3, while probability of freeze response was 56 % (109 /195) on Trial 1 and 60 % (103 / 171 trials) on Trial 3 (**Figure 10 B**). These results indicate consistency in responses to the same visual stimuli as the probability of response is similar

between the 1st and 2nd exposure. Mice responded similarly to both the 1st and 2nd loom, as well as to the 1st and 2nd sweep stimuli, within a given session.

3.5.1 Parameters of behaviour response.

I then aimed to characterise further the acquired responses by investigating the latency of escape and freezing responses, the maximum escape speed and freeze duration. **Figure 11** (and **Table 3**) shows that response parameters (latency, movement speed, freeze duration) varied only slightly within or across sessions. Escape latency (median: S1 = 0.59 s, S2 = 0.99 s, S3 = 0.66 s, S4 = 0.72 s, S5 = 0.59 s), was similar across the five sessions (**Figure 11 A**). Freeze latency (median: S1 = 0.8 s, S2 = 0.49 s, S3 = 0.47 s, S4 = 0.42 s, S5 = 0.51 s), was slightly longer during the 1st session, at least compared to the 5th session (ANOVA p = 0.016). Maximum escape speed (median: S1 = 61, S2 = 70.2, S3 = 72.66, S4 = 76.13, S5 = 73.47), was also slightly slower in the first session, at least in comparison to S4 (ANOVA p = 0.049) (**Figure 11 B**). Within Session, escape latency (median: T1 = 1.79 s, T3 = 1.89 s; T2 = 0.37 s, T4 = 0.4 s) (**Figure 11 A**), freeze latency (median: T1 = 0.5 s, T3 = 0.49 s; T2 = 0.54 s, T4 = 0.51 s), escape speed (median: T1 = 58.85, T3 = 60.63; T2 = 78.73, T4 = 77.56), and freeze duration (median: T1 = 0.92 s, T3 = 0.97 s; T2 = 1.5 s, T4 = 1.3 s) were similar in the first and second presentation of each stimulus type.

In summary, behavioural responses in the initial session were slightly different to those in subsequent sessions, with lower detection percentage more equal probability of escape and freeze responses. However, repeated exposure to visual stimuli within a single session did not significantly influence subsequent responses. The order of presentation of stimuli similarly showed consistency on the behavioural responses obtained.

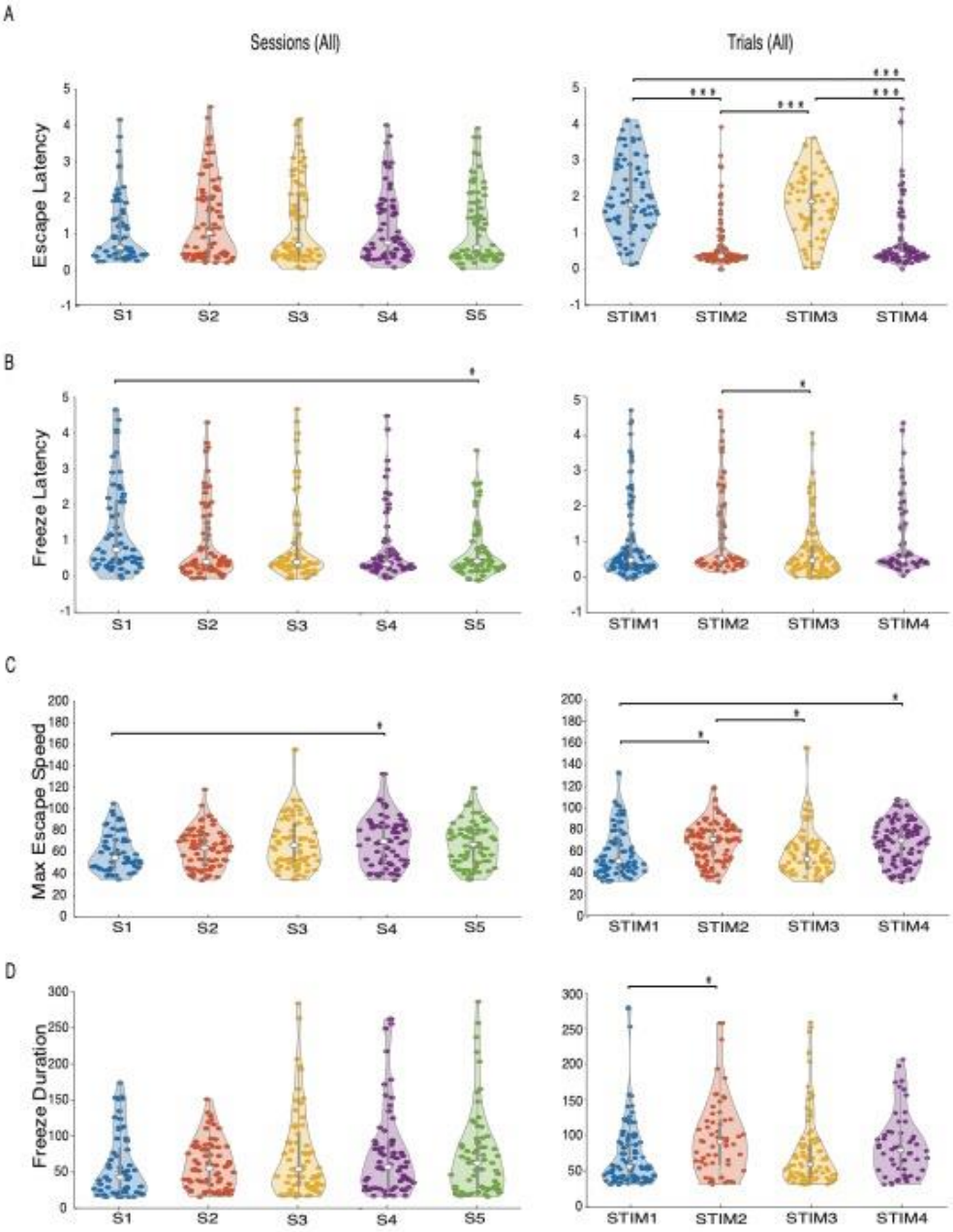
A
Sessions (All)
Trials (All)
Escape Latency
S1
S2
S3
S4
S5
STIM1
STIM2
STIM3
STIM4
B
Freeze Latency
C
Max Escape Speed
D
Freeze Duration

Figure 11: The reproducibility of response characteristics of visually induced avoidance behaviours in mice.

Visual representation of the distribution and probability density of behavioural response characteristics: escape latency, freeze latency, maximum escape speed and freeze duration. Latency of escape and freezing responses were defined as the time between stimulus onset and the initiation of escape or freezing events respectively. Peak escape speed was defined as the maximum speed achieved between the initiation of an escape response and, freeze duration was defined as the time between the initiation and ceased of a freeze response. Left Panels: Violin plots of the distribution and probability density of behavioural response characteristics: escape latency (A), freeze latency (B), maximum escape speed (D) and freeze duration (E) for the session analysis. Right Panels: Violin plots of the distribution and probability density of behavioural response characteristics: escape latency (A), freeze latency (B), maximum escape speed (C) and freeze duration (D) for the trials analysis. $p<0.05$= statistically significant *, $p<0.001$= highly significant ***

3.6 Comparison of repeated measurements.

As highlighted in the Introduction, my aim was to establish a simple framework where visually induced innate behavioural responses could be used as an assessment of visual function in mouse models of retinal (dys)function. This assessment is crucial to understand disease progression and to establish a functional behavioural test for evaluating the impact of innovative therapies. In this context, it is essential to determine whether re-testing mice at multiple time points is feasible and reliable. To assess the impact of repeated measurements, animals were re-tested within the same protocol 28 days after their initial exposure (1st Timepoint: **Figure 12 A and C**; 2nd Timepoint: **Figure 12 B and C**). This analysis spanned across the various protocol designs, including “Tonic”, “Burst”, “Intense”, and “Optimal”, all conducted within the same research institution (UCL). The objective was to examine how mice responded to re-testing at multiple time points and whether this re-exposure influenced their behavioural responses to Loom and Sweep visual stimuli.

The data presented in **Figure 12** summarizes the responses of 40 mice tested under the various protocols. The detection percentage remained consistent between both testing time points. This consistency is reassuring

and suggests an absence of habituation or behavioural extinction to the visual stimuli. For Loom stimuli, 88 % (471 / 535) and 87 % (429 / 493) of trials elicited a behavioural response at the first and second time points respectively (**Figure 12 A and B**). For Sweep stimuli, detection probability was 80 % (455 / 569 trials) at the first time point and 89 % (473 / 531 trials) at the second. This could suggest that mice were more aware of their surroundings and paid greater attention to stimulus onset during the re-testing. However, the baseline data showed an overall increase in the likelihood of response of animals at the 2nd time point. The baseline assessment indicated higher probabilities of escaping, freezing, and detecting, implying that mice moved more and exhibited more episodes of escape and/or freezing behaviour in the baseline assessment before any stimulus presentation.

A reduced escape probability was found for Loom stimuli, from 60 % (321 / 535 trials) to 44 % (217 / 493 trials) between the 1st and 2nd time points, respectively. This decrease in escape responses was mirrored by increase in probability of freeze responses (32 %, 171 / 535 trials, to 48 %, 237 / 493 trials). For Sweep stimuli, there was a slight rise in freeze behaviour (57 %, 324 / 569 trials to 63 %, 335 / 531 trials) but escape probability remained consistent (43 %, 245 / 569 trials; to 44 %, 234 / 531 trials) (**Figure 12 C)**.

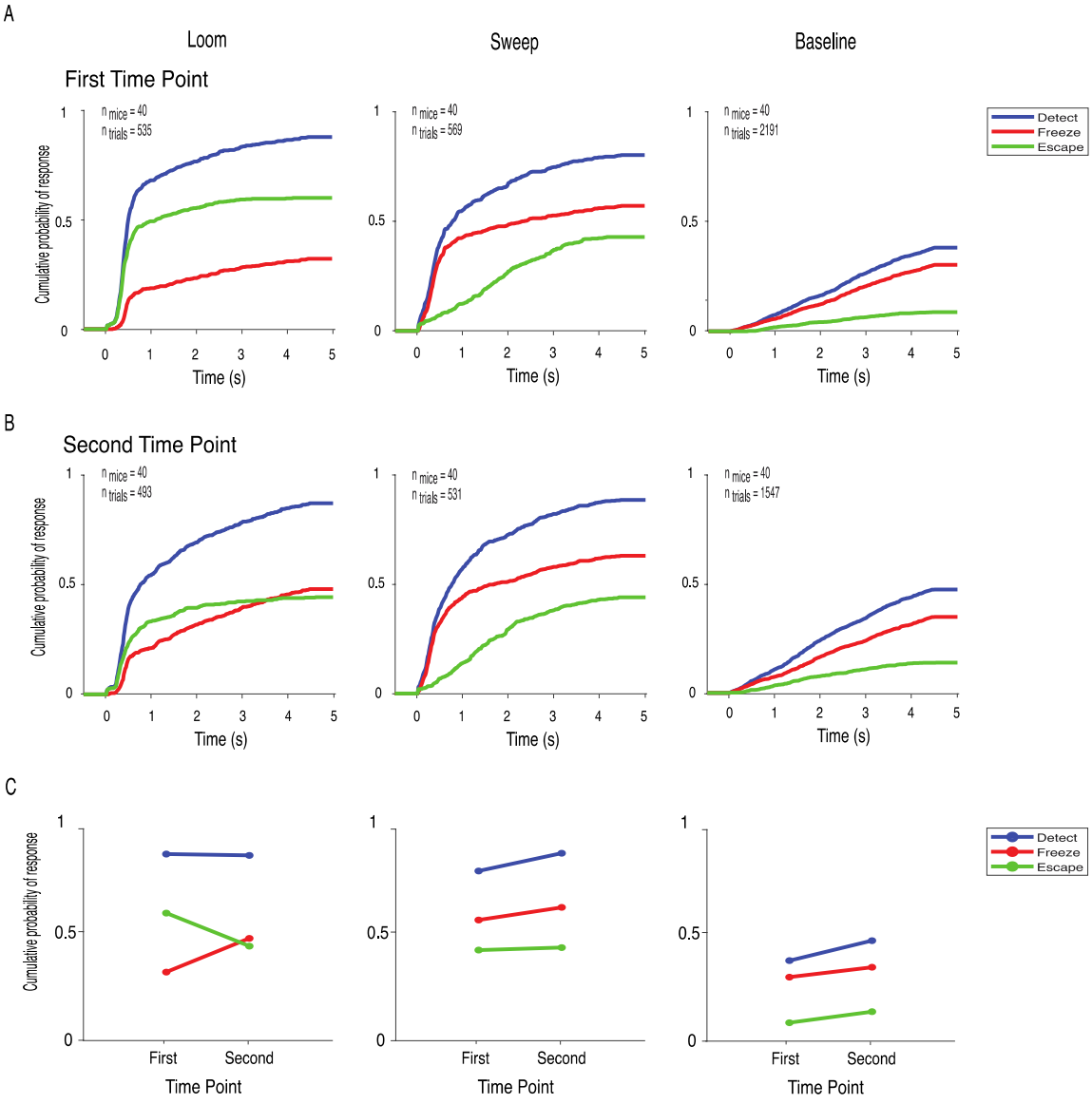

Figure 12: Effect of repeated measurements on avoidance behaviour.

(A) 1st Time point assessment: Cumulative probability of having observed either an escape and/or freeze response – detect (*blue*), an escape response (*green*) and a freeze response (*red*) over time on the tonic, burst, intense and optimal protocols. (B) 2nd Time point assessment: Cumulative probability of having observed either an escape and/or freeze response – detect (*blue*), an escape response (*green*) and a freeze response (*red*) over time on the Tonic, Burst, Intense and Optimised protocols. (C) Average cumulative probability of having observed either an escape and/or freeze response – detect (*blue*), an escape response (*green*) and a freeze response (*red*) over time across all datasets. Time point analysis across all datasets.

3.6.1 Parameters of behaviour response.

Analysis of behavioural parameters (**Figure 13** and **Table 3**) showed increased escape latency for Loom stimuli (median: 0.41 s vs. 0.49 s, Rank Sum p = 0.0338) between the initial and subsequent exposures (**Figure 12 A**). Similarly, freeze latency increased (median: 0.62 s, vs. 1.21 s, Rank Sum p = 0.0087) (**Figure 13 B**). No differences were observed for maximum escape speed (median: 78.41 vs. 77.88) or freeze duration (median: 1.28 s vs. 1.12 s) (**Figure 13 C and D,** respectively).

Freeze duration during presentation of Sweep stimuli increased slightly when mice were re-exposed (median: 0.95 s vs. 1.15 s, Rank Sum p = 0.0245) (**Figure 13 D** and **Table 3**) but there were no differences in escape latency (median: 1.65 s vs. 1.5 s), freeze latency (median: 0.4 s vs. 0.45 s), or maximum escape speed (median: 68.74 vs. 70.19) (**Figure 13 A, B and C** respectively).

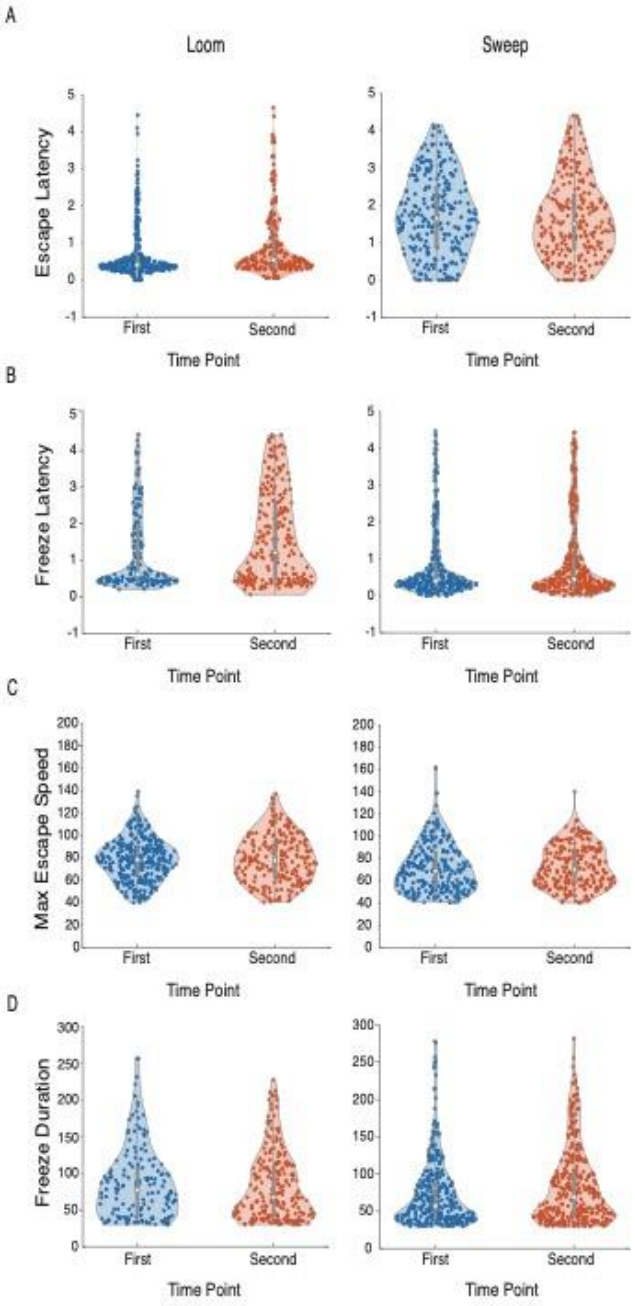
A
Loom
Sweep
Escape Latency
5
4
3
2
1
0
-1
First
Second
Time Point
B
Freeze Latency
C
Max Escape Speed
200
180
160
140
120
100
80
60
40
20
0
D
Freeze Duration
300
250
200
150
100
50

Figure 13: Effect of repeated measurements on the response characteristics of visually induced avoidance behaviours in mice.

Visual representation of the distribution and probability density of behavioural response characteristics: escape latency, freeze latency, maximum escape speed and freeze duration. Latency of escape and freezing responses were defined as the time between stimulus onset and the initiation of escape or freezing events respectively. Peak escape speed was defined as the maximum speed achieved between the initiation of an escape response and, freeze duration was defined as the time between the initiation and ceased of a freeze response. Left Panels: Violin plots of the distribution and probability density of behavioural response characteristics: escape latency (A), freeze latency (B), maximum escape speed (D) and freeze duration (E) for the 1st Time Point analysis. Right Panels: Violin plots of the distribution and probability density of behavioural response characteristics: escape latency (A), freeze latency (B), maximum escape speed (C) and freeze duration (D) for the 2nd Time Point analysis. $p<0.05$= statistically significant *

3.7 Conclusion

In summary, the data presented here shows that behaviours remain very consistent between testing time points 28 days apart. This consistency suggests a lack of habituation or behavioural extinction to the visual stimuli. While re-testing led to a slight decrease in escape probability for Loom stimuli, escape responses persisted in both time points, even with a high number of sessions being conducted. Interestingly, an increase in detection probability was noted for Sweep stimuli during the second time point, suggesting potential heightened awareness or attention to stimulus onset during re-testing. However, baseline data indicated an overall increase in mouse activity profiles at the second time point, suggesting that mice exhibited more escape and/or freezing behaviour even before stimulus presentation.

Further characterization of behavioural responses, showed that mice exhibited quicker responses to Loom stimuli during the initial exposure, indicating a potential adaptation or familiarisation effect during re-testing. However, no significant differences were observed for Sweep stimuli, suggesting that retesting had minimal impact on these parameters.

In conclusion, this Chapter findings demonstrate the feasibility and reliability of re-testing mice at multiple time points. These results suggest the establishment of a functional behavioural test for evaluating the efficacy of therapeutic interventions in retinal dysfunction models.

CHAPTER 4: The Influence of Sex, Age and Strain on visually evoked avoidance behaviour.

The purpose of this Chapter is to establish the potential impact of sex, age, and background strain in a longitudinal and cross-sectional approach. I seek to determine if and how these characteristics interact with and potentially modulate the avoidance responses triggered by visual stimuli and how these could shape the reliability of this tool as a pre-clinical behavioural assay to measure vision function in mice.

4.1 Effect of Sex on visually evoked ennate behaviours.

Sexual dimorphism, the distinctions in biological traits between males and females within a species, is a well-explored phenomenon and there is consensus on the existence of disparities between female and male brains across biochemistry, physiology, structure, and function, supported by studies in basic neuroscience (Becker et al., 2005; McCarthy et al., 2012; Panzica and Melcangi 2016). Despite the prevailing acceptance of these differences, research in neuroscience and pharmacology using non-human mammals generally lacks comparison of male and female subjects, and the literature includes about five studies exclusively using male subjects for every one study exclusively using female subjects (Shansky and Woolley, 2016; Shansky, 2019). Sex-based divergences in sensory perception and behavioural responses have been documented across various species, spanning spatial navigation to social interactions (Mowrey and Portman, 2012; Cholerisa et al., 2017; Munion et al., 2019; Shaqiri et al., 2018).

Identification of any potential sex-dependent disparities is vital for experimental design and accurate result interpretation. Therefore, I prioritized addressing possible sex differences early in the project by analysing a reasonable number of mice from both sexes to shape the project accordingly. To address this question, I focused my analysis on the "Tonic," "Burst," and

"Optimised" protocols, which included male (n=20) and female (n=14) C57BL/6J mice (see **Table 1**). **Figure 14** summarises in the usual way responses to Loom and Sweep stimuli (and **Table 2**) among male and female mice. Overall response is strikingly similar across female and male subjects. For example, 89 % (242 / 272) of Loom trials evoked either freeze or escape response in female mice; and this was 88 % (287 / 326) in male mice. Advanced analysis yielded no difference between female and male mice, in the fraction of Loom trials that evoked escape (54% vs 54% trials respectively) or freezing response (40% vs 39%). Similarly, 87 % (245 / 282) of Sweep trials evoked a response in female mice and this was 86 %, (292 / 339) in male mice. Female mice were slightly more likely than male mice to freeze during Sweep (69% vs 59% respectively), and slightly less likely to escape (42% vs. 49%). Analysis of baseline activity (**Figure 14 C**) also showed no sex differences.

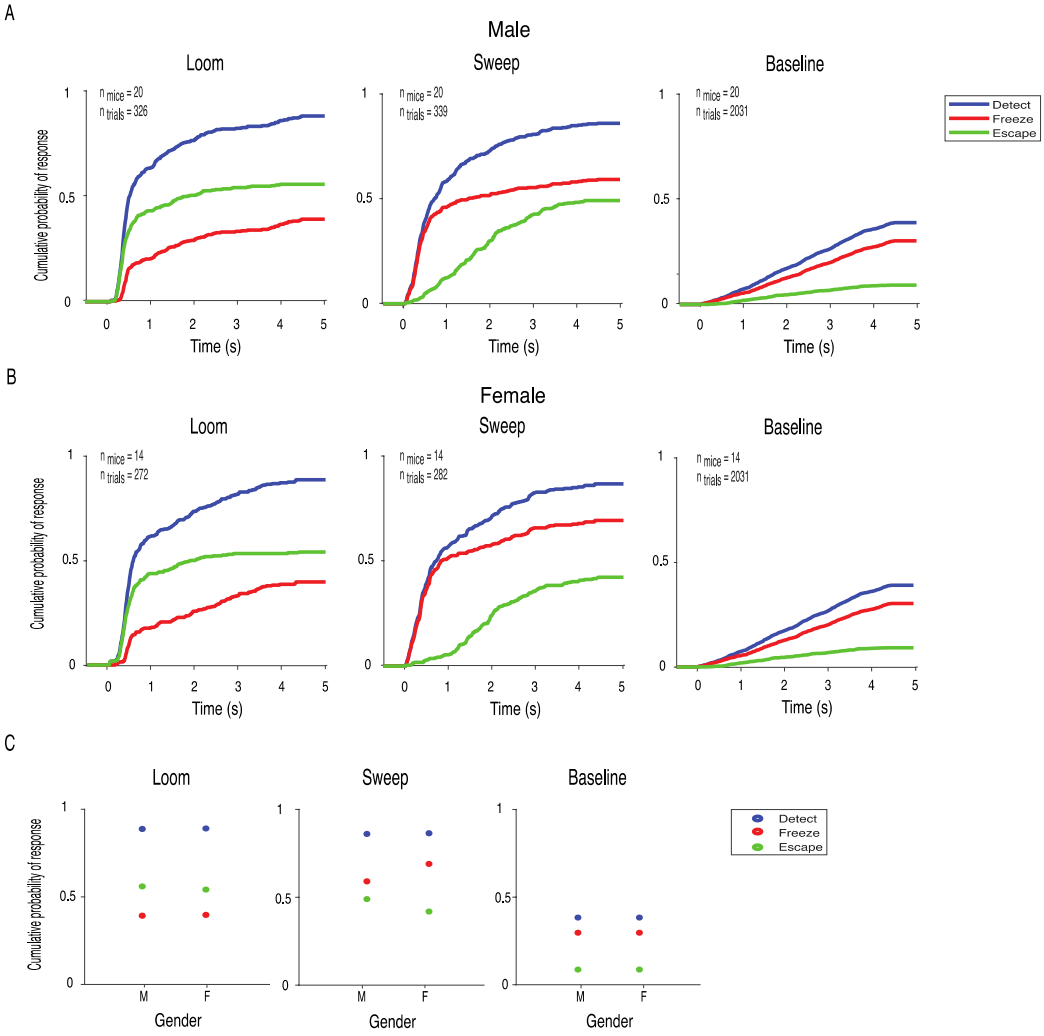

Figure 14*: Effect of sex on visually evoked innate responses.*

(A) Graphs representing the cumulative probability of having observed either an escape and/or freeze response (*blue*), an escape response (*green*) and a freeze response (*red*) over time for male mice. Cumulative probability of responses to (*Left*) Loom stimuli, (*Middle*) Sweep stimuli, and (*Right*) during baseline assessment where no visual stimuli was triggered. (B) Graphs representing the cumulative probability of having observed either an escape and/or freeze response (*blue*), an escape response (*green*) and a freeze response (*red*) over time for female mice. Cumulative probability of responses to (*Left*) Loom stimuli, (*Middle*) Sweep stimuli, and during (*Right*) baseline assessment where no visual stimuli was triggered. (C) Comparisons of the average cumulative probability of detecting either of the visual stimuli by having observed either an escape and/or freeze response (*blue*), an escape response (*green*) and a freeze response (*red*) in response to the stimuli. Cumulative probability of responses to (*Left*) Loom stimuli, (*Middle*) Sweep stimuli, and (*Right*) during baseline assessment where no visual stimuli was triggered.

4.1.1 Parameters of behaviour response.

Additional analyses of escape and freezing response latencies, maximum escape speed, and freeze duration (**Figure 15** and **Table 3**) showed no obvious differences for Loom (median escape latency: Female = 0.44 s, Male = 0.42 s; freeze latency: Female = 1.2 s, Male = 0.8 s; maximum escape speed: Female = 77.14, Male = 76.1; freeze duration: Female = 1.06 s, Male = 1.08 s) or Sweep (median escape latency: Female = 1.92 s, Male = 1.62 ; freeze latency: Female = 0.45 s, Male = 0.4 s; maximum escape speed: Female = 65.41, Male = 60.76; freeze duration: Female = 0.95s, Male = 1.13s). In summary, the responses to Loom and Sweep stimuli were strikingly similar across female and male subjects. There may be a minor difference in response to Sweep (**Figure 15** and **Table 3**), with females slightly more likely to freeze and less likely to escape (**Figure 15 C**), but my results indicate that sex is unlikely to be an experimental confound, I therefore proceeded with mixed cohorts in the remaining experiments in this chapter.

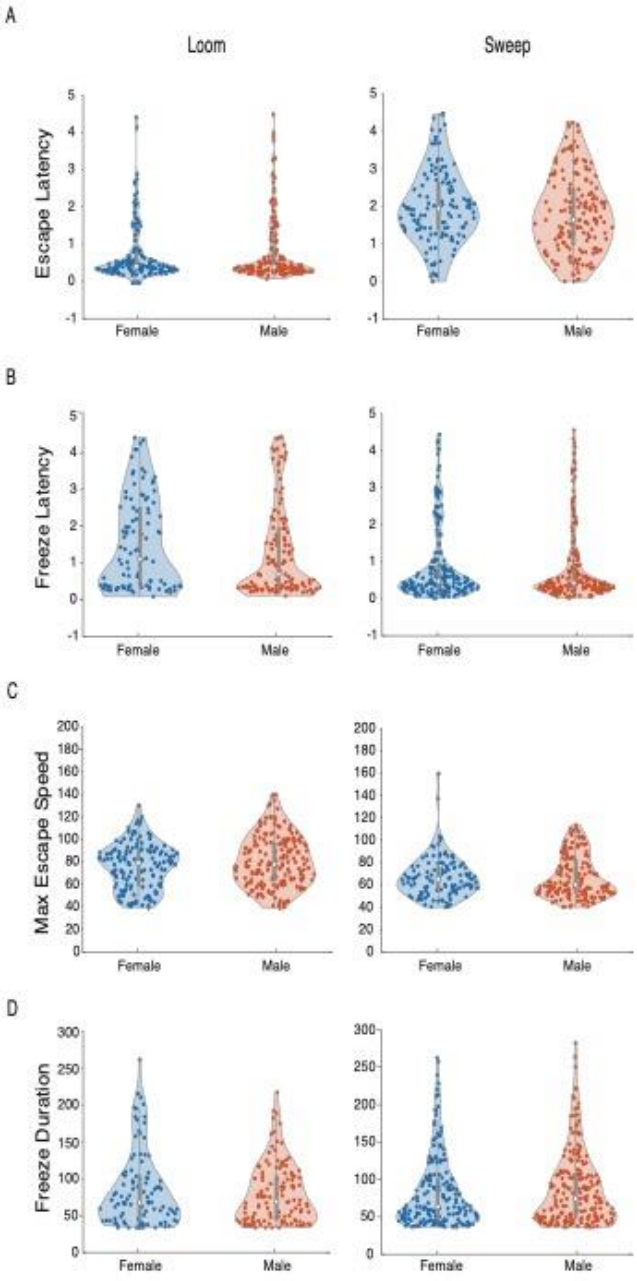

Figure 15: Effect of sex on the response characteristics of visually induced avoidance behaviours in mice.

Visual representation of the distribution and probability density of behavioural response characteristics: escape latency, freeze latency, maximum escape speed and freeze duration. Latency of escape and freezing responses were defined as the time between stimulus onset and the initiation of escape or freezing events, respectively. Peak escape speed was defined as the maximum speed achieved between the initiation of an escape response and freeze duration was defined as the time between the initiation and ceased of a freeze response. *Left Panel*: Violin plots of the distribution and probability density of behavioural response characteristics: escape latency (A), freeze latency (B), maximum escape speed (C) and freeze

duration (D) for male and female mice to Loom stimuli. *Right Panel:* Violin plots of the distribution and probability density of behavioural response characteristics: escape latency (A), freeze latency (B), maximum escape speed (C) and freeze duration (D) for male and female mice to Sweep stimuli.

4.2 Effect of Age on Visually Evoked Innate Behaviour

Age can significantly impact on an individual's perception, cognition, and responses to the environment (Andersen, 2012; Roberts and Allen, 2016; Ferreira et al., 2023). The process of aging affects the structure and function of the brain, along with its interconnected sensory, motor, and cognitive processes leading to age-related behavioural impairments. Increasing research efforts have been directed towards comprehending the ramifications of the aging process on visual function, predominantly focussing on age-related impairments of visual perception, with specific attention to basic elements of vision like orientation, contrast sensitivity, and spatial frequency (Andersen, 2012). Moreover, various cell types comprising the retina experience selective age-related alterations, which may contribute to decline in visual acuity (Samuel et al., 2011; Sugita et al., 2020; Zhu et al., 2023).

Such age-related alterations must be understood if these visually evoked innate responses are be used as a behaviour tool to access vision function in mouse models of progressive retinal diseases and evaluate the effect of therapeutic treatments over time. Here, I assessed whether age affects the avoidance responses triggered by Loom and Sweep visual stimuli, using a longitudinal approach to examine how age-related changes manifest over time within individual mice, and, in parallel, a cross-sectional approach, to assess how naïve mice at different ages respond when subjected to the same visual stimuli.

4.2.1 Longitudinal study.

Despite all efforts to maintain consistency with respect to where these experiments were conducted, unforeseen circumstances, including the COVID-19 pandemic and a subsequent move of laboratories between universities, made it necessary to conduct some of these experiments in different locations. This change was a result of the commitment to progress with our experiments under challenging conditions and timelines. I acknowledge the potential impact that this change in experimental locations may have on my research (also discussed in Chapter 3). In the interests of full transparency, we have clearly indicated in the summary **Table 1** the instances where experiments were conducted in different sites. This will allow readers to consider any variations that may arise due to these changes in experimental environments. Careful measures were taken to ensure that animals were only allocated to an experimental cohort approximately four months after the animals were transferred to King's College London (KCL). This extended acclimatization period was implemented to allow the mice sufficient time to adapt to their new environment and to minimize any potential confounding factors related to the site change.

A total of 11 wildtype (C57BL/6J) mice were randomly allocated to the longitudinal study at 21 days of age. Of these, 5 mice begun testing at UCL and moved to KCL, while the remaining 6 underwent testing entirely at KCL. I have opted to present the results together, but the reader should note that effects may relate to the change in site location. As detailed in **Table 1**, we performed experiments at several time points, including 21 days, and 1, 2, 6 and 12 months. Note that the 6-month time point coincided with the transition between universities, and due to access constraints imposed by the COVID-19 pandemic, we were unable to perform experiments at this specific time point for the 5 mice that began the study at UCL, resulting in a lower sample size for this time point. Nevertheless, we recorded data for the 12-month time point for these mice at KCL, and this data is included in the overall analysis, as summarized in **Figure 16 D**. I have chosen to graphically display the time points that we found particularly interesting and that contribute novelty to this

chapter; these are 21 days, 6 months, and 12 months. However, all the data for all time points are displayed in **Table 2**.

Mice were first exposed to Loom and Sweep visual stimuli at 21 days of age (**Figure 16 A**). These young mice exhibited the expected array of behavioural responses (escape, freeze, or a combination of both) when presented with either Loom or Sweep, but the distribution of responses was different to that of older animals. First, we found responses to 75 % (83 / 11) Loom trials, but a notably lower-than-expected 60 % (70 / 117) for Sweep. Second, finer analysis showed that Loom evoked freezing behaviours in 55 % (61 / 110) trials, and escape on only 20 % (22 / 110) (**Figure 16 A**). Third, we found episodes of freezing, in 51 % (60 / 117) of Sweep trials, but escape was rare, observed in only 11 % (13 / 117) (**Figure 16 A**). Thus, young mice display distinct behavioural responses to Loom and Sweep stimuli, compared to the 6–8-week-old mice examined in Chapter 3 and earlier in this Chapter.

As mentioned above, it was not possible to record the 6-month time point for 5 of the cohort (**Figure 16 B**) as this coincided with the transition between universities and the relocation of mice from UCL to KCL. The smaller cohort of 6 mice housed only at KCL are shown here. As shown in **Figure 17** and further elaborated in **Table 2,** these mice exhibited distinctive responses. The probability of detection was 76 % for Loom (38 / 50 trials) and 83 % for Sweep (48 / 58) (**Figure 16 B**). Analysing specific behaviours **Figure 16 B**, we found strong escape-base response to Loom in the 6-month-old mice (60%; 30 / 50), and low probability of a freeze response (16 %; 8 / 50). Similarly, Sweep stimuli also evoked a strong probability of escape (66 %; 38 / 58) (**Figure 16 B)**. Indeed, escape responses were the most frequently observed behaviour exhibited by the 6-month-old mice.

The oldest age examined was 12 months. These assessments were conducted at KCL and included the 5 mice whose experiments had commenced at UCL and were transferred to KCL (see **Table 1**). All mice demonstrated a robust capability to detect both Loom and Sweep stimuli, responding on an 83 % (38 / 46 trials) and 79 % (38 / 48) to Loom and Sweep, respectively. Closer analysis, however, revealed, marked absence of escape

responses in these older mice in response to both types of visual stimuli (**Figure 16 C**); instead, the predominant response was to freeze, possibly reflecting age-related effects on their mobility capabilities. For Loom, only two escape responses were observed (0.04 %, 2 / 46), while freezing was common (78%; 36 / 46) (**Figure 16 C)**. Similarly, Sweep usually evoked freeze response (77 %, 37 / 48), and only one escape response was observed.

Figure 16 D summarises responses across all the time points. Escape behaviour is rare at the earliest time point (21 days), gradually increasing as mice age, peaking at 6 months, then dropping markedly between 6 and 12 months, such that older mice exhibit few or no escape responses. This trend is consistent for both types of visual stimulus. In contrast, freezing behaviours are consistent before declining at 6 months, then increasing at 12 months. It is worth noting that the 6-month time point appears somewhat inconsistent in terms of escape and freeze responses, likely attributed to the lower number of animals tested under this protocol, so some caution is advised. Interestingly, however, a similar trend is observed even at baseline, where escape type behaviours are increasingly observed as mice mature, peaking at 2-6 months, and then declining in older age. Freezing behaviours follow an opposing trajectory, with mice exhibiting more freezing at earlier and later developmental stages.

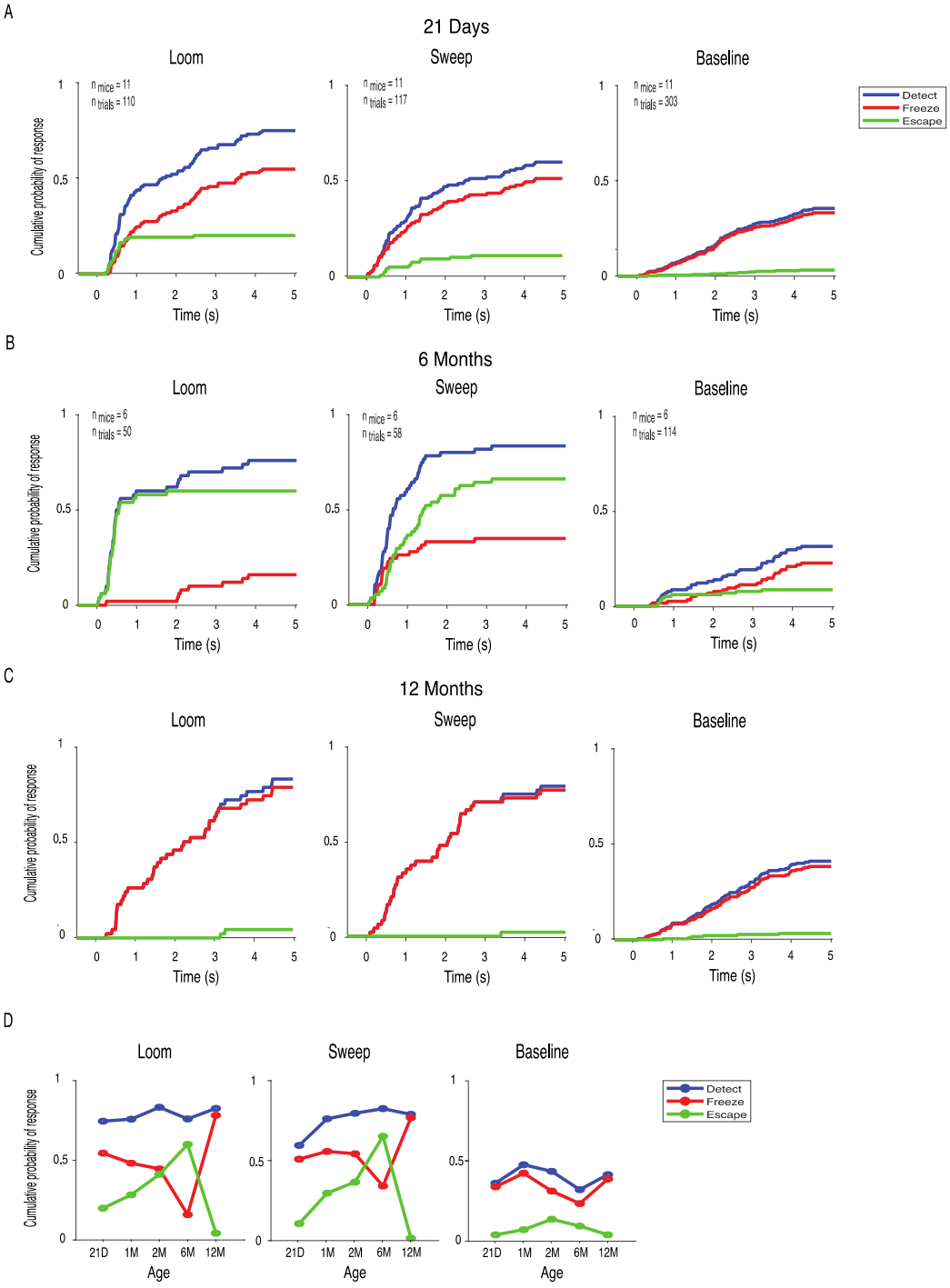
A
21 Days
Loom
Sweep
Baseline
n mice = 11
n trials = 110
n mice = 11
n trials = 117
n mice = 11
n trials = 303
Detect
Freeze
Escape
Cumulative probability of response
Time (s)
B
6 Months
Loom
Sweep
Baseline
n mice = 6
n trials = 50
n mice = 6
n trials = 58
n mice = 6
n trials = 114
C
12 Months
Loom
Sweep
Baseline
D
Loom
Sweep
Baseline
Detect
Freeze
Escape
Cumulative probability of response
21D
1M
2M
6M
12M
Age

Figure 16: Effect of Age on Visually Evoked Innate Behaviours - Longitudinal approach.

(A) Graphs representing the cumulative probability of having observed either an escape and/or freeze response (blue), an escape response (green) and a freeze response (red) over time for the 21 days' time point. Cumulative probability of responses to (Left) Loom stimuli, (Middle) Sweep stimuli, and (Right) during baseline assessment where no visual stimuli was triggered. (B) Graphs representing the cumulative probability of having observed either an escape and/or freeze response (blue), an escape response (green) and a freeze response (red) over time for the 6 months' time point. Cumulative probability of responses to (Left) Loom stimuli, (Middle) Sweep stimuli, and (Right) during baseline assessment where no visual stimuli was triggered. (C) Graphs representing the cumulative probability of having observed either an escape and/or freeze response (blue), an escape response (green) and a freeze response (red) over time for the 12 months' time point. Cumulative probability of responses to (Left) Loom stimuli, (Middle) Sweep stimuli, and (Right) during baseline assessment where no visual stimuli was triggered. (D) Comparisons of the average cumulative probability of detecting either of the visual stimuli by having observed either an escape and/or freeze response (blue), an escape response (green) and a freeze response (red) in response to the stimuli for all the time points taken in account in the longitudinal study: 21 days, 1, 2, 6 and 12 months. Cumulative probability of responses to (Left) Loom stimuli, (Middle) Sweep stimuli, and (Right) during baseline assessment where no visual stimuli was triggered.

4.2.1.1 Parameters of Behaviour Response

Additional analyses of behavioural parameters suggested little change across age (**Figure 17**). For Loom, median escape latency was preserved across the first 6 months (21D = 0.44 s, 1M = 0.44 s, 2M = 0.45 s, 6M = 0.38 s, 12M = 3.21 s), while median freeze latency (21D = 1.14 s, 1M = 1.95 s, 2M = 2.24 s, 6M = 2.17 s, 12M = 1.64 s), showed a slight difference only between 21 days and 2 months (ANOVA: 21 days vs 2 months p = 0.011) (**Figure 17 B**). No significant differences were observed in maximum escape speed (21D = 69.32, 1M = 81.96, 2M = 79.87, 6M = 76.92, 12M = 53.46) or freeze duration (21D = 1.27 s, 1M = 1.12 s, 2M = 0.96 s, 6M = 0.88 s, 12M = 1.37s) (**Figure 17 C and D**). The picture was similar for Sweep, though median of escape latency (21D = 1.11 s, 1M = 0.45 s, 2M = 0.48 s, 6M = 0.35 s, 12M = 1.22 s) suggested older mice (12 months) took longer to initiate an escape response compared to younger age points (21 days and 6 months) (ANOVA: 21 days vs 6 months p = 0.036 ; 6 months vs 12 months p = 0.020) (**Figure 17 A**). Older

mice also took significantly longer to engage in a freeze response (median freeze latency: 21D = 0.987 s, 1M = 1.1 s, 2M = 1.13 s, 6M = 0.9 s, 12M = 2.89 s; multiple comparison of means ANOVA: 6 months vs 12 months p = 0.033) (**Figure 17 B**) No significant differences were observed in maximum escape speed (21D = 65.93, 1M = 72.72, 2M = 75.42, 6M = 79.78, 12M = 46.21) or in freeze duration (21D = 1.18 s, 1M = 1.05 s, 2M = 1.13 s, 6M = 0.88 s, 12M = 1.28 s).

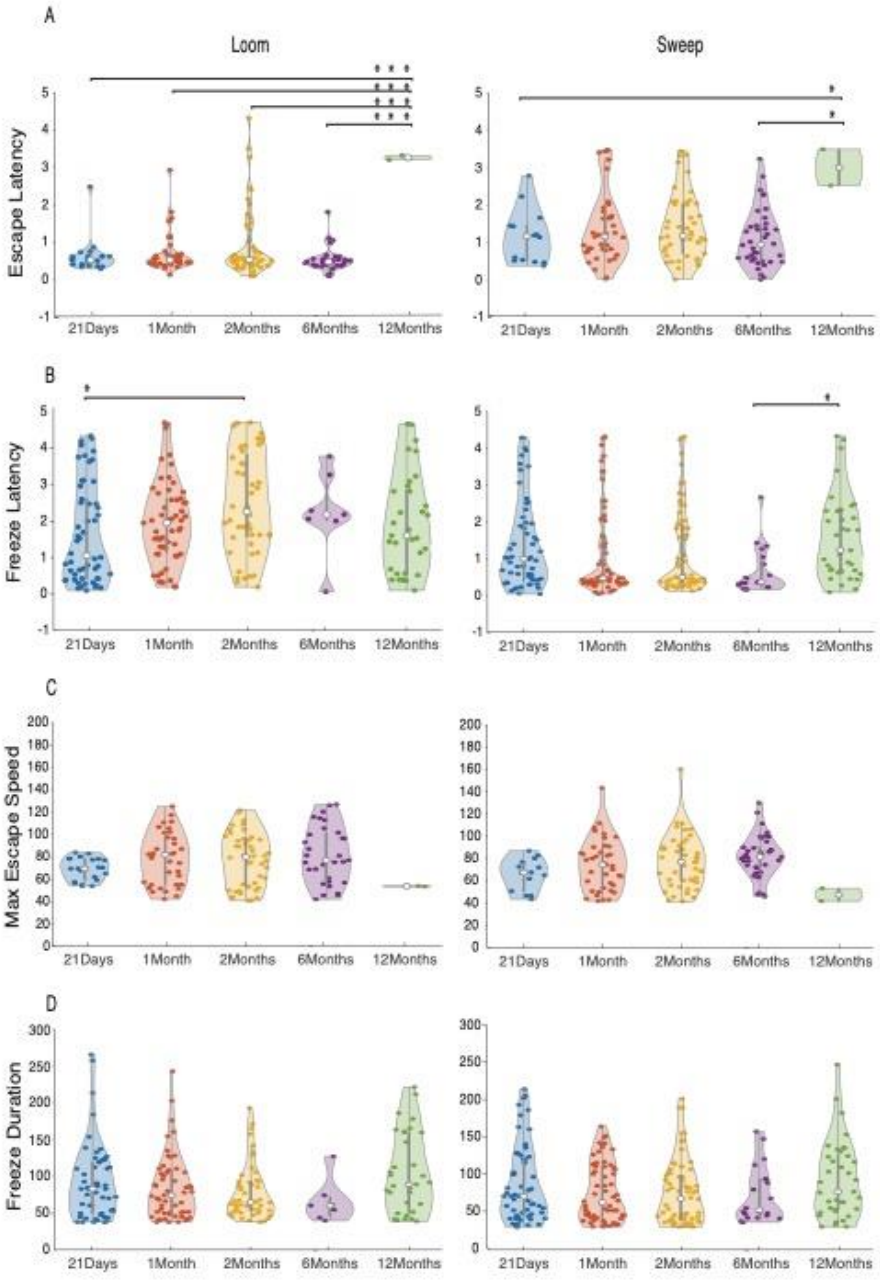
A
Loom
Sweep
Escape Latency
B
Freeze Latency
C
Max Escape Speed
D
Freeze Duration
21Days
1Month
2Months
6Months
12Months

Figure 17: Effect of age on the response characteristics of visually induced avoidance behaviours in mice - Longitudinal approach.

Visual representation of the distribution and probability density of behavioural response characteristics: escape latency, freeze latency, maximum escape speed and freeze duration. Latency of escape and freezing responses were defined as the time between stimulus onset and the initiation of escape or freezing events respectively. Peak escape speed was defined as the maximum speed achieved between the initiation of an escape response and, freeze duration was defined as the time between the initiation and ceased of a freeze response. Left Panel: Violin plots of the distribution and probability density of behavioural response characteristics: escape latency (A), freeze latency (B), maximum escape speed (C) and freeze duration (D) for 21 days, 1-, 2-, 6- and 12-months' time points to loom stimuli. Right Panel: Violin plots of the distribution and probability density of behavioural response characteristics: escape latency (A), freeze latency (B), maximum escape speed (C) and freeze duration (D) for 21 days, 1-, 2-, 6- and 12-months' time points to sweep stimuli. $p<0.05$= statistically significant *, $p<0.001$= highly significant ***

4.2.2 Cross-sectional study.

In addition to the longitudinal investigation, I conducted a cross-sectional study with independent cohorts of differently aged mice (ages as for the longitudinal study), each naïve at the time of testing. The cumulative probability of response data for all analysed time points is available in **Table 2**. Despite challenges incurred because of the COVID-19 pandemic and a change in universities, efforts were made to minimize the impact on the study. Instances of experimental site change are noted in the summary **Table 1**.

The 21-day group is the same cohort as used in the longitudinal study (**Figure 18 A)** and comprises 11 wildtype (C57BL/6JBL/6J) mice, 5 mice tested at UCL and 6 at KCL, and their response profile is described in detail above. In the cross-sectional study, 13 mice were assigned to the 6 months old cohort, with 9 mice tested at UCL and 4 at KCL, all subjected to identical visual stimuli (**Figure 18 B and Table 2**). As for the 6-month cohort in the longitudinal study, these mice exhibited a robust probability of detecting visual stimuli, reaching 80 % for both Loom (118 / 148 trials) and Sweep stimuli (118 / 147 trials). Analysis of specific behaviours showed low probability of escape response to Loom (36 %, 53 / 148), and higher likelihood of freeze responses

(53 %, 78 / 148). Similarly, freeze responses prevailed for Sweep (71 %, 105 / 148), with escape on 27 % (40 / 148). Taken together with the longitudinal study, comparison of 21 day and 6-month-old cohorts suggests an enhanced probability of detecting visual stimuli, especially Sweep, as age increased. However, 6-month-old mice in the cross-sectional study were less likely to escape than those in the longitudinal study, making comparison difficult.

Ten 12-month-old mice were assessed in this cross-sectional study (experiments all conducted at KCL). Consistent with the longitudinal study, these older mice maintained the ability to detect both Loom and Sweep, with escape and freeze responses observed in 73 % (84 / 115 trials) and 68 % (79 / 116), respectively (**Figure 18 C**). Analysing specific responses, 12-month-old mice were less likely to escape for both Loom and Sweep, similar to the 6-month cohort and consistent with observations from the longitudinal study (**Figure 16 C**). In the cross-sectional study, 12-month-old mice escaped on 23 % (26 / 115) of Loom trials, and freezing responses were more prevalent (51 %; 59 / 115). Similarly, Sweep elicited freezing on 60 % (70 / 116) trials, and few escapes (19%, 22 / 116). Thus, in this cross-sectional study, unlike in the longitudinal study, escape behaviour appears to diminish from 6-months.

Figure 18 D summarises the results of the cross-sectional study. Escape behaviour is low in young mice, increasing as mice mature and peaking at 2 months, before later exhibiting a progressive decrease in the amount of escape responses observed. This trend is consistent for both visual stimuli presented to the mice. In contrast, freezing behaviours are predominant in young mice, declining as they mature, before reasserting dominance at older (> 6 months) ages. Of note, at 15 months of age, only freezing responses were observed in response to Loom and Sweep. The baseline data suggests little change in mouse behaviour in the absence of visual stimulus.

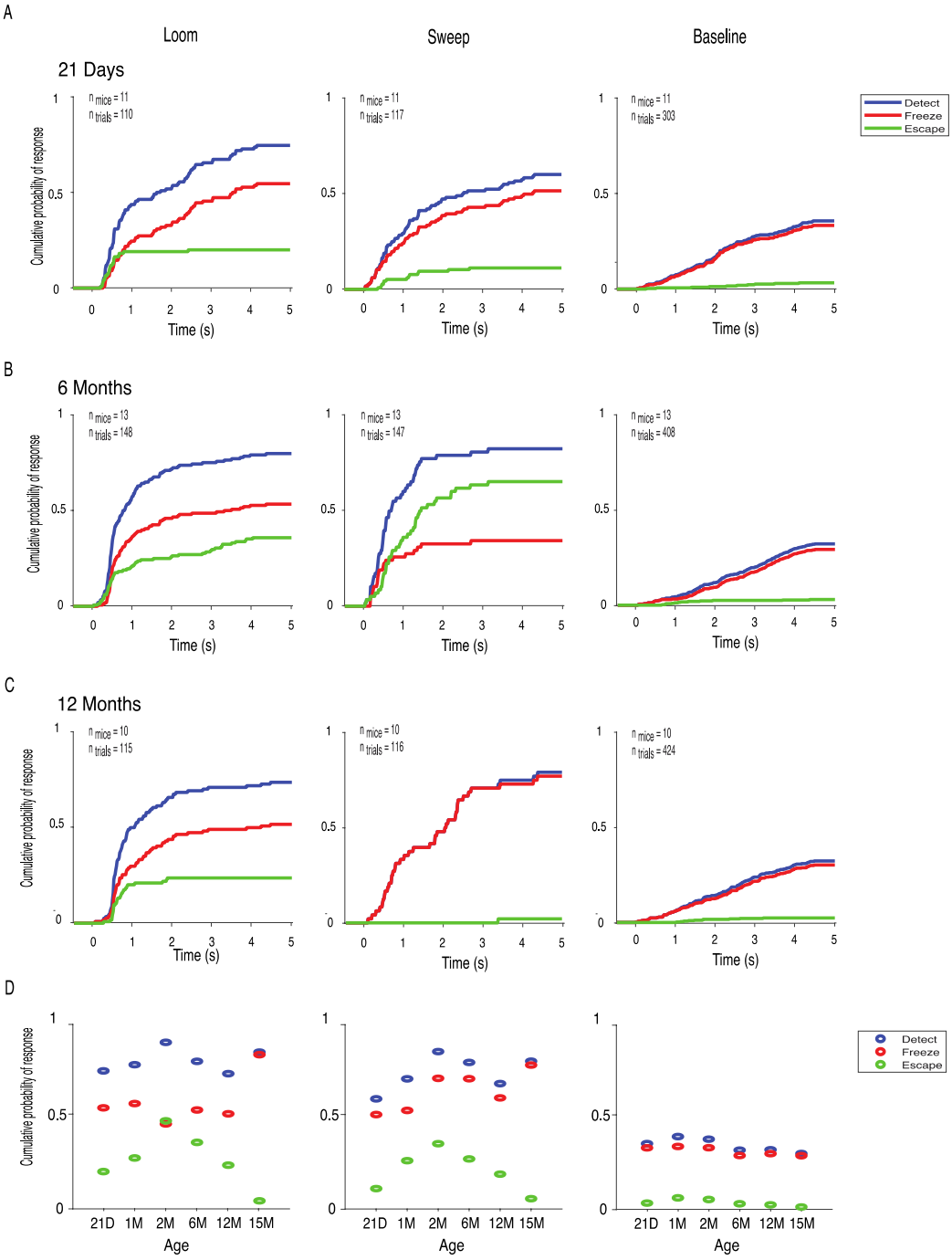
A
Loom
Sweep
Baseline
21 Days
n mice = 11
n trials = 110
n mice = 11
n trials = 117
n mice = 11
n trials = 303
Detect
Freeze
Escape
Cumulative probability of response
Time (s)
B
6 Months
n mice = 13
n trials = 148
n mice = 13
n trials = 147
n mice = 13
n trials = 408
C
12 Months
n mice = 10
n trials = 115
n mice = 10
n trials = 116
n mice = 10
n trials = 424
D
21D 1M 2M 6M 12M 15M
Age

Figure 18: Effect of age on visually evoked innate behaviours – Cross-sectional approach.

(A) Graphs representing the cumulative probability of having observed either an escape and/or freeze response (blue), an escape response (green) and a freeze response (red) over time for the 21 days' time point. Cumulative probability of responses to (Left) Loom stimuli, (Middle) Sweep stimuli, and (Right) during baseline assessment where no visual stimuli was triggered. (B) Graphs representing the cumulative probability of having observed either an escape and/or freeze response (blue), an escape response (green) and a freeze response (red) over time for the 6 months' time point. Cumulative probability of responses to (Left) Loom stimuli, (Middle) Sweep stimuli, and (Right) during baseline assessment where no visual stimuli was triggered. (C) Graphs representing the cumulative probability of having observed either an escape and/or freeze response (blue), an escape response (green) and a freeze response (red) over time for the 12 months' time point Cumulative probability of responses to (Left) Loom stimuli, (Middle) Sweep stimuli, and (Right) during baseline assessment where no visual stimuli was triggered. (D) Comparisons of the average cumulative probability of detecting either the visual stimuli by having observed either an escape and/or freeze response (blue), an escape response (green) and a freeze response (red) in response to the stimuli for all the time points taken in account in the longitudinal study: 21 days, 1, 2, 6, 12 and 15 months. Cumulative probability of responses to (Left) Loom stimuli, (Middle) Sweep stimuli, and (Right) during baseline assessment where no visual stimuli was triggered.

4.2.2.1 Parameters of behaviour response.

Consistent with the longitudinal study, there were significant differences in responses characteristics across age (**Figure 19**). Escape latency was variable but increased with age (21D = 0.44 s, 1M = 1.362 s, 2M = 0.44 s, 6M = 0.70 s, 12M = 0.74 s, 15M = 3.25 s); (ANOVA: 21 days vs 1 month p = 0.014, 21 days vs 6 months p = 0.011, 1 month vs 2 month p = 0.056, 1 month vs 15 months p = 0.039, 2 months vs 6 month p = 0.035, 6 months vs 15 months p = 0.012, 12 months vs 15 months p = 0.022) (**Figure 19 A**). Freeze latency was also variable with some indication of faster response at intermediate age (21D = 1.14 s, 1M = 0.72 s, 2M = 0.76 s, 6M = 0.63 s, 12M = 1.19 s, 15 M = 1.06 s); (ANOVA: 21 days vs 1 months p = 0.014, : 21 days vs 6 months p = 0.012 , 1 month vs 2 months p = 0.056, 1 month and 15 months: p = 0.039, 2 months vs 6 months p = 0.035, 6 and 12 months p = 0.012, 12 months and 15 months p = 0.022). No significant differences were observed in maximum escape speed (21D = 69.32, 1M = 55.89, 2M = 70.7, 6M = 62.02, 12M = 75.79, 15M = 54.16) or freeze duration (21D = 1.27 s, 1M = 1.18 s, 2M = 1.41 s, 6M

= 1.52 s, 12M = 0.83 s, 15M = 1.72 s) indicating consistent behavioural patterns (**Figure 19 C and D**).

Likewise, analysis of responses to Sweep (**Figure 19 Right panel**), were variable but suggest increase escaped latency with age (21D = 1.11 s, 1M = 1.85 s, 2M = 1.82 s, 6M = 2.07 s, 12M = 1.4 s, 15M = 3.41 s); (ANOVA: 21 days vs 1 months p =0.044, : 21 days vs 2 months p = 0.024 , 21 days vs 6 months p = 0.008, 1 month vs 15 months: p = 0.014, 2 months vs 15 months p = 0.008, 6 vs 15 months p = 0.021, 12 months and 15 months p = 0.000) (**Figure 19 A**). Freeze latency was shortest at intermediate ages (21D = 0.99 s, 1M = 0.89 s, 2M = 0.38 s, 6M = 0.5 s, 12M = 1.17 s, 15M = 0.921 s) (ANOVA: 21 days vs 2 months p =0.014, 21 days vs 6 months p = 0.037). The 12M group exhibited higher escape speed in response to sweep stimuli compared to the 1-, 2-, and 15-months groups, as depicted in the graph (**Figure 19 C**). Freeze duration was consistent across age (21D = 1.18 s, 1M = 0.92 s, 2M = 1.33 s, 6M = 1.43 s, 12M = 1.43, 15M = 1.46).

These longitudinal and cross-sectional investigations into the age-related effects on visually evoked innate behaviours in mice offer a critical foundation for designing interventional experiments with a temporal dimension. Remarkably, both longitudinal and cross-sectional approaches demonstrate similar response probabilities at earlier time points, namely 21 days, 1 month, and 2 months. However, distinctions arise between the approaches at the 6-month time point, possibly attributable to idiosyncratic differences that could contribute to group disparities. Based on the patterns observed at previous time points, one would anticipate a similar trajectory of behaviour, highlighting the importance of accounting for such nuances in experimental design and interpretation.

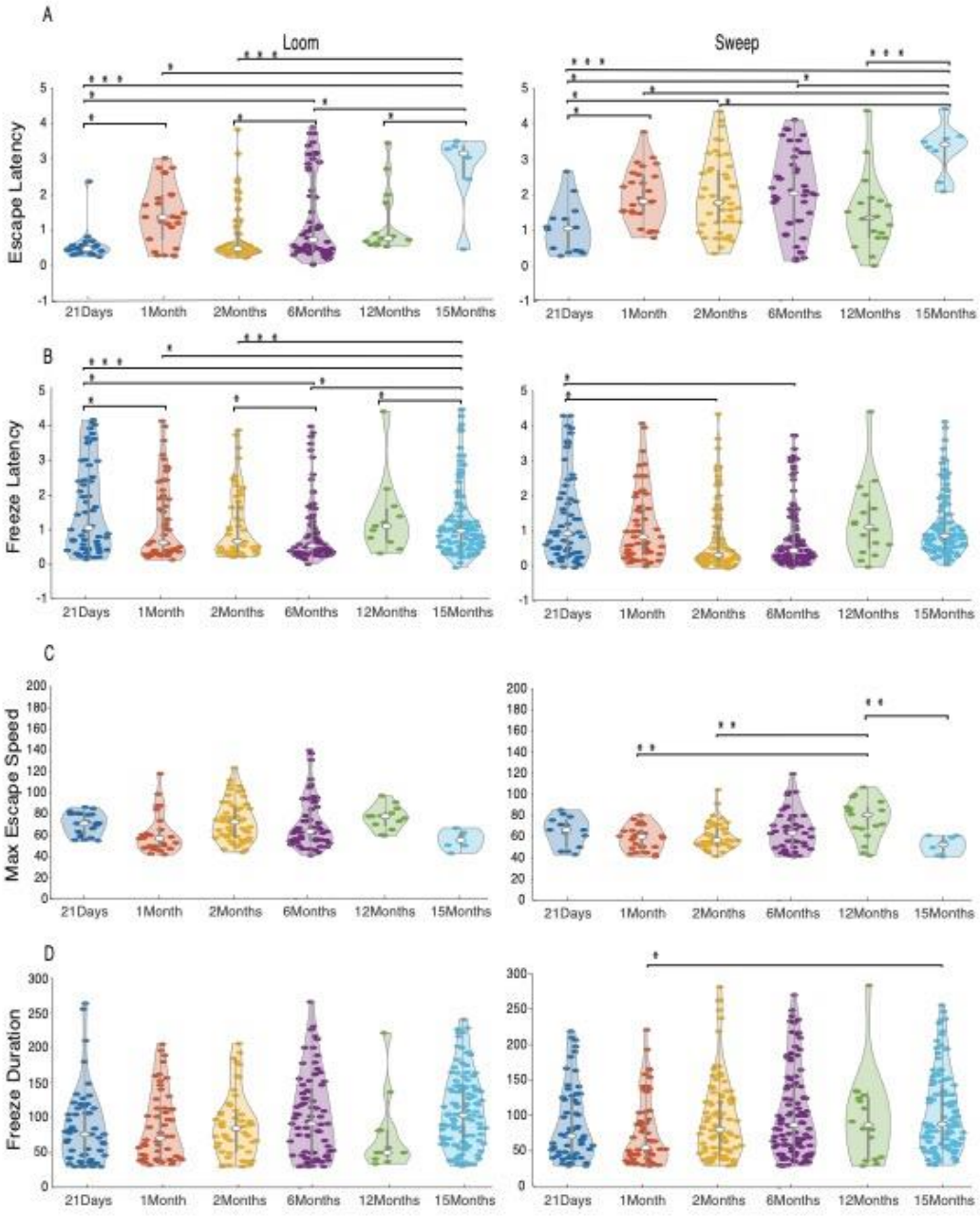
A
Loom
Sweep
Escape Latency
B
Freeze Latency
C
Max Escape Speed
D
Freeze Duration
21Days
1Month
2Months
6Months
12Months
15Months

Figure 19: Effect of age on the response characteristics of visually induced avoidance behaviours in mice – Cross-sectional approach.

Visual representation of the distribution and probability density of behavioural response characteristics: escape latency, freeze latency, maximum escape speed and freeze duration. Latency of escape and freezing responses were defined as the time between stimulus onset and the initiation of escape or freezing events respectively. Peak escape speed was defined as the maximum speed achieved between the initiation of an escape response and, freeze duration was defined as the time between the initiation and ceased of a freeze response. Left Panel: Violin plots of the distribution and probability density of behavioural response characteristics: escape latency (A), freeze latency (B), maximum escape speed (C) and freeze duration (D) for 21 days, 1, 2-, 6-, 12- and 15-months' time points to Loom stimuli. Right Panel: Violin plots of the distribution and probability density of behavioural response characteristics: escape latency (A), freeze latency (B), maximum escape speed (C) and freeze duration (D) for 21 days, 1, 2-, 6-, 12- and 15-months' time points to Sweep stimuli. $p<0.05$= statistically significant *, $p<0.005$ = very significant **, $p<0.001$= highly significant ***

4.3 Effect of wild-type mouse strains on visually evoked innate behaviours.

Experimental research utilises a range of inbred and outbred mouse strains. Mice share approximately 90 % of their genes with humans and ~85 % of the protein-coding region of the genome is conserved (Weitzman, 2002; Breschi et al, 2017), providing a robust model for investigating understanding human health and disease (Sultana et al, 2019). There are, however, multiple mouse strains used in pre-clinical work and behavioural assays can, in part, be influenced by the genetic background of the experimental animal, with subtle differences in behaviour known to exist between strains (Chang et al., 2002; Serpi et al., 2013; Sultana et al, 2019). Often, little consideration is given to the strain of 'wild-type' animal beyond it broadly matching the genetic background of a transgenic or mutant strain being used in an experimental context. Surprisingly few behavioural studies have compared the behaviours of the most commonly used 'wild-type' mouse lines.

Thus, when studying visually evoked avoidance behaviours, particularly when seeking to establish this as a tool to measure the benefit of therapeutics products to improve vision, understanding the potential impact of

such characteristics takes on a heightened significance. Here, I compared visually evoked innate behaviours in three commonly used wildtype or background stains for transgenic models: C57BL/6J, DBA1/J and 129/SV. Understanding the potential variations among wildtype strains is vital not only for advancing the accuracy and reliability of visually evoked behaviours in vision research, but also for broadening our understanding of the nuances in behaviours exhibited between strains.

Wild-type adult mice (2 ± 1 month old: see summary **Table 1** for details) were randomly allocated, regardless of sex. Note that the C57BL/6J cohort used here are a new, naïve cohort, to provide a fairer test by examining animals with equivalent experiences prior to onset of testing. **Figure 20** (and **Table 2** summarizes all the cumulative response probabilities) shows in the usual way responses to Loom and Sweep in the different strains. As before, this study was had to be performed across two sites (further details on summary **Table 1**). A total of 12 adult C57BL/6J mice (7 at UCL and 5 at KCL) were recorded, the group consisted of 8 male and 4 female mice. As expected from the results presented above, C57BL/6J mice (**Figure 20 A**) show escape and or freeze responses in Loom (90%; 198 / 220 trials) and Sweep (90%; 212 /235). Mice in this cohort showed similar propensity for escape and freeze response to Loom (escape: 50%, 110 / 220 trials; freeze: 48%, 106 / 220 trials), while Sweep was more likely to evoke freezing behaviour (escape: 48%, 113/235; freeze: 66 %, 155 / 235).

Nine DBA1/J mice (4 recorded at UCL and 5 at KCL, **Table 1**) were allocated to this study, of these 3 were male and 6 were female. This strain exhibited strikingly different behaviours even in the absence of visual stimuli, displaying minimal exploratory behaviour, often remaining stationary in a corner of the arena or, if venturing out, subsequently retreating to the nest for the entire session. This behaviour posed significant challenges in delivering stimuli and collecting data, reflected in the small sample size for this strain (just 36 Loom trials across 9 mice, out of a potential 216 trials). This minimal movement is reflected in the shaped of the baseline data trace, shown in **Figure 20 B**. Perhaps relatedly, DBA1/J mice assigned to this study

demonstrated a surprisingly low probability of detecting Loom (53 %, 19 / 36) **(Figure 20 B**).

Despite the limited chance to present and the reduced responses to visual stimuli, DBA1/J mice did still exhibit the characteristic responses to Loom stimuli (**Table 2**), escaping in 39% (14 / 36) of all Loom trials, and freezing in 17% (6 / 36) (**Figure 20 B**). Sweeps were more likely to evoke a response (80 %, 33 / 41 trials), indicating that most mice were able to detect the stimulus. Where mice responded, escape responses were seen in 44 % of all Sweep trials (18 / 41), and freeze responses accounted for 39 % (16 / 41) (**Figure 20 B and Table 2**).

The 129/SV wild-type mouse strain is widely used in research, particularly in the establishment of transgenic lines. Ten mice, 5 male and 5 female, were assessed (5 recorded at UCL and 5 at KCL, see summary **Table 1**). Similar to the DBA1/J strain, 129/SV mice exhibited reduced exploratory behaviour compared to the C57BL/6J, often staying in a corner or returning to the nest during the session, which posed challenges for stimulus delivery and data collection. In the absence of stimulus, the baseline data (**Figure 20 C**) indicates that this strain's general behaviour closely resembled that of the C57BL/6J strain. Moreover, as shown in **Figure 20 C** (**Table 2**), 129/SV mice could detect both types of visual stimuli, with response rates (Loom: 89 %, 34 / 38; Sweep: 94 %, 45 / 48) similar to that observed for the C57BL/6J strain.

Finer analysis showed Loom evoked more escape responses (58 %, 22 / 38) than freeze (37 %, 14 / 38). As illustrated in **Figure 20 C**, we often observed freeze followed by escape behaviour in these animals. Interestingly, Sweep (**Figure 20 C**), which typically initiates freezing behaviours in C57BL/6Jmice, often evoked escapes in 129/SV mice: escape responses were observed in 73 % (35 / 48), while freezing behaviour occurred in 33 % (16 / 48). Thus, escape behaviour was noticeably more pronounced in these mice compared to the other two strains.

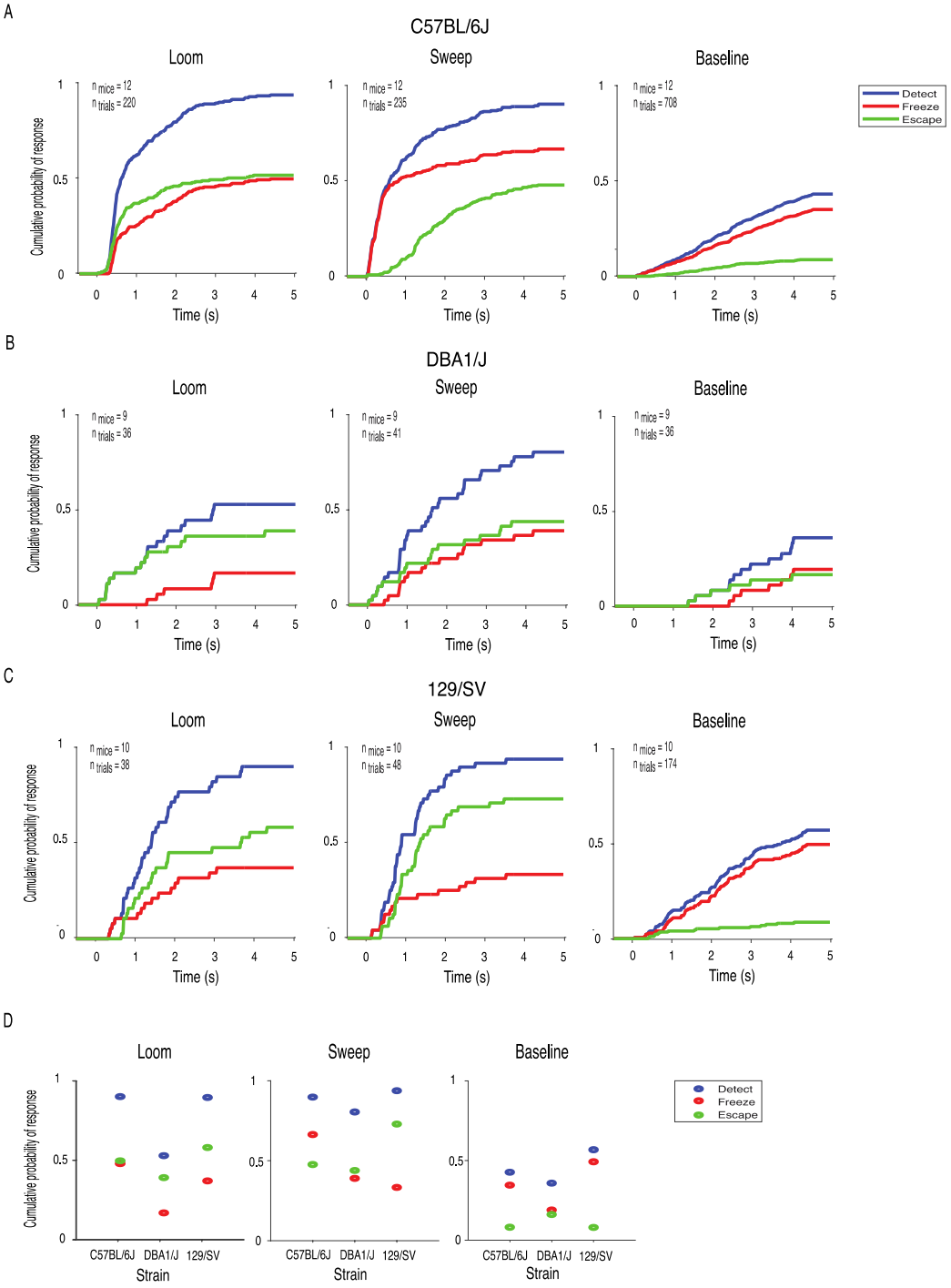
A
C57BL/6J
Loom
Sweep
Baseline
n mice = 12
n trials = 220
n mice = 12
n trials = 235
n mice = 12
n trials = 708
Detect
Freeze
Escape
Cumulative probability of response
Time (s)
B
DBA1/J
Loom
Sweep
Baseline
n mice = 9
n trials = 36
n mice = 9
n trials = 41
n mice = 9
n trials = 36
C
129/SV
Loom
Sweep
Baseline
n mice = 10
n trials = 38
n mice = 10
n trials = 48
n mice = 10
n trials = 174
D
Loom
Sweep
Baseline
C57BL/6J DBA1/J 129/SV
Strain

Figure 20: Effect of wild-type mouse strains on visually evoked innate behaviours.

(A) Graphs representing the cumulative probability of having observed either an escape and/or freeze response (blue), an escape response (green) and a freeze response (red) over time for the C57BL/6J mouse strain. Cumulative probability of responses to (Left) Loom stimuli, (Middle) Sweep stimuli, and (Right) during baseline assessment where no visual stimuli was triggered. (B) Graphs representing the cumulative probability of having observed either an escape and/or freeze response (blue), an escape response (green) and a freeze response (red) over time for 129/SV mouse strain. Cumulative probability of responses to (Left) Loom stimuli, (Middle) Sweep stimuli, and (Right) during baseline assessment where no visual stimuli was triggered. (C) Graphs representing the cumulative probability of having observed either an escape and/or freeze response (blue), an escape response (green) and a freeze response (red) over time for the DBA1/J mouse strain. Cumulative probability of responses to (Left) Loom stimuli, (Middle) Sweep stimuli, and (Right) during baseline assessment where no visual stimuli was triggered. (D) Comparisons of the average cumulative probability of detecting either the visual stimuli by having observed either an escape and/or freeze response (blue), an escape response (green) and a freeze response (red) in response to the stimuli for all the wild-type strains analysed: C57BL/6J, 129/SV, DBA1/J. Cumulative probability of responses to (Left) Loom stimuli, (Middle) Sweep stimuli, and (Right) during baseline assessment where no visual stimuli was triggered.

4.3.1 Parameters of behaviour response

In-depth analysis of the distribution and probability density of escape and freezing response latencies, maximum escape speed, and freeze duration revealed notable differences between the three wild-type strains (**Figure 21** and **Table 3**). However, it's important to note that the data points for the 129/SV and DBA1/J mouse lines were limited in number, potentially impacting the statistical significance of the observed differences, especially for the DBA1/J line. Further studies with increased sample sizes are warranted to validate these findings.

For Loom, significant differences emerged in escape latency (C57BL/6J= 0.52 s, DBA1/J = 0.82, 129/SV = 1.42), particularly between C57BL/6J and 129/SV (ANOVA: $p = 0.0001$). DBA1/J strains took longer to engage both in escape response (**Figure 21 A**) and freeze responses (C57BL/6J= 0.79 s, DBA1/J= 2.87, 129/SV = 1.72), compared to C57BL/6J (ANOVA: $p = 0.0348$) (**Figure 21 B**). C57BL/6J also typically ran faster than 129/SV during escape (C57BL/6J= 64.81, DBA1/J = 58.27, 129/SV = 57.24)

(ANOVA: p = 0.0004). Freeze duration (C57BL/6J= 1.12 s, DBA1/J = 0.97 s, 129/SV = 1.13 s) was consistent across strains (**Figure 21 C and D**). For Sweep, C57BL/6J were instead typically slowest to escape (C57BL/6J= 1.62, DBA1/J = 1.26, 129/SV = 1.16) (for C57BL/6J vs.129/SV ANOVA: p = 0.008) (**Figure 21 A**) but fastest to freeze (C57BL/6J= 0.34, DBA1/J = 1.81, 129/SV = 0.75) (C57BL/6J vs.129/SV ANOVA: p = 0.0085 , C57BL/6J vs. DBA1/J ANOVA: p = 0.0000). In this case C57BL/6J ran slower during escape than other strains (C57BL/6J= 59.03, DBA1/J= 65.24, 129/SV = 63.35; C57BL/6J vs. DBA1/J ANOVA: p = 0.0086) (**Figure 21 C**). Freeze duration (C57BL/6J= 1.23, DBA1/J= 0.78, 129/SV = 1.01) was similar across strains (**Figure 21 D**).

To summarise, I investigated the effect of different genetic background on visually triggered innate behavioural responses. I found reduction in exploratory behaviour in DBA1/J mice, and 129/SV mice but the latter still responded well to Loom and Sweep. Distinct differences in escape and freeze latencies, maximum escape speed, and freeze duration highlight strain-specific variations, contributing to a comprehensive understanding of how genetic factors shape diverse responses to visual stimuli in mice.

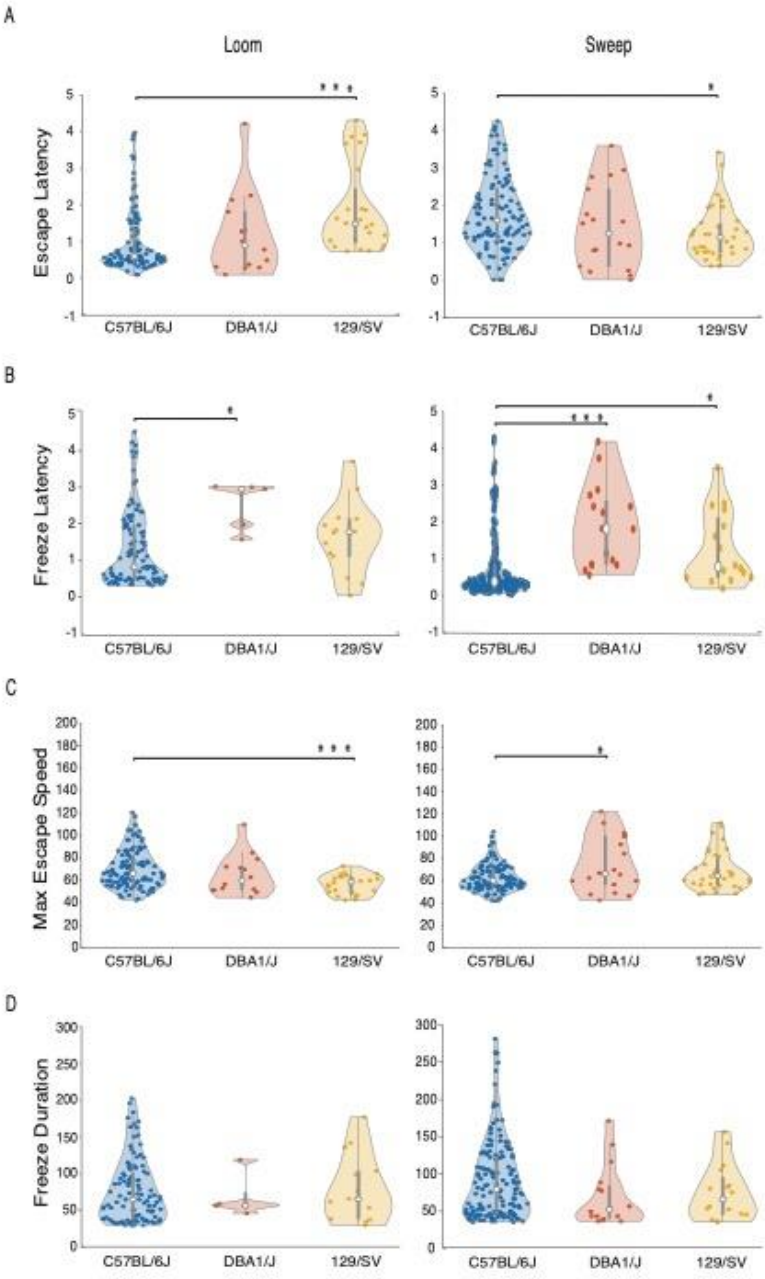
A
Loom
Sweep
Escape Latency
B
Freeze Latency
C
Max Escape Speed
D
Freeze Duration
C57BL/6J
DBA1/J
129/SV

Figure 21: Effect of wild-type mouse strains on the response characteristics of visually induced avoidance behaviours in mice.

Visual representation of the distribution and probability density of behavioural response characteristics: escape latency, freeze latency, maximum escape speed and freeze duration. Latency of escape and freezing responses were defined as the time between stimulus onset and the initiation of escape or freezing events respectively. Peak escape speed was defined as the maximum speed achieved between the initiation of an escape response and, freeze duration was defined as the time between the initiation and ceased of a freeze response. Left Panel: Violin plots of the distribution and probability density of behavioural response characteristics: escape latency (A), freeze latency (B), maximum escape speed (C) and freeze duration (D) for all the wild-type strains analysed: C57BL/6J, 129/SV, DBA1/J to Loom stimuli. Right Panel: Violin plots of the distribution and probability density of behavioural response characteristics: escape latency (A), freeze latency (B), maximum escape speed (C) and freeze duration (D) for all the wild-type strains analysed: C57BL/6J, 129/SV, DBA1/J to Sweep stimuli. $p<0.05$= statistically significant *, $p<0.001$= highly significant ***

4.4 Conclusion.

In this Chapter, I provide a comprehensive examination of the impact of sex, age and strain on visually evoked avoidance behaviours. This careful exploration is vital in the context of using visually evoked avoidance behaviours as a tool to measure therapeutic benefits for improving vision in mice and provides important information about the interactions between these characteristics and mouse behaviour more broadly.

I found that male and female mice exhibit comparable behavioural responses to visual stimuli. Indeed, the consistency of the data across the two sexes highlights the reliability and consistency of the observed visual responses within an age-matched and strain-matched cohort.

The exploration into age-related effects presents a nuanced understanding of how mice respond to visual stimuli at different developmental stages. Both the longitudinal and cross-sectional studies revealed significant alterations in behavioural profiles as mice age, with initial increases and later decreases in escape behaviour and the converse pattern for freezing

behaviours. Careful characterisation of the more subtle changes in escape and freeze response latencies, maximum escape speed, and freeze duration contribute to a robust framework for studying vision in mice, considering the evolving nature of responsiveness with age.

The investigation into the effect of genetic background further adds to the complexity, revealing strain-specific behavioural patterns and variations in responses to visual stimuli. These findings contribute to a comprehensive framework for assessing visual function in mouse models, crucial for understanding ocular disease progression and evaluating potential therapeutic strategies. Moreover, they underscore the importance of considering strain-specific differences and their impact on the reliability and accuracy of behavioural neuroscience-based research and provides researchers with valuable insights for comparing and interpreting results across different strains. In conclusion, this chapter offers a comprehensive understanding of the complex interplay between age, sex, genetics, and environmental factors, contributing significantly to the broader scientific community's knowledge in this intriguing field.

CHAPTER 5: The relative contributions of photosensitive cells in sculpting visually evoked avoidance behaviour.

In the intricate realm of neurobehavioral studies, understanding the intricate interplay between sensory input and behavioural responses is fundamental. This chapter asks how different photosensitive cells – rod and cone photoreceptors, and melanopsin-containing intrinsically photosensitive retinal ganglion cells - sculpt visually evoked avoidance behaviour in mice. To address this, I investigated the behaviour of well-characterized mouse models harbouring mutations in different components of phototransduction. Cohorts of 2 ± 1 months *Gnat1*$^{-/-}$ (herein called GNAT1, n=6 ; a non-degenerative model of stationary night blindness, in which the rod photoreceptors are stable but non-functional, and cones are unaffected), *Cnga3*$^{-/-}$ (herein called CNGA3, n=8 ; a model where cones are non-functional and die within 3 months, but the rods are unaffected) and *Gnat1*$^{-/-}$*x Cnga3*$^{-/-}$ *x Opn4*$^{-/-}$ (herein called OGC; triple-knockout mouse model in which both rods and cones are non-functional, in addition to the light-sensitive melanopsin (m)RGCs), alongside wild-type C57BL/6J (n=7) (please see **Table 1** for details), were exposed to Sweep and Loom stimuli under scotopic and photopic conditions following appropriate dark/light adaptation.

To establish the contribution of different photoreception mechanisms under both photopic and scotopic light conditions, we adjusted the design to make measurements during three sessions in photopic light levels (mean luminance 30 to 40 candela/m^2), and three sessions in scotopic levels (mean luminance 0.1 candela/m^2). Each mouse was randomly assigned, either tested initially under scotopic levels, and under photopic levels on the subsequent day; or tested first under photopic and then under scotopic.

5.1 Photopic responses.

Figure 22 and **Table 2** summarizes, in the usual way, the responses to Loom and Sweep under photopic light levels. CNG3A mice (**Figure 22 A**) showed robust responses to both Loom (93%, 28 / 30 trials) and Sweep (97%, 36 / 37). This suggests rod pathways can support these behaviours under photopic conditions, at least when the cone pathway is compromised. In response to Loom, CNG3A mice exhibited a remarkably high escape probability of 93% (28 / 30 trials), and no freeze responses were observed (**Figure 22 A**). Escape behaviour was also the predominant response to Sweep (78 %, 29/37 of Sweep trials), but Sweep also triggered freeze responses (35%, 13/37 trials).

I made counterpart measurements in 2-month-old (see Summary Table for details) GNAT1 mice, in which the rod pathway is disrupted (**Figure 22 B**). GNAT1 mice were able to detect Loom (63%,19/30 trials) and Sweep (71 %, 22 / 31). GNAT1 mice showed a mixture of freeze (37 %, 11 / 30), and escape responses (27 %, 8 / 30) to Loom, while Sweep elicited more freezing (52%, 16/31) than escape responses (29 %, 9 / 31).

I also made measurements from OGC triple-knockout mice, in which all photosensitive cells are disrupted, including melanopsin, rod, and cone cells. OCG mice showed a reduced ‘detection rate’ for both Loom (58 %, 26 /4 5) and Sweep (70 %, 32 / 46) stimuli. Moreover, all of these events exhibited ‘freezing’ behaviour and there was no evidence of escape responses in these mice. In addition, the cumulative probability of ‘freezing’ behaviour in baseline measurements (**Figure 22 C**) are higher than observed for wild-type strains. Thus, we find no clear response to visual stimuli in OGC mice, as expected.

The control C57BL/6Jmice exhibited responses consistent with previous findings in this thesis. This alignment was expected, given that all experiments thus far were performed under a consistent mean luminance of 30 to 40 candela/m^2 (photopic light levels). In this study, C57BL/6J mice demonstrated a 76 % detection rate for Loom stimuli (26 / 34) and a 79 %

detection rate for Sweep stimuli (30 / 38). Escape responses were predominant, particularly in reaction to Loom stimuli (41 %, 14 / 34 trials), with a lower proportion of trials resulting in freezing responses (35 %, 12 / 34 trials). As expected, Sweep stimuli elicited freezing behaviour in most trials (50%, 19 / 38), while also inducing escape responses in 47 % of trials (16 / 25).

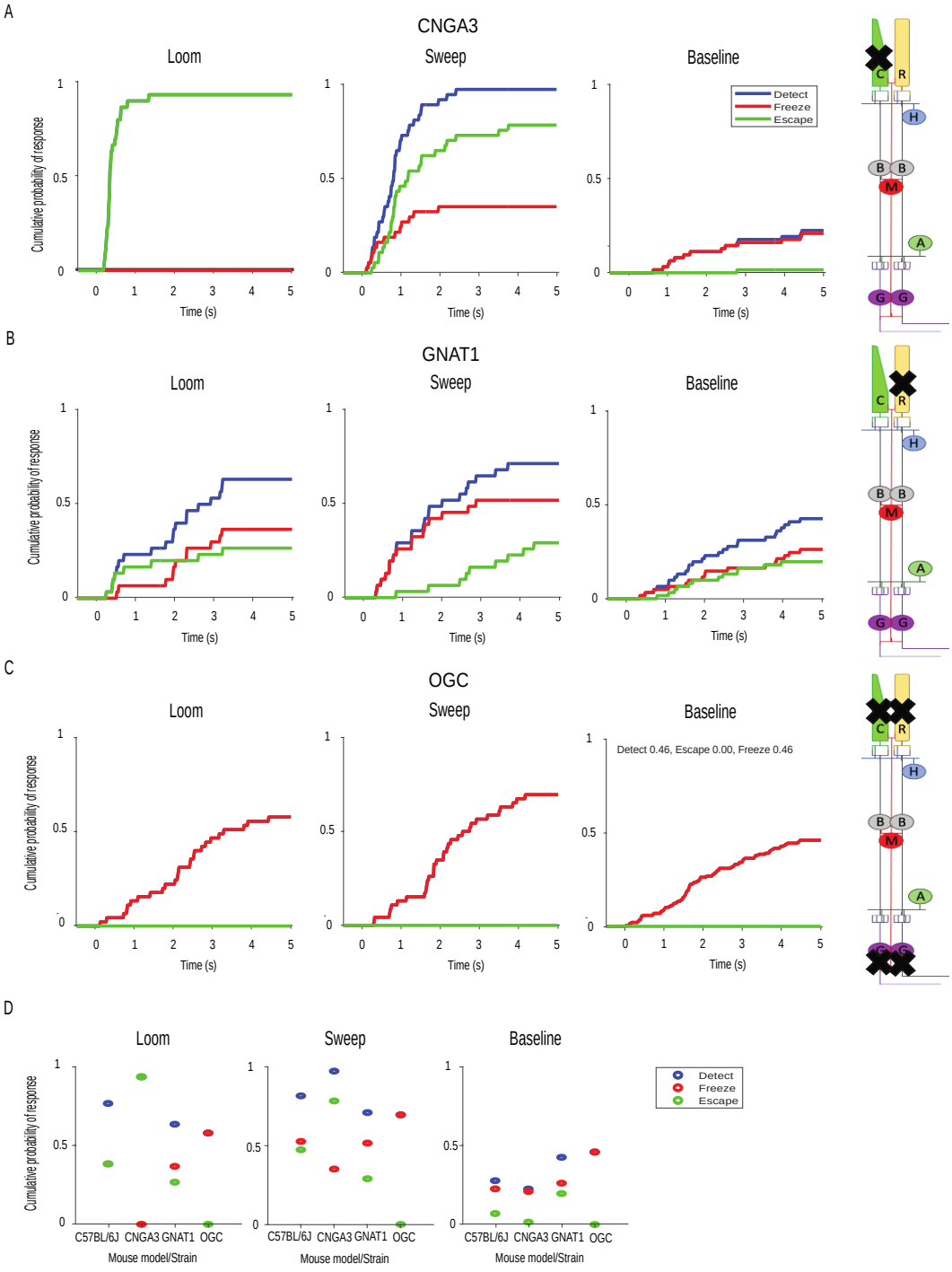
A
CNGA3
Loom
Sweep
Baseline
Detect
Freeze
Escape
Cumulative probability of response
Time (s)
B
GNAT1
C
OGC
Detect 0.46, Escape 0.00, Freeze 0.46
D
C57BL/6J CNGA3 GNAT1 OGC
Mouse model/Strain

Figure 22: The relative contributions of photosensitive cells in sculpting visually evoked avoidance behaviour in photopic conditions.

(A) Graphs representing the cumulative probability of having observed either an escape and/or freeze response (*blue*), an escape response (*green*) and a freeze response (*red*) over time for the CNG3A mouse strain. Cumulative probability of responses to Loom (1st panel) and Sweep (2nd panel) stimuli, and during baseline assessment where no visual stimuli was triggered (3rd panel). *Far right,* Schematic representation of the affected component of the photo cascade-cones, in the CNG3 mouse model. (B) As above, but for the GNAT1, and (C) OGC mouse strain. (D) Comparisons of the average cumulative probability of detecting either the visual stimuli by having observed either an escape and/or freeze response (*blue*), escape response (*green*) or freeze response (*red*) in response to the stimuli for all the strains analysed: C57Bl/6J, CNGA3, GNAT1 and OCG. Cumulative probability of responses to the Loom (*left*) and Sweep (*middle*) stimuli, and during baseline assessment (*right*) where no visual stimuli was triggered. Background mean luminance 30 to 40 candela/m^2.

5.1.1 Parameters of behaviour response.

Analysis of behavioural parameters suggested additional differences between the three transgenic mouse lines. First, GNAT1 took longer to escape from Loom, compared to C57BL/6 and CNGA3 (median escape latency C57BL/6J= 0.51 s, CNGA3 = 0.32 s, GNAT1 = 0.72 s, OGC = NA; ANOVA: C57BL/6Jvs GNAT1 p = 0.0024, CNGA3 vs GNAT1 p = 0.0001; **Figure 23 A**). Similarly, escape speed was lower in GNAT1 than CNGA3 (median of maximum escape speed: C57BL/6J= 71, CNGA3 = 77.61, GNAT1 = 47.13, OGC = NA; ANOVA: p = 0.0015). By contrast, freeze latency (median: C57BL/6J= 1.73 s, CNGA3 = NA, GNAT1 = 1.99 s, OGC = 2.16 s) and freeze duration (median of freeze duration: C57BL/6J= 1.15 s, CNGA3 = NA, GNAT1 = 0.84 s, OGC = N/A) was consistent across lines (**Figure 23 B, D**).

GNAT1 were also slower to escape from Sweep (median of escape latency: C57BL/6J= 1.65 s, CNGA3 = 0.86 s, GNAT1 = 2.7 s, OGC = NA; ANOVA: C57BL/6Jvs GNAT1 p = 0.0068, CNGA3 vs GNAT1 p = 0.0001) (**Figure 23 A**), and their escape speed was again lower (median of maximum escape speed: C57BL/6J= 75.53 s, CNGA3 = 72.55, GNAT1 = 45.61, OGC = NA; ANOVA: C57BL/6J vs. GNAT1, p = 0.0004; CNGA3 vs. GNAT1, p = 0.0005; **Figure 23 C**). GNAT1 were also the slowest to freeze (median of

freeze latency: C57BL/6J= 0.95 s, CNGA3 = 0.69 s, GNAT1 = 1.05 s, OGC = 2.09 s; ANOVA: C57BL/6J vs. GNAT1, p = 0.0011; CNGA3 vs. GNAT1, p = 0); no discernible differences were found in freeze duration (median of freeze duration: C57BL/6J= 1.03 s, CNGA3 = 0.98 s, GNAT1 = 1.17 s, OGC = 1.9=38 s; **Figure 23 D**).

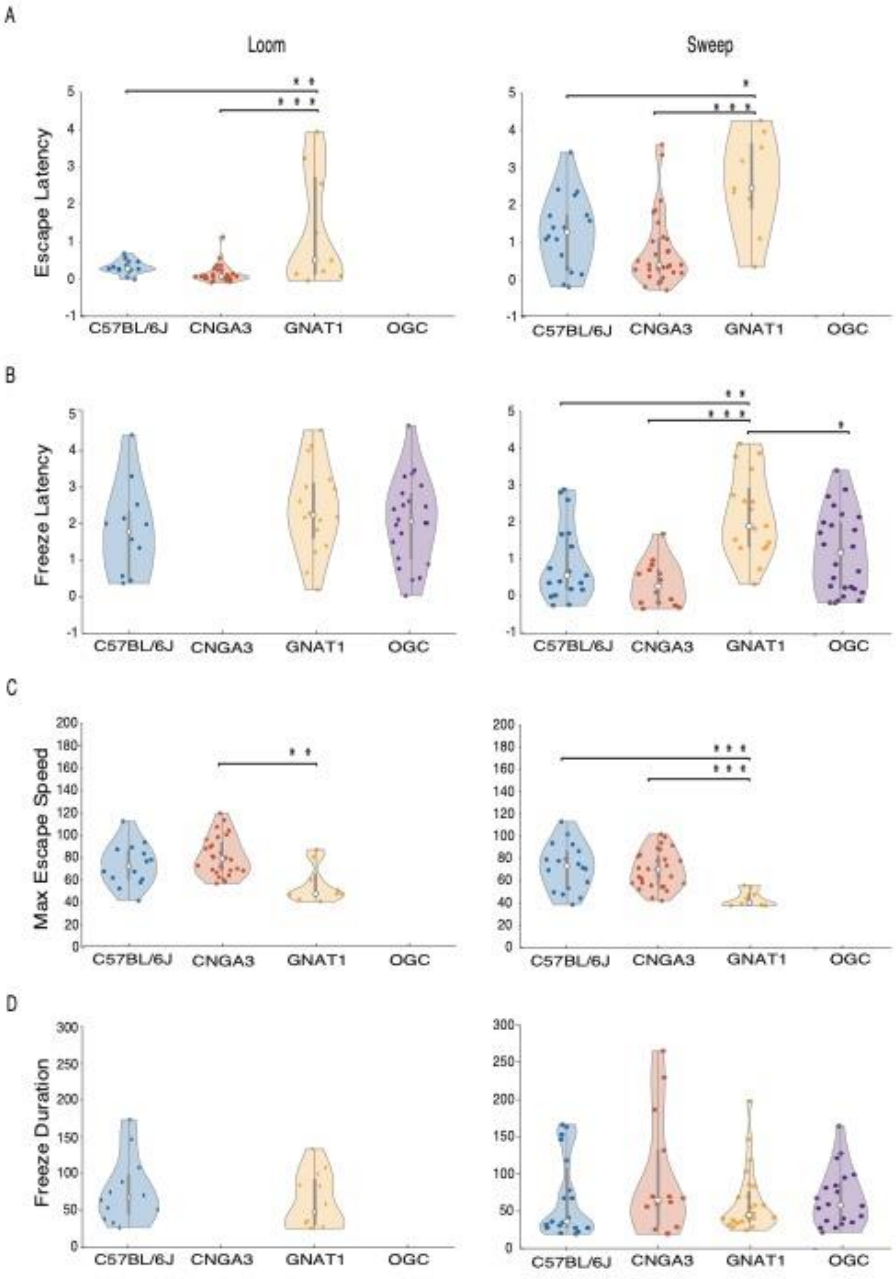
A
Loom
Sweep
Escape Latency
B
Freeze Latency
C
Max Escape Speed
D
Freeze Duration
C57BL/6J
CNGA3
GNAT1
OGC

Figure 23: The relative contributions of photosensitive cells on the response characteristics of visually induced avoidance behaviours in photopic conditions.

Visual representation of the distribution and probability density of behavioural response characteristics: escape latency, freeze latency, maximum escape speed and freeze duration. Latency of escape and freezing responses were defined as the time between stimulus onset and the initiation of escape or freezing events respectively. Peak escape speed was defined as the maximum speed achieved between the initiation of an escape response and, freeze duration was defined as the time between the initiation and ceased of a freeze response. *Left*: Violin plots of the distribution and probability density of behavioural response characteristics: escape latency (A), freeze latency (B), maximum escape speed (C) and freeze duration (D) for all the wild-type strains analysed: C57BL/6J, CNGA3, GNAT1 and OCG to Loom stimuli. *Right*: Violin plots of the distribution and probability density of behavioural response characteristics: escape latency (A), freeze latency (B), maximum escape speed (C) and freeze duration (D) for all the strains analysed: C57BL/6J, CNGA3, GNAT1 and OCG to Sweep stimuli. $p<0.05$= statistically significant *, $p<0.005$ = very significant **, $p<0.001$= highly significant ***

In summary, CNGA3 mice, in which cone phototransduction cascade is impaired, show robust detection rates for both Loom and Sweep, with escape responses predominating. GNAT1 mice, representative of a non-functional rod pathway, also showed robust detection despite ongoing degeneration, but freeze responses were more prominent, especially in response to Sweep. GNAT1 mice exhibited longer escape latencies and lower maximum escape speeds, while CNGA3 mice displayed faster escape responses. OGC mice, in which all photosensitive cells are impaired, showed no escape behaviour and detection rates similar to baseline data, suggesting responses were unlikely to be driven by visual stimuli. These observations suggest that both rod and cone pathways may contribute to instinctive behaviours in photopic conditions.

5.2 Scotopic responses.

CNGA3 mice (**Figure 24 A**), where cone function is impaired, but rod function is normal, responded to a striking 100 % of scotopic Loom (32 / 32) and Sweep (39 / 39) trials. CNGA3 mice almost always (Loom: 97 %, 31 / 32) or always (Sweep) responded by escaping (**Figure 24 A**), with freezing

responses seen in just 3% (1 / 32) of Loom and 18% (7 / 39) of Sweep trials; all freeze responses followed by a subsequent escape response (**Figure 24 A**). Comparison with the responses at photopic levels suggests an important role for the rod pathway in Loom and Sweep responses, even in photopic conditions.

GNAT1 mice (**Figure 24 B**), showed weaker visually-induced responses. Loom stimuli induced a response on 57% (20 / 35) of trials, and Sweep stimuli triggered a response on 61% (22 / 36) of trials, with escape only on 1 Loom (3%, 1 / 32) and 1 Sweep (3%, 1 / 36) trial. Instead, GNAT1 mice showed modest freezing responses to Loom (54%, 19 / 35) and Sweep (58%, 21 / 36) of all Sweep trials. Moreover, the slope of the cumulative probabilities was shallow, indicating limited relationship to visual stimuli.

The response of OCG mice (**Figure 24 C**) was similar to that seen in photopic conditions; ‘Detection’ events were almost exclusively freezing behaviour (Loom: 74%, 31 / 42; Sweep: 69%, 31 / 46) with an escape response observed in only 1 Sweep. Moreover, as seen in photopic evaluation, the overall likelihood of 'freezing' behaviour in baseline measurements (**Figure 24 C**) persists at a higher level compared to that observed in wild-type strains. Consequently, we observe no distinct reaction to visual stimuli in OGC mice, as anticipated.

Control C57BL/6J mice exhibited an enhanced behavioural response profile under scotopic light conditions, successfully detecting 100% of both Loom (22 trials) and Sweep (25 trials). Notably, all Loom trials prompted escape responses (100%), while a substantial proportion of Sweep trials resulted in escape responses (68 %, 17 / 25 trials). Additionally, Sweep stimuli elicited freeze responses in 64% of trials (16 / 25), with half of these responses being a combination of freeze+escape. Comparing these outcomes to previous observations across C57BL/6J mice, it appears that scotopic light levels enhance innate behavioural responses to visual stimuli.

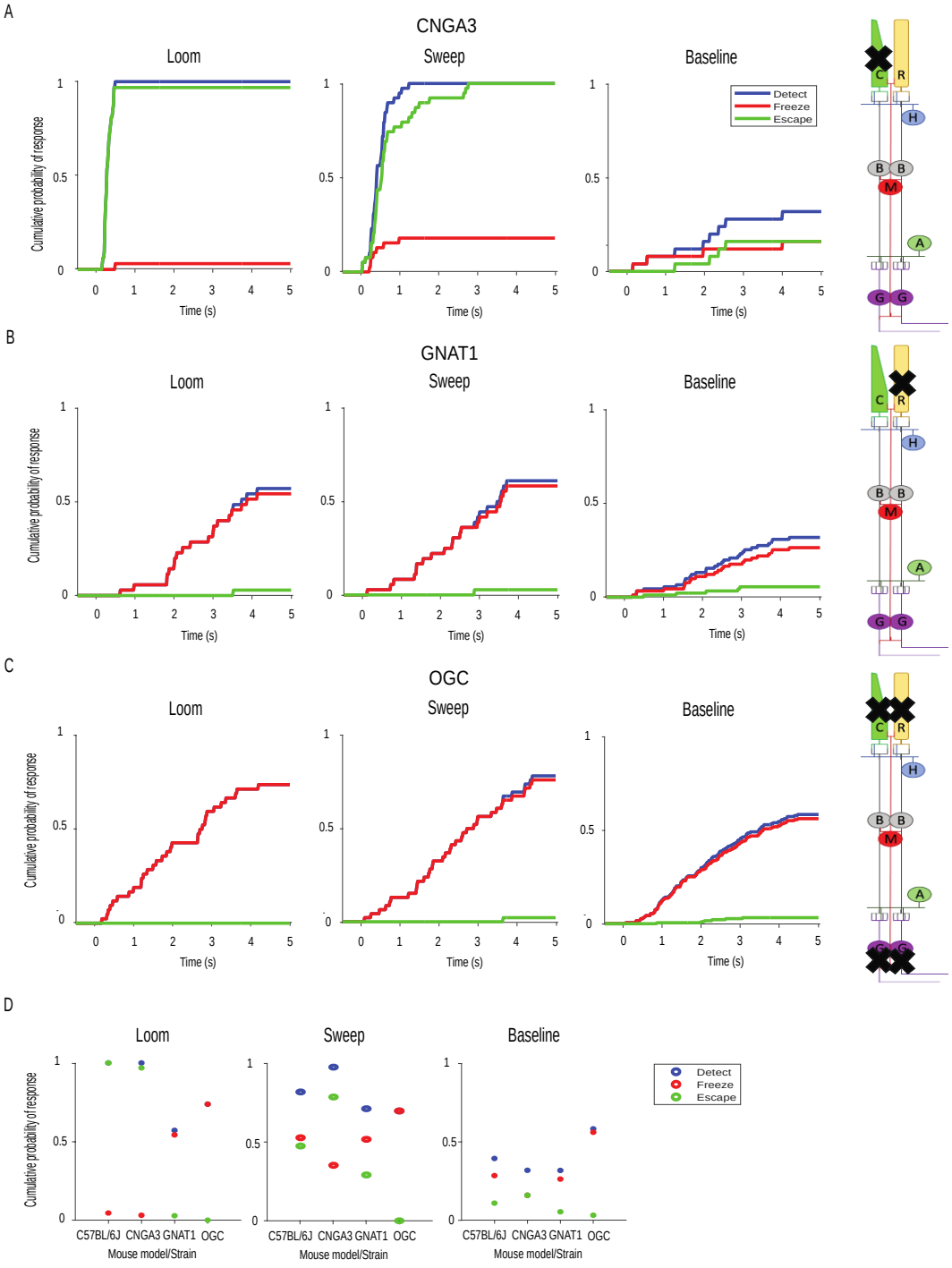
A
CNGA3
Loom
Sweep
Baseline
Detect
Freeze
Escape
Cumulative probability of response
Time (s)
B
GNAT1
C
OGC
D
C57BL/6J CNGA3 GNAT1 OGC
Mouse model/Strain

Figure 24: The relative contributions of photosensitive cells in sculpting visually evoked avoidance behaviour in scotopic conditions.

(A) Graphs representing the cumulative probability of having observed either an escape and/or freeze response (*blue*), an escape response (*green*) and a freeze response (*red*) over time for the CNG3A mouse strain. Cumulative probability of responses to Loom (1st panel) and Sweep (2nd panel) stimuli, and during baseline assessment where no visual stimuli was triggered (3rd panel). *Far right,* Schematic representation of the affected component of the phototransduction cascade in the CNGA3 mouse model. (B) As above, but for the GNAT1, and (C) OGC mouse strain. (D) Comparisons of the average cumulative probability of detecting either the visual stimuli by having observed either an escape and/or freeze response (*blue*), escape response (*green*) or freeze response (*red*) in response to the stimuli for all the strains analysed: C57BL/6J, CNGA3, GNAT1 and OCG. Cumulative probability of responses to the Loom (*left*) and Sweep (*middle*) stimuli, and during baseline assessment (*right*) where no visual stimuli was triggered. Background mean luminance 0.1 candela/m^2.

5.2.1 Parameters of behaviour response

Analysis of behavioural parameters again suggested GNAT1 took longest to escape from Loom, while CNGA3 were quickest (median of escape latency: C57BL/6J = 0.44 s, CNGA3 = 0.26 s, GNAT1 = 2.79 s, OGC = NA; ANOVA: C57BL/6J vs GNAT1 p = 0.0000, CNGA3 vs GNAT1 p = 0.0000; C57BL6 vs CNGA3 p = 0.0010) (**Figure 25 A**), and GNAT1 escaped more slowly (median of maximum escape speed: C57BL/6J = 85.91, CNGA3 = 92.75, GNAT1 = 52.59, OGC = NA; ANOVA: C57BL6 vs GNAT1 p = 0.0165, CNGA3 vs GNAT1 p = 0.0013) (**Figure 25 C**). Freeze duration and latency (median of freeze latency: C57BL/6J = NA, CNGA3 = NA, GNAT1 = 0.67 s, OGC = 1.40 s) showed no discernible differences (**Figure 25D**).

Similarly, CNGA3 were quickest to escape from Sweep (median of escape latency: C57BL/6J = 1.74 s, CNGA3 = 0.54 s, GNAT1 = 2.72 s, OGC = 3.47; ANOVA: C57BL/6J vs CNGA3 p = 0.0002, CNGA3 vs GNAT1 p = 0.0025, CNGA3 vs OGC p = 0.0007) (**Figure 25 A**), and ran faster when doing so (median of maximum escape speed: C57BL/6J = 78.80, CNGA3 = 90.06, GNAT1 = 42.97, OGC = 47.39; ANOVA: C57BL/6J vs CNGA3, p = 0.0487; C57BL/6J vs GNAT1 , p = 0.0042; CNGA3 vs. GNAT1, p = 0.0000; CNGA3 vs OGC, p = 0.0339). CNGA3 were also faster to freeze (median of freeze

latency: C57BL/6J = 0.95 s, CNGA3 = 0.69 s, GNAT1 = 1.05 s, OGC = 2.09 s; ANOVA: C57BL/6J vs. GNAT1, p = 0.0000; C57BL/6J vs. OGC, p = 0.0000; CNGA3 vs. GNAT1, p = 0.0003; CNGA3 vs OGC, p = 0.0016; **Figure 25 C**). No significant differences were found in freeze duration (median of freeze duration: C57BL/6J = 1.03 s, CNGA3 = 0.98 s, GNAT1 = 1.17 s, OGC = 1.38 s).

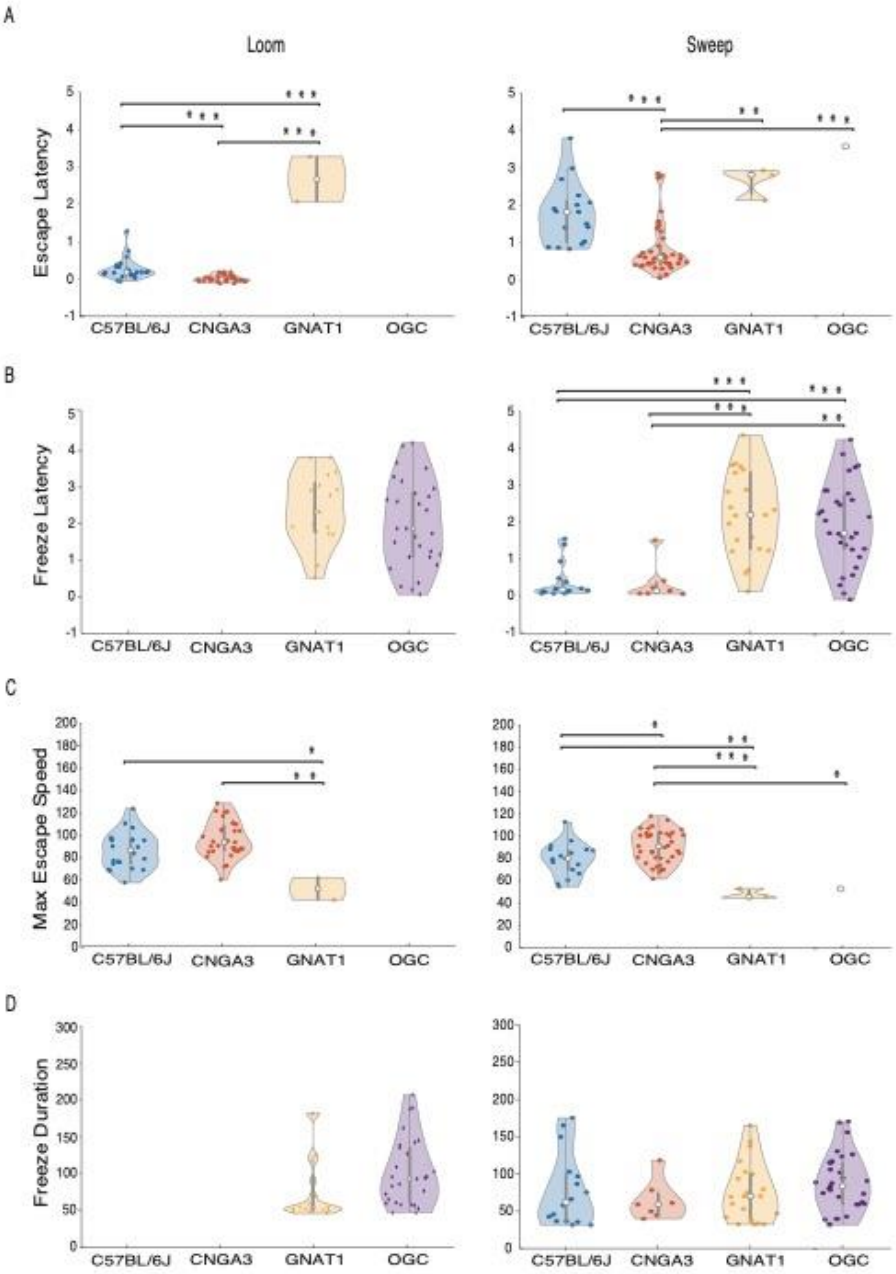
A
Loom
Sweep
Escape Latency
B
Freeze Latency
C
Max Escape Speed
D
Freeze Duration
C57BL/6J
CNGA3
GNAT1
OGC

Figure 25: The relative contributions of photosensitive cells on the response characteristics of visually induced avoidance behaviours in scotopic conditions.

Visual representation of the distribution and probability density of behavioural response characteristics: escape latency, freeze latency, maximum escape speed and freeze duration. Latency of escape and freezing responses was defined as the time between stimulus onset and the initiation of escape or freezing events respectively. Peak escape speed was defined as the maximum speed achieved between the initiation of an escape response and, freeze duration was defined as the time between the initiation and ceased of a freeze response. *Left*: Images of the distribution and probability density of behavioural response characteristics: escape latency (A), freeze latency (B), maximum escape speed (C) and freeze duration (D) for all the wild-type strains analysed C57BL/6J, CNGA3, GNAT1 and OCG to Loom stimuli. *Right*: Images of the distribution and probability density of behavioural response characteristics: escape latency (A), freeze latency (B), maximum escape speed (C) and freeze duration (D) for all the wild-type strains analysed: C57BL/6J, CNGA3, GNAT1 and OCG to Sweep stimuli. $p<0.05$= statistically significant *, $p<0.005$ = very significant **, $p<0.001$= highly significant ***

5.3 Conclusion.

This study shows the responses of several mouse models, each with specific defects in the phototransduction cascade, to Loom and Sweep under both photopic and scotopic light conditions. C57BL/6J mice exhibited heightened responses under scotopic conditions, compared to photopic conditions, underscoring the relevance of these light levels for (largely nocturnal) mice. We observed robust responses in CNGA3 mice, which have impaired cone function, in both photopic and scotopic conditions. Responses were fast and were dominated by escape behaviour in both conditions (particularly scotopic). GNAT1 mice, lacking rod function, also responded in both photopic and scotopic conditions, but freeze responses were much more prevalent, especially in response to Sweep stimuli, but were not tightly locked to the onset of stimulus for Loom. OGC triple-knockout mice, in which rods, cones and melanopsin RGCs are all impaired, displayed detection rates similar to baseline data, suggesting that the observed responses are unlikely to be specifically driven by visual stimuli.

Overall, these findings contribute to a more comprehensive understanding of how specific defects in photosensitive cells impact innate

behaviours in response to visual stimuli. The dual exploration of photopic and scotopic conditions broadens the scope of my study, offering insights applicable to diverse light levels and disease models. This work lays the groundwork for future investigations into the contributions of distinct photosensitive cell types, such as rods, cones, and photosensitive retinal ganglion cells, to the observed behavioural outcomes, advancing our understanding of visual processing in different mouse models.

CHAPTER 6: Idiosyncratic behaviour influences behavioural responses to visual stimuli.

In this Chapter, I sought to determine the influence of idiosyncratic behaviours on the responses of mice to common visual stimuli, by examining the effect of repeated measurements, focusing on the data collected for animals that underwent multiple measurement (day 0 and day 28, see Chapter 3; and the longitudinal cohort where individual mice were re-tested at 21 days, 1, 2, 6 and 12 months, see Chapter 4) to understand if and how these behaviours evolve.

Individual animal occupancy plots allow for examination of how protocol design can affect baseline behaviours. In **Figure 26 A**, occupancy maps of an individual mouse tested under the “Intense” protocol show a marked decrease in exploratory behaviour between the first and last session performed in a single day. By Session 5, many mice remained in the nest for long periods of time and made fewer journeys into the arena (**Figure 26 A**). Strikingly, however, exploratory behaviour returned in the first session the following day (see 2nd time point plot, **Figure 26 A**), before declining in subsequent sessions, as before. This pattern of is maintained across consecutive days and when re-testing 28 days later, strongly indicating that there is robust daily recovery in exploratory behaviour that declines with consecutive sessions in one day.

It is important to acknowledge that this trend could also be partially reflect a "time of day" effect. Experiments were consistently conducted around the same time, coinciding with the mice's light period, during which they are typically less active as nocturnal species. This suggests that mice might have been more active when experiments started in the morning while performing the first sessions compared to later in the afternoon when the last sessions were recorded.

As discussed in Chapter 3, this reduction in exploratory behaviour across sessions in a day limits the utility of the Intense and Burst protocols since it

can prove difficult to deliver all 4 stimuli (Sweep-Loom-Sweep-Loom) in the set time window of 20 minutes.

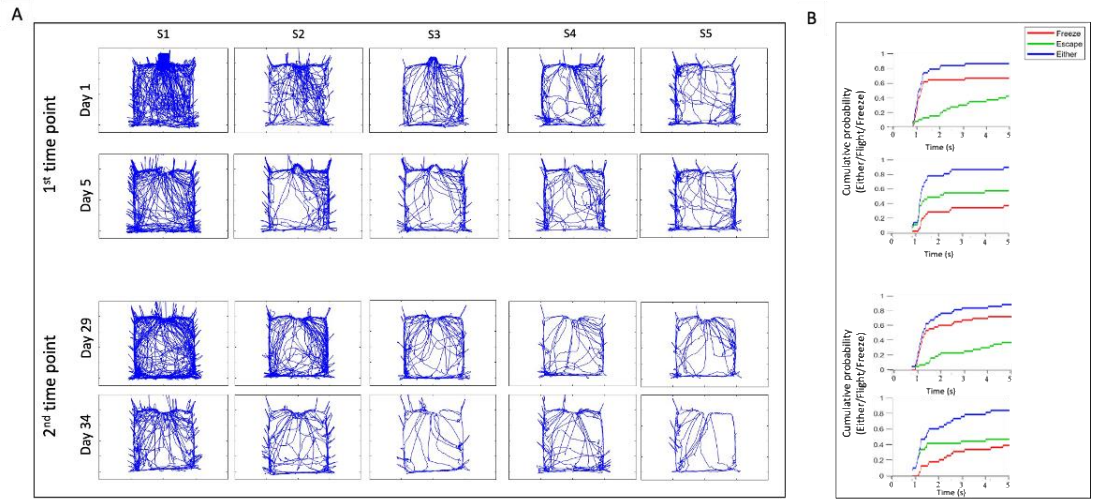

Figure 26: Impact of experimental design on exploratory behaviour.

(A) Occupancy maps representative track plots from an individual female *C57B L/6J* mouse during the intense protocol on the 1st and 2nd experimental time-points (*top*, day 1 and day 5; *bottom,* day 29 and day 34). (B) Cumulative probability of having observed either an escape and/or freeze response (*blue*), an escape response (*green*) and a freeze response (*red*) over time for an individual mouse tested under the intense protocol (*top,* day 1 and day 5; *bottom*, day 29 and day 34).

I next examined inter- versus intra-animal variability in stimulus-induced responses. Whilst there is a strong *group* preference for mice to escape a Loom stimulus and freeze in response to Sweep stimuli, individual animals can still show distinct preferences for a particular type of response. For example, within the same group one mouse might preferentially freeze then escape in response to a Loom stimulus, whilst another might simply freeze. This reflects inter-animal variability. Strikingly, however, intra-animal variability was remarkably low, with individual animals maintaining their preferred behaviour in response to a given visual stimuli regardless of the number of sessions exposure. This is illustrated in **Figure 26 B**, where the cumulative probability of response plots for each individual mouse (one mouse per row) during the initial set of exposures to the visual stimuli under the assigned protocol compared to the second exposure 28 days later, illustrates that for a given

visual stimulus, the behavioural response remained consistent over time. This consistency persisted despite repeated measures and a reduction in exploratory behaviour observed within daily testing sessions. Furthermore, the average cumulative probability of response for individual animals assigned to the 'Tonic' protocol (**Figure 27**) reveal a remarkable consistency in their response preferences to Loom and Sweep stimuli; each animal responded in a highly reproducible manner (escape or freeze behaviours) in response to a given visual stimulus, both during the initial exposure (**Figure 27 A**), and when re-tested 28 days later (**Figure 27 B**). This consistency is further evident in the Pearson correlation graphs, which compare the cumulative probability of response types between the initial and subsequent (re-testing 28 days later) testing events when mice were exposed to Loom and Sweep stimuli (**Figure 27 B**).

The Pearson correlation (**Figure 27 B**) also provides a measure of how well the responses of individual mice at the first time point predict their responses at the second time point. ‘Detection’ of Loom and Sweep stimuli presented a weak positive linear relationship between the first and second time points (correlation coefficient $r_{detection}$ = 0.1915 and 0.1958; p-values 0.494 and 0.484, respectively). In contrast, freeze responses evoked by Loom stimuli showed a strong and highly significant positive linear relationship (correlation coefficient: r_{freeze}= 0.71973; p-value 0.0025), suggesting that individual mice consistently maintain their response to this stimulus across the two time points. A positive, but non-significant, linear relationship was seen for both freeze and escape responses to Sweep stimuli (Freeze: correlation coefficient r_{freeze} = 0.10312; p-value 0.71459. Escape: correlation coefficient r_{escape} = 0.38276; p-value 0.1591).

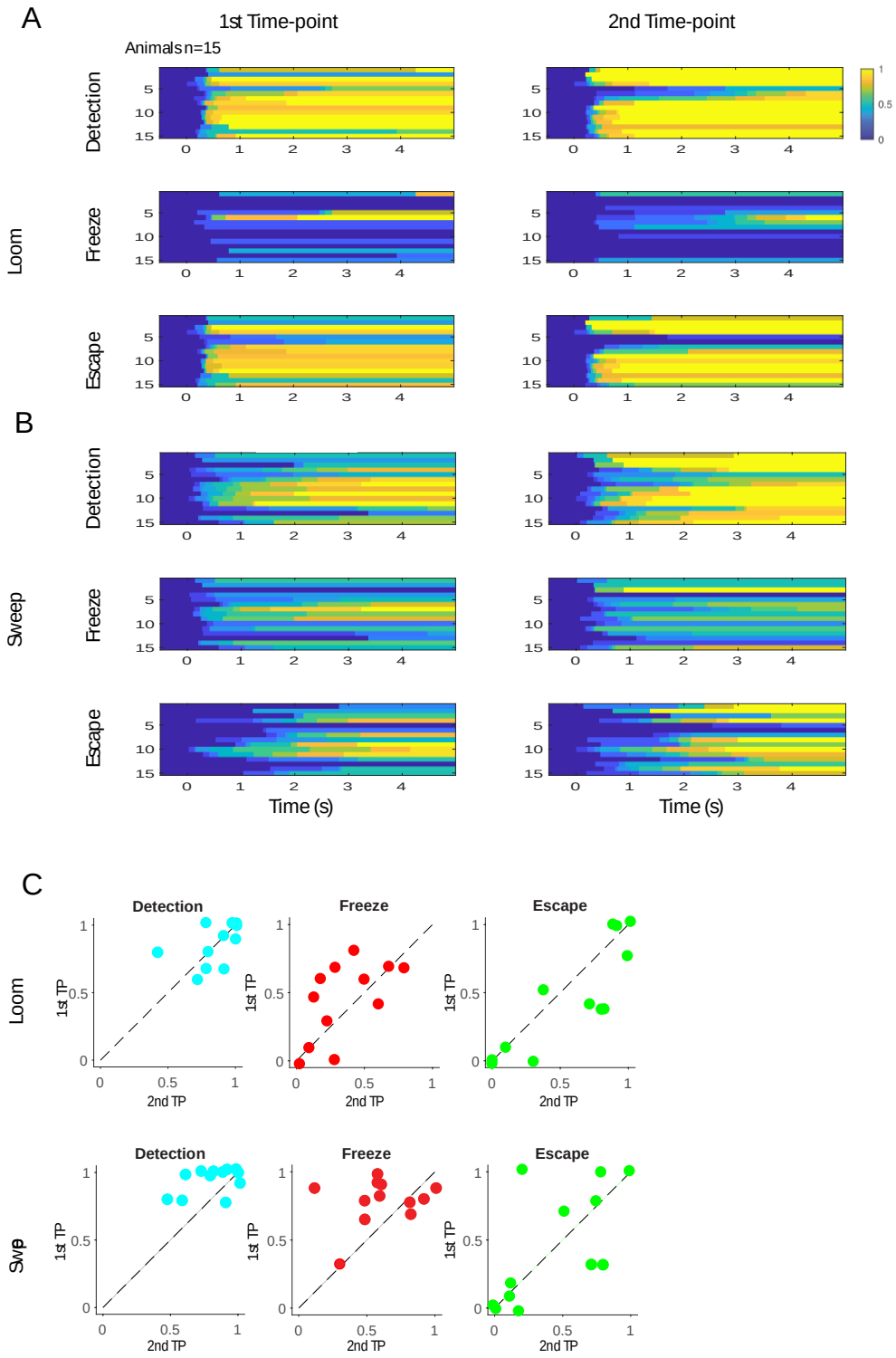
A
1st Time-point
2nd Time-point
Animals n=15
Loom
Detection
Freeze
Escape
B
Sweep
Detection
Freeze
Escape
Time (s)
Time (s)
C
Loom
Sweep
Detection
Freeze
Escape
1st TP
2nd TP

Figure 27 - Correlation Analysis of cumulative response probability for individual animals tested at two distant time point under Tonic Protocol

(A) Average of natural logarithm images of cumulative response probability detection, freeze, and escape for individual animals (one mice per row) assigned to Tonic protocol during Loom stimuli at the 1st Time Point (1st panel, sessions 1-5) and 2nd Time Point (2nd panel, sessions 6-10) 28 days later. *Blue* indicates low cumulative probability of response and *yellow* indicates high cumulative probability of response. (B) Average of natural logarithm images of cumulative response probability detection, freeze, and escape for individual animals (one mice per row) assigned to Tonic protocol during Sweep stimuli on the 1st Time Point (1st panel, sessions 1-5) and on the 2nd Time Point (2nd panel, sessions 6-10). (C) Pearson correlation graphs illustrating the cumulative probability of detection, freeze, and escape to Loom (*above*) and Sweep (*below*) stimuli between the 1st and 2nd exposure Time Points for individual animals assigned to Tonic protocol.

Similarly, animals assigned to the 'Burst' protocol also maintained their preferred behavioural responses to Loom and Sweep stimuli across sessions separated by time (**Figure 28 A**). This consistency is visually apparent in the heat maps and is further supported by correlation analyses (**Figure 28 B**). For Loom stimuli, a moderate positive corelation ($r_{detection}$ = 0.56705; p-value = 0.055) was observed between the first assessment and the second, 28 days later, for "detection", and a strong positive correlation for “freezing” behaviours (r_{freeze} = 0.6251; p-value = 0.030). An even stronger correlation was observed for escape responses (r_{escape} = 0.87392; P-value = 0.00020). Thus, an individual mouse’s idiosyncratic preference for freezing or escape behaviour in response to a Loom stimulus appears to be maintained over time. For Sweep stimuli, both detection and freeze responses displayed limited correlation ($r_{detection}$ = 0.40661; p-value = 0.1896 and r_{freeze} = 0.27132; p-value = 0.3937, respectively) indicating greater variation in idiosyncratic behaviours across time. Of note, escape responses exhibited a stronger and statistically significant positive correlation (r_{escape} = 0.65832; p-value = 0.0199), suggesting a more consistent retention of escape responses by individual mice across time.

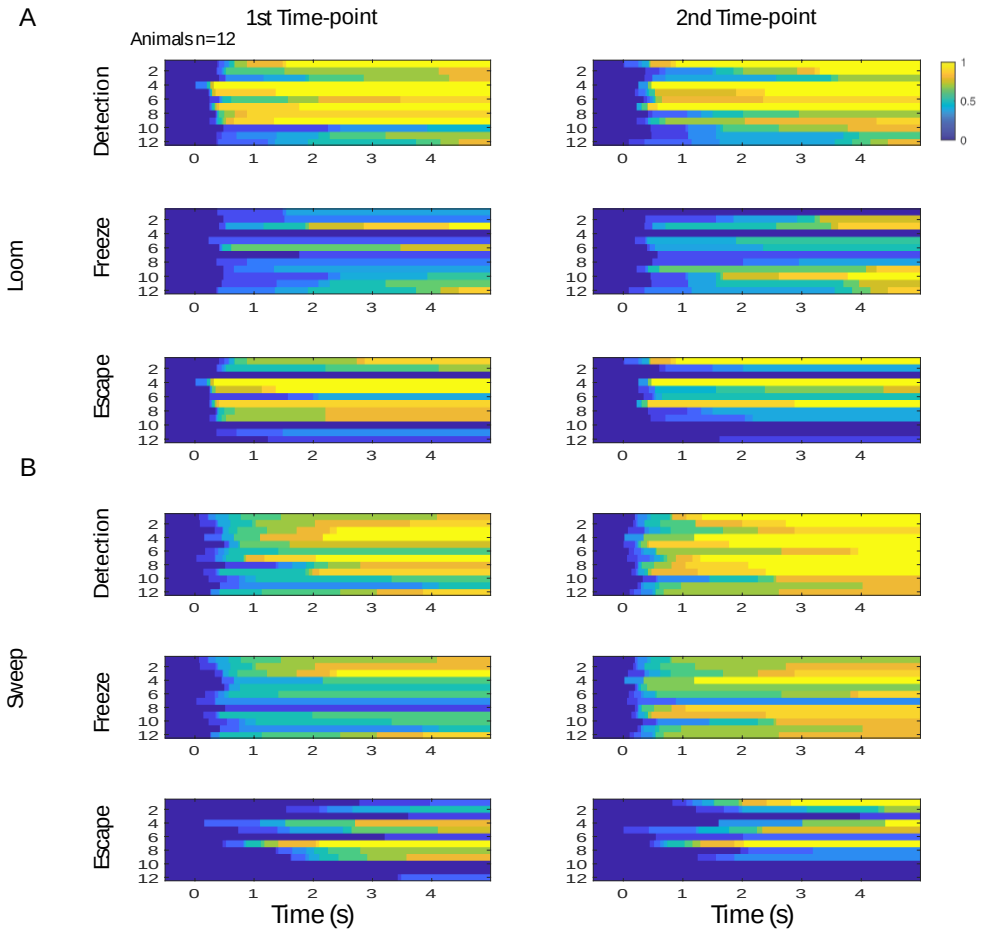
A
1st Time-point
2nd Time-point
Animals n=12
Detection
Freeze
Escape
Loom
B
Sweep
Time (s)
C
Detection
Freeze
Escape
1st TP
2nd TP

Figure 28: Correlation Analysis of cumulative response probability for individual animals tested at two distant time point under Burst Protocol

(A) Average of natural logarithm images of cumulative response probability detection, freeze, and escape for individual animals (one mice per row) assigned to Burst protocol during Loom stimuli at the 1st Time Point (1st panel, sessions 1-5) and 2nd Time Point (2nd panel, sessions 6-10) 28 days later. *Blue* indicates low cumulative probability of response and *yellow* indicates high cumulative probability of response. (B) Average of natural logarithm images of cumulative response probability detection, freeze, and escape for individual animals (one mice per row) assigned to Burst protocol during Sweep stimuli at the 1st Time Point (1st panel, sessions 1-5) and 2nd Time Point (2nd panel, sessions 6-10). (C) Pearson correlation graphs illustrating the cumulative probability of detection, freeze, and escape to Loom (*above*) and Sweep (*below*) stimuli between the 1st and 2nd exposure Time Points for individual animals assigned to Burst protocol.

Animals assessed under the "Intense" protocol also showed a reasonable degree of uniformity in their behavioural responses to both Loom and Sweep stimuli across the two analysed time points (**Figure 29 A; Figure 29 B**). Fewer animals were tested in this protocol, but for Loom stimuli, a positive correlation was observed for all three responses ($r_{detection}$ = 0.33743, r_{freeze} 0.70754 =, r_{escape} = 0.50096) but these were not statistically significant ($p_{detection}$ = 0.5131, p_{freeze} = 0.1158, p_{escape} = 0.3114). A similar pattern was seen in response to Sweep stimuli for detection and freeze responses (correlation coefficient $r_{detection}$= 0.56977, r_{freeze}= 0.70537; $p_{detection}$= 0.2378, p_{freeze}= 0.1174). However, there was a much stronger conservation of escape behaviours triggered by Sweep stimuli (r_{escape} = 0.94225, p_{escape} = 0.0049) between the first and second time point.

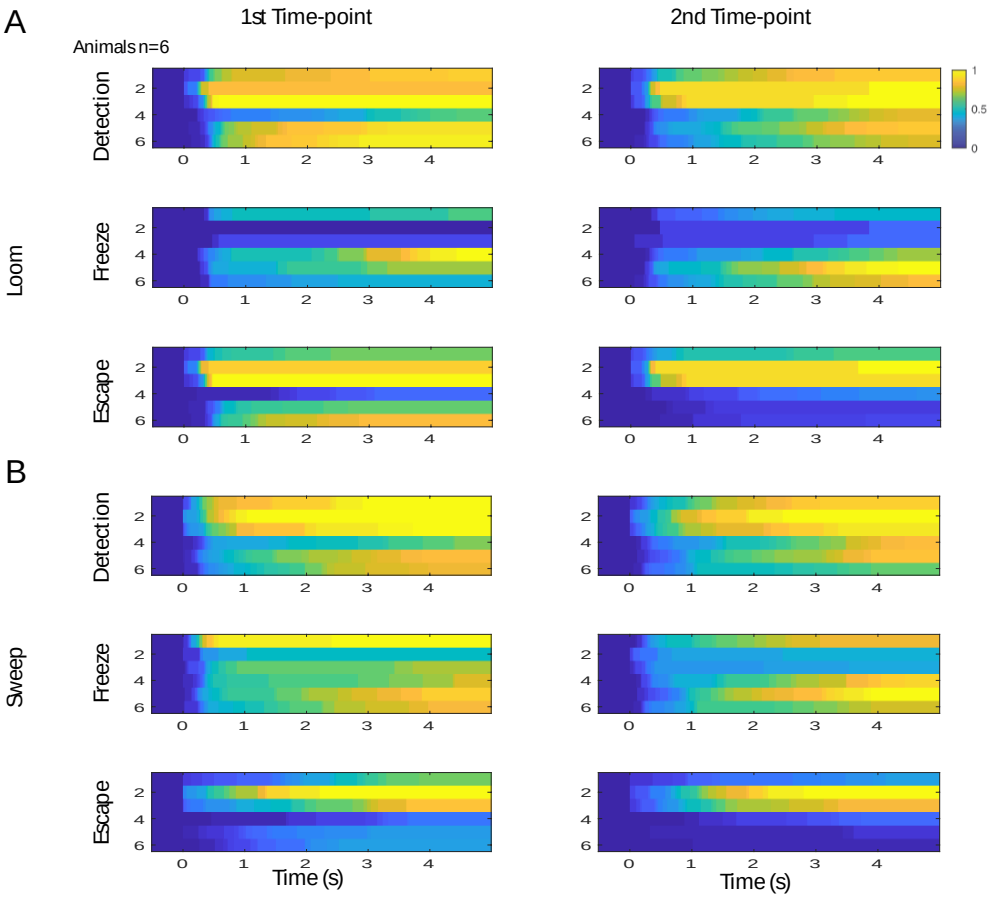
A
1st Time-point
2nd Time-point
Animals n=6
Loom
Detection
Freeze
Escape
B
Sweep
Detection
Freeze
Escape
Time (s)
Time (s)

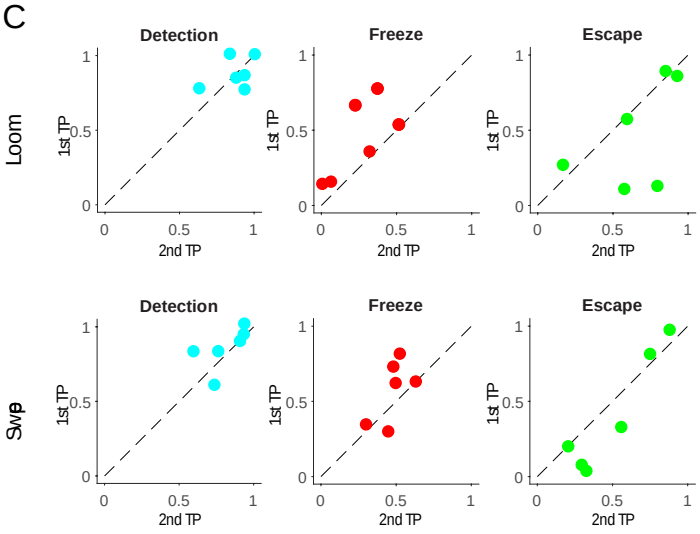
C
Loom
Sweep
Detection
Freeze
Escape
1st TP
2nd TP

Figure 29: Correlation Analysis of cumulative response probability for individual animals tested at two distant time point under Intense Protocol

(A) Average of natural logarithm images of cumulative response probability detection, freeze, and escape for individual animals (one mice per row) assigned to Intense protocol during Loom stimuli at the 1st Time Point (1st panel, sessions 1-5) and 2nd Time Point (2nd panel, sessions 6-10) 28 days later. *Blue* indicates low cumulative probability of response and *yellow* indicates high cumulative probability of response. (B) Average of natural logarithm images of cumulative response probability detection, freeze, and escape for individual animals (one mice per row) in the Intense protocol during Sweep stimuli at the 1st Time Point (1st panel, sessions 1-5) and 2nd Time Point (2nd panel, sessions 6-10). (C) Pearson correlation graphs illustrating the cumulative probability of detection, freeze, and escape to Loom (*above*) and Sweep (*below*) stimuli between the 1st and 2nd exposure Time Points for individual animals assigned to Intense protocol.

Idiosyncratic behavioural responses were also largely maintained across time in mice assessed using the "Optimised" protocol (**Figure 30 A).** Pearson correlation analysis (**Figure 30 B**) indicates that detection responses to both stimuli are broadly consistent, but the associations were not statistically significant (Loom, $r_{detection}$ = 0.40591, $p_{detection}$ = 0.36625; Sweep, $r_{detection}$ = 0.69026, $p_{detection}$ = 0.08606). Escape behaviour in response to Loom showed a strong positive correlation, which approached significance (r_{escape} = 0.68363, p_{escape} = 0.09038), while freeze responses exhibited a weak negative correlation (r_{freeze} = -0.13951, p_{freeze} = 0.76546). Positive correlations were found for both freeze and escape behaviours in response to Sweep stimuli (r_{freeze} = 0.53705, p_{freeze} = 0.21385), with that of escape being statistically significant (r_{escape} = 0.81265, p_{escape} = 0.02631). Thus, consistent behavioural responses to Loom and Sweep stimuli are generally maintained by individual animals across the two time points, particularly escape behaviour.

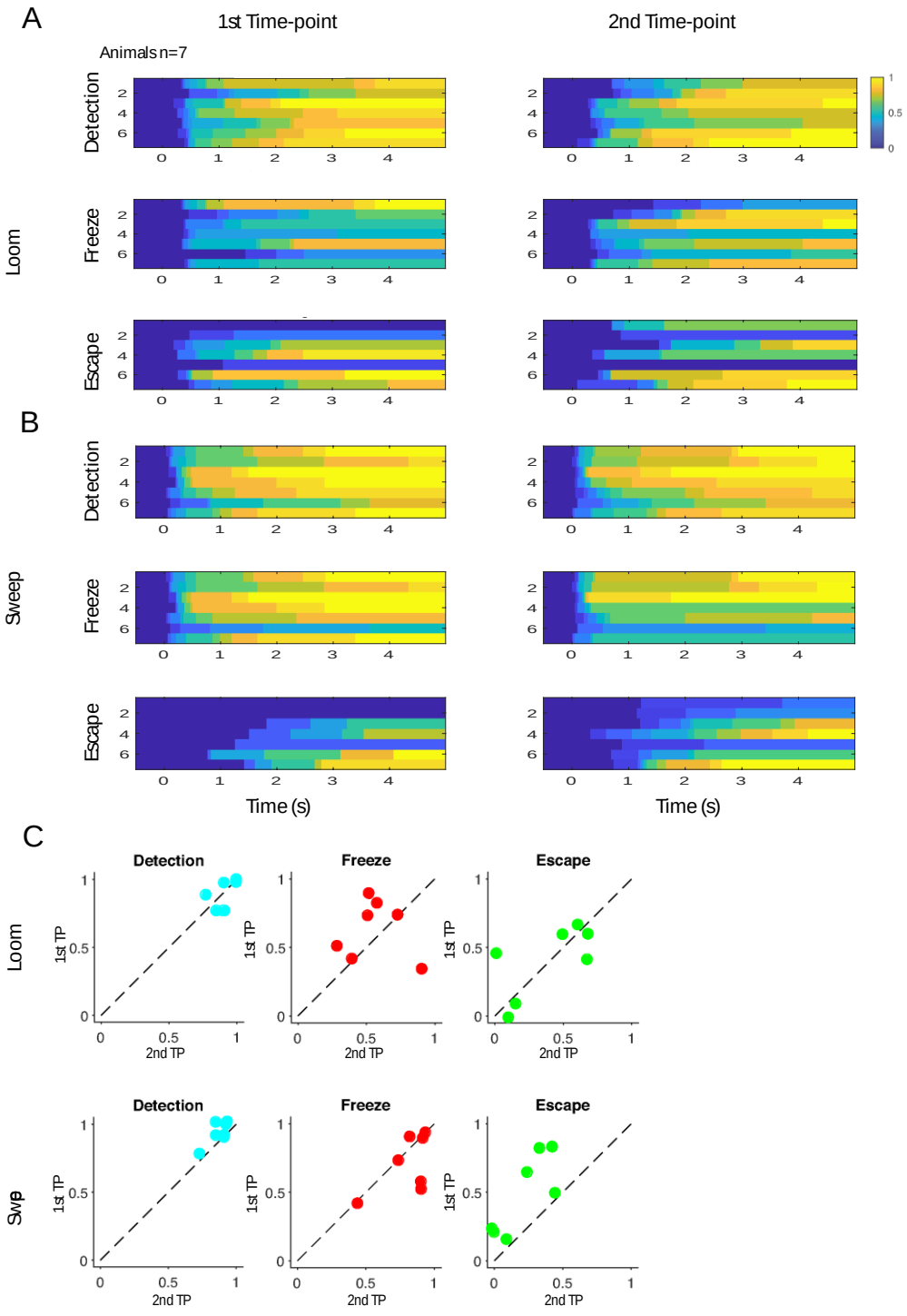
A
1st Time-point
2nd Time-point
Animals n=7
Loom
Detection
Freeze
Escape
B
Sweep
Detection
Freeze
Escape
Time (s)
Time (s)
C
Loom
Sweep
Detection
Freeze
Escape
1st TP
2nd TP

Figure 30: Correlation Analysis of cumulative response probability for individual animals tested at two distant time point under Optimised Protocol

(A) Average of natural logarithm images of cumulative response probability detection, freeze, and escape for individual animals (one mice per row) assigned to Optimised protocol during Loom stimuli at the 1st Time Point (1st panel, sessions 1-6) and 2nd Time Point (2nd panel, sessions 7-12) 28 days later. *Blue* indicates low cumulative probability of response and *yellow* indicates high cumulative probability of response. (B) Average of natural logarithm images of cumulative response probability detection, freeze, and escape for individual animals (one mice per row) in the Optimised protocol during Sweep stimuli at the 1st Time Point (1st panel, sessions 1-6) and 2nd Time Point (2nd panel, sessions 7-12). (C) Pearson correlation graphs illustrating the cumulative probability of detection, freeze, and escape to Loom (*above*) and Sweep (*below*) stimuli between the 1st and 2nd exposure Time Points for individual animals assigned to Optimised protocol.

The analyses above indicate that individual mice will generally exhibit a preferred idiosyncratic behavioural response to a given stimulus and maintain this type of response over time, at least across two time points separated by one month. To further explore retention of preferred behaviours I analysed individual mice participating in the longitudinal study, described in Chapter 4. Originally designed to investigate the impact of age on visually triggered innate behaviours, this study also revealed striking consistency in the response patterns of individual animals over time. **Figure 31** shows the cumulative probability of all responses (detecting, freezing, and escaping) for individual animals exposed to both Loom and Sweep stimuli. Whilst different animals exhibited distinct and sometimes opposing preferences for escape or freeze responses to the same visual stimuli, these individual preferences were maintained, and were consistent between the 1 and 6 month time points. Despite the passage of time, mice consistently maintained their idiosyncratic behaviours, demonstrating a clear preference for either escape or freeze responses to specific visual stimuli. It is important to note, as determined in Chapter 4, that age itself also introduces changes in mouse behaviour, particularly evident in older mice (>12 months) where a marked reduction in escape behaviour is observed. This appears more closely related to the age of the animal, rather than an extinction of the escape behaviour due to repeated exposure to visual stimuli.

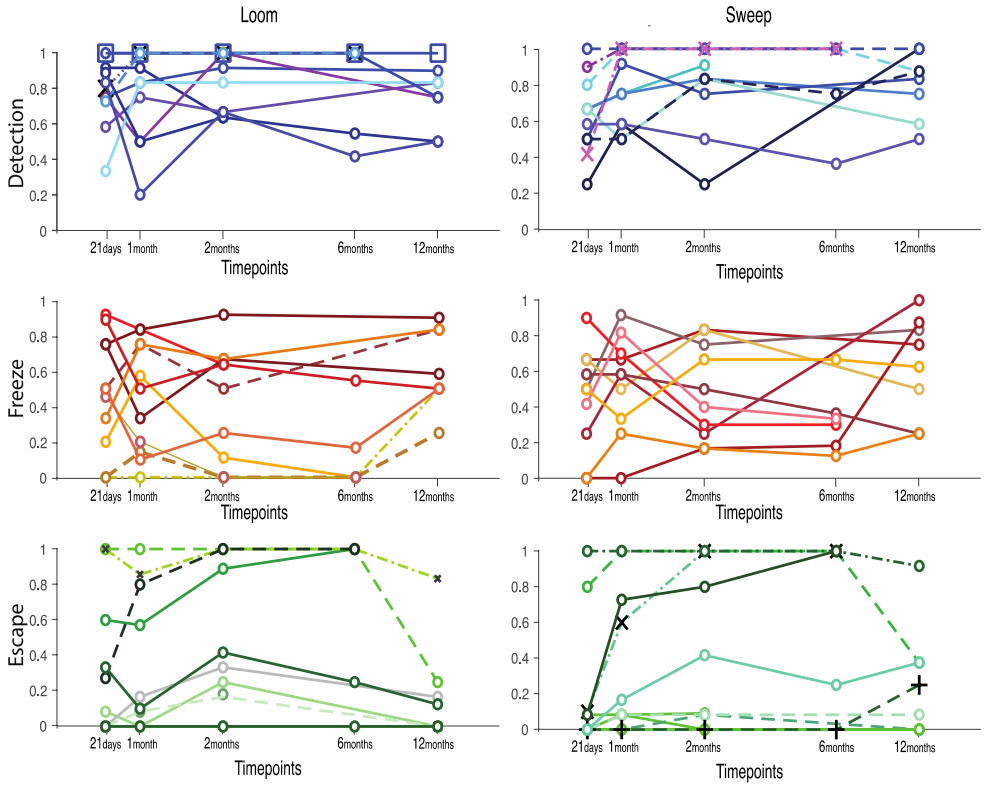

Figure 31: Idiosyncratic behaviour in longitudinal study.

Graph representing the cumulative probability of response for detect, freeze, escape for individual animals in the Longitudinal study tested at for Loom stimuli (left panel) and for Sweep (2nd panel, sessions 6-10), exposed to the visual stimuli at 21 days (n= 11), 1 month (n=11) , 2 months (n=11), 6 months (n=6) and 12 months (n=10).

6.1. Conclusion.

In this chapter, I explored the presence of idiosyncratic behaviour in the responses of mice to common visual stimuli, focusing on repeated measurements. The study involves re-testing mice at different time points, including a protocol establishment with a 28-day re-test (as outlined in Chapter 3) and a longitudinal study for age with multiple time points at 21 days, 1, 2, 6, and 12 months (as outlined in Chapter 4). The aim was to understand how these behaviours evolve with time.

Habituation was observed in responses to Loom stimuli, suggesting mice can identify repeated (**Figure 12**) , harmless stimuli experienced over a short time frame (within a day), leading to a gradual reduction in threat perception. Importantly, however exploratory behaviour returned to normal the following day; this pattern was observed in “Tonic”, "Burst" and "Intense" protocols, emphasizing the role of daily recovery in exploratory behaviour.

Despite habituation, freeze and escape behaviours persist, and mice maintain idiosyncratic responses across sessions and over time. Whilst not uniformly achieving statistical significance, response hear maps and correlation analysis for mice assigned to each of the three original protocols, "Tonic", “Burst” and “Intense”, as well as the “Optimised” protocol, showed remarkable consistency in their preferred responses to both Loom and Sweep stimuli. Behavioural preferences related to freezing and escaping are generally maintained, such that individual mice will respond in a predictable manner in response to a given visual stimulus. This was particularly notable in the preservation of escape responses between first and second time points.

Examination of idiosyncratic behaviours in the longitudinal study highlights the endurance of specific behaviours, especially during adulthood. This assessment further illustrated the changes in behaviour that occur in older age, with a reduction in escape responses. These findings contribute valuable insights into understanding the interplay between age, individual preferences, and the sustained reliability of visually induced avoidance behaviours.

CHAPTER 7: Vision-dependent avoidance behaviours as a non-invasive assessment for evaluating the effectiveness of gene therapy.

Having established a robust framework with which to test and analyse visually evoked avoidance behaviours in mice, finally, I sought to examine whether this methodology can be used as a non-invasive tool for assessing the efficacy of therapeutic interventions for restoring vision, such as gene therapy, cell therapy or opt genetics. The most commonly used methods of assessment test at the level of the *in vivo* or *ex vivo* retina (electroretinograms, pupil reflex, multielectrode array recordings on explant retina), or visual reflexes such as optokinetic head tracking. Tests involving cortical processing of visual information, such as water-maze and fear conditioning paradigms, involve lengthy and stressful training, which is poorly suited to assessing sight restoring therapeutics as the animal cannot be trained beforehand. As novel therapeutics, such as gene and cell therapies advance, the need for easy, reliable, and non-invasive methods to evaluate their effectiveness becomes imperative in pre-clinical research.

To determine the utility of the developed methodology, I used an AAV-mediated gene supplementation therapy previously reported by our lab (Nishiguchi et al. 2015). The *PDE6β*$^{rd1/rd1}$ mouse model of autosomal recessive retinitis pigmentosa (Carter-Dawson et al., 1978), herein referred as *Rd1*, exhibits rapid photoreceptor loss, with rod degeneration starting as early as P10, and near complete loss by P25; cones are present as a single layer together with a few remaining cones (Bowes and Farber, 1987). Our lab has previously used *AAV2/8.RK.βPDE* to successfully rescue photoreceptor degeneration and restore long term retinal function (Nishiguchi et al., 2015).

Following the same protocol, *Rd1* mice were randomly assigned to treated or untreated groups, with treated mice receiving gene replacement in both eyes at P7-9. All mice were assessed using Loom and Sweep, ERG and Optomotor testing at 6 weeks post-injection, with the Loom and Sweep test performed first to minimize handling. For clarity, I am presenting the histological data first, followed by the functional assessments. This is because,

as will be explained below, the viral rescue did not work as anticipated, but this was not known until after all the assessments had been completed.

After completing all assessments, the eyes were histologically examined to verify retinal rescue, as reported by Nishiguchi et al. (2015). Surprisingly, the observed degree of rescue was variable, contrary to our expectations based on previous work with the same plasmid (although a different batch of virus was used). **Figure 32** illustrates this variability well: in this mouse treated in both eyes, the left eye shows robust rescue and preservation of the outer nuclear layer (ONL), whereas the ONL in the right eye is almost entirely absent. Other animals in the cohort displayed varying levels of rescue. It is not clear why this occurred as the surgeon is highly experienced, the injections went without incident and the virus did demonstrate efficacy in some cases. Unfortunately, time constraints prevented a repeat of this experiment.

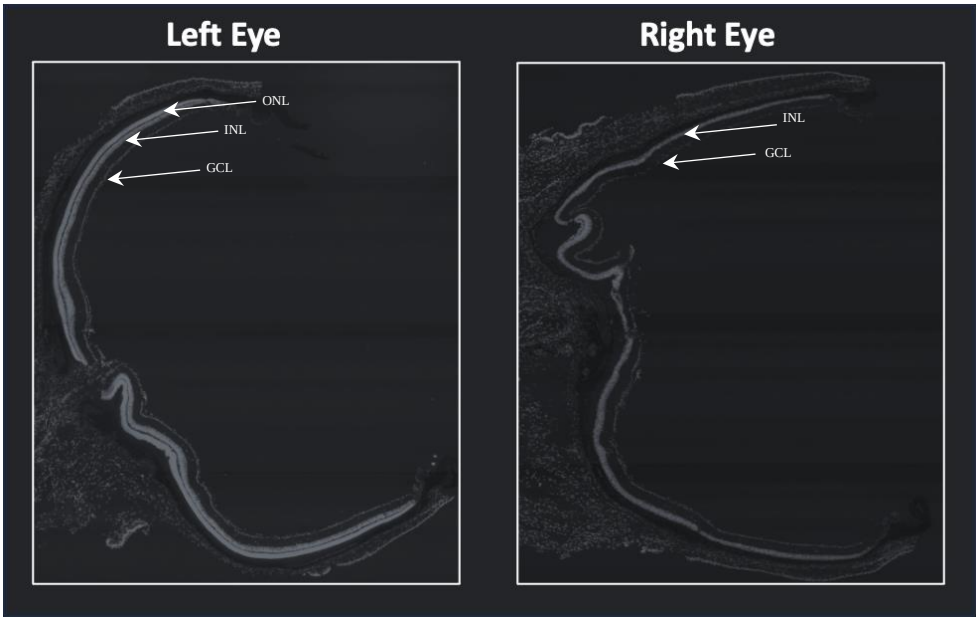

Figure 32: Histological assessment of retinal preservation of treated RD1 mouse.

Representative histological retinal cryosections from a treated Pde6b$^{rd1/rd1}$ mouse (both eyes treated), illustrating the variability in rescue, where the left eye shows robust rescue of the ONL throughout the eye, whilst the right eye exhibited only very limited rescue. The representative tissue was fixed in 4% PFA and 15μm cryosections were performed and stained with DAPI (1:1000). ONL-Outer Nuclear Layer; INL-Inner Nuclear Layer; GCL-Ganglion Cell Layer.

Following the histological characterization and the understanding that the rescue observed was not consistent across all treated animals, I will now present the functional outcomes through behaviour assessments. As before, **Figure 33** shows the cumulative probability of responses to Loom and Sweep stimuli under photopic conditions for both untreated (n=8) and treated (n=8) *Rd1* mice. Surprisingly, very little difference was detected between treated and untreated mice, for either stimulus. Untreated *Rd1* mice exhibited 58% (37 / 64) chance of detection, 5% (3 / 64) of escape and 53% (34 / 64) of freeze responses to presentation of Loom stimuli. Very similar values were observed for Sweep stimuli: 53% (43 / 81) of detection, 4 % (3 / 81) escape and 49% (40 / 81) freeze responses. Treated *Rd1* mice exhibited near identical response profiles to untreated mice, with Loom stimuli evoking 49% (44 / 89) detection, 4% (4 / 89) escape, and 47% (42 / 89) freeze responses, while for Sweep stimuli they had response rates of 58% (56/96) detection, 2% (2 / 96) escape, and 57% (55 / 96 trials) freeze. There is thus a slightly higher

probability of freeze responses following presentation of Sweep stimuli by *Rd1* treated mice (**Figure 33 C**), but the effect is marginal. Baseline data showed consistent, low response probabilities in both untreated (detection 30%, n = 65/217; escape 4%, n = 9 / 217; and freeze 26%, n = 56 / 217) and treated *Rd1* mice (detection 28 %, n = 68 / 243; escape 3 %, n= 7 / 243; and freeze 26 %, n= 63 / 243).

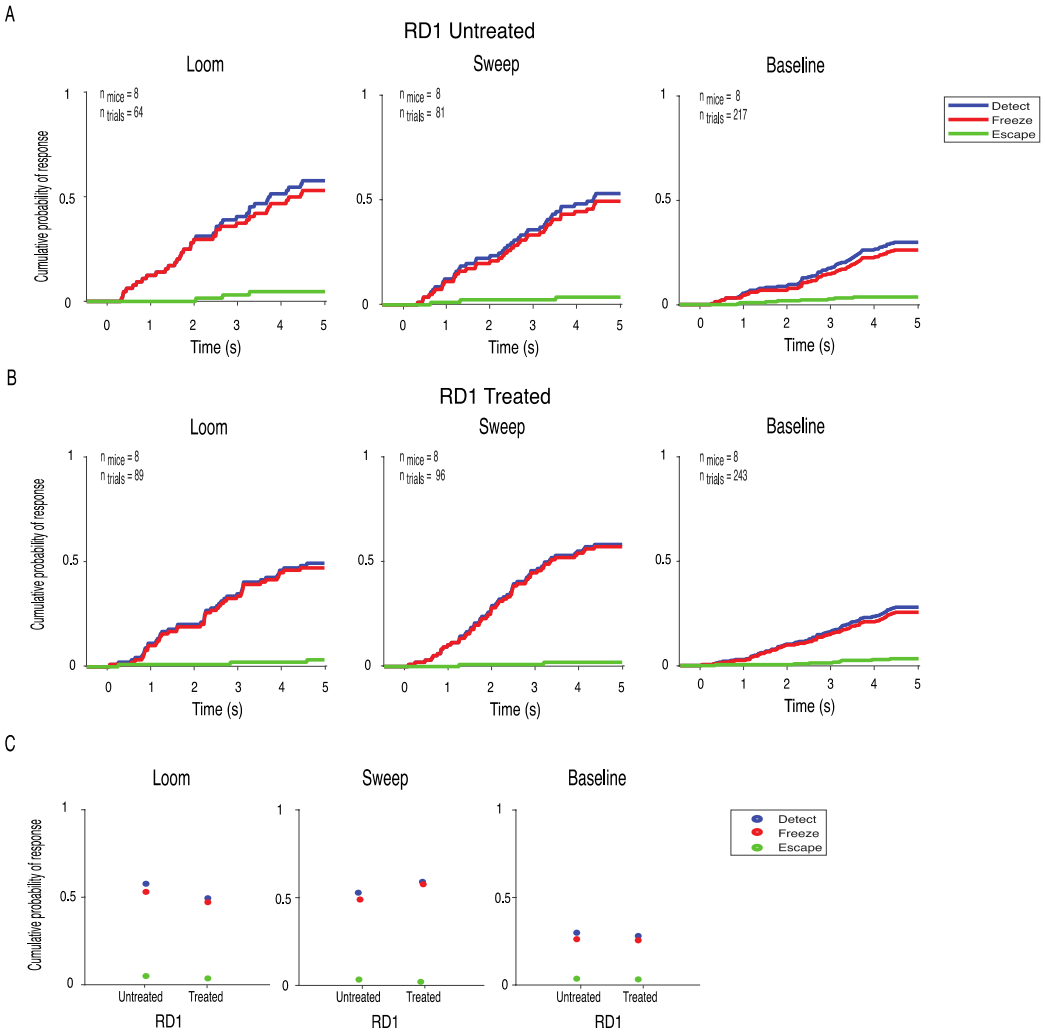

Figure 33: Evaluating gene therapy in Rd1 mice by assessing avoidance behaviour.

(A, B) Cumulative probability of having observed either an escape and/or freeze response – detect (*blue*), an escape response (*green*) and a freeze response (*red*) over time. (A) untreated control *Rd1* cohort, and (B) *Rd1* mice treated with *AAV.RK.βPDE*. (C) Average cumulative probability of having observed either an escape and/or freeze response – detect (*blue*), an escape response (*green*) and a freeze response (*red*) over time across untreated and untreated *Rd1*mice datasets.

It is noteworthy that the results obtained in this study for untreated Rd1 mice (lacking both rods and cones) closely resemble those obtained in Chapter 5 for the OGC (triple-knockout mouse model lacking functional rods and cones, in addition to light-sensitive melanopsin (m)RGCs). In the OGC model, we observed detection rates of 58 % and 70 % for Loom (n= 26 / 45) and Sweep trials (n= 32 / 46), respectively, with the majority of these responses categorized as freezing behaviour (**Figure 22 C**). Similarly, baseline measurements (**Figure 22 C**) were higher than those observed for wild-type strains, indicating the absence of a clear response to visual stimuli in OGC mice, as anticipated. The resemblance in results between Rd1 and OGC implies a foundational level of response in rod-less and cone-less models, characterized by increased instances of freezing overall, as indicated by the baseline data. This suggests higher cumulative probabilities of freezing and, consequently, detection as well. This suggests a distinct behavioural profile and, consequently, a different background level of response in these non-vision function mice, which is evident even during baseline assessments.

When initially designing this study, I anticipated that treated Rd1 mice would exhibit escape and freeze responses to visual stimuli, considering our previous report of robust gene therapy-mediated rescue of retinal function for this mouse model using electroretinogram recordings (ERGs) (Nishiguchi et al., 2015). However, the variability in retinal rescue observed could potentially explain the lack of anticipated results. Additionally, to the best of my knowledge, no hierarchical study comparing methods of retinal and visual function assessment has been conducted to date. Therefore, it is conceivable that avoidance behaviour, as triggered by Loom and Sweep stimuli, may necessitate greater retinal function than that required to elicit an electrical response in the retina, or even other visually evoked responses.

To explore the comparative sensitivity of this test, the mice involved in this study underwent a secondary behavioural assessment using the optomotor test. The optokinetic motor reflex is characterised by slow head movements elicited by visual stimuli, typically a slowly rotating vertically striped pattern (**Figure 34 A**). Mice track the rotating pattern, with clockwise

rotations being driven predominantly by responses from the left eye, and counter-clockwise rotations being driven by activity in the right eye, enabling assessment of each eye individually. Moreover, this technique permits a measure of contrast sensitivity and visual acuity, by modifying the contrast, thickness, and rotation speed of the vertical bars. For this project, contrast sensitivity was evaluated at each of three different spatial frequencies (0.1, 0.2 and 0.4 cycles per degree; c/d) (see Methods Chapter 2, Section 5) 6 weeks post-injection.

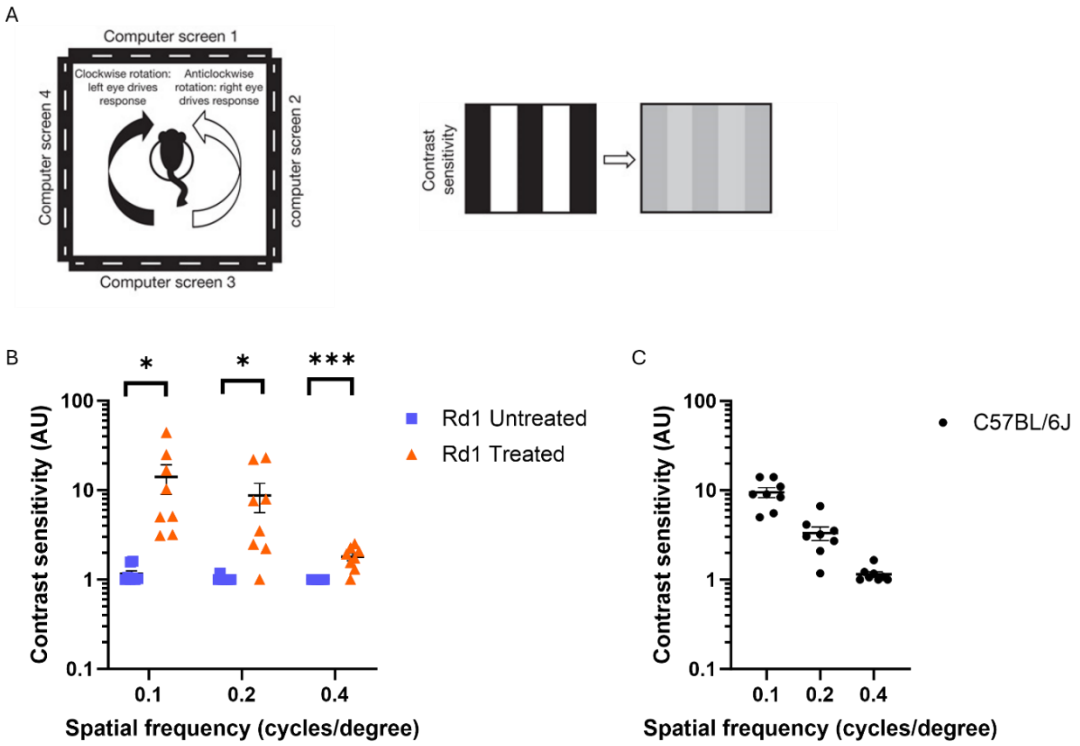

Figure 34: Evaluating contrast sensitivity in untreated and treated RD1 mice.

(A) Schematic of the optomotor set-up and representation of contrast sensitivity. Figure adapted with permission from Rachael A. Pearson et. al, Nature. 10.1038, 2012. (B) Contrast sensitivity thresholds for untreated (orange) and treated (blue) *Pde6b*$^{rd1/rd1}$ mice at three different spatial frequencies: 0.1, 0.2 and 0.4 (cycles/degree) obtained by optomotor test at 6 weeks post treatment. Data points shows the average of 3 independent assessments at each spatial frequency, per mouse. (C) Responses from adult wildtype mice (*C57Bl/6J*) are shown for comparison. $p<0.05$= statistically significant *, $p<0.001$= highly significant ***

Although variable, the mean contrast sensitivity thresholds were significantly higher for treated Rd1 mice (n=8), compared to the untreated cohort (n=8) values at all three acuity settings assessed (0.1 c/d : p=0.024, unpaired t-test, 1.2 ± 0.09 vs 14.1 ± 5.1; 0.2 c/d : p=0.025, 1.02 ± 0.02 vs 8.75 ± 3.15; 0.4 c/d: p=0.0003, 1.01 ± 0 vs 1.8 ± 0.18 untreated vs treated, respectively) (**Figure 34 B**). Notably, the contrast measurements obtained for the treated cohort are similar to those obtained for adult wildtype (*C57Bl/6J*, n=3) mice (0.1 c/d: 9.52 ± 1.2; 0.2 c/d: 3.33 ± 0.57; 0.4 c/d: 1.15 ± 0.08), suggesting a substantial degree of rescue was achieved in the treated cohort (**Figure 34 C**).

Next, the mice enrolled in this study underwent ERG recordings (**Figure 35**), a well-established technique that measures alterations in electrical activity across the eye in response to light stimuli. The changes in polarity detected by electrodes positioned on the corneal surface, with respect to a reference electrode, reflect changes in the polarity of cells in the retina. Typically, a negative deflection, referred to as the a-wave, is seen first, driven by the hyperpolarization of photoreceptor cells in response to the light stimulus. Subsequently, a more pronounced positive deflection ensues, referred to as the b-wave, and this is thought to derive from the depolarization of inner retinal neurons. Treated and untreated mice (n= 8 mice per group) were assessed 6-8 weeks post-treatment, after Loom and Sweep and Optomotor testing.

Again, somewhat surprisingly, we failed to observe a significant improvement in ERG function in the treated cohort; the mean amplitude of both a- and b- waves following light flash from dark adapted conditions (0.01 and 10 cd.s/m^2, respectively) was slightly higher in the treated cohort, but this was not statistically significant (**Figure 35**).

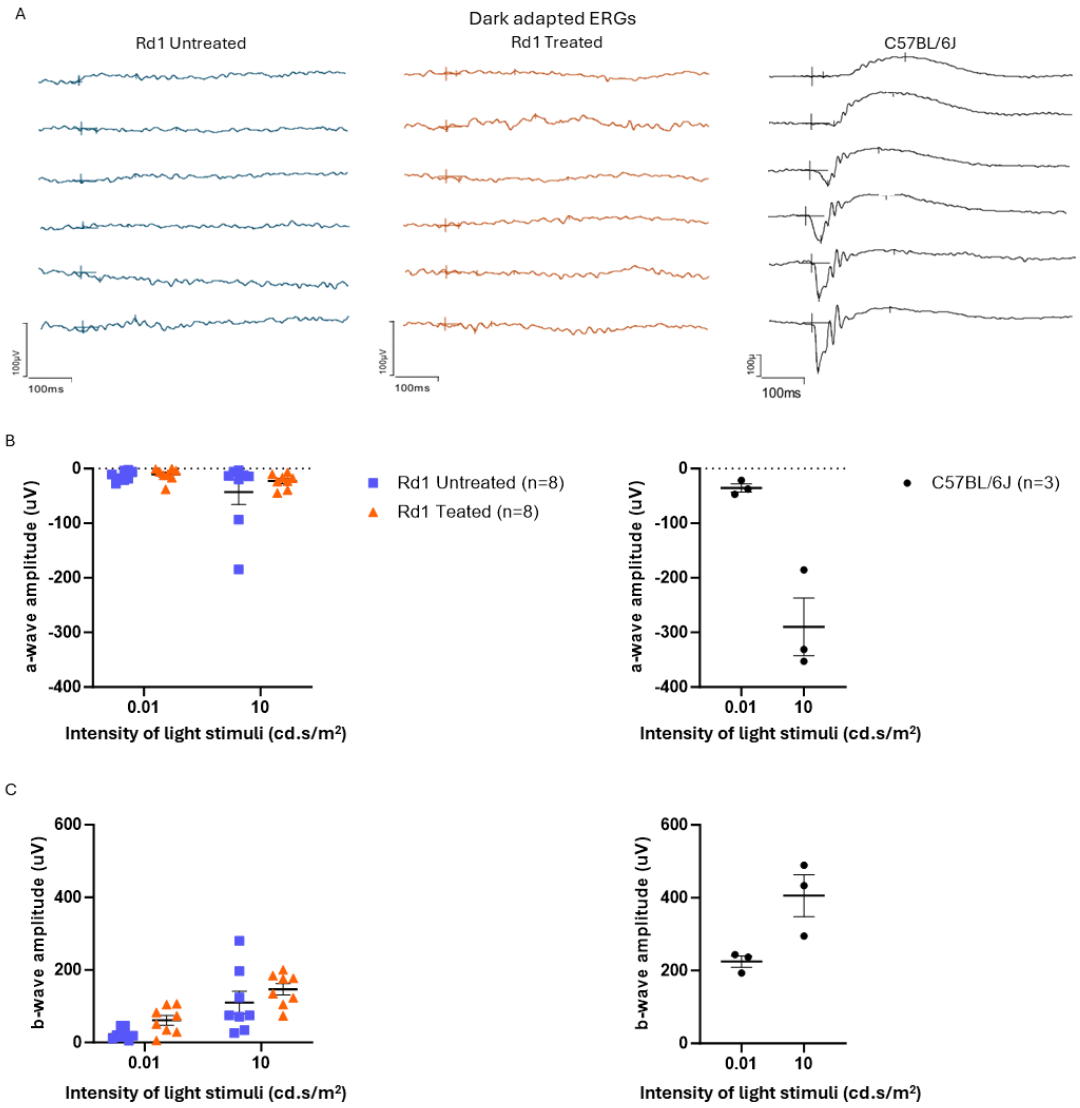

Figure 35: Dark-adapted electroretinogram recordings of untreated and treated Rd1 mice 6 weeks after gene transfer.

(A) Examples of dark-adapted electroretinogram (ERG) traces elicited by a series of white light flash intensities from 0.001, 0.01, 0.1, 1, 10 and 30 cd.s/m^2 respectively in untreated *Pde6b$^{rd1/rd1}$*(*blue)*, treated *Pde6b$^{rd1/rd1}$* (*orange*) and wildtype mice *C57Bl/6J* from left to right respectively. (B) Quantification of the a-wave amplitudes in treated (*blue*, n=8) and untreated eyes (*orange*, n=8) from *Pde6b$^{rd1/rd1}$* mice (left) and for wildtype mice *C57Bl/6J (right, n=3*) in response to 0.01 and 10 cd.s/m^2 light flashes from a dark-adapted background. (C) Quantification of the b-wave amplitudes in treated (*blue*, n=8) and untreated eyes (*orange*, n=8) from *Pde6b$^{rd1/rd1}$* mice (left) and for wildtype mice *C57Bl/6J (right, n=3*) in response to 0.01 and 10 cd.s/m^2 light flashes from a dark-adapted background. Adult wildtype mice (*C57Bl/6J*) data are shown for comparison.

Similarly, in the light adapted conditions the mean amplitudes of both a- and b-waves (10 and 50 cd.s/m², respectively) were slightly higher in the treated cohort compared to the control. However, this increase was not statistically significant (**Figure 36**). Furthermore, the observed effect for dark and light adapted conditions was considerably smaller than the magnitude of rescue we previously reported for this model using the same construct.

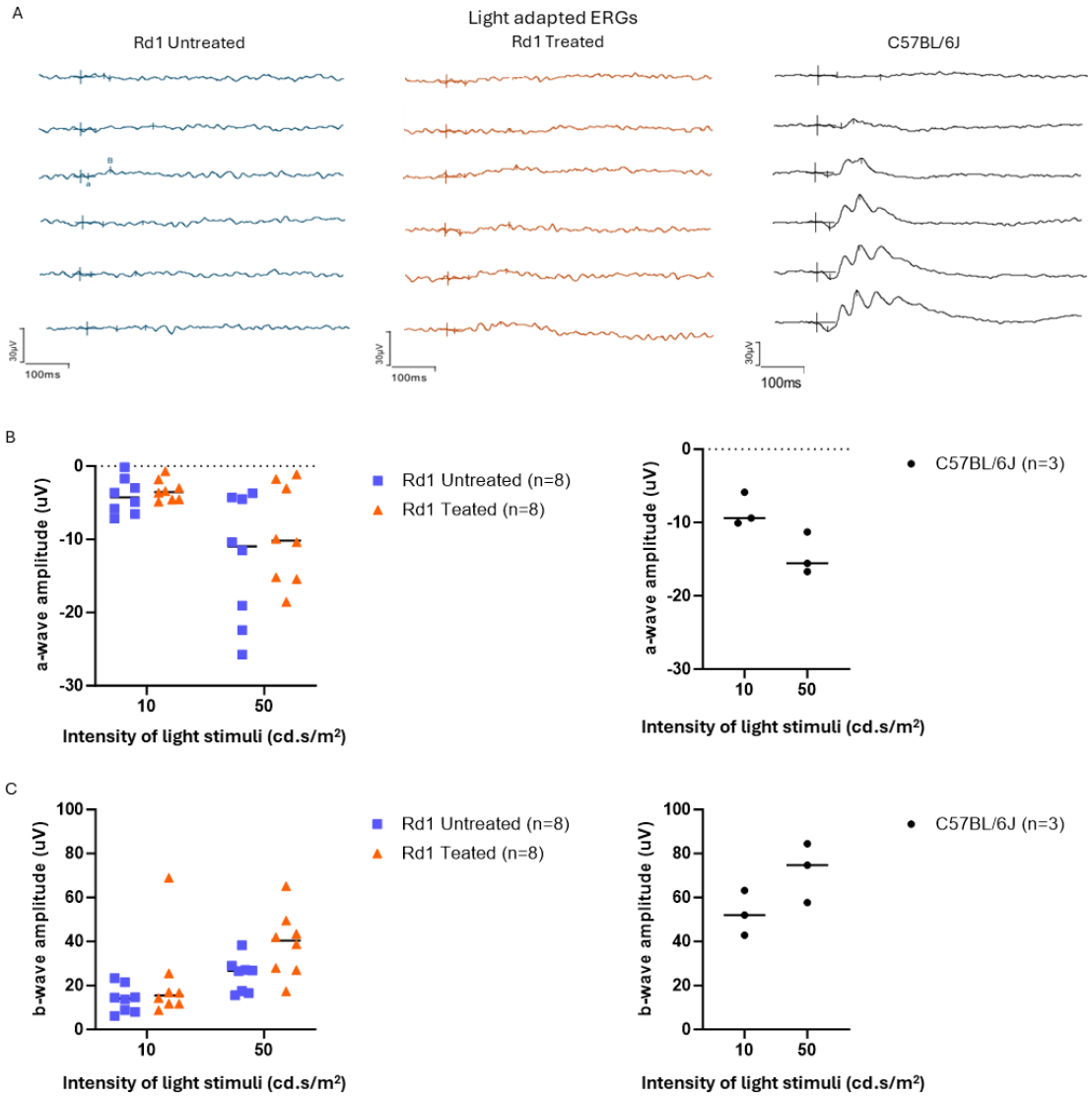

Figure 36: Light-adapted electroretinogram recordings of untreated and treated Rd1 mice 6 weeks after gene transfer.

(A) Examples of light-adapted electroretinogram (ERG) traces elicited by a series of white light flash intensities from 0.1, 1, 3, 10, 30 and 50 cd.s/m^2 respectively in untreated *Pde6b*$^{rd1/rd1}$(*blue)*, treated *Pde6b*$^{rd1/rd1}$ (*orange*) and wildtype mice *C57Bl/6J* from left to right respectively. (B) Quantification of the a-wave amplitudes in treated (*blue*, n=8) and untreated eyes (*orange*, n=8) from *Pde6b*$^{rd1/rd1}$ mice (left) and for wildtype mice *C57Bl/6J (right, n=3*) in response to 10 and 50 cd.s/m^2 light flashes from a light-adapted background. (C) Quantification of the b-wave amplitudes in treated (*blue*, n=8) and untreated eyes (*orange*, n=8) from *Pde6b*$^{rd1/rd1}$ mice (left) and for wildtype mice *C57Bl/6J (right, n=3*) in response to 10 and 50 cd.s/m^2 light flashes from a light-adapted. Adult wildtype mice (*C57Bl/6J*) data are shown for comparison.

7.1 Conclusion.

The variability observed in rescue outcomes poses challenges when interpreting results obtained from Loom and Sweep experiments. While gene therapy experiments conventionally adopt a design where one eye is injected while the other serves as an internal control, our approach deliberately diverged by injecting both eyes to enhance the likelihood of achieving sufficient rescue to support the behavioural responses triggered by Loom and Sweep. However, the variation of rescue observed even within an animal imposes limitations on the interpretation of the Loom and Sweep data. Nevertheless, this variability does not undermine the reliability of Loom and Sweep results, as evidenced by the remarkable consistency demonstrated throughout the preceding chapters. The inability to achieve significant rescue in the Rd1 mouse with this vector raises significant concerns. This issue, however, pertains more to the efficacy of the viral vector rather than the methodology of the Loom and Sweep experiments. While acknowledging this concern, it's also important to note that addressing the efficacy of the viral vector may be tangential to the primary focus of this thesis.

In conclusion, this chapter sought to examine the potential of vision-dependent avoidance behaviours as a non-invasive tool for assessing the efficacy of therapeutic interventions in the treatment of retinal degenerative

diseases. The unexpected variability in gene therapy rescue together with the decision to treat both eyes make it challenging to rigorously compare Loom and Sweep against the other tests. However, optomotor does appear to be the most sensitive of the assessments, followed by ERG and then Loom and Sweep, although further experiments including single eye treatments are required to confirm this provisional finding.

CHAPTER 8: Discussion.

The visual system has long been the subject of significant research interest both to understand the neurobiology underlying visual processing and as a model to understand the mechanisms underlying neurodegenerative disorders. The pre-clinical development of potential therapies for retinal degeneration relies heavily on the use of mouse models, requiring the ability to assess visual function before, during and after treatment. Current methods used to assess vision in mice are largely restricted to: a) electrophysiological recordings, which provide a useful measure of retinal function; b) pupillary light reflex, optokinetic and optomotor reflexes, which all share the same limitation, being sub-conscious reflex responses where activity is only indirectly related to perceptual vision (Abdeljalil et al. 2005; Hall and Chilcott 2018); and c) visually associated-fear conditioning, food and water regulation, and water-maze tests, which allow a measure of perceptual and cortically modulated vision, but rely on learning, and are lengthy and often stressful techniques (Prusky et al., 2000), limiting their use in progressively visually impaired animals. Developing new non-invasive, repeatable, and reliable methods for behavioural measurements of visual sensitivity is crucial. Visually induced avoidance responses (escape or freeze) may be a potential alternative to assess low- and high-level visual function.

8.1 Overall characterisation of avoidance behaviours.

The initial aim of this project was to establish a standardized framework for assessing visual stimulus-induced escape/freeze response in wild-type mice. To confirm the presence of visually induced avoidance behaviours randomly allocated wild-type mice were exposed to a single session per day for five consecutive days (a “Tonic” protocol). In the present study, I was able to observe freezing and escape avoidance behaviours in response to, respectively, a sweeping or looming visual stimuli (**Figure 5A-D**), as previously

reported by De Franceschi et al. (2016). Specifically, a small black disk crossing the monitor overhead (“Sweep” stimulus) primarily induced a substantial decrease in movement speed of the mice (freeze behaviour). I also observed combined freeze+escape behaviours in response to the Sweep stimuli, as described by De Franceschi et al. (2016). Further, I established that the presentation of an expanding black disk (“Loom” stimulus) reliably caused mice to escape to the refuge.

The most commonly used experimental design in similar behavioural studies consists of testing the mice in a a small number of sessions, over a couple of days (De Franceschi et al. 2016; Huang et al. 2017; Lenzi et al. 2022), similar to the “Tonic” protocol in the present study. However, no work has been done so far to establish whether this is represents an optimal experimental design. Habituation or extinction may be more prominent in some designs than others, and inter- and intra-animal variability may similarly differ between protocols (Zhou et al., 2009; Raderschall et al., 2011; Bell and Peeke, 2012; Tafreshiha et al., 2021). Therefore, in addition to the “Tonic” protocol, two other protocols were designed with an increasing number of sessions per day: “Burst” (five sessions in one day) and “Intense” (five sessions per day for five consecutive days) (**Figure 6 A**). The comparison of the three designs enabled assessment of whether session intensity leads to habituation &/or behavioural extinction, and the significant data collection per animal permitted analysis of intra- and inter-animal variability.

The comparison of the different experimental protocols demonstrated that the characteristic avoidance behaviours were observed and broadly maintained in all three protocols (**Figure 6 E**) but session intensity led to subtle differences in behaviour. The behaviour profiles of mice tested on the “Tonic” and “Intense” protocols were very similar in terms of overall response and preferred behavioural response to the visual stimuli. There was a heightened likelihood of response across all trials and an increased tendency to escape in response to visual stimuli on “Burst” protocol (**Figure 6 C and E**), likely reflecting the specific preferences of mice assigned to this protocol. Notably, the consistency observed in the behavioral profiles and the analysis of

response characteristics such as freeze latency, maximum escape speed, and freeze duration to Loom stimuli across different experimental protocols revealed remarkable similarities, suggesting that these behaviors maintain consistency and reproducibility irrespective of protocol dynamics (**Figure 7 A**).

The consistency of innate behaviours within individual animals, which persist across varying stimuli presentations and over time was particularly striking. This consistency highlights the robust and recurrent nature of these individual personal preference responses to visual stimuli, further reinforcing their relevance and significance in our research. The discussion of these idiosyncratic preferences will be discussed in detailed later on.

The feasibility of employing these instinctive behaviours as a pre-clinical test to evaluate vision function in mice, along with the findings obtained, prompted us to devise an Optimized protocol by merging aspects of the "Tonic" and "Burst" design protocols. This protocol would comprise of 3 sessions per day for two consecutive days, whilst the session design and the sequence of stimuli remained unchanged. Due to establishment changes part-way through the project, two cohorts of mice housed at different Universities were assigned to this protocol, one that moved between UCL and KCL, and a another that was bred at KCL (**Figure 8 E**). Some differences were noted between sites, where the UCL cohort showed a lower cumulative probability of escape in response to both visual stimuli. It is interesting that the KCL cohort exhibit similar behaviour profiles to the earlier UCL response profiles (**Figure 8 E**), so it would seem reasonable that UCL Optimised cohort experienced different environmental impacts associated with the move that influenced their later behaviours.

Indeed, it became evident that despite best efforts to maintain consistency in experimental conditions, handling procedures, user practices, and protocol design, individual mice can display distinct behavioural responses to Loom and Sweep stimuli. Although escape responses are commonly observed with Loom stimuli and freeze responses with Sweep stimuli, this pattern does not hold true for every mouse, with many showing combination responses and

some showing strong preference for one or other response, regardless of the stimulus. It is important to keep this in mind when designing studies and interpreting data accurately, but the central tenet of the hypothesis – that visually triggered innate behaviours can reliably indicate visual capability – remains unchanged: mice consistently detect and respond, regardless of the behaviour, to both Loom and Sweep stimuli. Establishing the “Optimised Protocol” not only highlights a commitment to practicality and utility within a research context, but also ensures the scientific validity of our research, laying a strong groundwork for subsequent chapters.

8.2 Choice of experimental design.

During the development of optimal study design, I sought to examine the impact of session number on mouse avoidance behaviour. Notably, across all data sets (“Tonic”, “Burst”, “Intense”, “Optimised”, focusing on the initial five sessions for each design protocol) I observed that mice responded less to the first presentation of the visual stimuli in the first session than on the remaining sessions (2-5), where the responses were quite consistent (**Figure 10 A**). On session 1 mice were allowed to explore/adapt to the arena for 10 minutes whereas only 5 minutes of adaptation was given on the remaining sessions. This could indicate that longer periods of adaptation might affect the mouse’s level of anxiety in the arena , or that they have not yet learnt to pay attention to the potential for overhead threat. Avoidance behaviours depend on learned information about the spatial environment (Vale et al. 2017). As mice are re-exposed to looming or sweeping visual stimuli overhead, they are continually learning about their spatial environment, which is reflected in the higher probabilities of responses to the same visual stimuli in the following sessions, 2-5.

Analyzing the trial data, where each trial involves the presentation of visual stimuli in the defined Sweep-Loom-Sweep-Loom order, it becomes evident that the sequence of stimulus presentation does not exert a significant

influence on the probability of response: mice responded similarly to both the 1st and 2nd Loom, and to the 1st and 2nd Sweep stimuli within a given session (**Figure 10**). Furthermore, the order of stimulus presentation exhibited minimal influence on response characteristics (**Figure 11**). The behavioral profile remained consistent across repetitions of the same stimuli, indicating stability in response patterns regardless of presentation sequence.

8.3 Impact of mouse characteristics on visually evoked avoidance behaviour.

In biomedical research, particularly in ophthalmology, behavioural testing of animals, especially mice models, plays a crucial role in understanding visual function and developing treatments for retinal degeneration. The Loom and Sweep test established here offers a simple and reliable method to assess vision in mice. However, it is imperative to consider the potential impact of variables such as sex, age, and background strain differences, as these characteristics have been shown to significantly influence behaviour in other settings (Joel and McCarthy 2017; Shaqiri et al. 2018; Sultana, Ogundele, and Lee 2019).

8.4 Sex.

Sex is a particularly significant factor in experimental design, as there is consensus on the existence of disparities between female and male brains across biochemistry, physiology, structure, and function, supported by studies in basic neuroscience (Becker et al., 2005; McCarthy et al., 2012; Panzica and Melcangi, 2016; Joel et al., 2015). Differences in hormonal profiles and genetic predispositions between male and female mice can lead to variations in sensory perception and sex differences in behavioural responses have been documented across various species, spanning spatial navigation to social interactions (William Mowrey and Portman, 2012; Choleris et al., 2018; Munion et al., 2019; Shaqiri et al., 2018). In the present study, the responses to Loom

and Sweep stimuli across female and male cohorts were remarkably similar (see **Figure 14** and **15**). In depth analysis revealed a slight trend for females to exhibit a higher freeze response and a lower inclination for escape responses compared to males, particularly in response to the Sweep stimuli (refer to **Figure 15**). However, these disparities were marginal, and overall, my findings suggest that sex is unlikely to represent a confounding factor in experimental design. The observed trend in freeze behavior among female mice is consistent with findings from other studies. For instance, Borkar et al. utilized a fear conditioning paradigm that induces both freezing and flight responses and similarly discovered no gender disparity in conditioned flight behavior between male and female mice. However, they noted a significantly higher occurrence of freezing behavior in females (Borkar et al., 2020). Furthermore, reports from various studies indicate that female mice exhibit increased freezing behavior, as evidenced by studies documenting impaired cued fear extinction memory in female mice and rats (Baran et al., 2009; 2010). While different studies may report sex-dependent differences (Colom-Lapetina et al., 2019), it is crucial to acknowledge that the majority of studies still predominantly focus on experiments involving only one sex. Consequently, obtaining a comprehensive understanding across all paradigms of behavior, reflecting an even distribution of data for both male and female subjects would improve biomedical reaserch (Shansky and Woolley, 2016; Joel and McCarthy, 2017).

8.5Age.

Age is another important variable that can influence an individual's perception, cognition, and responses to the environment (Shoju et al., 2016; Roberts and Allen, 2016). The aging process profoundly affects the brain's structure and function, including its sensory, motor, and cognitive processes, and can lead to behavioural changes. A considerable amount of research has been devoted to understanding how aging impacts visual function (Andersen, 2012), focusing mainly on age-related impairments in visual perception, such as orientation, contrast sensitivity, and spatial frequency. Moreover, various

cell types within the retina undergo age-related alterations, potentially contributing to a decline in visual acuity (Lehmann et al., 2021; Qianli Meng, 2019; Samuel et al., 2011; Calkins, 2013; Sugita et al., 2020; Radulescu et al., 2021). It was important to determine in what ways, if any, age affects visually evoked innate responses, if we are to utilise it as a tool to assess visual function in mouse models of progressive retinal diseases and evaluate therapeutic interventions over time. The trend of age-related effects on visually triggered innate behaviours observed in this study can be described as an increased likelihood of escape behaviour, starting at low levels in young mice, increasing as mice mature, before decreasing again in old age. This trend is consistent for both visual stimuli presented to the mice. Freezing behaviour presented the opposite trajectory, with mice showing more freezing at very young and old ages, compared to 6 week - 6 month old adult stages.

These trends align with the biology of mice, as younger mice may be less familiar with the stimuli and therefore exhibit freezing responses as a cautious approach to novel stimuli. As mice mature, they become more familiar with threats (Lenzi et al. 2022) and may develop more efficient defence behaviours, leading to prominent escape responses. However, escaping requires substantial energy expenditure and may result in missed opportunities. Thus, as mice reach older age (middle age to old), they may prefer freezing as a strategy to conserve energy and resume normal activities once the threat has dissipated. Ultimately, as mice age further, escaping becomes less feasible due to energy constraints.

8.6 Genetic background.

Experimental research relies on a diverse range of inbred and outbred mouse strains, which serve as robust models for exploring various facets of human biology, each harbouring unique genetic backgrounds (Guenet JL., 2005; Vandamme TF., 2014). However, the selection of mouse strains for pre-clinical studies demands careful consideration, as behavioural responses can be influenced by the genetic makeup of the experimental animals. Notably,

differences in behaviour have been documented among different strains (Bothe et al., 2005; Can et al., 2012). Bothe et al. (2005) found significant behavioral differences among 14 inbred mouse strains across three behavioral tests: rotorod, open-field activity-habituation, and contextual and cued fear conditioning, where some strains consistently outperformed others in these assays (Bothe et al., 2005). Additionally, Sultana et al. (2019) reported that animals from different genetic background strains displayed distinct behavioral patterns when evaluated for sociability/novelty, memory function, and negative behaviors like despair and stress calls (Sultana et al., 2019). These findings suggest that genetic variation among strains contributes, at least partially, to strain-specific behavioral traits.

Here, I compared visually evoked innate behaviours across three wildtype strains that are commonly used as background strains for transgenic models: C57BL/6J, DBA1/J, and 129/SV (**Figure 20**). Distinct behavioural differences were observed, with C57BL/6J mice displaying a greater willingness to explore the environment, resulting in more frequent triggering of the visual stimuli and higher trial numbers per stimulus. Conversely, 129/SV, and especially DBA1/J, mice exhibited a greater reluctance to explore novel environments, leading to a lower likelihood of triggering the visual stimuli. However, despite the overall lower cumulative probabilities of response for both visual stimuli in these two strains, the same characteristic innate behaviours were still observed. Escape behaviours were more common in response to both stimuli in DBA1/J and 129/SV mice, which differed from C57BL/6J, where Sweep stimuli elicited a higher probability of freezing (under photopic conditions). That all three strains showed stereotyped responses in response to the two stimuli supports the wider applicability and utility of this as a test of visual function. It does, however, also emphasise the need to generate robust background- and age-matched wildtype control data when using it to assess visual impairment and/or treatment efficacy.

A key challenge in using the DBA1/J, and to a lesser extent the 129/SV mice, was their reluctance to explore the arena, making it challenging to present sufficient trials within the pre-defined time limits of the test. Although

not tested here, it may be possible to modify the set up to make it more attractive for exploration, for example by introducing a food reward (Lockie et al., 2017; Spangenberg and Wichman, 2018) at the centre of the test arena or by trialling different durations of acclimatisation/testing. Other shapes of arena might alter exploration, for example circular versus square, as used here. Recognizing the potential for behavioural differences among wildtype strains is essential both for good experimental design and improving the reliability and accuracy of behavioural neuroscience-based research.

Investigating the interactions and potential modulation of characteristics on avoidance behaviours is essential for understanding the reliability of behavioural assays as preclinical tools for assessing vision function in mice. By systematically evaluating the influence of sex, age, and background strain on avoidance responses to visual stimuli, researchers can enhance the robustness and validity of their experimental designs and interpretations. The findings not only have immediate relevance for my current research, but they are also poised to make a significant contribution to the broader scientific community, as I have acquired a large, carefully controlled dataset examining these variables. I plan to share this comprehensive dataset as an open resource to provide a unique resource for understanding visually evoked behaviours in mice. Moreover, it may prove crucial in underpinning important aspects of vision perception and mouse behaviour for the wider scientific community.

8.7 The contribution of photosensitive cells in sculpting visually evoked avoidance behaviour.

In the complex field of neurobehavioral research, unravelling the intricate relationship between sensory input and behavioural responses holds paramount importance. In mice, a substantial proportion of retinal output neurons project to the Superior Colliculus (SC), where distinct populations of SC neurons exhibit responses to sweeping (Gale and Murphy, 2016) and

looming stimuli (Zhao et al., 2014). These studies have shown that key targets of the SC, such as the lateral posterior nucleus of the thalamus (LP) and the periaqueductal gray (PAG), have been implicated in freeze and escape responses, respectively (Wei et al., 2015; Evans et al., 2018).

While previous investigations have predominantly focused on the circuitry beyond the retina, delving into higher-level pathways and integration processes, less is known about the specific contributions of the different light-sensitive retinal cells, rod and cone photoreceptors and melanopsin-containing intrinsically photosensitive retinal ganglion cells, in shaping visually evoked avoidance behaviours in mice. To address this, I explored the behaviour of well characterised mouse models harbouring genetic knockouts for different components of phototransduction. Specifically, *Gnat1*$^{-/-}$ (referred to as GNAT1, a non-degenerative model of stationary night blindness with non-functional rod photoreceptors, but unaffected cones), *Cnga3*$^{-/-}$ (referred to as CNGA3; a model where cones are non-functional and degenerate within three months, while rods remain unaffected), and *Gnat1*$^{-/-}$ *x Cnga3*$^{-/-}$ *x Opn4*$^{-/-}$ (referred to as OGC; a triple-knockout mouse model with non-functional rods and cones, in addition to non-functional melanopsin retinal ganglion cells), were studied alongside wild-type C57BL/6J mice. These mice were exposed to Sweep and Loom stimuli under both photopic (normal light, **Figure 24** and **25**) and scotopic (low light, **Figure 26** and **27**) conditions following appropriate dark/light adaptation.

The findings from the photopic responses shed light on the intricate dynamics of visually evoked avoidance behaviours, revealing distinct patterns among the different mouse strains examined. Notably, the CNGA3 mice exhibited robust responses to both Loom and Sweep stimuli (**Figure 24**), indicating that rod pathways can sustain these behaviours under moderate photopic conditions, even when cone function is compromised. Conversely, in GNAT1 mice where the rod pathway is disrupted, a lower rate of detection for both Loom and Sweep stimuli was observed (**Figure 24**). While GNAT1 mice still exhibited a mix of freeze and escape responses to Loom and Sweep, freezing behaviour was more prevalent, compared to escape responses. As

expected, the OGC triple-knockout mice, lacking all photosensitive cells (rods, cones, and melanopsin-containing cells), displayed a reduced ability to detect both Loom and Sweep stimuli (**Figure 24**).

Recent studies have strated to adress the role of the retina, particularly retinal ganglion cells (RGCs), in facilitating these defence behaviors. For instance, K-RGCs have been identified as essential for looming-evoked innate defensive behavior (F. Wang et al. 2021), while another study revealed that a specific type of RGC projecting to the dorsal raphe nucleus in the mouse retina modulates looming-evoked defensive behavior through DRN GABAergic neurons (Huang et al. 2017). The data from the OGC mice supports the notion that the absence of retinal ganglion cells could compromise innate defensive behaviors. However, exploring other models of photoreceptor dysfunction, such as, Gnat1$^{-/-}$/Cnga3$^{-/-}$/Opn4$^{+/+}$, mice where only retinal ganglion cells are expressed, could provide additional valuable insights into the role of these cells in supporting innate defensive behaviors.

Consistent with the findings above, CNG3A mice exhibited robust responses to both stimuli in scotopic light conditions, detecting 100% of trials with escape responses predominating, GNAT1 mice, which lack rod function, displayed limited escape behaviours, preferentially freezing if they responded at all. This underscores the importance of intact rod function in mediating effective avoidance behaviours. Interestingly, in scotopic conditions, C57BL/6J wildtype mice exhibited notably heightened behavioural responses to all visual stimuli, compared to those tested under standard phoopic conditions earlier in the project (Chapters 3-4). They exhibited a remarkable ability to detect and respond to visual stimuli with high accuracy, and high probabilities of escape was observed in response to Loom and Sweep stimuli.

Taken together, these indicate that the rod pathway preferentially drives an escape-based response and, in the absence of cone function (low light levels or when cones are dysfunctional). When cones are functional, they appear to modulate this response and bring in a more nuanced response that may be a balance between freezing and escaping. Behaviourally, these

findings are consistent with a survival mode, where mice, being nocturnal prey animals most typically active in dim light conditions, need to “act first, think later” if they perceive a potential predator. By creating environments that mimic the natural nocturnal and/or low light habitat of mice, it is possible to experimentally enhance the triggering of these innate defensive behaviours. By considering the environmental context in which mice evolved and naturally navigate, researchers may optimize experimental conditions to more closely resemble the ecological conditions that shape their behaviours. This approach could lead to more ecologically valid experimental designs and better understanding of the neural mechanisms underlying visually evoked behaviours in mice.

Overall, these findings provide valuable insights into the intricate interplay between retinal photoreceptor function and visually evoked avoidance behaviours in mice, highlighting the essential role of the rod pathway in mediating effective responses under both photopic and scotopic light conditions. The heightened behavioural responses observed in C57BL/6J mice under scotopic, compared to photopic, conditions suggest the potential importance of replicating nocturnal environments to enhance visually triggered innate behaviours. This refinement of the protocol described in this thesis could facilitate the use of visually triggered behaviour as a preclinical tool to measure visual function in mice. However, they also raise important considerations for studying retinal diseases and using this behaviour as a test for assessing efficacy of therapeutic interventions aimed at preserving visual function.

8.8 Idiosyncratic behaviours.

For the application of Loom and Sweep as a test for assessing visual function, it was necessary to determine if re-testing mice at different time points would influence mice avoidance behaviours. To examine this, animals were re-tested within the same protocol 28 days after the first exposure. Re-

testing mice under any of the four (“Tonic”, “Burst”, “Intense” and “Optimised”) experimental protocols showed no habituation or behavioural extinction to the Sweep stimuli. Interestingly, evidence of habituation was observed in responses to the Loom stimuli, where mice showed a reduction in escape responses (**Figure 12**). This is consistent with reports by others, who also reported evidence of habituation in response to looming stimuli, most likely reflecting the ability of mice to identify repeated, harmless stimuli so that the perceived threat level reduces with repeated exposure, and mice can avoid energy-expensive escape behaviours (Raderschall et al. 2011; Evans et al. 2019).

Habituation occurs in all animals, characterised by a progressive decrease in responsiveness to a repeated event, and can in some cases lead to behaviour extinction (Raderschall, Magrath, and Hemmi 2011; Bell and Peeke 2012). Evidence of habituation was seen when comparing the “burst” and “intense” protocols, in a decrease in exploratory behaviour across the sessions performed in a single day. What was particularly striking is that this decrease in exploratory behaviour is proportional to the number of sessions that a mouse is exposed to within a single day, but returns to baseline the next day, suggesting that there is daily recovery in exploratory behaviour. It will be interesting to explore whether this resetting is time- or sleep-dependent i.e. does exploration reset in the absence of stimuli for a minimum period of time, or does it require a sleep-wake cycle to reset. Taken together, our data suggest that the number of sessions that a mouse is exposed per day, and the potential for habituation, are important considerations for optimal experimental design. However, it is important to highlight that although habituation is evident, we continued to observe freeze and/or escape behaviours in response to the visual stimuli, suggesting no behavioural extinction. More broadly, habituation appears to be stimulus dependent, and suggests that mice constantly assess their defence strategies, modifying their behaviour choices based on balancing the threat imminence and escaping costs.

Our data shows that mice show a strong maintenance of their given idiosyncratic behaviours across sessions and time; a given mouse’s preferred

behaviourial response (to freeze, or escape, or freeze then escape) in response to a specific visual stimulus was maintained across sessions and time points. Individual animals maintained their preferred idiosyncratic behaviour even through the “Intense” protocol where they were exposed to 50 sessions. Thus, visually induced avoidance behaviour has a very low intra-animal variability, which strengthens the applicability of using these behaviours as a measure of visual function over time and before and after treatment.

Animal behavioural studies invariably encounter individual differences, but these are often treated as experimental “noise”. However, growing evidence shows that these behavioural differences are maintained through time and across contexts (Wolf and Weissing, 2012; Sih et al., 2015). These differences or “animal personalities” could reflect social context and experience (Wolf et al. 2008; Wolf et al., 2011, Laskowski and Bell, 2014). In the present study, behavioural differences to specific visual stimuli highlight the potential impact of inter-animal variability; for example, in the “Burst” protocol a higher number of escape responses were observed in response to the Loom stimuli (**Figure 12 B**). Throughout our results, we observed trial clustering of individual animals that responded differently to the same visual stimuli. These differences in response to the same visual stimuli i.e. inter-animal variability, could be clearly observed when comparing the protocols. Nonetheless, as discussed above, the vast majority of the animals tested maintained their preferred behaviour response throughout trials, sessions and even between time-points suggesting that “animal personalities” are maintained leading to low intra-animal variability.

It is important to acknowledge these individual differences in behaviour profiles, but for the purpose of this project, *any* response to the visual stimuli, particularly given its consistency, would support the establishment of this straightforward framework as a behavioural assay for assessing visual function in mice. While idiosyncratic behaviours are an important consideration in experimental designs and data interpretation, analyses across different protocols (**Figure 27**, **28**, **29** and **30**) showed consistent behavioural

responses to visual stimuli over time, with notable preservation of escape behaviours between initial and subsequent assessments. The longitudinal (**Figure 31**) study further demonstrated the endurance of specific behaviours over time, particularly during adulthood, while also highlighting age-related changes in behaviour, such as a reduction in escape responses in older mice.

8.9 Vision-dependent avoidance behaviours as a non-invasive assessment for evaluating the effectiveness of therapeutic interventions.

Strochi et al. (2019) described how innate responses elicited by visual stimuli might offer a viable approach for measuring visual capabilities both in mice with intact visual function and in mouse models of retinal degeneration, allowing for discrimination between severity and type of retinal degeneration. My research has shown that Loom and Sweep stimuli can indeed elicit robust, reproducible and stereotypical behavioural responses. To assess the effectiveness of the developed methodology outlined in this thesis, which employs vision-dependent avoidance behaviours as a non-invasive means of evaluating visual function in mice, I implemented a protocol previously described by Nishiguchi et al. (2015) to treat RD1 mice. This study encompassed a comprehensive approach, utilizing the Loom and Sweep behaviour test (**Figure 33**), optomotor assessment (**Figure 34**), and ERG recordings (**Figure 35**) to gauge the response of Rd1 mice to gene supplementation therapy. Surprisingly, and in contrast to previous experiments utilising the same construct to generate the therapeutic viral vector, histological analysis revealed variable degrees of rescue, with some eyes displaying robust preservation of retinal layers while others exhibited little or no improvement, despite receiving identical treatment protocols.

In the design of these experiments, meticulous consideration was given to the utilization of the Loom and Sweep behavioural test to measure vision function post-treatment. However, both eyes of the RD1 mice were treated to

achieve full rescue and maximize visual function, thereby aiming for clearer results from the Loom and Sweep behaviour test and exploring the sensitivity of this test subsequently.

The optomotor testing (**Figure 34**) revealed some improvements in contrast sensitivity thresholds in treated mice, indicating an enhanced level of rescue comparable to untreated RD1 mice. However, ERG recordings failed to demonstrate a significant improvement in retinal function in the majority of treated eyes. Despite observing some rescue of the retinal phenotype, treated RD1 mice exhibited minimal differences in avoidance behaviours compared to untreated mice, suggesting that the variability in the rescue could be affecting the results. This discrepancy could also indicate that avoidance behaviours may require greater retinal function than that required to drive the optomotor response, underscoring the need for a comprehensive evaluation of the different methods of visual assessment used in pre-clinical research.

In conclusion, while vision-dependent avoidance behaviours show promise as a non-invasive tool for assessing therapeutic efficacy in retinal degenerative diseases, the unexpected variability in gene therapy outcomes underscores the importance of comprehensive evaluation methods, assessing multiple modalities in any given experiment. Further exploration into the sensitivity and reliability of Loom and Sweep behavioural test is required and I would seek to examine whether it is possible to achieve rescue by treating a single eye, as this would enable within animal testing of optomotor and ERG responses against control. Optomotor testing appears to be the most sensitive assessment, followed by ERG, but additional experiments, including single-eye treatments, are necessary to confirm these findings and elucidate the relative sensitivities of different evaluation methods.

CHAPTER 9: Summary of Key Results and Contributions.

The main contributions of this doctoral project are:

- Demonstrated the potential utility of and established a standardized framework for assessing visual stimulus-induced spontaneous behaviours as a low-impact measure of vision.

- Defined best protocol design for eliciting visual stimulus-induced innate behaviours, exploring variations in trial intensity over different time frames, resulting in a comprehensive and valuable dataset. This dataset has already garnered attention from researchers within and outside our lab and has been incorporated into their work and Ph.D. thesis (Wheatcroft, T. 2021. Projection-specific anatomy, physiology and behaviour in the mouse superior colliculus, PhD Thesis, University College London).

- Generated new understanding into the impact of background strain, sex, and different age groups in both longitudinal and cross-sectional studies, and various mouse models of visual dysfunction.

- Revealed that observed differences in behaviours are highly specific to individual animals, with individual behavioural response preferences maintained across time and repeated testing.

- Laid the foundation for further investigation into the biological mechanisms underlying visually induced innate behaviours (escape and freeze responses) elicited by salient visual stimuli, such as Loom and Sweep.

CHAPTER 10: Future Work.

The dataset I have generated is, to my knowledge, one of the most comprehensive available for assessing visually evoked behaviours. Although beyond the scope and time available in this thesis, we seek to exploit this dataset by employing various statistical tests that encompass all variables and parameters to provide a comprehensive overview. By integrating multiple factors into the analysis, such as sex, age, strain, and treatment effects, we expect to gain a greater understanding of how these influence behavioural responses more generally. In this thesis, detection was defined based on any escape or freeze responses, however, refining this definition, for example to encompassing other behaviours such as rearing, could capture subtle nuances in animal movements and behaviour indicative of stimuli perception. This could present an opportunity to develop more sensitive methods for detecting or accounting for stimuli perception, which in turn could provide for a more meaningful evaluation of the impact of novel therapies on visual function, compared to current measures which largely rely on assessment of retinal function (MEAs, ERGs) or reflexes (optokinetic headtracking, pupil reflex).

Indeed, a key aim of this project had been to validate the utility of the Loom and Sweep response framework as a metric for evaluating the effectiveness of novel therapies. Unfortunately, for reasons that are not entirely clear, we were unable to replicate the previously successful gene therapy rescue of Rd1 mice. It will be important to repeat these experiments, once viral vector efficacy has been re-established, and compare, as had been intended, the outcomes of the Loom and Sweep behavioural test with existing assessments, such as ERG and Optomotor, to establish the relative sensitivities of these different tests and how they can complement each other in assessing the level of rescue achieved post-treatment. To further establish the broader utility of the Loom and Sweep behavioural test, it will be important to extend this aspect of my investigation to other successfully treated (gene or

cell therapy) mouse models to understand the wider application of Loom and Sweep test as a behavioural test for measuring vision sensibility.

Dissecting the circuitry involved in driving freezing and escape behaviour is of particular interest for behavioural neuroscience. Further analysis of my dataset conducted in the group after the completion of this thesis is already revealing intriguing new insights, for example that the Escape response appears to be driven by rod, rather than cone, photoreceptors. Further investigation into the existing dataset and other models of photoreceptor dysfunction (e.g. $Gnat1^{-/-}$/$Cnga3^{-/-}$/$Opn4^{+/+}$) may offer further important insights. Related to this, an exciting avenue for exploration involves utilizing these visual stimuli (Loom and Sweep) in retinal explants to explore the responses at a retinal level. Understanding how different cells within the retina respond to these stimuli could shed light on the intricate biology underlying vision pathways. This is also important for improving our understanding of how well therapeutic approaches restore meaningful vision, as opposed to simply restoring light sensitivity. Recent unpublished work in our group using spatially defined stimuli (horizontal and vertical bars) and MEA analysis has found that photoreceptor transplantation therapy can yield sufficient acuity for the retinal ganglion cells to detect vertical and horizontal bars. How this might relate to driving behavioural responses to more salient shapes, such as looming disks, will be very interesting to determine.

By addressing these aspects, future research endeavours can further elucidate the utility and mechanisms underlying visually triggered innate behaviours, ultimately advancing our understanding of vision function, and paving the way for more effective therapeutic interventions in retinal degenerative diseases.

Table of copyright and reprint permissions

Page Number	Type of Work	Name of Work	Citation	Do I have permission?	Permission note
21	Figure	Figure 37: Schematic representation of the eye and retina of humans and primates.	Aikaterini A. Kalargyrou et. al, Front. Mol. Neuroscience. 15:1042469, 2023	Yes	Written permission
25	Figure	Figure 38: The visual pathway in primates.	Solomon and Lennie, Nature Reviews Neuroscience 8(4): 276-86, 2007	Yes	Written permission
29	Figure	Figure 39: Schematic illustration depicting the phototransduction cascade in a vertebrate rod and cone photoreceptor cell.	Larhammar, D., Nordström, K. and Larsson, T. A., Philosophical Transactions of the Royal Society B: Biological Sciences.10:1098, 2009	Yes	Written permission
155	Figure	Figure 34: Evaluating contrast sensitivity in untreated and treated RD1 mice.	Rachael A. Pearson et. al, Nature. 10.1038, 2012	Yes	Written permission

References

Abdeljalil, Jellali, Meziane Hamid, Ouagazzal Abdel-Mouttalib, Rousseau Stéphane, Romand Raymond, Auwerx Johan, Sahel José, Chambon Pierre, and Picaud Serge. 2005. “The Optomotor Response: A Robust First-Line Visual Screening Method for Mice.” Vision Research 45 (11): 1439–46.

Aghaizu, Nozie D., Kamil Kruczek, Anai Gonzalez-Cordero, Robin R. Ali, and Rachael A. Pearson. 2017. Pluripotent Stem Cells and Their Utility in Treating Photoreceptor Degenerations. Progress in Brain Research. 1st ed. Vol. 231. Elsevier B.V.

Ali, Robin R., Martin B. Reichel, Adrian J. Thrasher, Roland J. Levinsky, Christine Kinnon, Naheed Kanuga, David M. Hunt, and Shomi S. Bhattacharya. 1996. “Gene Transfer into the Mouse Retina Mediated by an Adeno-Associated Viral Vector.” Human Molecular Genetics 5 (5): 591–94.

Ali, Robin R., Gian Marco Sarra, Clare Stephens, Mahesh De Alwis, James W.B. Bainbridge, Peter M. Munro, Sascha Fauser, et al. 2000. “Restoration of Photoreceptor Ultrastructure and Function in Retinal Degeneration Slow Mice by Gene Therapy.” Nature Genetics 25 (3): 306–10.

Allen, Annette E., Morven A. Cameron, Timothy M. Brown, Anthony A. Vugler, and Robert J. Lucas. 2010. “Visual Responses in Mice Lacking Critical Components of All Known Retinal Phototransduction Cascades.” PLoS ONE 5 (11).

Andersen, George J. 2012. “Aging and Vision: Changes in Function and Performance from Optics to Perception.” Wiley Interdiscip Rev Cogn Sci. 3 (3): 11–18.

Armstrong, R.A., and R.C. Cubbidge. 2019. The Eye and Vision: An Overview. Handbook of Nutrition, Diet, and the Eye. 2nd ed. Elsevier Inc.

Athanasiou, Dimitra, Monica Aguila, James Bellingham, Wenwen Li, Caroline McCulley, Philip J. Reeves, and Michael E. Cheetham. 2018. “The Molecular and Cellular Basis of Rhodopsin Retinitis Pigmentosa Reveals Potential Strategies for Therapy.” Progress in Retinal and Eye Research 62(October 2017): 1–23.

Auricchio, Alberto, Alexander J. Smith, and Robin R. Ali. 2017. “The Future Looks Brighter After 25 Years of Retinal Gene Therapy.” Human Gene Therapy 28 (11): 982–87.

Bainbridge, James W.B., Manjit S. Mehat, Venki Sundaram, Scott J. Robbie, Susie E. Barker, Caterina Ripamonti, Anastasios Georgiadis, et al. 2015. “Long-Term Effect of Gene Therapy on Leber’s Congenital Amaurosis.” New England Journal of Medicine 372 (20): 1887–97.

Bainbridge, James W.B., Alexander J. Smith, Susie S. Barker, Scott Robbie, Robert Henderson, Kamaljit Balaggan, Ananth Viswanathan, et al. 2008. “Effect of Gene Therapy on Visual Function in Leber’s Congenital Amaurosis.” New England Journal of Medicine 358 (21): 2231–39.

Baran, Sarah E., Charles E. Armstrong, Danielle C. Niren, and Cheryl D. Conrad. 2010. “Prefrontal Cortex Lesions and Sex Differences in Fear Extinction and Perseveration.” Learning and Memory 17 (5): 267–78.

Baran, Sarah E., Charles E. Armstrong, Danielle C. Niren, Jeffery J. Hanna, and Cheryl D. Conrad. 2009. “Chronic Stress and Sex Differences on the Recall of Fear Conditioning and Extinction.” Neurobiology of Learning and Memory 91 (3): 323–32.

Barber, Amanda C., Claire Hippert, Yanai Duran, Emma L. West, James W.B. Bainbridge, Katherine Warre-Cornish, Ulrich F.O. Luhmann, et al. 2013. “Repair of the Degenerate Retina by Photoreceptor Transplantation.” Proceedings of the National Academy of Sciences of the United States of America 110 (1): 354–59.

Barnard, Alun R., Joanne M. Appleford, Sumathi Sekaran, Krishna Chinthapalli, Aaron Jenkins, Matheas Seeliger, Martin Biel, et al. 2004. “Residual Photosensitivity in Mice Lacking Both Rod Opsin and Cone Photoreceptor Cyclic Nucleotide Gated Channel 3 α Subunit.” Visual Neuroscience 21 (5):675–83.

Becker, Jill B., Arthur P. Arnold, Karen J. Berkley, Jeffrey D. Blaustein, Lisa A. Eckel, Elizabeth Hampson, James P. Herman, et al. 2005. “Strategies and Methods for Research on Sex Differences in Brain and Behavior.” Endocrinology 146 (4): 1650–73.

Becker, Jill B., Brian J. Prendergast, and Jing W. Liang. 2016. “Female Rats Are Not More Variable than Male Rats: A Meta-Analysis of Neuroscience Studies.” Biology of Sex Differences 7 (1): 1–7.

Bell, Alison M., and Harman V.S. Peeke. 2012. “Individual Variation in Habituation: Behaviour over Time toward Different Stimuli in Threespine Sticklebacks (Gasterosteus Aculeatus).” Behaviour 149 (13–14): 1339–65.

Borkar, Chandrashekhar D., Mariia Dorofeikova, Quan Son Eric Le, Rithvik Vutukuri, Catherine Vo, Daniel Hereford, Alexis Resendez, Samhita Basavanhalli, Natalia Sifnugel, and Jonathan P. Fadok. 2020. “Sex Differences in Behavioral Responses during a Conditioned Flight Paradigm.” Behavioural Brain Research 389 (April): 112623.

Bothe, Gerald W.M., Valerie J. Bolivar, Michelle J. Vedder, and James G. Geistfeld. 2005. “Behavioral Differences among Fourteen Inbred Mouse Strains Commonly Used as Disease Models.” Comparative Medicine 55 (4): 326–34.

Botto, Catherine, Marco Rucli, Müge Defne Tekinsoy, Juliette Pulman, José Alain Sahel, and Deniz Dalkara. 2022. “Early and Late Stage Gene Therapy Interventions for Inherited Retinal Degenerations.” Progress in Retinal and Eye Research 86.

Bowes, Cathy, and Debora B. Farber. 1987. “MRNAs Coding for Proteins of the CGMP Cascade in the Degenerative Retina of the Rd Mouse.” Experimental Eye Research 45 (4): 467–80.

Breschi, Alessandra, Thomas R. Gingeras, and Roderic Guigó. 2017. “Comparative Transcriptomics in Human and Mouse.” Nat Rev Genet. 18 (7): 425–440.

Busse, Laura. 2018. “The Mouse Visual System and Visual Perception.” Handbook of Behavioral Neuroscience 27: 53–68.

Calvert, Gemma A., Ruth Campbell, and Michael J. Brammer. 2000. “Evidence from Functional Magnetic Resonance Imaging of Crossmodal Binding in the Human Heteromodal Cortex.” Current Biology 10 (11): 649–57.

Calvert, Peter D., Katherine J. Strissel, William E. Schiesser, Edward N. Pugh, and Vadim Y. Arshavsky. 2006. “Light-Driven Translocation of Signaling Proteins in Vertebrate Photoreceptors.” Trends in Cell Biology 16 (11): 560–68.

Carter-Dawson, L. D., M. M. LaVail, and R. L. Sidman. 1978. “Differential Effect of the Rd Mutation on Rods and Cones in the Mouse Retina.” Investigative Ophthalmology and Visual Science 17 (6): 489–98.

Celesia, Gastone G., and Paul J. DeMarco. 1994. “Anatomy and Physiology of the Visual System.” Journal of Clinical Neurophysiology 11 (5): 482–92.

Chang, B., N. L. Hawes, R. E. Hurd, M. T. Davisson, S. Nusinowitz, and J. R. Heckenlively. 2002. “Retinal Degeneration Mutants in the Mouse.” Vision Research 42 (4): 517–25. https://doi.org/10.1016/S0042-6989(01)00146-8.

Cholerisa, Elena, Liisa A. M. Galea, Farida Sohrabji, and Karyn M. Frick. 2017. “Sex Differences in the Brain: Implications for Behavioral and Biomedical Research.” Neurosci Biobehav 176 (3): 139–48.

Cideciyan, Artur V., Samuel G. Jacobson, William A. Beltran, Alexander Sumaroka, Malgorzata Swider, Simone Iwabe, Alejandro J. Roman, et al. 2013. “Human Retinal Gene Therapy for Leber Congenital Amaurosis Shows Advancing Retinal Degeneration despite Enduring Visual Improvement.” Proceedings of the National Academy of Sciences of the United States of America 110 (6): 517–25.

Clark, Damon A., Raphael Benichou, Markus Meister, and Rava Azeredo da Silveira. 2013. “Dynamical Adaptation in Photoreceptors.” PLoS Computational Biology 9 (11).

Colom-Lapetina, José, Anna J. Li, Tatiana C. Pelegrina-Perez, and Rebecca M. Shansky. 2019. “Behavioral Diversity across Classic Rodent Models Is Sex-Dependent.” Frontiers in Behavioral Neuroscience 13 (March): 1–8.

Einthoven, W., and W. A. Jolly. 1908. “The Form and Magnitude of the Electrical Response of the Eye to Stimulation by Light at Various Intensities.” Experimental Physiology 1 (4): 373–416.

Ellis, Erika M., Gregory Gauvain, Benjamin Sivyer, and Gabe J. Murphy. 2016. “Shared and Distinct Retinal Input to the Mouse Superior Colliculus and Dorsal Lateral Geniculate Nucleus.” Journal of Neurophysiology 116 (2): 602–10.

Evans, Dominic A., A. Vanessa Stempel, Ruben Vale, and Tiago Branco. 2019. “Cognitive Control of Escape Behaviour.” Trends in Cognitive Sciences 23 (4): 334–48.

Evans, Dominic A, A Vanessa Stempel, Ruben Vale, Sabine Ruehle, Yaara Lefler, and Tiago Branco. 2018. “A Synaptic Threshold Mechanism for Computing Escape Decisions.” Nature 558: 590–94.

Ferreira, Ana Catarina, Nuno Sousa, João Carlos Sousa, and Fernanda Marques. 2023. “Age-Related Changes in Mice Behavior and the Contribution of Lipocalin-2.” Frontiers in Aging Neuroscience 15 (April): 1–11.

Field, G. D., and E. J. Chichilnisky. 2007. “Information Processing in the Primate Retina: Circuitry and Coding.” Annual Review of Neuroscience 30: 1–30.

Franceschi, Gioia De, Tipok Vivattanasarn, Aman B. Saleem, and Samuel G. Solomon. 2016. “Vision Guides Selection of Freeze or Flight Defense Strategies in Mice.” Current Biology 26 (16): 2150–54.

Gale, Samuel D., and Gabe J. Murphy. 2014. “Distinct Representation and Distribution of Visual Information by Specific Cell Types in Mouse Superficial Superior Colliculus.” Journal of Neuroscience 34 (40): 13458–71.

Gotch, Francis. 1903. “The Time Relations of the Photo-electric Changes in the Eyeball of the Frog.” The Journal of Physiology 29 (4–5): 388–410.

Hall, Charlotte A., and Robert P. Chilcott. 2018. “Eyeing up the Future of the Pupillary Light Reflex in Neurodiagnostics.” Diagnostics 8 (1).

Hattar, S., R. J. Lucas, N. Mrosovsky, S. Thompson, R. H. Douglas, M. W. Hankins, J. Lem, et al. 2003. “Melanopsin and Rod–Cone Photoreceptive Systems Account for All Major Accessory Visual Functions in Mice.” Nature 462 (1): 76–81.

Hejtmancik, J. Fielding, and John M. Nickerson. 2015. Overview of the Visual System. Progress in Molecular Biology and Translational Science. 1st ed. Vol. 134. Elsevier Inc.

Hooser, Stephen D. Van. 2007. “Similarity and Diversity in Visual Cortex: Is There a Unifying Theory of Cortical Computation?” Neuroscientist 13 (6): 639–56.

Howlett, Marcus H.C., Robert G. Smith, and Maarten Kamermans. 2017. “A Novel Mechanism of Cone Photoreceptor Adaptation.” PLoS Biology 15 (4): 1–28.

Huang, Lu, Tifei Yuan, Minjie Tan, Yue Xi, Yu Hu, Qian Tao, Zhikai Zhao, et al. 2017. “A Retinoraphe Projection Regulates Serotonergic Activity and Looming-Evoked Defensive Behaviour.” Nature Communications 8.

Jerath, Ravinder, Molly W. Crawford, and Vernon A. Barnes. 2015. “Functional Representation of Vision within the Mind: A Visual Consciousness Model Based in 3D Default Space.” Journal of Medical Hypotheses and Ideas 9 (1): 45–56.

Joel, Daphna, and Margaret M. McCarthy. 2017. “Incorporating Sex As a Biological Variable in Neuropsychiatric Research: Where Are We Now and Where Should We Be?” Neuropsychopharmacology 42 (2): 379–85.

Kalargyrou, Aikaterini A., Siobhan E Guilfoyle, J Alexander, Robin R Ali, and Rachael A Pearson. 2023. “Extracellular Vesicles in the Retina - Putative Roles in Physiology and Disease.” Frontiers in Molecular Neuroscience, no. January: 1–16.

Keeler, Clyde E. 1924. “The Inheritance of a Retinal Abnormality in White Mice.” Proceedings of the National Academy of Sciences 10 (7): 329–33.

Kim, Ungsoo Samuel, Omar A. Mahroo, John D. Mollon, and Patrick Yu-Wai-Man. 2021. “Retinal Ganglion Cells—Diversity of Cell Types and Clinical Relevance.” Frontiers in Neurology 12 (May): 1–20.

Kretschmer, Friedrich, Momina Tariq, Walid Chatila, Beverly Wu, and Tudor Constantin Badea. 2017. “Comparison of Optomotor and Optokinetic Reflexes in Mice.” Journal of Neurophysiology 118 (1): 300–316.

Laskowski, Kate L., and Alison M. Bell. 2014. “Strong Personalities, Not Social Niches, Drive Individual Differences in Social Behaviours in Sticklebacks.” Animal Behaviour, no. 90: 287–95.

Lees, Rebecca Nicole, Armaan Fazal Akbar, and Tudor Constantin Badea. 2020. “Retinal Ganglion Cell Defects Cause Decision Shifts in Visually Evoked Defense Responses.” Journal of Neurophysiology 124 (5): 1530–49.

Lenzi, Stephen C., Lee Cossell, Benjamin Grainger, Sarah F. Olesen, Tiago Branco, and Troy W. Margrie. 2022. “Threat History Controls Flexible Escape Behavior in Mice.” Current Biology.

Lockie, Sarah H., Clare V. McAuley, Sasha Rawlinson, Natalie Guiney, and Zane B. Andrews. 2017. “Food Seeking in a Risky Environment: A Method for Evaluating Risk and Reward Value in Food Seeking and Consumption in Mice.” Frontiers in Neuroscience 11 (JAN): 1–7.

Lopes, Gonçalo, Niccolò Bonacchi, João Frazão, Joana P. Neto, Bassam V. Atallah, Sofia Soares, Luís Moreira, et al. 2015. “Bonsai: An Event-Based Framework for Processing and Controlling Data Streams.” Frontiers in Neuroinformatics 9 (APR): 1–14.

Lopes, Gonçalo, Karolina Farrell, Edward Horrocks, Chi-Yu Lee, Mai Morimoto, Tomaso Muzzu, Amalia Papanikolaou, et al. 2020. “BonVision – an Open-Source Software to Create and Control Visual Environments.” BioRxiv 983775 [Preprint], 1–11.

Lucas, Robert J., Gurprit S. Lall, Annette E. Allen, and Timothy M. Brown. 2012. How Rod, Cone, and Melanopsin Photoreceptors Come Together to Enlighten the Mammalian Circadian Clock. Progress in Brain Research. 1st ed. Vol. 199. Elsevier B.V.

Mannu, Gurdeep S. 2014. “Retinal Phototransduction.” Neurosciences.

Martersteck, Emily M., Karla E. Hirokawa, Mariah Evarts, Amy Bernard, Xin Duan, Yang Li, Lydia Ng, et al. 2017. “Diverse Central Projection Patterns of Retinal Ganglion Cells.” Cell Reports 18 (8): 2058–72.

Masland, Richard H. 2012. “The Neuronal Organization of the Retina.” Neuron 76 (2): 266–80.

McCarthy, Margaret M., Arthur P. Arnold, Gregory F. Ball, Jeffrey D. Blaustein, and Geert J. de Vries. 2012. “Sex Differences in the Brain: The Not so Inconvenient Truth.” Journal of Neuroscience 32 (7): 2241–47.

McClements, Michelle E., Federica Staurenghi, Robert E. MacLaren, and Jasmina Cehajic-Kapetanovic. 2020. “Optogenetic Gene Therapy for the Degenerate Retina: Recent Advances.” Frontiers in Neuroscience 14 (November).

Michalakis, Stylianos, Regine Mühlfriedel, Naoyuki Tanimoto, Vidhyasankar Krishnamoorthy, Susanne Koch, M. Dominik Fischer, Elvir Becirovic, et al. 2010. “Restoration of Cone Vision in the CNGA3-/- Mouse Model of Congenital Complete Lack of Cone Photoreceptor Function.” Molecular Therapy 18 (12): 2057–63.

Mowrey, William R, and Douglas S Portman. 2012. “Sex Differences in Behavioral Decision-Making and the Modulation of Shared Neural Circuits.” Biology of Sex Differences 3 (1): 8.

Münch, Thomas A., Rava Azeredo Da Silveira, Sandra Siegert, Tim James Viney, Gautam B. Awatramani, and Botond Roska. 2009. “Approach Sensitivity in the Retina Processed by a Multifunctional Neural Circuit.” Nature Neuroscience 12 (10): 1308–16.

Munion, Ascher K., Jeanine K. Stefanucci, Ericka Rovira, Peter Squire, and Michael Hendricks. 2019. “Gender Differences in Spatial Navigation: Characterizing Wayfinding Behaviors.” Psychonomic Bulletin and Review 26 (6): 1933–40.

Nishiguchi, Koji M., Livia S. Carvalho, Matteo Rizzi, Kate Powell, Sophia Martha Kleine Holthaus, Selina A. Azam, Yanai Duran, et al. 2015. “Gene Therapy Restores Vision in Rd1 Mice after Removal of a Confounding Mutation in Gpr179.” Nature Communications 6: 1–10.

Pahlberg, Johan, and Alapakkam P. Sampath. 2011. “Visual Threshold Is Set by Linear and Nonlinear Mechanisms in the Retina That Mitigate Noise: How Neural Circuits in the Retina Improve the Signal-to-Noise Ratio of the Single-Photon Response.” BioEssays.

Pang, Ji jing, Wen Tao Deng, Xufeng Dai, Bo Lei, Drew Everhart, Yumiko Umino, Jie Li, et al. 2012. “AAV-Mediated Cone Rescue in a Naturally Occurring Mouse Model of CNGA3-Achromatopsia.” PLoS ONE 7 (4): 1–9.

Panzica, Gian Carlo, and Roberto C. Melcangi. 2016. “Structural and Molecular Brain Sexual Differences: A Tool to Understand Sex Differences in Health and Disease.” Neuroscience and Biobehavioral Reviews 67: 2–8.

Prusky, Glen T., Paul W.R. West, and Robert M. Douglas. 2000. “Behavioral Assessment of Visual Acuity in Mice and Rats.” Vision Research 40 (16): 2201–9.

Raderschall, Chloé A., Robert D. Magrath, and Jan M. Hemmi. 2011. “Habituation under Natural Conditions: Model Predators Are Distinguished by Approach Direction.” Journal of Experimental Biology 214 (24): 4209–16.

Reinhard, Katja, Chen Li, Quan Do, Emily G. Burke, Steven Heynderickx, and Karl Farrow. 2019. “A Projection Specific Logic to Sampling Visual Inputs in Mouse Superior Colliculus.” ELife 8: 1–42.

Roberts, Katherine L., and Harriet A. Allen. 2016. “Perception and Cognition in the Ageing Brain: A Brief Review of the Short- and Long-Term Links between Perceptual and Cognitive Decline.” Frontiers in Aging Neuroscience 8 (MAR): 1–7.

Samuel, Melanie A., Yifeng Zhang, Markus Meister, and Joshua R. Sanes. 2011. “Age-Related Alterations in Neurons of the Mouse Retina.” Journal of Neuroscience 31 (44): 16033–44.

Seabrook, Tania A., Timothy J. Burbridge, Michael C. Crair, and Andrew D. Huberman. 2017. “Architecture, Function, and Assembly of the Mouse Visual System.” Annual Review of Neuroscience 40 (1): 499–538.

Serpi, Raisa, Tanja Klein-Rodewald, Julia Calzada-Wack, Frauke Neff, Tibor Schuster, Valérie Gailus-Durner, Helmut Fuchs, Matti Poutanen, Martin Hrabé de Angelis, and Irene Esposito. 2013. “Inbred Wild Type Mouse Strains Have Distinct Spontaneous Morphological Phenotypes.” Histology and Histopathology 28 (1): 79–88.

Shang, Congping, Zijun Chen, Aixue Liu, Yang Li, Jiajing Zhang, Baole Qu, Fei Yan, et al. 2018. “Divergent Midbrain Circuits Orchestrate Escape and Freezing Responses to Looming Stimuli in Mice.” Nature Communications 9 (1): 1–17.

Shansky, Rebecca M., and Catherine S. Woolley. 2016. “Considering Sex as a Biological Variable Will Be Valuable for Neuroscience Research.” Journal of Neuroscience 36 (47): 11817–22.

Shansky, Rebecca M. 2019. “Animal Studies in Both Sexes.” Science 364 (6443): 825–26.

Shaqiri, Albulena, Maya Roinishvili, Lukasz Grzeczkowski, Eka Chkonia, Karin Pilz, Christine Mohr, Andreas Brand, Marina Kunchulia, and Michael H. Herzog. 2018. “Sex-Related Differences in Vision Are Heterogeneous.” Scientific Reports 8 (1): 1–10.

Sih, Andrew, Kimberley J. Mathot, María Moirón, Pierre Olivier Montiglio, Max Wolf, and Niels J. Dingemanse. 2015. “Animal Personality and State-Behaviour Feedbacks: A Review and Guide for Empiricists.” Trends in Ecology and Evolution 30 (1): 50–60.

Spangenberg, Elin M.F., and Anette Wichman. 2018. “Methods for Investigating the Motivation of Mice to Explore and Access Food Rewards.” Journal of the American Association for Laboratory Animal Science 57 (3): 244–52.

Storchi, R., J. Rodgers, M. Gracey, F. P. Martial, J. Wynne, S. Ryan, C. J. Twining, T. F. Cootes, R. Killick, and R. J. Lucas. 2019. “Measuring Vision Using Innate Behaviours in Mice with Intact and Impaired Retina Function.” Scientific Reports 9 (1).

Sugita, Yuko, Haruka Yamamoto, Yamato Maeda, and Takahisa Furukawa. 2020. “Influence of Aging on the Retina and Visual Motion Processing for Optokinetic Responses in Mice.” Frontiers in Neuroscience 14 (December): 1–16.

Sultana, Razia, Olalekan M. Ogundele, and Charles C. Lee. 2019. “Contrasting Characteristic Behaviours among Common Laboratory Mouse Strains.” Royal Society Open Science 6 (6).

Sundaram, Venki, Anthony T. Moore, Robin R. Ali, and James W. Bainbridge. 2012. “Educational Paper: Retinal Dystrophies and Gene Therapy.” European Journal of Pediatrics 171 (5): 757–65.

Tafreshiha, Azadeh, Sven A.Vander Burg, Kato Smits, Laila A. Blomer, and J. Alexander Heimel. 2021. “Visual Stimulus-Specific Habituation of Innate Defensive Behaviour in Mice.” Journal of Experimental Biology 224 (6).

Thaung, Caroline, Karen Arnold, Ian J. Jackson, and Peter J. Coffey. 2002. “Presence of Visual Head Tracking Differentiates Normal Sighted from Retinal Degenerate Mice.” Neuroscience Letters 325 (1): 21–24.

Vale, Ruben, Dominic A. Evans, and Tiago Branco. 2017. “Rapid Spatial Learning Controls Instinctive Defensive Behavior in Mice.” Current Biology 27 (9): 1342–49.

Wang, Fei, E. Li, Lei De, Qiwen Wu, and Yifeng Zhang. 2021. “OFF-Transient Alpha RGCs Mediate Looming Triggered Innate Defensive Response.” Current Biology 31 (11): 2263-2273.e3.

Wang, Nan Kai, Pei Kang Liu, Yang Kong, Sarah R. Levi, Wan Chun Huang, Chun Wei Hsu, Hung Hsi Wang, et al. 2021. “Mouse Models of Achromatopsia in Addressing Temporal ‘Point of No Return’ in Gene-therapy.” International Journal of Molecular Sciences 22 (15).

Wei, Pengfei, Nan Liu, Zhijian Zhang, Xuemei Liu, Yongqiang Tang, Xiaobin He, Bifeng Wu, et al. 2015. “Processing of Visually Evoked Innate Fear by a Non-Canonical Thalamic Pathway.” Nature Communications 6.

Weitzman, Jonathan B. 2002. “The Mouse Genome.” Genome Biology 3 (1): 1729–40.

West, Emma L., Joana Ribeiro, and Robin R. Ali. 2020. “Development of Stem Cell Therapies for Retinal Degeneration.” Cold Spring Harbor Perspectives in Biology 12 (8): 1–23.

Wissinger, Bernd, Daphne Gamer, Herbert Jägle, Roberto Giorda, Tim Marx, Simone Mayer, Sabine Tippmann, et al. 2001. “CNGA3 Mutations in Hereditary Cone Photoreceptor Disorders.” American Journal of Human Genetics 69 (4): 722–37.

Wolf, Max, and Franz J. Weissing. 2012. “Animal Personalities: Consequences for Ecology and Evolution.” Trends in Ecology and Evolution 27 (8): 452–61.

Yilmaz, Melis, and Markus Meister. 2013. “Rapid Innate Defensive Responses of Mice to Looming Visual Stimuli.” Current Biology 23 (20): 2011–15.

Zhao, Xinyu, Mingna Liu, and Jianhua Cang. 2014a. “Visual Cortex Modulates the Magnitude but Not the Selectivity of Looming-Evoked Responses in the Superior Colliculus of Awake Mice.” Neuron 84 (1): 202–13.

Zhou et al. 2009. “Intrasession and Intersession Habituation in Mice: From Inbred Strain Variability to Linkage Analysis.” Neurobiol Learn Mem. 92 (2): 206–14.

Zhu, Jeffrey D., Sharma Pooja Tarachand, Qudrat Abdulwahab, and Melanie A. Samuel. 2023. “Structure, Function, and Molecular Landscapes of the Aging Retina.” Annual Review of Vision Science 9: 177–99.

Zingg, Brian, Xiao lin Chou, Zheng gang Zhang, Lukas Mesik, Feixue Liang, Huizhong Whit Tao, and Li I. Zhang. 2017. “AAV-Mediated Anterograde Transsynaptic Tagging: Mapping Corticocollicular Input-Defined Neural Pathways for Defense Behaviors.” Neuron 93 (1): 33–47.

Supplementary data

Table 1: Summary table of animal allocated to each experimental study.

FILENAME	COHORT	STRAIN	DOB	GENDER	Date of 1st day of session Experiment	Age on of 1st day of session Experiment (months)	Age on of 1st day of session Experiment (days)	Location	User
MF19044_S1_0	Intense	C57BL6	31/05/2019	F	29/07/2019	2.0		UCL	MM
MF19045_S1_0	Intense	C57BL6	31/05/2019	F	29/07/2019	2.0		UCL	MM
MF19046_S1_0	Intense	C57BL6	31/05/2019	F	29/07/2019	2.0		UCL	MM
MF19047_S1_0	Burst	C57BL6	31/05/2019	F	22/08/2019	2.8		UCL	MM
MF19048_S1_0	Burst	C57BL6	31/05/2019	F	22/08/2019	2.8		UCL	MM
MF19049_S1_0	Burst	C57BL6	31/05/2019	F	22/08/2019	2.8		UCL	MM
MF19052_S1_0	Burst	C57BL6	04/06/2019	F	23/08/2019	2.7		UCL	MM
MF19053_S1_0	Burst	C57BL6	04/06/2019	F	23/08/2019	2.7		UCL	MM
MM19050_S1_0	Burst	C57BL6	04/06/2019	M	23/08/2019	2.7		UCL	MM
MM19082_S1_0	Burst	C57BL6	07/09/2019	M	29/11/2019	2.8		UCL	MM
MF19086_S1_0	Intense	C57BL6	07/09/2019	F	02/12/2019	2.9		UCL	MM
MF19088_S1_0	Intense	C57BL6	07/09/2019	F	02/12/2019	2.9		UCL	MM
MF19089_S1_0	Intense	C57BL6	07/09/2019	F	02/12/2019	2.9		UCL	MM
MM19093_S1_0	Burst	C57BL6	07/11/2019	M	13/01/2020	2.2		UCL	MM
MF19090_S1_0	Tonic	C57BL6	07/11/2019	F	13/01/2020	2.2		UCL	MM
MF19091_S1_0	Tonic	C57BL6	07/11/2019	F	13/01/2020	2.2		UCL	MM
MM19095_S1_0	Burst	C57BL6	12/11/2019	M	14/01/2020	2.1		UCL	MM
MM19094_S1_0	Burst	C57BL6	12/11/2019	M	14/01/2020	2.1		UCL	MM
MF19096_S1_0	Burst	C57BL6	12/11/2019	F	15/01/2020	2.1		UCL	MM
MM19098_S1_0	Burst	C57BL6	18/11/2019	M	15/01/2020	1.9		UCL	MM
MF19097_S1_0	Tonic	C57BL6	12/11/2019	F	20/01/2020	2.3		UCL	MM
MM19099_S1_0	Tonic	C57BL6	09/12/2019	M	20/01/2020	1.4		UCL	MM
MF190100_S1_0	Tonic	C57BL6	19/11/2019	F	20/01/2020	2.1		UCL	MM
MF190101_S1_0	Tonic	C57BL6	19/11/2019	F	20/01/2020	2.1		UCL	MM
MF190102_S1_0	Tonic	C57BL6	19/11/2019	F	20/01/2020	2.1		UCL	MM
MM190103_S1_0	Tonic	C57BL6	19/11/2019	M	20/01/2020	2.1		UCL	MM
MM190104_S1_0	Tonic	C57BL6	19/11/2019	M	20/01/2020	2.1		UCL	MM
MM190105_S1_0	Tonic	C57BL6	19/11/2019	M	20/01/2020	2.1		UCL	MM
MM190106_S1_0	Tonic	C57BL6	19/11/2019	M	20/01/2020	2.1		UCL	MM
MM190107_S1_0	Tonic	C57BL6	19/11/2019	M	20/01/2020	2.1		UCL	MM
MM19009_S1_0	Age_15months	C57BL6	26/03/2019	M	08/07/2020	15.7		UCL	MM
MM19010_S1_0	Age_15months	C57BL6	26/03/2019	M	08/07/2020	15.7		UCL	MM
MM19011_S1_0	Age_15months	C57BL6	26/03/2019	M	08/07/2020	15.7		UCL	MM
MF19015_S1_0	Age_15months	C57BL6	26/03/2019	F	06/07/2020	15.6		UCL	MM
MF19016_S1_0	Age_15months	C57BL6	26/03/2019	F	06/07/2020	15.6		UCL	MM
MF19017_S1_0	Age_15months	C57BL6	11/04/2019	F	06/07/2020	15.1		UCL	MM
MF19018_S1_0	Age_15months	C57BL6	11/04/2019	F	06/07/2020	15.1		UCL	MM
MM19024_S1_0	Age_15months	C57BL6	17/04/2019	M	06/07/2020	14.9		UCL	MM
MM19025_S1_0	Age_15months	C57BL6	17/04/2019	M	06/07/2020	14.9		UCL	MM
MF19035_S1_0	Age_15months	C57BL6	01/05/2019	F	08/07/2020	14.5		UCL	MM
MF19036_S1_0	Age_15months	C57BL6	01/05/2019	F	08/07/2020	14.5		UCL	MM
MF19037_S1_0	Age_15months	C57BL6	01/05/2019	F	08/07/2020	14.5		UCL	MM
MM190108_S1_0	Age_6months	C57BL6	09/12/2019	M	23/07/2020	7.6		UCL	MM
MM190110_S1_0	Age_6months	C57BL6	09/12/2019	M	23/07/2020	7.6		UCL	MM
MM190111_S1_0	Age_6months	C57BL6	09/12/2019	M	23/07/2020	7.6		UCL	MM
MF190114_S1_0	Age_6months	C57BL6	09/12/2019	F	23/07/2020	7.6		UCL	MM
MF190117_S1_0	Age_6months	C57BL6	03/01/2020	F	23/07/2020	6.7		UCL	MM
MF2002051_S1_0	Opt_DBAs_2months	DBA	19/05/2020	F	10/08/2020	2.8		UCL	MM
MM2002052_S1_0	Opt_DBAs_2months	DBA	19/05/2020	M	10/08/2020	2.8		UCL	MM
MM2002053_S1_0	Opt_DBAs_2months	DBA	19/05/2020	M	10/08/2020	2.8		UCL	MM
MM2002054_S1_0	Opt_DBAs_2months	DBA	19/05/2020	M	10/08/2020	2.8		UCL	MM
MM2001089_S1_0	Opt_129SV_2months	129SV	10/06/2020	M	10/08/2020	2.0		UCL	MM
MM2001090_S1_0	Opt_129SV_2months	129SV	10/06/2020	M	10/08/2020	2.0		UCL	MM
MF200127_S1_0	Opt_C57BL6_2months	C57BL6	11/06/2020	F	12/08/2020	2.1		UCL	MM
MF200128_S1_0	Opt_C57BL6_2months	C57BL6	11/06/2020	F	12/08/2020	2.1		UCL	MM
MM200123_S1_0	Opt_C57BL6_2months	C57BL6	02/07/2020	M	12/08/2020	1.4		UCL	MM
MM200124_S1_0	Opt_C57BL6_2months	C57BL6	02/07/2020	M	12/08/2020	1.4		UCL	MM
MF2001091_S1_0	Opt_129SV_2months	129SV	11/06/2020	F	12/08/2020	2.1		UCL	MM
MF2001092_S1_0	Opt_129SV_2months	129SV	11/06/2020	F	12/08/2020	2.1		UCL	MM
MF2001093_S1_0	Opt_129SV_2months	129SV	11/06/2020	F	12/08/2020	2.1		UCL	MM
MM200135_S1_0	AgeLS_21Days	C57BL6	16/08/2020	M	07/09/2020		22.0	UCL	MM
MM200136_S1_0	AgeLS_21Days	C57BL6	16/08/2020	M	07/09/2020		22.0	UCL	MM
MM200137_S1_0	AgeLS_21Days	C57BL6	16/08/2020	M	07/09/2020		22.0	UCL	MM
MM200138_S1_0	AgeLS_21Days	C57BL6	16/08/2020	M	07/09/2020		22.0	UCL	MM
MF200139_S1_0	AgeLS_21Days	C57BL6	16/08/2020	F	07/09/2020		22.0	UCL	MM

MM200130_S1_0	Opt_C57BL6_2months/Age_2M	C57BL6	03/07/2020	M	01/09/2020	2.0		UCL	MM
MM200131_S1_0	Opt_C57BL6_2months/Age_2M	C57BL6	03/07/2020	M	01/09/2020	2.0		UCL	MM
MM200132_S1_0	Opt_C57BL6_2months/Age_2M	C57BL6	03/07/2020	M	01/09/2020	2.0		UCL	MM
MF200141_S1_0	Age_1 month	C57BL6	21/08/2020	F	26/09/2020	1.2		UCL	MM
MF200142_S1_0	Age_1 month	C57BL6	21/08/2020	F	26/09/2020	1.2		UCL	MM
MF200143_S1_0	Age_1 month	C57BL6	21/08/2020	F	26/09/2020	1.2		UCL	MM
MF200144_S1_0	Age_1 month	C57BL6	21/08/2020	F	26/09/2020	1.2		UCL	MM
MM200119_S1_0	Age_6months	C57BL6	27/03/2020	M	10/09/2020	5.6		UCL	MM
MM200120_S1_0	Age_6months	C57BL6	27/03/2020	M	10/09/2020	5.6		UCL	MM
MF200121_S1_0	Age_6months	C57BL6	27/03/2020	F	10/09/2020	5.6		UCL	MM
MF200122_S1_0	Age_6months	C57BL6	27/03/2020	F	10/09/2020	5.6		UCL	MM
MF210158_S1_0	Opt_C57BL6_2months	C57BL6	03/03/2021	F	11/05/2021	2.3		KCL	MM
MM210152_S1_0	Opt_C57BL6_2months	C57BL6	03/03/2021	M	11/05/2021	2.3		KCL	MM
MF210151_S1_0	Opt_C57BL6_2months	C57BL6	09/02/2021	F	11/05/2021	3.0		KCL	MM
MM210156_S1_0	Opt_C57BL6_2months	C57BL6	03/03/2021	M	12/05/2021	2.3		KCL	MM
MM210157_S1_0	Opt_C57BL6_2months	C57BL6	03/03/2021	M	12/05/2021	2.3		KCL	MM
MF2102060_S1_0	Opt_DBAs_2months	DBA1	11/02/2021	F	13/05/2021	3.0		KCL	MM
MF2102061_S1_0	Opt_DBAs_2months	DBA1	11/02/2021	F	13/05/2021	3.0		KCL	MM
MF2102062_S1_0	Opt_DBAs_2months	DBA1	11/02/2021	F	13/05/2021	3.0		KCL	MM
MF2102063_S1_0	Opt_DBAs_2months	DBA1	11/02/2021	F	20/05/2021	3.3		KCL	MM
MF2102064_S1_0	Opt_DBAs_2months	DBA1	11/02/2021	F	20/05/2021	3.3		KCL	MM
MM2101120_S1_0	Opt_129SV_2months	129SV	26/03/2021	M	20/05/2021	1.8		KCL	MM
MF2101108_S1_0	Opt_129SV_2months	129SV	11/02/2021	F	20/05/2021	3.3		KCL	MM
MF2101109_S1_0	Opt_129SV_2months	129SV	11/02/2021	F	20/05/2021	3.3		KCL	MM
MM2101103_S1_0	Opt_129SV_2months	129SV	11/02/2021	M	26/05/2021	3.5		KCL	MM
MM2101104_S1_0	Opt_129SV_2months	129SV	11/02/2021	M	26/05/2021	3.5		KCL	MM
MM2101112_S1_0	CA_129SV_2months	129SV	08/03/2021	M	26/05/2021	2.6		KCL	MM
MM2101113_S1_0	CA_129SV_2months	129SV	08/03/2021	M	26/05/2021	2.6		KCL	MM
MM2102065_S1_0	CA_DBA1_2months	DBA1	09/03/2021	M	26/05/2021	2.6		KCL	MM
MM2102065_S1_0	CA_DBA1_2months	DBA1	09/03/2021	M	26/05/2021	2.6		KCL	MM
EM210180_S1_0	AgeLS_21Days	C57BL6	20/06/2021	M	12/07/2021		22.0	KCL	EY
EM210181_S1_0	AgeLS_21Days	C57BL6	20/06/2021	M	12/07/2021		22.0	KCL	EY
EF210182_S1_0	AgeLS_21Days	C57BL6	20/06/2021	F	12/07/2021		22.0	KCL	EY
EM210183_S1_0	AgeLS_21Days	C57BL6	30/06/2021	M	21/07/2021		21.0	KCL	EY
EM210184_S1_0	AgeLS_21Days	C57BL6	30/06/2021	M	21/07/2021		21.0	KCL	EY
EF210185_S1_0	AgeLS_21Days	C57BL6	30/06/2021	F	21/07/2021		21.0	KCL	EY
MM200142_S1_0	Age_12Month	C57BL6	04/09/2020	M	20/09/2021	13.7		KCL	EY
MM200148_S1_0	Age_12Month	C57BL6	10/01/2021	M	20/09/2021	13.7		KCL	EY
MM200149_S1_0	Age_12Month	C57BL6	10/01/2021	M	20/09/2021	13.7		KCL	EY
MM200150_S1_0	Age_12Month	C57BL6	10/01/2021	M	20/09/2021	12.6		KCL	EY
EF210168_S1_0	Age_6Month	C57BL6	26/03/2021	F	27/09/2021	6.5		KCL	EY
EF210177_S1_0	Age_6Month	C57BL6	15/04/2021	F	27/09/2021	6.5		KCL	EY
EF210178_S1_0	Age_6Month	C57BL6	15/04/2021	F	27/09/2021	6.5		KCL	EY
EF210179_S1_0	Age_6Month	C57BL6	15/04/2021	F	27/09/2021	6.5		KCL	EY
EF2104003_S1_0	Control / GT_Rd1	Rd1	04/09/2021	F	01/11/2021	1.9		KCL	EY
EF2104004_S1_0	Control / GT_Rd1	Rd1	04/09/2021	F	01/11/2021	1.9		KCL	EY
EM2104005_S1_0	Control / GT_Rd1	Rd1	04/09/2021	M	01/11/2021	1.9		KCL	EY
EM2104006_S1_0	Control / GT_Rd1	Rd1	04/09/2021	M	01/11/2021	1.9		KCL	EY
EM2204011_S1_0	Control / GT_Rd1	Rd1	04/09/2021	M	01/11/2021	1.9		KCL	EY
EM2204012_S1_0	Control / GT_Rd1	Rd1	04/09/2021	M	01/11/2021	1.9		KCL	EY
EM2204013_S1_0	Control / GT_Rd1	Rd1	04/09/2021	M	01/11/2021	1.9		KCL	EY
EM2204014_S1_0	Control / GT_Rd1	Rd1	04/09/2021	M	01/11/2021	1.9		KCL	EY
EF220153_S1_0	Age_12Month	C57BL6	03/03/2021	F	19/04/2022	13.7		KCL	EY
EF220154_S1_0	Age_12Month	C57BL6	03/03/2021	F	19/04/2022	13.7		KCL	EY
EF220155_S1_0	Age_12Month	C57BL6	03/03/2021	F	19/04/2022	13.7		KCL	EY
EM220170_S1_0	Age_12Month	C57BL6	14/04/2021	M	26/04/2022	12.6		KCL	EY
EM220171_S1_0	Age_12Month	C57BL6	14/04/2021	M	26/04/2022	12.6		KCL	EY
EM220172_S1_0	Age_12Month	C57BL6	14/04/2021	M	26/04/2022	12.6		KCL	EY
MF220188_S1_0	Scotopic_C57BL6	C57BL6	13/04/2022	F	30/06/2022	2.6		KCL	MM
MF2205002_S1_0	Scotopic_Gnat1	Gnat1-/-	04/04/2022	M	30/06/2022	2.9		KCL	MM
MF2205003_S1_0	Scotopic_Gnat1	Gnat1-/-	04/04/2022	M	30/06/2022	2.9		KCL	MM
MF2205004_S1_0	Scotopic_Gnat1	Gnat1-/-	04/04/2022	M	30/06/2022	2.9		KCL	MM
MF2205005_S1_0	Photopic_Gnat1	Gnat1-/-	04/04/2022	M	26/07/2022	3.8		KCL	MM
MF2205006_S1_0	Photopic_Gnat1	Gnat1-/-	04/04/2022	M	26/07/2022	3.8		KCL	MM
MF2205007_S1_0	Photopic_Gnat1	Gnat1-/-	04/04/2022	M	26/07/2022	3.8		KCL	MM
MF220189_S1_0	Photopic_C57BL6	C57BL6	12/03/2022	F	28/07/2022	4.6		KCL	MM
MF220190_S1_0	Photopic_C57BL6	C57BL6	12/03/2022	F	28/07/2022	4.6		KCL	MM
MF220191_S1_0	Photopic_C57BL6	C57BL6	12/03/2022	F	28/07/2022	4.6		KCL	MM
MF2207000_S1_0	Photopic_OGC	OGC	03/04/2022	F	26/07/2022	3.8		KCL	MM
MF2207001_S1_0	Photopic_OGC	OGC	03/04/2022	F	26/07/2022	3.8		KCL	MM
MM2207002_S1_0	Photopic_OGC	OGC	04/04/2022	M	26/07/2022	3.8		KCL	MM
MM2207003_S1_0	Photopic_OGC	OGC	04/04/2022	M	26/07/2022	3.8		KCL	MM
MM2207004_S1_0	Photopic_OGC	OGC	04/04/2022	M	26/07/2022	3.8		KCL	MM
MM220192_S1_0	Photopic_C57BL6	C57BL6	13/04/2022	M	28/07/2022	3.5		KCL	MM
MM220193_S1_0	Photopic_C57BL6	C57BL6	13/04/2022	M	28/07/2022	3.5		KCL	MM
MM220194_S1_0	Photopic_C57BL6	C57BL6	13/04/2022	M	28/07/2022	3.5		KCL	MM
MM220195_S1_0	Scotopic_C57BL6	C57BL6	13/04/2022	M	11/08/2022	4.0		KCL	MM
MF2207005_S1_0	Scotopic_OGC	OGC	27/04/2022	F	11/08/2022	3.5		KCL	MM
MF2207006_S1_0	Scotopic_OGC	OGC	27/04/2022	F	11/08/2022	3.5		KCL	MM
MF2207007_S1_0	Scotopic_OGC	OGC	27/04/2022	M	11/08/2022	3.5		KCL	MM
MM2208000_S1_0	Photopic_CNG3A	CNG3A	15/05/2022	M	17/08/2022	3.1		KCL	MM
MM2208001_S1_0	Photopic_CNG3A	CNG3A	15/05/2022	M	17/08/2022	3.1		KCL	MM
MF2208002_S1_0	Photopic_CNG3A	CNG3A	15/05/2022	M	17/08/2022	3.1		KCL	MM
MF2208003_S1_0	Photopic_CNG3A	CNG3A	15/05/2022	M	17/08/2022	3.1		KCL	MM
MM2208004_S1_0	Photopic_CNG3A	CNG3A	15/05/2022	M	23/08/2022	3.3		KCL	MM
MM2208005_S1_0	Photopic_CNG3A	CNG3A	15/05/2022	M	23/08/2022	3.3		KCL	MM
MF2208006_S1_0	Photopic_CNG3A	CNG3A	15/05/2022	M	23/08/2022	3.3		KCL	MM

MF2208007_S1_0	Photopic_CNG3A	CNG3A	15/05/2022	M	23/08/2022	3.3		KCL	MM
MM220180_S1	Age_1Month	C57BL6	02/11/2022	M	08/12/2022	1.2		KCL	MM
MM220181_S1	Age_1Month	C57BL6	02/11/2022	M	08/12/2022	1.2		KCL	MM
MM220182_S1	Age_1Month	C57BL6	02/11/2022	M	08/12/2022	1.2		KCL	MM
MM220183_S1	Age_1Month	C57BL6	02/11/2022	M	08/12/2022	1.2		KCL	MM
MM220184_S1	Age_1Month	C57BL6	02/11/2022	M	08/12/2022	1.2		KCL	MM
MM2204018_S1_0	Subret injections / GT_Rd1	Rd1	14/01/2022	M	10/03/2022	1.8		KCL	MM
MM2204019_S1_0	Subret injections / GT_Rd1	Rd1	14/01/2022	M	10/03/2022	1.8		KCL	MM
MF2204020_S1_0	Subret injections / GT_Rd1	Rd1	06/10/2022	F	30/11/2022	1.8		KCL	MM
MF2204021_S1_0	Subret injections / GT_Rd1	Rd1	07/10/2022	F	30/11/2022	1.8		KCL	MM
MM2304022_S1_0	Subret injections / GT_Rd1	Rd1	20/03/2023	M	15/05/2023	1.9		KCL	MM
MF2304023_S1_0	Subret injections / GT_Rd1	Rd1	20/03/2023	F	15/05/2023	1.9		KCL	MM
MF2304024_S1_0	Subret injections / GT_Rd1	Rd1	20/03/2023	F	15/05/2023	1.9		KCL	MM
MF2304025_S1_0	Subret injections / GT_Rd1	Rd1	20/03/2023	F	15/05/2023	1.9		KCL	MM

Table 2: Summary of behavioural responses characterization.

Protocols	Tonic 1st Time Point			Burst 1st Time Point			Intense 1st Time Point			Optimal UCL- 1st Time Point			Optimal KCL- 1st Time Point		
sex	male	female	total	male	female	total	male	female	total	male	female	total	male	female	total
n mice	6	6	12	9	6	15	0	6	6	5	2	7			
stimuli	Loom	Sweep	Baseline	Loom	Sweep	Baseline	Loom	Sweep	Baseline	Loom	Sweep	Baseline	Loom	Sweep	Baseline
ntrial	111	113	359	122	130	512	220	243	995	82	83	325	38	41	169
CPR detect	0.86	0.81	0.34	0.9	0.78	0.32	0.87	0.79	0.43	0.9	0.87	0.37	0.89	0.83	0.41
CPR F+E	0.07	0.21	0	0.02	0.26	0	0.04	0.16	0.01						
CPR escape	0.55	0.41	0.1	0.76	0.52	0.06	0.62	0.46	0.11	0.38	0.22	0.05	0.68	0.63	0.05
CPR freeze	0.38	0.61	0.24	0.16	0.52	0.26	0.29	0.5	0.34	0.57	0.82	0.32	0.21	0.49	0.36
n detect	95	92	122	110	101	164	191	192	428	74	72	120	34	34	69
n f+e	8	24	0	2	34	0	9	39	10	0	0	0	0	0	0
n escape	61	46	36	93	68	31	136	112	109	31	18	16	26	26	8
n freeze	42	69	86	20	68	133	64	122	338	47	68	104	8	20	61

Sessions (All)												
sex	male	female	total									
n mice	20	20	40									
stimuli	Loom						Sweep					
session	**S1**	**S2**	**S3**	**S4**	**S5**	**Baseline**	**S1**	**S2**	**S3**	**S4**	**S5**	**Baseline**
nsession	80	75	69	63	64	1423	80	76	71	71	69	1423
CPR detect	0.81	0.91	0.9	0.87	0.92	0.33	0.55	0.78	0.83	0.89	0.87	0.33
CPR escape	0.04	0.61	0.67	0.59	0.64	0.07	0.17	0.43	0.44	0.48	0.48	0.07
CPR freeze	0.54	0.36	0.28	0.33	0.33	0.26	0.44	0.57	0.69	0.63	0.71	0.26
n detect	65	68	62	55	59	470	44	59	59	63	60	470
n escape	3	46	46	37	41	100	14	33	31	34	33	100
n freeze	43	27	19	21	21	370	35	43	49	45	49	370

Trials (All)	T1	T2	T3	T4	Baseline
ntrial total	686	673	641	628	1423
CPR detect	0.82	0.82	0.82	0.82	0.33
CPR escape	0.51	0.51	0.49	0.48	0.07
CPR freeze	0.45	0.45	0.46	0.46	0.26
n detect	563	552	526	515	470
n escape	350	343	314	301	100
n freeze	309	303	295	289	370

Optimised Protocol	Optimal UCL- 1st Time Point			Optimal KCL- 1st Time Point			Optimal UCL - 2nd Time Point			Optimal KCL - 2nd Time Point		
sex	male	female	total	male	female	total	male	female	total	male	female	total
n mice	5	2	7				5	2	7			
stimuli	Loom	Sweep	Baseline	Loom	Sweep	Baseline	Loom	Sweep	Baseline	Loom	Sweep	Baseline
ntrial	82	83	325	38	41	169	76	80	174	24	31	40
CPR detect	0.9	0.87	0.37	0.89	0.83	0.41	0.88	0.94	0.59	0.96	0.97	0.33
CPR escape	0.38	0.22	0.05	0.68	0.63	0.5	0.39	0.5	0.16	0.92	0.9	0.2
CPR freeze	0.57	0.82	0.32	0.21	0.49	0.36	0.64	0.71	0.44	0.04	0.35	0.13
CPR F+E								0.28			0.29	
n detect	74	72	120	34	34	69	67	75	103	23	30	13
n escape	31	18	16	26	26	85	30	40	28	22	28	8
n freeze	47	68	104	8	20	61	49	57	77	1	11	5
n f+e							0	0	0	0	9	0

1st and 2 nd Time Point (All)	All 1st Time Point			All 2nd Time Point		
sex	male	female	total	male	female	total
n mice	20	20	40	20	20	40
stimuli	Loom	Sweep	Baseline	Loom	Sweep	Baseline
ntrial	535	569	2191	493	531	1547
CPR detect	0.88	0.8	0.38	0.87	0.89	0.48
CPR escape	0.6	0.43	0.09	0.44	0.44	0.14
CPR freeze	0.32	0.57	0.3	0.48	0.63	0.35
n detect	471	455	833	429	473	743
n escape	321	245	197	217	234	217
n freeze	171	324	657	237	335	541
n f+e						

Female vs Male						
sex	**male**	**female**	**total**			
n mice	20	14	34			
	Female			Male		
stimuli	Loom	Sweep	Baseline	Loom	Sweep	Baseline
ntrial	272	282	2031	326	339	2031
CPR detect	0.89	0.87	0.39	0.88	0.86	0.39
CPR escape	0.54	0.42	0.09	0.56	0.49	0.09
CPR freeze	0.4	0.69	0.3	0.39	0.59	0.3
n detect	242	245	792	287	292	792
n escape	147	118	183	183	166	183
n freeze	109	195	609	127	200	609

Age Longitudinal Study	12M			6M			2M			1M			21D		
sex	male	female	total	male	female	total	male	female	total	male	female	total	male	female	total
n mice - ucL	4		10			6	4	1	11	4	1	11	4	1	11
n mice -nkcl	4	2		4	2		4	2		4	2		4	2	
stimuli	Loom	Sweep	Baseline	Loom	Sweep	Baseline	Loom	Sweep	Baseline	Loom	Sweep	Baseline	Loom	Sweep	Baseline
n trial total	46	48	183	50	58	114	114	119	323	116	123	246	110	117	303
CPR detect	0.83	0.79	0.41	0.76	0.83	0.32	0.83	0.8	0.43	0.76	0.76	0.47	0.75	0.6	0.36
CPR F+E	0	0	0	0	0.17	0	0.02	0.12	0	0.01	0.1	0.01	0	0.03	0.01
CPR escape	0.04	0.02	0.03	0.6	0.66	0.09	0.41	0.37	0.13	0.28	0.3	0.07	0.2	0.11	0.03
CPR freeze	0.78	0.77	0.38	0.16	0.34	0.23	0.45	0.55	0.31	0.48	0.56	0.42	0.55	0.51	0.33
n detect (trials)	38	38	75	38	48	36	95	95	139	88	93	116	83	70	109
n f+e (trials)	0	0	0	0	10	0	2	14	0	1	12	2	0	4	3
n escape (trials)	2	1	5	30	38	10	47	44	42	32	37	17	22	13	9
n freeze (trials)	36	37	70	8	20	26	51	65	100	56	69	103	61	60	100

Age Cross-sectional Study	15M			12M			6M			2M			1M			21D		
sex	male	female	total	male	female	total	male	female	total	male	female	total	male	female	total	male	female	total
n mice - ucL	5	7	12	-	-		5	4		5	2			4		4	1	
n mice -nkcl	-	-	-	7	3	10		4	13	3	2	12		4	8	4	2	11
stimuli	Loom	Sweep	Baseline	Loom	Sweep	Baseline	Loom	Sweep	Baseline	Loom	Sweep	Baseline	Loom	Sweep	Baseline	Loom	Sweep	Baseline
n trial total	144	142	588	115	116	424	148	147	408	120	124	494	95	99	261	110	117	303
CPR detect	0.85	0.8	0.3	0.73	0.68	0.32	0.8	0.8	0.32	0.9	0.85	0.38	0.78	0.71	0.39	0.75	0.6	0.36
CPR F+E	0.03	0.04	0	0.02	0.11	0	0.09	0.18	0	0.03	0.21	0.01	0.06	0.09	0	0	0.03	0.01
CPR escape	0.04	0.06	0.01	0.23	0.19	0.02	0.36	0.27	0.03	0.47	0.35	0.05	0.27	0.26	0.06	0.2	0.11	0.03
CPR freeze	0.83	0.78	0.29	0.51	0.6	0.3	0.53	0.71	0.29	0.46	0.71	0.33	0.57	0.54	0.34	0.55	0.51	0.33
n detect (trials)	122	114	176	84	79	136	118	118	131	108	105	188	74	70	102	83	70	109
n f+e (trials)	4	6	0	2	13	0	13	26	0	4	26	5	6	9	0	0	4	3
n escape (trials)	6	9	6	26	22	8	53	40	12	56	43	25	26	26	16	22	13	9
n freeze (trials)	120	111	171	59	70	127	78	104	118	55	88	163	54	53	89	61	60	100

WT Strains	C57BL6			DBA1			129SV		
sex	male	female	total	male	female	total	male	female	total
n mice	8	4	12	3	6	9	5	5	10
stimuli	Loom	Sweep	Baseline	Loom	Sweep	Baseline	Loom	Sweep	Baseline
ntrial	220	235	708	36	41	36	38	48	174
CPR detect	0.9	0.9	0.43	0.53	8	0.36	0.89	0.94	0.57
CPR escape	0.5	0.48	0.09	0.39	0.44	0.17	0.58	0.73	0.09
CPR freeze	0.48	0.66	0.35	0.17	0.39	0.19	0.37	0.33	0.49
CPR freeze+escape									
n detect	198	212	304	19	328	13	34	45	99
n escape	110	113	64	14	4	6	22	1	16
n freeze	106	155	248	6	0	7	14	0	85
n f+e									

Photopic	C57BL6			CNGA3			GNAT1			OGC		
sex	male	female	total	male	female	total	male	female	total	male	female	total
n mice												
stimuli	Loom	Sweep	Baseline	Loom	Sweep	Baseline	Loom	Sweep	Baseline	Loom	Sweep	Baseline
ntrial	34	38		30	37		30	31		45	46	
CPR detect	0.76	0.79		0.93	0.97		0.63	0.71		0.58	0.7	
CPR escape	0.41	0.47		0.93	0.78		0.27	0.29		0	0	
CPR freeze	0.35	0.5		0	0.35		0.37	0.52		0.58	0.7	
CPR freeze+escape												
n detect	26	30		28	36		19	22		26	32	
n escape	14	18		28	29		8	9		0	0	
n freeze	12	19		0	13		11	16		26	32	
n f+e												

Scotopic	C57BL6			CNGA3			GNAT1			OGC		
sex	male	female	total	male	female	total	male	female	total	male	female	total
n mice												
stimuli	Loom	Sweep	Baseline	Loom	Sweep	Baseline	Loom	Sweep	Baseline	Loom	Sweep	Baseline
ntrial	22	25		32	39		35	36		42	46	
CPR detect	1	1		1	1		0.57	0.61	0.39	0.74	0.7	0.58
CPR escape	1	0.68		0.97	1		0.03	0.03	0.23	0	0.02	0.03
CPR freeze	0.05	0.64		0.03	0.18		0.54	0.58	0.2	0.74	0.67	0.56
CPR freeze+escape		0.32										0
n detect	22	25		32	39		20	22		31	32	
n escape	22	17		31	39		1	1		0	1	
n freeze	1	16		1	7		19	21		31	31	
n f+e		8										

Table 3: Statistics ananlysis summary of behaviour caracteristics.

Protocols

		Loom			Comparison p-value			Sweep			Comparison p-value		
		Mean	S.D	Median				Mean	S.D	Median			
Escape Latency	Tonic	0.81	0.93	0.40	0.0089	0.4030	0.0837	2.04	0.98	1.98	0.2989	0.0036	0.1708
	Burst	0.49	0.43	0.37				1.75	0.97	1.70			
	Intense	0.68	0.65	0.46				1.46	1.13	1.35			
Freeze Latency	Tonic	1.53	1.28	1.26	0.4503	0.2697	0.9969	1.01	1.06	0.55	0.1635	0.0092	0.6635
	Burst	1.13	1.13	0.53				0.77	0.88	0.47			
	Intense	1.15	1.11	0.50				0.82	1.06	0.35			
Max Escape Speed	Tonic	75.87	19.80	76.45	0.2038	0.1211	0.9858	70.27	20.75	67.29	0.8317	0.1613	0.0159
	Burst	81.03	17.08	84.26				67.89	22.49	61.51			
	Intense	81.43	18.79	79.20				77.15	21.98	73.67			
Freeze Duration	Tonic	1.18	0.61	1.06	0.3769	0.2266	0.9902	1.27	0.74	1.13	0.0181	0.3501	0.2128
	Burst	1.50	1.04	1.18				0.95	0.48	0.78			
	Intense	1.47	0.90	1.32				1.12	0.74	0.89			

Sessions (All)

		Mean	S.D	Median	Comparison p-value								
Escape Latency	S1	1.06	0.93	0.59	0.6332	0.6936	0.9843	0.9627	1.0000	0.8963	0.9398	0.9297	0.9631	0.9999
	S2	1.31	1.11	0.99										
	S3	1.30	1.15	0.66										
	S4	1.16	0.99	0.72										
	S5	1.18	1.04	0.59										
Freeze Latency	S1	1.31	1.16	0.80	0.3545	0.2703	0.0646	0.0165	0.9998	0.9125	0.6774	0.9601	0.7828	0.9917
	S2	0.98	1.01	0.49										
	S3	0.95	1.08	0.47										
	S4	0.84	0.93	0.42										
	S5	0.76	0.72	0.51										
Max Escape Speed	S1	66.40	18.11	61.00	0.8671	0.0848	0.0485	0.2976	0.4353	0.2954	0.8269	0.9987	0.9715	0.9026
	S2	69.86	17.67	70.20										
	S3	75.44	24.24	72.66										
	S4	76.38	22.64	76.13										
	S5	73.37	19.38	73.47										
Freeze Duration	S1	1.15	0.69	0.92	0.9998	0.4720	0.2676	0.5317	0.5452	0.3171	0.6087	0.9954	1.0000	0.9879
	S2	1.18	0.51	1.11										
	S3	1.39	0.92	1.08										
	S4	1.45	0.98	1.13										
	S5	1.38	0.92	1.22										

Trials (All)

		Mean	S.D	Median	Comparison p-value					
Escape Latency	T1	2.02	1.04	1.79	0.0000	0.4316	0.0000	0.0000	0.5793	0.0000
	T2	0.63	0.68	0.37						
	T3	1.81	0.89	1.89						
	T4	0.79	0.86	0.43						
Freeze Latency	T1	0.93	1.03	0.50	0.1589	0.5509	0.8797	0.0087	0.6685	0.2682
	T2	1.26	1.18	0.54						
	T3	0.75	0.79	0.49						
	T4	1.05	0.99	0.51						
Max Escape Speed	T1	67.50	22.58	58.85	0.0186	0.9985	0.0436	0.0421	0.9915	0.0866
	T2	76.36	18.18	78.73						
	T3	68.05	23.55	60.63						
	T4	75.53	18.99	77.56						
Freeze Duration	T1	1.18	0.78	0.92	0.0109	0.9076	0.3672	0.0623	0.6102	0.7197
	T2	1.59	0.91	1.50						
	T3	1.26	0.85	0.97						
	T4	1.40	0.75	1.30						

Optimised Protocol

		Loom				Sweep			
		Mean	S.D	Median	Comparison p-value	Mean	S.D	Median	Comparison p-value
Escape Latency	UCL	2.17	1.41	2.02	0.0000	2.20	0.95	1.92	0.2957
	KCL	0.36	0.09	0.37		1.87	1.05	1.73	
Freeze Latency	UCL	1.10	0.84	0.69	0.0328	0.83	0.99	0.37	0.4011
	KCL	1.16	0.94	0.87		0.89	0.83	0.69	
Max Escape Speed	UCL	61.60	10.76	61.37	0.0000	54.20	8.34	53.00	0.0036
	KCL	82.76	18.38	84.07		64.79	13.53	61.80	
Freeze Duration	UCL	1.57	0.77	1.49	0.0138	1.63	0.96	1.40	0.2028
	KCL	0.83	0.37	0.63		1.35	0.85	1.13	

1st and 2nd Time Point (All)

		Loom				Sweep			
		Mean	S.D	Median	Comparison p-value	Mean	S.D	Median	Comparison p-value
Escape Latency	1st TP	0.69	0.72	0.41	0.0338	1.70	1.07	1.65	0.5333
	2nd TP	0.88	0.92	0.49		1.66	1.08	1.50	
Freeze Latency	1st TP	1.23	1.09	0.62	0.0087	0.85	1.01	0.40	0.3016
	2nd TP	1.61	1.27	1.21		0.96	1.09	0.45	
Max Escape Speed	1st TP	78.33	18.76	78.41	0.9139	71.54	22.02	68.74	0.1758
	2nd TP	78.94	21.49	77.88		72.52	18.44	70.19	
Freeze Duration	1st TP	1.43	0.83	1.28	0.4534	1.23	0.78	0.95	0.0245
	2nd TP	1.36	0.78	1.12		1.38	0.86	1.15	

Female vs Male

		Loom				Sweep			
		Mean	S.D	Median	Comparison p-value	Mean	S.D	Median	Comparison p-value
Escape Latency	Female	0.73	0.75	0.44	0.4975	1.97	0.97	1.92	0.0881
	Male	0.81	0.84	0.42		1.77	1.01	1.62	
Freeze Latency	Female	1.61	1.23	1.20	0.1916	0.85	0.97	0.45	0.6280
	Male	1.40	1.22	0.80		0.82	0.99	0.40	
Max Escape Speed	Female	74.08	18.77	77.14	0.1042	67.20	18.33	65.41	0.8744
	Male	78.50	20.80	76.09		67.96	19.32	60.76	
Freeze Duration	Female	1.31	0.35	1.27	0.8569	1.13	0.32	1.01	0.2910
	Male	0.02	0.01	0.02		0.02	0.01	0.02	

Age Longitudinal Study

		Loom										
		Mean	S.D	Median	Comparison p-value							
Escape Latency	21Days	0.53	0.45	0.44	0.9843	0.2924	0.9945	0.0000	0.4822	0.8352	0.0000	0.0596	0.0000	0.0000
	1Month	0.62	0.54	0.44										
	2Months	0.86	0.95	0.45										
	6Months	0.45	0.33	0.39										
	12Months	3.21	0.08	3.21										
Freeze Latency	21Days	1.68	1.26	1.14	0.6954	0.0114	0.7956	0.8831	0.2781	0.9869	0.9997	0.9905	0.3136	0.9773
	1Month	1.98	1.04	1.95										
	2Months	2.44	1.27	2.24										
	6Months	2.22	1.08	2.17										
	12Months	1.93	1.25	1.64										
Max Escape Speed	21Days	68.75	9.93	69.32	0.5089	0.5707	0.2283	0.8879	0.9996	0.9719	0.5440	0.9129	0.5783	0.4153
	1Month	78.35	23.14	81.96										
	2Months	77.33	23.84	79.87										
	6Months	81.75	25.70	76.92										
	12Months	53.46	0.42	53.46										
Freeze Duration	21Days	1.42	0.88	1.27	0.8863	0.6270	0.6219	0.8354	0.9867	0.8698	0.3428	0.9539	0.1622	0.3098
	1Month	1.28	0.75	1.12										
	2Months	1.20	0.64	0.96										
	6Months	0.98	0.50	0.88										
	12Months	1.61	0.93	1.37										

		Sweep										
		Mean	S.D	Median	Comparison p-value							
Escape Latency	21Days	1.10	0.70	1.11	0.8750	0.8370	0.9999	0.0356	1.0000	0.5512	0.0781	0.4543	0.0817	0.0204
	1Month	1.34	0.94	1.10										
	2Months	1.36	0.85	1.13										
	6Months	1.06	0.74	0.90										
	12Months	2.89	0.66	2.89										
Freeze Latency	21Days	1.39	1.24	0.99	0.7038	0.8933	0.0926	0.9517	0.9952	0.4871	0.3403	0.3231	0.5389	0.0330
	1Month	1.12	1.21	0.45										
	2Months	1.20	1.19	0.48										
	6Months	0.64	0.63	0.35										
	12Months	1.57	1.16	1.22										
Max Escape Speed	21Days	64.25	14.06	65.93	0.6873	0.4108	0.1197	0.7908	0.9798	0.5730	0.4097	0.8644	0.3084	0.1780
	1Month	72.84	22.79	72.72										
	2Months	75.45	23.28	75.42										
	6Months	79.99	18.77	79.78										
	12Months	46.21	7.99	46.21										
Freeze Duration	21Days	1.47	0.87	1.18	0.6016	0.5313	0.6955	0.9868	1.0000	0.9985	0.3852	0.9995	0.3307	0.5024
	1Month	1.27	0.66	1.05										
	2Months	1.26	0.72	1.13										
	6Months	1.22	0.63	0.88										
	12Months	1.55	0.86	1.28										

Age Cross-Sectional Study

Loom

		Mean	S.D	Median	Comparison p-value													
Escape Latency	21Days	0.53	0.45	0.44														
	1Month	1.45	0.89	1.36														
	2Months	0.80	0.80	0.44	0.0142	0.8762	0.0109	0.2879	0.0000	0.0558	0.9983	0.9897	0.0392	0.0348	0.6774	0.0000	0.9992	0.0116	0.0224
	6Months	1.35	1.27	0.70														
	12Months	1.24	0.99	0.74														
	15Months	2.74	1.20	3.25														
Freeze Latency	21Days	1.68	1.26	1.14														
	1Month	1.31	1.09	0.72														
	2Months	1.23	0.97	0.76	0.0142	0.8762	0.0109	0.2879	0.0000	0.0558	0.9983	0.9897	0.0392	0.0348	0.6774	0.0000	0.9992	0.0116	0.0224
	6Months	1.04	0.93	0.63														
	12Months	1.45	1.11	1.19														
	15Months	1.26	0.98	1.06														
Max Escape Speed	21Days	68.75	9.93	69.32														
	1Month	60.21	18.28	55.89														
	2Months	71.25	18.05	70.70	0.5978	0.9944	1.0000	0.9548	0.5300	0.1142	0.2929	0.2122	0.9811	0.9949	0.9944	0.2647	0.9544	0.4001	0.2367
	6Months	69.39	22.93	62.02														
	12Months	74.32	10.64	75.79														
	15Months	54.32	8.64	54.16														
Freeze Duration	21Days	1.42	0.88	1.27														
	1Month	1.44	0.82	1.18														
	2Months	1.48	0.77	1.41	1.0000	0.9996	0.5920	0.9952	0.0602	0.9999	0.6526	0.9933	0.0820	0.8217	0.9810	0.1782	0.7110	0.8564	0.3422
	6Months	1.68	0.98	1.52														
	12Months	1.27	0.93	0.83														
	15Months	1.83	0.89	1.72														

Sweep

		Mean	S.D	Median	Comparison p-value													
Escape Latency	21Days	1.10	0.70	1.11														
	1Month	2.01	0.73	1.85														
	2Months	2.01	1.01	1.82	0.0441	0.0240	0.0080	0.7917	0.0000	1.0000	0.9985	0.5827	0.0144	0.9961	0.4976	0.0079	0.2763	0.0208	0.0003
	6Months	2.11	1.10	2.07														
	12Months	1.54	1.03	1.40														
	15Months	3.27	0.72	3.41														
Freeze Latency	21Days	1.39	1.24	0.99														
	1Month	1.20	1.03	0.89														
	2Months	0.85	0.95	0.38	0.9122	0.0143	0.0372	1.0000	0.8733	0.3138	0.5151	0.9954	1.0000	0.9980	0.4298	0.1060	0.5729	0.2396	0.9957
	6Months	0.91	0.96	0.50														
	12Months	1.35	1.10	1.17														
	15Months	1.21	0.89	0.92														
Max Escape Speed	21Days	64.25	14.06	65.93														
	1Month	58.00	11.58	59.59														
	2Months	60.32	12.67	56.12	0.8195	0.9608	1.0000	0.2438	0.3664	0.9896	0.4397	0.0014	0.8622	0.7203	0.0028	0.6017	0.0934	0.1664	0.0015
	6Months	64.94	19.18	63.13														
	12Months	76.21	18.82	80.27														
	15Months	50.92	8.83	51.90														
Freeze Duration	21Days	1.47	0.87	1.18														
	1Month	1.29	0.79	0.92														
	2Months	1.56	0.93	1.33	0.9088	0.9915	0.5548	0.9978	0.4745	0.5282	0.0622	0.8712	0.0435	0.8358	1.0000	0.7642	0.9940	1.0000	0.9899
	6Months	1.72	1.03	1.43														
	12Months	1.59	1.03	1.43														
	15Months	1.74	0.91	1.46														

WT strains

		Loom			Comparison p-value			Sweep			Comparison p-value		
		Mean	S.D	Median				Mean	S.D	Median			
Escape Latency	C57BL6	0.92	0.89	0.52				1.81	1.01	1.62			
	DBA1	1.12	1.15	0.82	0.7590	0.0001	0.0808	1.43	1.13	1.26	0.2700	0.0077	0.7956
	129SV	1.82	1.20	1.42				1.25	0.73	1.16			
Freeze Latency	C57BL6	1.27	1.03	0.79				0.73	0.94	0.34			
	DBA1	2.43	0.67	2.87	0.0348	0.5094	0.2466	1.88	1.16	1.81	0.0000	0.0085	0.4308
	129SV	1.59	0.97	1.72				1.26	1.02	0.75			
Max Escape Speed	C57BL6	68.89	17.24	64.81				62.02	12.71	59.03			
	DBA1	63.45	17.96	58.27	0.4651	0.0004	0.2706	73.78	25.69	65.24	0.0086	0.1071	0.4281
	129SV	55.02	8.60	57.24				68.14	17.90	63.35			
Freeze Duration	C57BL6	1.33	0.77	1.12				1.44	0.90	1.23			
	DBA1	1.16	0.51	0.97	0.8791	0.9677	0.8419	1.07	0.68	0.78	0.2240	0.4251	0.9515
	129SV	1.38	0.80	1.13				1.16	0.62	1.01			

Photopic

Loom

		Mean	S.D	Median	Comparison p-value						Mean	S.D	Median	Comparison p-value					
Escape Latency	C57BL6	0.55	0.17	0.51							1.62	0.89	1.65						
	CNGA3	0.39	0.23	0.32	0.7017	0.0024	Na	0.0001	Na	Na	1.20	0.88	0.86	0.2971	0.0068	Na	0.0001	Na	Na
	GNAT1	1.47	1.40	0.72							2.83	1.17	2.70						
	OGC	Na	Na	Na							Na	Na	Na						
Freeze Latency	C57BL6	1.71	1.17	1.73							1.24	0.90	0.95						
	CNGA3	Na	Na	Na	NA	0.7407	0.3441	Na	Na	0.6866	0.74	0.54	0.69	0.4117	0.0011	0.8144	0.0000	0.0746	0.0066
	GNAT1	2.02	0.87	1.99							1.20	0.85	1.05						
	OGC	2.19	1.19	2.16							2.17	1.04	2.09						
Max Escape Speed	C57BL6	72.41	18.38	71.00							74.68	18.87	75.53						
	CNGA3	79.82	16.97	77.61	0.3961	0.0613	Na	0.0015	Na	Na	72.55	14.97	72.55	0.8896	0.0004	Na	0.0005	Na	Na
	GNAT1	55.22	16.40	47.13							48.66	6.31	45.61						
	OGC	Na	Na	Na							Na	Na	Na						
Freeze Duration	C57BL6	1.31	0.71	1.15							1.26	0.85	0.77						
	CNGA3	Na	Na	Na	Na	0.3937	Na	Na	Na	Na	1.66	1.27	1.23	0.5445	0.9937	1.0000	0.3652	0.5430	0.9924
	GNAT1	1.08	0.59	0.84							1.41	0.77	1.28						
	OGC	Na	Na	Na							1.14	0.55	0.88						

Scotopic

Loom

		Mean	S.D	Median	Comparison p-value						Mean	S.D	Median	Comparison p-value					
Escape Latency	C57BL6	0.52	0.28	0.44							1.70	0.82	1.74						
	CNGA3	0.28	0.09	0.26	0.0010	0.0000	Na	0.0000	Na	Na	0.74	0.69	0.54	0.0002	0.0922	0.2631	0.0025	0.0007	0.6776
	GNAT1	2.79	0.80	2.79							2.53	0.43	2.72						
	OGC	Na	Na	Na							3.47	0.00	3.47						
Freeze Latency	C57BL6	Na	Na	Na							0.55	0.47	0.34						
	CNGA3	Na	Na	Na	Na	Na	Na	Na	Na	0.2445	0.51	0.52	0.30	0.9999	0.0000	0.0000	0.0003	0.0016	0.7328
	GNAT1	2.48	0.96	2.41							2.35	1.13	2.32						
	OGC	2.08	1.18	1.96							2.07	1.11	1.84						
Max Escape Speed	C57BL6	85.59	15.64	85.91							78.18	15.53	78.80						
	CNGA3	95.18	15.67	92.75	0.0804	0.0165	Na	0.0013	Na	Na	89.68	14.96	90.06	0.0487	0.0042	0.1966	0.0000	0.0339	0.9990
	GNAT1	52.59	13.52	52.59							45.01	5.08	42.97						
	OGC	Na	Na	Na							47.39	0.00	47.39						
Freeze Duration	C57BL6	Na	Na	Na							1.28	0.80	1.03						
	CNGA3	Na	Na	Na	Na	Na	Na	Na	Na	0.1089	1.07	0.44	0.98	0.8967	0.9996	0.8394	0.9147	0.5224	0.7373
	GNAT1	1.12	0.84	0.67							1.26	0.65	1.17						
	OGC	1.54	0.84	1.40							1.45	0.63	1.38						